

Tectonic and Metamorphic Evolution of the Central Himalayan Domain in Southeast Zaskar (Kashmir, India)

by Pierre Dèzes



Mémoires de Géologie (Lausanne)

Section des Sciences de la Terre

Université de Lausanne

BFSH-2, 1015 Lausanne, Suisse

Mémoires de Géologie (Lausanne)

EDITEUR

Jean Guex
Institut de Géologie et Paléontologie
BFSH-2 Université de Lausanne
CH-1015, Lausanne SUISSE

COMITE EDITORIAL

Clark Blake
U.S. Geological Survey
345 Middlefield Road
94025 Menlo Park, California, U.S.A.

Francis Hirsch
Geological Survey of Israel
30 Malkhe Israel Street
95501 Jerusalem, ISRAEL

Gilles S. Odin
Géochronologie et Sédimentologie
Université P. et M. Curie, 4 Place Jussieu
75252 Paris Cedex 05 FRANCE

Jean Chaline
Centre des Science de la Terre
Uni. de Bourgogne, 6 bvd. Gabriel
21000 Dijon, FRANCE

Alan R. Lord
Department of Earth Science
University College, Gower Street
WC1E 6BT, London, U.K.

José Sandoval
Dpto.Estratigrafía y Paleontología
Universidad de Granada
18002, Granada, ESPAGNE

Jim T.E. Channell
Department of Geology
University of Florida
Gainesville, FL 32611-2036, U.S.A.

Jean Marcoux
Géologie Paris VII et IPGP
Tour 25 1er étage, 2 place Jussieu
75251 Paris Cedex 05 FRANCE

Rudolph Trumphy
Geologisches Institut, ETH-zentrum
Sonnegstrasse 5
CH-8092, Zurich, SUISSE

Giorgio Martinotti
Dipartimento di Scienze della Terra
Università, Via Valperga Caluso 37
10125 Torino ITALIE

Mémoires de Géologie (Lausanne)

Section des Sciences de la Terre
Institut de Géologie et Paléontologie
Université de Lausanne
BFSH-2, CH-1015 Lausanne

DÈZES, Pierre

Tectonic and metamorphic evolution of the Central Himalayan Domain in Southeast Zaskar (Kashmir, India)

Mém. Géol. (Lausanne), n°32, 1999, 145 p., X fig., 1 Map.

ISSN: 1015-3578

Imprimeur:

Cover photo: Along the paths of Zaskar, the traveller is often confronted with Mani walls. These stone structures are a compilation of many exquisitely carved stone tablets, each with the inscription "Om Mani Padme Hum" which translates to "Hail to the jewel in the lotus". These walls should be passed or circumvented from the left side, the clockwise direction in which the earth and the universe revolve, according to Buddhist doctrine.

Tectonic and Metamorphic Evolution of the Central Himalayan Domain in Southeast Zaskar (Kashmir, India)

Pierre Dèzes

Mémoires de Géologie (Lausanne) No. 32, 1999

Table of Contents

Résumé	1
Abstract	1
Acknowledgements	2
1. INTRODUCTION	5
1.1 Geography	6
1.2 Climate:	8
1.3 Population:	8
1.4 History:.....	10
1.5 Etymology:	11
1.6 Toponymy:	11
1.7 Cartography:.....	12
2. GEOLOGICAL OVERVIEW	15
2.1 Introduction	15
2.2 The making of the Himalaya	15
2.3 Major tectonic subdivisions of the Himalaya	17
2.4 Geological frame of this study	20
2.5 Purposes of the present work	22
3. STRATIGRAPHY	25
3.1 Introduction	25
3.2 The Phe Formation	25
3.3 The Karsha Formation	27
3.4 The Kurgiakh Formation	27
3.5 The Thaple Formation	28
3.6 The Muth Formation	28
3.7 The Lipak Formation	29
3.8 The Po Formation	29
3.9 The Ganmachidam Formation	32
3.10 The Chumik Formation	32
3.11 The Panjal Traps	33
3.12 The Kuling Formation	33
3.13 The Lilang Group	34
3.14 The Tamba Kurkur Formation	34
3.15 The Hanse Formation	34
3.16 The Zozar Formation	35
3.17 The Quartzites Series	35
3.18 Synthesis of the stratigraphic observations	36
3.19 Pre-Himalayan tectonics in Zanskar	38

4. TECTONICS	41
4.1 Introduction	41
4.1.1: Main Structural elements in the NW Himalaya	42
4.1.2: Chronology of deformation in the NW Himalaya (Fig 4.1)	44
4.2: Structural observations in SE Zaskar	46
4.2.1: Phase D1: the NE-directed Shikar Beh Nappe	46
4.2.2: Phase D2: The SW-directed Nyimaling - Tsarap Nappe	46
4.2.3: Phase D3: ductile underthrusting of the HHCS below the TH	48
4.2.4: Phase D4: ductile top to the NE extension along the ZSZ	50
4.2.5: Phase D5: Doming	53
4.2.6: Phase D6: High-angle normal faults	56
4.3 Discussion:	56
5. METAMORPHISM	59
5.1 Introduction	59
5.2 The prograde regional metamorphism M1	60
5.3 The prograde regional metamorphism M2	65
5.3.1 Introduction	65
5.3.2 Metamorphism in the Paleozoic-Mesozoic (Tethyan) series	65
5.3.3 High-grade Metamorphism along the Kamirup valley	69
5.3.4 The metamorphic transition between the TH and the HHCS across the ZSZ	70
5.3.4.1 The Biotite Zone	70
5.3.4.2 The Garnet Zone	73
5.3.4.3 The Staurolite Zone	74
5.3.4.4 The Kyanite Zone	75
5.3.4.5 The Intrusion Zone	77
5.3.4.6 The Migmatitic Zone	77
5.3.4.7 Discussion	81
5.3.5 Thermobarometry	83
5.3.5.1 Analytical procedure	83
5.3.5.2 Results:	84
5.4 The retrograde metamorphism M3	87
5.4.1 Sillimanite	87
5.4.2 Cordierite	88
5.4.3 K-feldspar	88
5.4.4 Andalusite	89
5.4.5 Margarite	89
5.4.6 Other minerals	89
5.4.7 Discussion	91
5.5 Conclusion	93
6. LEUCOGRANITES	99
6.1 Introduction	99
6.2 Geological setting	100
6.3 Petrography	104
6.4 Geochemistry	105

6.4.1	Major elements	105
6.4.2	Trace elements:	108
6.5	Geochronology	110
6.6	Origin of the leucogranites and melt migration	113
6.6	Discussion	114
7. THE ZSZ: AGE AND AMOUNT OF SHEAR		119
7.1	Introduction	119
7.2	Displacement along the ZSZ	119
7.3	Timing of extensional shearing along the ZSZ	123
7.4	Discussion	124
8. MODELS FOR SYN-OROGENIC EXTENSION		125
8.1	Introduction:	125
8.2	Gravity collapse	126
8.3	Ductile extrusion-channel flow model	128
8.4	Analogic physical modelling	129
8.5	Discussion	133
9. CONCLUSIONS		135
10. BIBLIOGRAPHY		137



Résumé

La région du Zaskar, étudiée dans le cadre de ce travail, se situe au passage entre deux domaines himalayens fortement contrastés, la Séquence Cristalline du Haut Himalaya (HHCS), composée de roches métamorphiques et l'Himalaya Tethysien (TH), composé de séries sédimentaires. La transition entre ces deux domaines est marquée par une structure tectonique majeure, la Zone de Cisaillement du Zaskar (ZSZ), au sein de laquelle on observe une augmentation extrêmement rapide, mais néanmoins graduelle, du degré du métamorphisme entre le TH et le HHCS.

Il a été établi que le HHCS n'est autre que l'équivalent métamorphique des séries sédimentaires de la base du TH. C'est principalement lors d'un épisode de mise en place de nappes à vergence sud-ouest, entre l'Eocène moyen et l'Oligocène, que les séries sédimentaires de la base du TH ont été entraînées en profondeur où elles ont subi un métamorphisme de type barrovien. Au début du Miocène, le HHCS a été exhumé en direction du sud-ouest sous forme d'une grande nappe, délimitée à sa base par le MCT (principal chevauchement central) et à son sommet par la Zone de Cisaillement du Zaskar. L'ensemble des zones barroviennes, de la zone à biotite jusqu'à la zone à disthène, a été cisailée par les mouvements en faille normale au sommet du HHCS et se retrouve actuellement sur une épaisseur d'environ 1 kilomètre au sein de la ZSZ. La décompression associée à l'exhumation du HHCS a provoqué la fusion partielle d'une partie du HHCS et a donné naissance à des magmas de composition leucogranitiques.

Grâce à la géothermobarométrie, et connaissant la géométrie de la ZSZ, il nous a été possible de déterminer que le rejet le long de cette structure d'extension est d'au moins 35 ± 9 kilomètres. Une série d'arguments nous permet cependant de suggérer que ce rejet aurait pu être encore bien plus important (~ 100 km).

Les données géochronologiques nous permettent de contraindre la durée des mouvements d'extension le long de la ZSZ à 2.4 ± 0.2 Ma entre 22.2 ± 0.2 Ma et 19.8 ± 0.1 Ma.

Ce travail apporte de nouvelles données sur les processus métamorphiques, magmatiques et tectoniques liés aux phénomènes d'extension syn-orogéniques.

Abstract

The southeastern part of Zaskar is located at the transition between two major Himalayan domains of contrasting metamorphic grade, the High Himalayan Crystalline Sequence (HHCS) and the Tethyan Himalaya (TH). The transition between the TH and the HHCS is marked by a very rapid, although perfectly gradual, decrease in metamorphic grade, which coincides with a major tectonic structure, the Zaskar Shear Zone (ZSZ).

It is now an established fact that the relation between the HHCS and the TH is not one of basement-cover type, but that the metasedimentary series of the HHCS represent the metamorphic equivalent of the lowermost sedimentary series of the TH. This transformation of sedimentary series into metamorphic rocks, and hence the differentiation between the TH and the HHCS, is the consequence of crustal thickening associated to the formation of large scale southwest vergent nappes within the Tethyan Himalaya sedimentary series. This, Middle Eocene to Oligocene, episode of crustal thickening and associated Barrovian metamorphism is followed, shortly after, by the exhumation of the HHCS as a, large scale, south-west vergent, nappe.

The exhumation of the HHCS nappe is marked by the activation of two contemporaneous structures, the Main Central Thrust at its base and the Zaskar Shear Zone at its top. Extensional movements along the ZSZ, caused the Barrovian biotite to the kyanite zones to be sheared and constricted within the ~1 km thick shear zone. Decompression associated with the exhumation of the HHCS induced the formation of leucogranitic magmas through vapour-absent partial melting of the highest-grade rocks.

The combination of geothermobarometric data with a geometric model of the ZSZ allowed us to constrain the net slip at the top of the HHCS to be at least 35 ± 9 kilometres. A set of arguments however suggests that these movements might have been much more important (~ 100 km).

Geochronological data coupled with structural observations constrain the duration of ductile shearing along the ZSZ to 2.4 ± 0.2 Ma between 22.2 ± 0.2 Ma and 19.8 ± 0.1 Ma.

This study also addresses the consequences of synorogenic extension on the metamorphic, tectonic and magmatic evolution of the upper parts of the High Himalayan Crystalline Sequence.

Acknowledgements

Although a Ph.D. thesis is essentially a solitary adventure, where one is most of the time left to one's own devices, this work could not have been carried out without the help of many persons which I sincerely wish to thank for their commitment and support.

First I would like to express my gratitude towards my parents for their moral and financial support without which this work could never have been achieved.

Of course, this work would not even have started in the first place without my thesis director Albrecht Steck, who generously entrusted me with an absolutely fascinating research theme in a superb area. Shall he be assured of my eternal gratefulness.

I want to particularly thank Mark Handy, Henri Masson, Johannes Hunziker and Albrecht Steck who reviewed this manuscript thoroughly and contributed greatly to several improvements.

It is in Zaskar that I experienced my greatest moments of happiness and exhilaration (mountain sickness?). For this I have to thank my dear colleagues and friends who accompanied me to this beautiful region. Maria-Laetizia Filippi, Andrea De Bono, Pascale and Romano Dalla Piazza and Sabine Vibe-Rheymer were the perfect friends one could wish to share such moments with. Johannes Hunziker and Albrecht Steck also joined me during the second field mission and provided me with their valuable experience and advices. I also spare a special thought to Yann Caloz and Laurent de Schoulepnikov, for it is with them that I first discovered Zaskar in 1987. This first journey to the Himalaya was such a memorable experience that it accounts for a large part in my decision to undertake a study in this region. Last but not least, these geologic missions in Zaskar would not have been the same without my efficient horseman Shukroo Ram Thakur and his eleven facetious horses, my great cook Tara Chand and the people of Zaskar.

I am greatly in debt to Jean-Claude Vannay who, with his unfailing enthusiasm provided me with the necessary motivation to pursue this work in those critical moments when I was running out of steam. Jean-Claude also often put me back on the right track when my train of thoughts was rolling head-down into some scientific dead-end. I sincerely hope that this work reflects some of the patience, didactic talents and scientific rigour he gratified me with.

Jean-Luc Epard also provided a lot of ideas, suggestions and critical comments which certainly contributed to ameliorate this manuscript.

Bernhard Grasemann, François Bussy and Viorel Atudorei were kind enough to review and comment several chapters of this work, for which I am very grateful.

I also sincerely wish to thank François Bussy who carried out the U/Pb analyses at the Royal Ontario Museum, Mike Cosca who helped me with the interpretation of the muscovite argon ages, Philippe Thelin, Michel Jaboyedoff, François Girod and Liliane Dufresne who helped me with X-Ray analyses and interpretation, as well as Anne-Marie Magnenat, Néjia Ghazinouri and Huguette Fluri for administrative support.

My often ugly samples were metamorphosed into beautiful thin sections thanks to the talented craftsmanship of Raymond Ansermoz and Laurent Nicod.

Georges Mascle and the people at the French embassy in Delhi were kind enough to provide the logistic support to fly my samples safely to Europe, for which I am more than grateful.

I also want to thank Alice H., Anna-Chiara B., Aymon B., Christian B., Christian S., Dave K., David G., Giovanni A., Guido V., Elisabeth C., Filomena A., Gerard S., Hans-Ruedi P., Iannis V., Jean G., Jean H., John M., Mac Intosh, Markus B., Makus S., Marc-Henri D., Martin R., Martin W., Micha S., Nicolas K., the Pannatiers, Popoff, Raffaele L., Robin M., Michel M., Nicolas M., Peter B., Sabrina P., Stephane C., Stephane A., Tatiana B., Vincent S and Zack S.

Finally, I am utterly glad that Brahma, Shiva, Ganesh, Hanupatta, Lakshmi, Parvati-Annapurna-Durga-Kali, Vishnu and his ten avatars, Rama, Saraswati and all the other deities kept a benevolent eye upon me whilst I was under their zone of influence.

This study was financed by the Université de Lausanne, the Swiss National Science Fund (FNRS grants 20-38917.93, 8220-028439, and 21-45650), and by the Herbette Fund.

The publishing of the present volume was financed by the Fondation du 450^e anniversaire de l'Université de Lausanne, by the Fonds de subsides pour l'impression des thèses de l'Université de Lausanne and by the Société Académique Vaudoise.

...Les faits appellent les faits. Quelque riche qu'on en soit, on en désire toujours... C'est surtout en histoire naturelle qu'on est toujours mécontent de ce qu'on a fait, parce que la nature nous montre à chaque pas qu'elle est inépuisable.

G. Cuvier, Leçons d'anatomie comparée, 1835

1. INTRODUCTION

«In this Zangskar valley which is full of wealth and happiness, first of all came the Gesar of gLing, the prime mover in this land. Then came Padmasambhava who gained control over the non-human spirits and put down the bad features of the area. The valley is shaped like a female demon lying on its back; so he built Kanika on its head. His statue was made on its heart at Pipiting and on the feet of the demon was built a shrine in a garden of the future Buddha Maitreya, Padmasambhava prophesied that Zangskar would be like the happy cemetery of Sukhavati in India. To the east is Tsere, to the south is Mahakali, to the west is Dur.lha.khrug.pa and in the north is the jewel of Cintamani. The owner of the valley is the Goddess with One Eye. The trees of the cemetery are the bushes at Sani and the birds there are the vultures thereof. So said Padmasambhava. It was a place where the Dakinis assembled, he said. And so far as human settlement is concerned, Rang.thags.sha and Ri.nam in the north and Pip.ca and Kumik in the south were established at the very beginning. After that appeared others. As it developed it became a part of Kashmir.»

The Bo-Yig document of Phugtal (trad. Osmaston, 1995)



Fig 1.1: Buddha carved on a Mani stone near Kurghiakh. Such stones carved with drawings or holy inscriptions (Om Mani Padme Hum) are found on the top of stone walls bordering Chortens (see fig. 1.9)

1.1 Geography

Zanskar together with the better known region of Ladakh were once known as Little or Western Tibet. These two ancient Buddhist kingdoms now belong to the state of Jammu and Kashmir in northwestern India. (figs. 1.3 and 1.10)



Fig 1.2: Prayer flag above the monastery (Gompa) of Tanze, in the Kurgiakh valley. The wind is believed to propagate the prayers printed on tissue

Zanskar covers an area of some 7000 km² at an elevation between 3500 and 7000 meters. It comprises the country lying along the two main tributaries of the Zanskar river. The first one, the Doda, has its source near the Pensi-La (4400m.) mountain-pass and then flows south-eastwards along the main valley leading towards Padum, the capital of Zanskar. The second branch is formed by two main tributaries known as Kurgiakh-chu with its source near the Shingo-La and Tsarap-chu with its source near the Baralacha-La. These two rivers unite below the village of Purne to form the Lungnak river (also named Lingti or Tsarap). The Lungnak-Chu then flows north-westwards along a narrow and precipitous gorge towards the Padum Valley where it unites with the Doda river to form the Zanskar river. The Zanskar river then takes globally a north-eastern course until it joins the Indus river in Ladakh. High mountain ridges lie on both sides of the NW-SE trending Doda and Lingti/Kurgiakh valleys. To the southwest is the Great Himalayan Range that separates Zanskar from the Kisthwar and Chamba basins. To the northeast lies the Zanskar Range separating Zanskar from Ladakh. Thus, the only outlet for the whole Zanskar hydrographic system is the Zanskar river which cuts a deep and narrow gorge through the Zanskar range.

These topographical features explain why access to Zanskar is difficult from all sides. Communication with the neighbouring Himalayan areas is maintained across mountain passes or along the Zanskar river when frozen. The easiest approach leads from Kargil through the Suru Valley and over the Pensi La. It is along this track that in 1979 the first and only road in Zanskar was built to connect Padum with the main road from Srinagar into Ladakh.

The remoteness of this region also explains why only a few western travellers have visited this area until recent times, the tibetologist Alexander Csoma de Körös in 1823 being probably one of the first. Moreover, because of the recent border conflicts between India and Pakistan or China, Zanskar was declared a restricted area and was reopened to foreigners only in 1974.

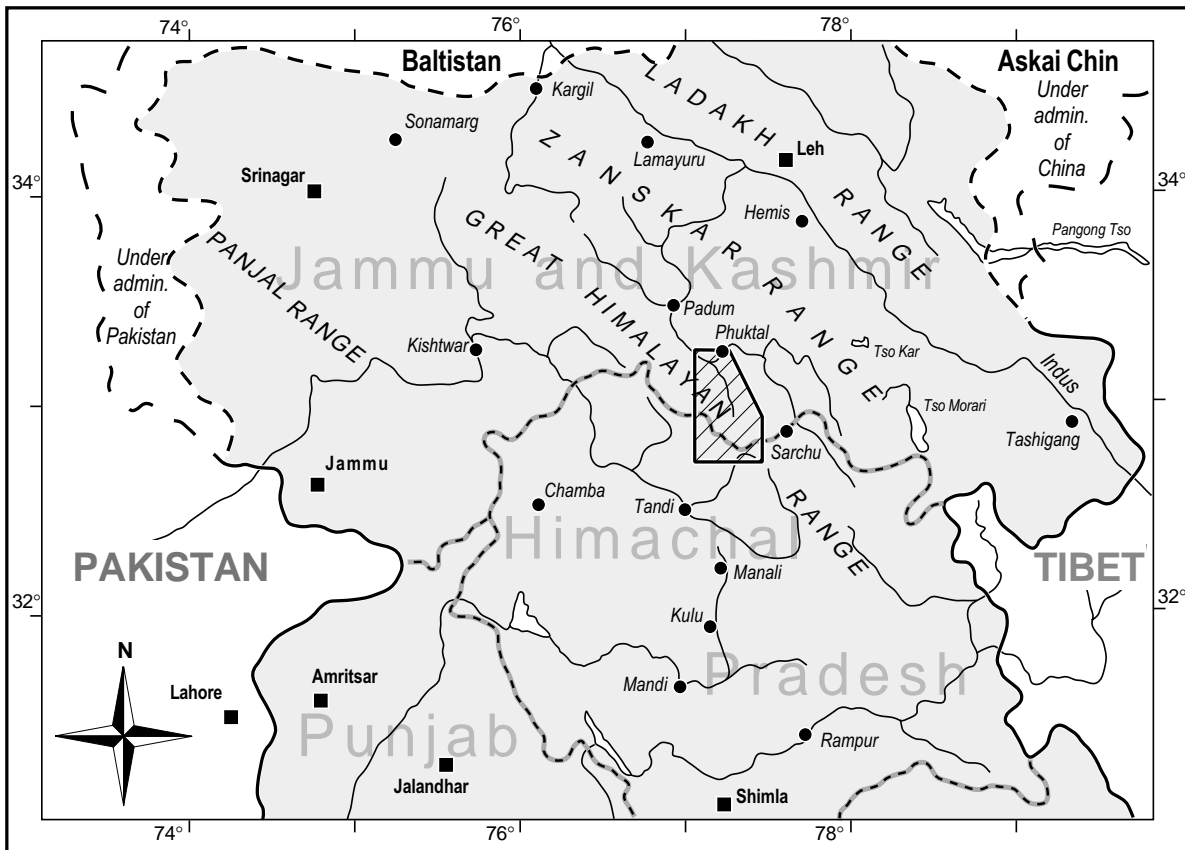


Fig. 1.3: Geographic map showing the location of the studied area of Zaskar in NW India

1.2 Climate:

Zanskar is a high altitude semi-desert lying on the Northern flank of the Great Himalayan Range. This mountain range acts as a climatic barrier protecting Ladakh and Zanskar from most of the monsoon, resulting in a pleasantly warm and dry climate in the summer. Precipitations during this season are thus scarce, although it seems that the last decades have seen an increase in pluviometry. We have indeed noticed several water driven mills, that were built, during ancient periods of drought at a great distance from the villages, but are now abandoned because running water is now available nearer to the houses. The Zanskari houses, which are otherwise especially well built, are not adapted to the recently increasing rainfalls as their roofs pretty fast start to leak, which catches their surprised inhabitants unprepared. Most of the precipitations occur as snowfalls during the harsh and extremely long lasting winter period. These winter snow falls are of vital importance since they feed the glaciers which will melt in the summer and provide most of the irrigation water.

1.3 Population:

The number of people living in Zanskar is very small, the last census of the population (1971) was of 6886 souls. Tibetan Buddhism is the religion that largely prevails among Zanskari people although slightly tinted with relicts of animistic and shamanistic rituals. A small minority of Muslims (Shiites) also lives in Zanskar. The population is scattered in small villages, the largest being Padum the «capital» with nearly 700 inhabitants. Most of the villages are distributed along the valley of the Zanskar river and its two main tributaries. Given the isolation of this region, the inhabitants are condemned to rely essentially upon themselves and until recently lived in almost complete autarky. Trade with the outside was however always necessary to acquire goods like tools, jewels or religious artefacts. The Zanskaris live from cattle-rearing and from the farming of land that they almost always own. Cultivable land is however scarce and restricted to alluvial fans and terraces (cultivated fields are rarely found at an altitude exceeding 4000 meters in Zanskar). The Zanskaris thus had to do their best to successfully develop a system of intensive arable agriculture and complex irrigation that produces enough food and avoids fallows. The scarcity of cultivable land also implies that the population has to remain stable. A rather efficient «birth control» system in Zanskar was achieved by the common practice of polyandrous marriage (several brothers are married to the same wife) and the widespread adoption of celibate religious life. A high (natural) infantile mortality rate did also certainly contribute to maintain a stable population.



Fig 1.4: Young Zanskari Girl on her way to see the Dalai Lama (picture by Yann Caloz, 1987)

The livestock and especially the yak is of paramount importance in Zanskar. Yaks are used to plough the land, to thresh the grain, to carry heavy loads (up to 200 kg), to heat the houses during the winter and their dung not only serves as fertiliser but is also the only heating fuel available in this region. They are also a vital source for milk, and sometimes but rarely, of meat. The yak's fur is used to make clothes, carpets, ropes and bed covers.



Fig. 1.5: White yak



Fig. 1.6: Black yak (in Transhimalaja, Swen Hedin, 1909)

*Oh! you beautiful yak!
Please walk fast so that our fields will be sown quickly.
Oh! you beautiful yak!
Your horns are so long that they reach the sky
and your tail is very long
Please plough our fields quickly
and then you can go on to the high pastures
and eat flowers and sit by the water on the green grass.*

Traditional Folk song

1.4 History:

The first traces of human activity in Zanskar seem to go back as far as the Bronze-age. Petroglyphs attributed to that period suggest that their creators were steppe hunters of central Asia living between Kazakstan and China. It is then suspected that an Indo-European population known



Fig. 1.7: The Royal Palace of Leh, home of the king of Ladakh, now transformed into a museum.

as the «Mon» might have lived in this region before being fused with, or replaced by, the next settlers, the Dards. Early Buddhism coming from Kashmir spread its influence in Zanskar maybe as early as 200 BC. The earliest monuments date from the Kushan period (100 BC - 500 AD). After this eastward propagation of Buddhism, Zanskar and a large part of Western Himalaya were overrun in the 7th century by the Tibetan who imposed their then animistic «Bon» religion. Buddhism regained its influence over Zanskar in the 8th century when Tibet was also converted to this religion. Between the 10th and 11th centuries, two Royal Houses were founded in Zanskar and the monasteries of Karsha and Phugtal (fig 1.8) were erected. Until the 15th century Zanskar existed as a more or less independent Buddhist Kingdom ruled by between two and four related royal families. Since the 15th century Zanskar however became subordinated to Ladakh, sharing its fortunes and misfortunes. In 1822, a coalition from Kulu, Lahoul and Kinnaur invaded Zanskar, plundering the country and destroying the Royal palace at Padum. From 1842 onward Zanskar and Ladakh became part of the state of Jammu and Kashmir. In the mid-20th century,

border conflicts between India, Pakistan and China caused Ladakh and Zanskar to be closed to foreigners. During these wars Ladakh lost two thirds of its original territory, leaving Baltistan to Pakistan and the Askai Chin to China. Ladakh and Zanskar, despite a tumultuous history of internal wars and external aggressions, never lost their cultural and religious heritage since the 8th century. Thanks to its adherence to the Indian Union, it is also one of the rare regions in the Himalaya where the traditional Tibetan culture, society and buildings survived the Chinese Cultural Revolution. In the last 20 years, the opening of a road and the massive influx of tourists and researchers however caused many changes in the traditional social organisation of Zanskar.

1.5 Etymology:

Zanskar is also often found to be written Zangskar in sociological studies or Zaskar in geographers reports or maps of the Himalaya fifty or so years ago. An etymological study (Snellgrove and Skorupsky, 1980) of the name “Zangskar” reveals that its origin might refer to the natural occurrence of copper within this region, the Tibetan word for which is *Zangs*. The second syllable however seems to be more challenging as it has various meanings: *Zangs-dkar* (white copper), *Zangs-mkhar* (copper palace) or *Zangs-sKar* (copper star). Crook (1994) partly shares this interpretation but suggests that the origin of this name might also be *Zan-mKhar* (food palace), because the staple food crops are so abundant in an otherwise rather arid region. Some of the religious scholars of the district, also cited by Snellgrove and Skorupsky (1980) and Crook (1994), held that it was originally bZang-dKar, meaning good (or beautiful) and white. «Good» refers to the shape of the Padum plain which is triangular, the symbol of Dharma and religion, «white» refers to the simplicity, goodness and religious inclinations of the Zanskaris. Thus, even if etymologically it would be more correct to use Zangskar, we decided to adopt the most frequently found spelling for this region which is undoubtedly Zanskar.

1.6 Toponymy:

The correct transcription of the names of localities is a rather challenging task when making a survey in a remote part of the Himalaya. This seems to be particularly true for Zanskar as there are notable discrepancies from one study to another in the spelling of villages, rivers or mountains. An illustration of this problem is already given above for the name of Zanskar itself. The source of these differences is not only due to the nationality of the researcher transcribing a Tibetan name in his mother tongue but is also clearly due to the inherent difficulty of translating Tibetan. In this work we have tried as much as possible to follow a hierarchy that gives priority to the spelling as found in previous geological publications for the same region so as to keep a certain homogeneity within our community. Indeed, certain names, like, for example, that of the Kurgiakh village, could be (and have been) spelled in many ways. As it has, however, also become the name of a member of a sedimentary formation (Garzanti et al. 1986), we will stick to that spelling. The second priority was to use the most frequently found modern spelling of names (as Zanskar). Certain names, however, had to be asked directly from the Zanskaris and their transcription might thus be slightly incorrect.

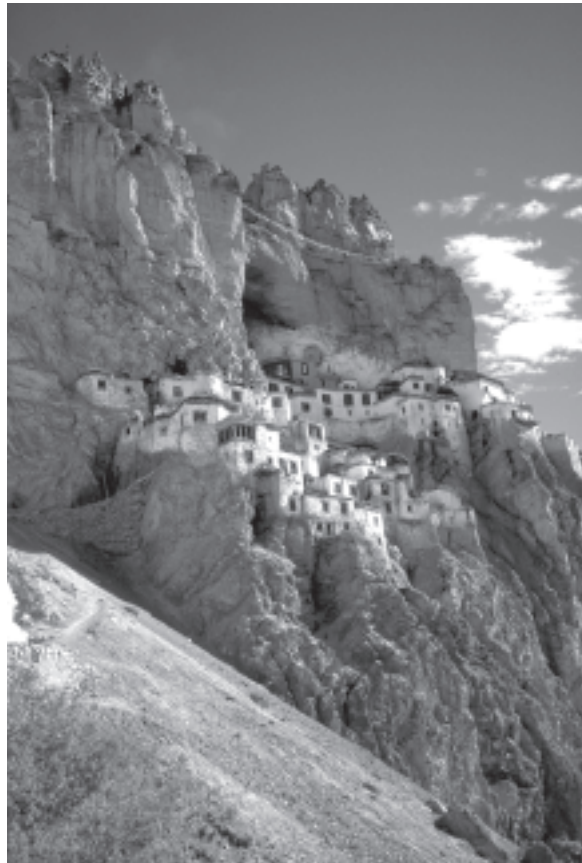


Fig 1.8: Hanging between earth and sky, the monastery of Phugtal dates from the XI century A.D.

1.7 Cartography:

Given the proximity of the Chinese and Pakistanese ill defined borders, Zanskar is considered by India as a sensitive area. Detailed topographical maps of this region are thus not available to non-Indian officials. For this reason, our geological map is essentially based on satellite imagery. We used both panchromatic Spot images with a ground resolution of 10m and Landsat images with a ground resolution of 80m. Other cartographic sources include:

- Indian Himalaya Maps, trekking routes sheets 2,3 (Jammu & Kashmir) and 5 (Himachal Pradesh). Scale 1:200'000. 1987. Leomann Maps U.K.
- US Army Maps: Palampur, (Jammu & Kashmir) NI 43-16, series U502, edition 2-AMS 1:250'000. 1962
- US Army Maps: Martselang, (Jammu & Kashmir) NI 43-12, series U502, edition 2-AMS 1:250'000. 1963
- Northern India, Special map: Ladakh/Zanskar. 1: 650'000, Nelles Verlag, Germany



Fig 1.9: Row of Chortens (or Stupas) at the village of Purne. Each of the elements forming these edifices, as well as their colour, has a symbolic meaning in Tibetan Buddhism.

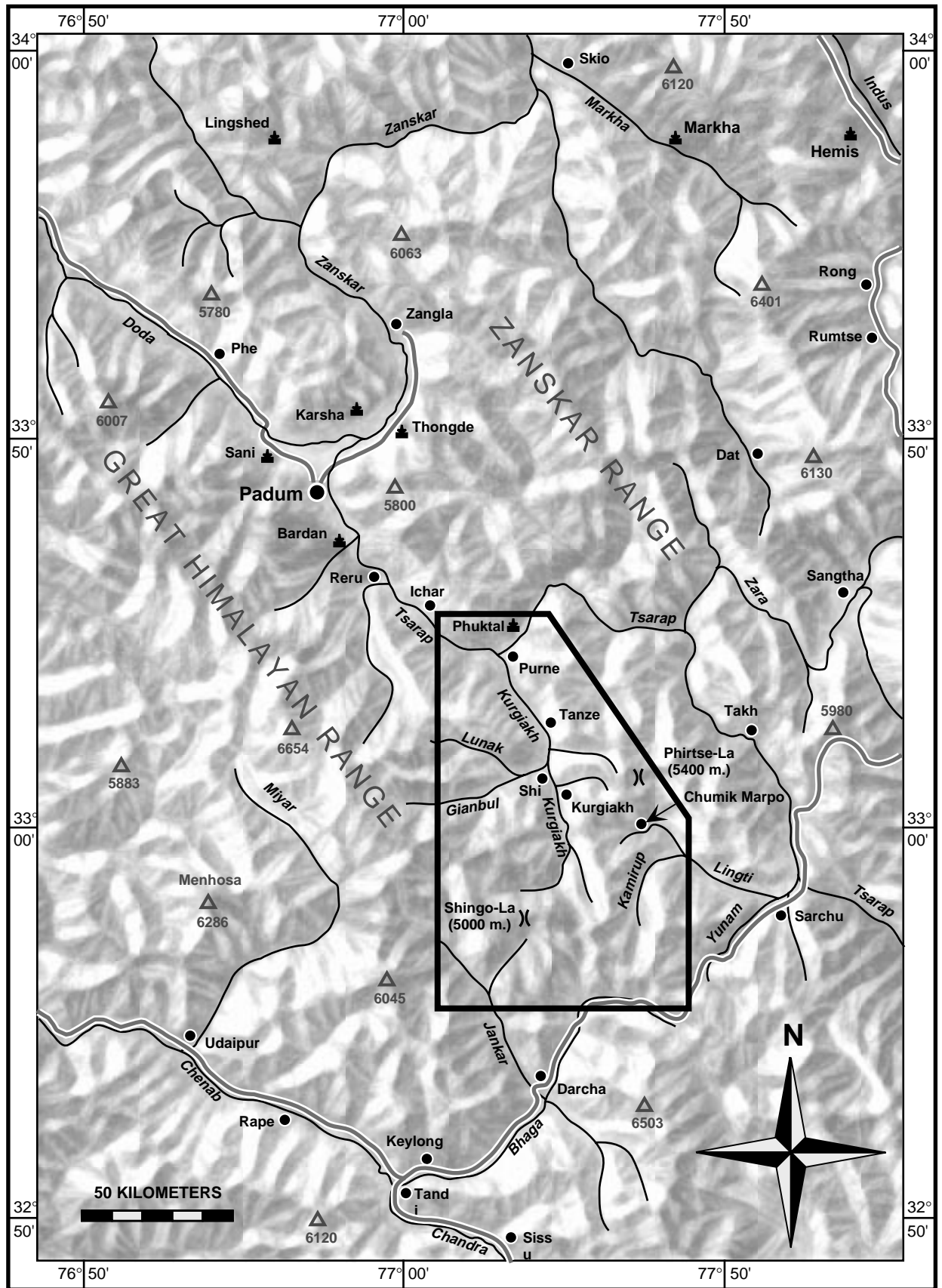


Fig. 1.10: Geographic map of the Ladakh, Zanskar and Upper Lahul regions. The studied area is shown in the bold lined box. Small black dots are villages, larger dots are county towns, stylised Chortens are monasteries, grey lines are roads and black lines are rivers.

2. GEOLOGICAL OVERVIEW

Shiva is deep in meditation in an ice-locked cave in the Himalayas. The goddess who loves him has been banished from his sight lest she disturb his meditation. She wanders the world trying to forget the great ascetic, determined not to look in his direction. But she cannot help herself and standing on a wave in the middle of the Indian Ocean, she turns and stretches her arms towards the mountains, beseeching the ascetic god to enter her embrace. Into the space between her arms explode rice fields and deserts and stone fortresses and elephants and glaciers and coconut palms and temples - in short the continent of India. This is why India is shaped in the semaphore of embrace

«Ladders and Snakes» Gita Mehta

2.1 Introduction

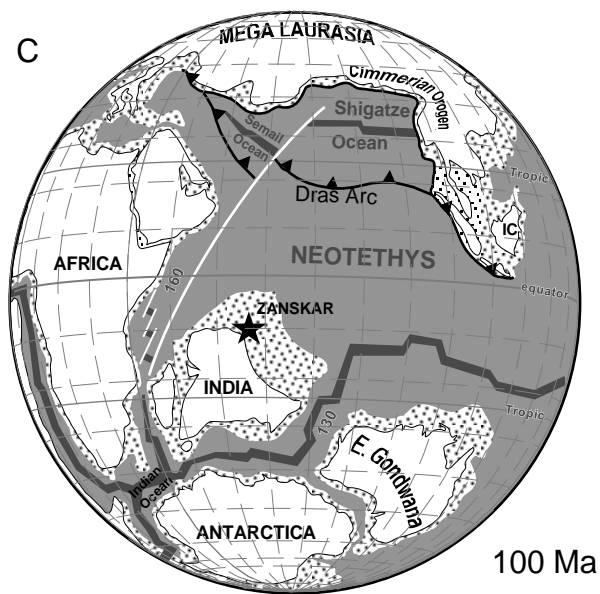
Among the most dramatic and visible creations of plate tectonic forces are the lofty Himalayas, which stretch over 2900 km along the border between India and Tibet. This immense mountain range was formed by huge tectonic forces and sculpted by powerful denudation processes. The Himalaya-Tibet region is virtually the water tower of Asia: it supplies freshwater for more than one-fifth of the world population, and it accounts for a quarter of the global sedimentation budget. Topographically, the belt has many superlatives: the highest rate of uplift (nearly 1 cm/year at Nanga Parbat), the highest relief (8848 m at Mt. Everest Chomolangma), the source of some of the greatest rivers and the highest concentration of glaciers outside of the polar regions. This last feature earned the Himalaya its name meaning in Sanskrit: «the abode of the snow».

2.2 The making of the Himalaya

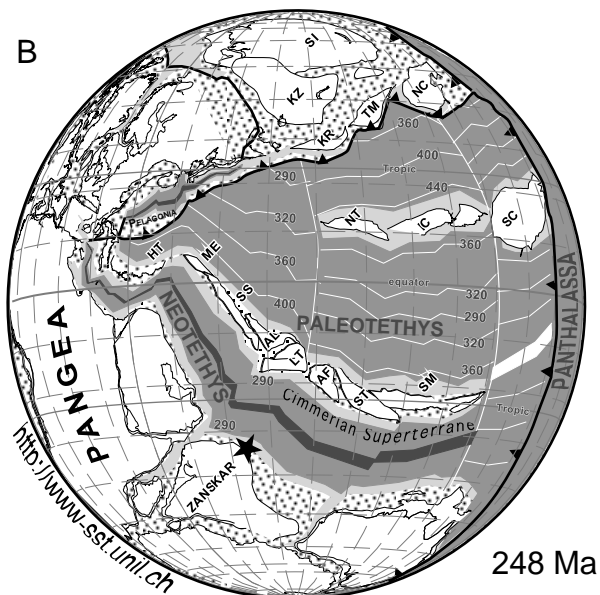
This paleogeographic reconstitution is mainly based on the following papers: Besse et al., 1984; Patriat and Achache, 1984; Dewey et al. 1989; Brookfield, 1993; Ricou, 1994; Rowley, 1996; Stampfli et al. 1998 (see also <http://www-sst.unil.ch>.)

During Late Precambrian and the Palaeozoic, the Indian continent, bounded to the north by the Cimmerian Superterrane, was part of Gondwana and was separated from Eurasia by the Paleotethys Ocean (Fig. 2.1 A). During that period, the northern part of India was affected by a late phase of the so-called “Cambro-Ordovician Pan-African event”, which is marked by an unconformity between Ordovician continental conglomerates and the underlying Cambrian marine sediments. Numerous granitic intrusions dated at around 500 Ma are also attributed to this event.

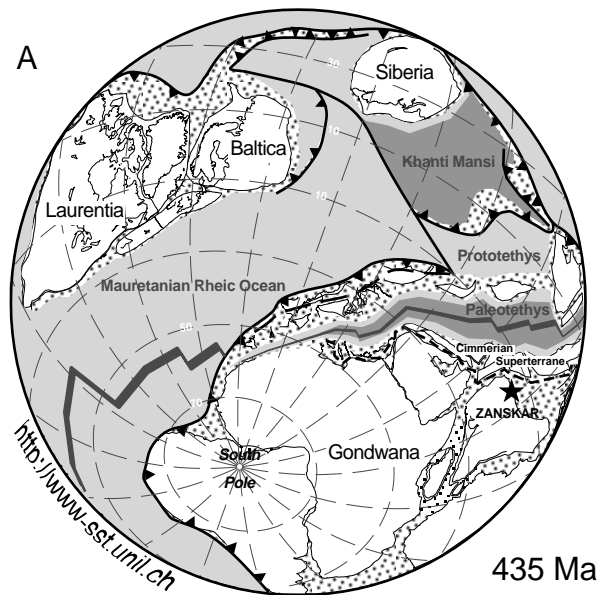
In the Early Carboniferous, an early stage of rifting is observed between the Indian continent and the Cimmerian Superterrane. During the Early Permian, this rift will develop into the Neotethys ocean (Fig 2.1 B). From that time on, the Cimmerian Superterrane drift away from Gondwana towards the north. Nowadays, Iran, Afghanistan and Tibet are partly made up of these terranes.



100 Ma



248 Ma



435 Ma

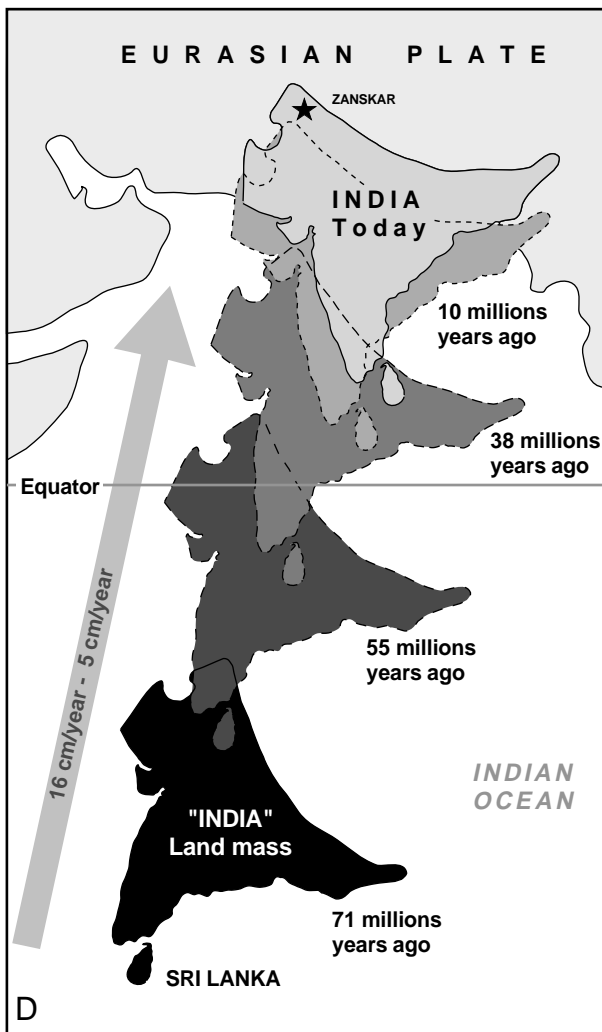


Fig 2.1: Paleogeographic reconstructions based on Stampfli and Mosar (1998) and Patriat and Achache (1984). Oceanic crust is shown in greys and continental crust in white or stippled. The position of Zanskar is shown by a black star.

A) The earth in the Early Silurian. At that time, India is part of Gondwana and bordered to the north by the Cimmerian Superterrane.

B) The earth at the Permian-Triassic boundary. The opening of the Neotethys separates the Cimmerian Superterrane from Gondwana. HT, Helenides-SW Taurides; ME, Menderes and Taurides; SS, Sanandaj and Sirjan; AL, Albroz; LT, Lut-Central Iran; AF, Afghanistan; ST, South Tibet; SM, Sibü Masu; NT, North Tibet; IC, Indochina; SC, South China; SI, Siberia; KZ, Kazakhstan; KR, Karakum; Tm, Tarim; NC, North China.

C) The earth in the Cretaceous. The Cimmerian Superterrane has accreted to Mega Laurasia, the oceanic crust of the Neotethys is subducted to the north along the Dras volcanic arc, the Shigatze Ocean opens as a consequence of back-arc spreading, India is separated from Africa and E. Gondwana and the Indian Ocean opens.

D) The northward drift of India from 71 Ma ago to present time. Note the simultaneous counter-clockwise rotation of India. Collision of the Indian continent with Eurasia occurred at about 55 Ma.

In the Norian (210 Ma), a major rifting episode splits Gondwana in two parts. The Indian continent becomes part of East Gondwana, together with Australia and Antarctica. However, the separation of East and West Gondwana, together with the formation of oceanic crust, occurred only in the Callovian (160-155 Ma). The Indian plate then broke off from Australia and Antarctica in the Early Cretaceous (130 - 125 Ma) with the opening of the “South Indian Ocean” (Fig. 2.1 C).

In the Upper Cretaceous (84 Ma), the Indian plate began its very rapid northward drift at an average speed of 16 cm/year, covering a distance of about 6000 km, until the collision of the north-western part of the Indian passive margin with Eurasia in the lower Eocene (48-52 Ma). Since that time and until today, the Indian continent continues its northwards ascent at a slower but still surprisingly fast rate of ~ 5 cm/year, indenting Eurasia by about 2400 km and rotating by just over 33° in an anticlockwise direction (Fig. 2.1 D).

Whilst most of the oceanic crust was “simply” subducted below the Tibetan block during the northward motion of India, at least three major mechanisms have been put forward, either separately or jointly, to explain what happened, since collision, to the 2400 km of “missing continental crust”. The first mechanism also calls upon the subduction of the Indian continental crust below Tibet. Second is the extrusion or escape tectonics mechanism (Molnar and Tapponier, 1975) which sees the Indian plate as an indenter that squeezed the Indochina block out of its way. The third proposed mechanism is that a large part (~1000 km, Dewey et al. 1989) of these 2400 km of crustal shortening since collision was accommodated by thrusting and folding of the sediments of the passive Indian margin together with the deformation of the Tibetan crust.

Even though it is more than reasonable to argue that this huge amount of crustal shortening most probably results from a combination of these three mechanisms, it is nevertheless the last mechanism which created the high topographic relief of the Himalaya.

2.3 Major tectonic subdivisions of the Himalaya

One of the most striking aspects of the Himalayan orogen is the lateral continuity of its major tectonic elements. Since Blanford & Medlicott, 1879 and Heim & Gansser, 1939, the Himalaya is classically divided into four tectonic units than can be followed for more than 2400 km along the belt (Fig. 2.2). In this work we will stick to these divisions but we introduce a slightly different terminology suggested by Steck (oral comm.). The ancient or frequently used terms are given within brackets.

- 1) The **Subhimalaya** forms the foothills of the Himalayan Range and is essentially composed of Miocene to Pleistocene molassic sediments derived from the erosion of the Himalaya. These molasses known as *Muree* and *Siwaliks* Formations are internally folded and imbricated. The Subhimalaya is thrust along the *Main Frontal Thrust* over the quaternary alluvium deposited by the rivers coming from the Himalaya (Ganges, Indus, Brahmaputra...), which demonstrates that the Himalaya is still a very active orogen.
- 2) The **Lesser Himalaya, LH** is mainly formed by Upper Proterozoic to Lower Cenozoic detrital sediments from the passive Indian margin intercalated with some granites and acid volcanics (1840± 70 Ma, Frank et al., 1977). These low-grade sediments are thrust over the Subhimalaya along the *Main Boundary Thrust* (MBT). The Lesser Himalaya often appears in tectonic windows (Kishtwar or Larji-Kulu-Rampur windows) within the *High Himalaya Crystalline Sequence*.

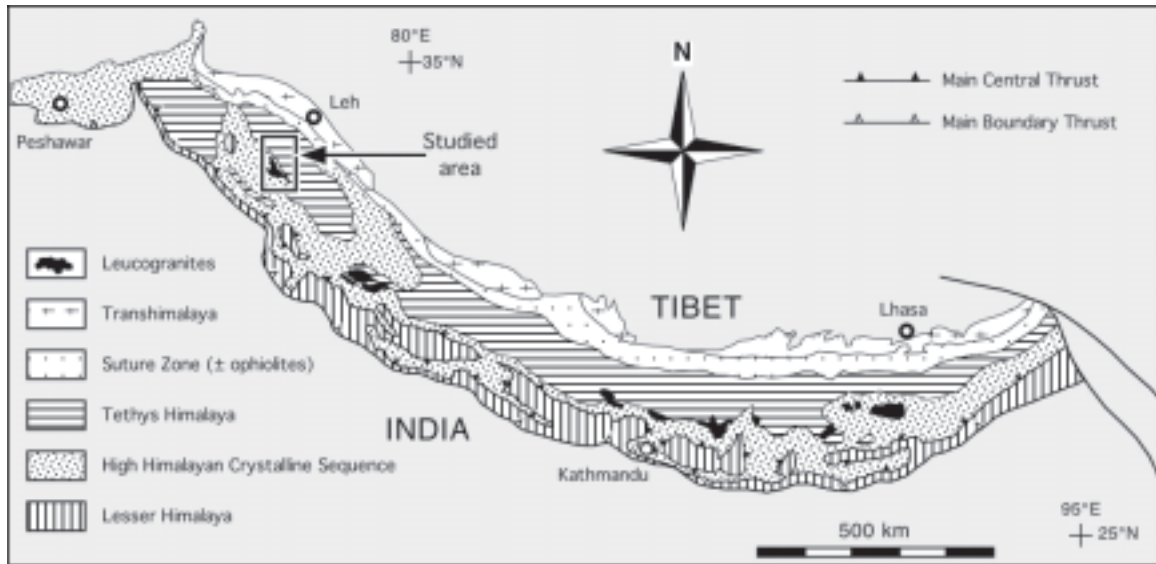


Fig. 2.2: Geologic - Tectonic map of the Himalaya, modified after Le Fort 1988

3) The **Central Himalayan Domain, CHD** (or High Himalaya) forms the backbone of the Himalayan orogen and encompasses the areas with the highest topographical relief. It is commonly separated into four zones.

- The **High Himalayan Crystalline Sequence, HHCS** (approximately 30 different names exist in the literature to describe this unit. The most frequently found equivalents are Greater Himalayan Sequence, Tibetan Slab and High Himalayan Crystalline) is a 30 km thick, medium- to high-grade metamorphic sequence of metasedimentary rocks which are frequently intruded by granites of Ordovician (~ 500 Ma) and Lower Miocene (~ 22 Ma) age. Although most of the metasediments forming the HHCS are of Upper Proterozoic to Lower Cambrian age, much younger metasediments can also be found in several areas (Mesozoic in the Tandi syncline and Warwan region, Permian in the Tschuldo slice, Ordovician to Carboniferous in the Sarchu Area). It is now generally admitted that the metasediments of the HHCS represent the metamorphic equivalent of the sedimentary series forming the base of the overlying Tethys Himalaya. The HHCS forms a major nappe which is thrust over the Lesser Himalaya along the *Main Central Thrust* (MCT).
- The **Tethys Himalaya, TH** is an approximately 100 km large synclinorium formed by strongly folded and imbricated, weakly metamorphosed sedimentary series. Several nappes, termed North Himalayan Nappes (Steck et al. 1993) have also been evidenced within this unit. An almost complete stratigraphic record ranging from the Upper Proterozoic to the Eocene is preserved within the sediments of the TH. The stratigraphic analyses of these sediments yields important indications on the geological history of the northern margin of the Indian continent from its Gondwanian evolution to its continental collision with Eurasia. The transition between the generally low-grade sediments of the Tethys Himalaya and the underlying low- to high-grade rocks of the High Himalayan Crystalline Sequence is usually progressive. Yet, in many places along the Himalayan belt, this transition zone is marked by a major extensional structure, the *Central Himalayan Detachment System* (also known as South Tibetan Detachment System or North Himalayan Normal Fault).
- The **Nyimaling–Tso Morari Metamorphic Dome, NTMD**: In the Ladakh region, the Tethys Himalaya synclinorium passes gradually to the north in a large dome of greenschist to eclogitic

metamorphic rocks. As with the HHCS, these metamorphic rocks represent the metamorphic equivalent of the sediments forming the base of the Tethys Himalaya. The Precambrian Phe Formation is also here intruded by several Ordovician (~480 Ma; Girard and Bussy, 1998) granites.

- The **Lamayuru and Markha Units, LMU** are formed by flyschs and olistholiths deposited in a turbiditic environment, on the northern part of the Indian continental slope and in the adjoining Neotethys basin. The age of these sediments ranges from Upper Permian to Eocene.

4) the **Indus Suture Zone, ISZ** (or Indus-Yarlung-Tsangpo Suture Zone) defines the zone of collision between the Indian Plate and the Ladakh Batholith (also Transhimalaya or Karakoram-Lhasa Block) to the north. This suture zone is formed by:

- the **Ophiolite Melanges**: which are composed of an intercalation of flyschs and ophiolites from the Neotethys oceanic crust;
- the **Dras Volcanics**: which are relicts of an Upper Cretaceous to Upper Jurassic volcanic island arc and consist of basalts, dacites, volcanoclastites, pillow lavas and minor radiolarian cherts;
- the **Indus Molasse**: which is a continental clastic sequence (with rare interbeds of marine saltwater sediments) comprising alluvial fan, braided stream and fluvio-lacustrine sediments derived mainly from the Ladakh batholith but also from the suture zone itself and the Tethyan Himalaya. These molasses are post-collisional and thus Eocene to post-Eocene.

The Indus Suture Zone represents the northern limit of the Himalaya. Further to the North is the so-called Transhimalaya, or more locally Ladakh Batholith, which corresponds essentially to an active margin of Andean type. Widespread volcanism in this arc was caused by the melting of the mantle at the base of the Tibetan bloc, triggered by the dehydration of the subducting Indian oceanic crust.

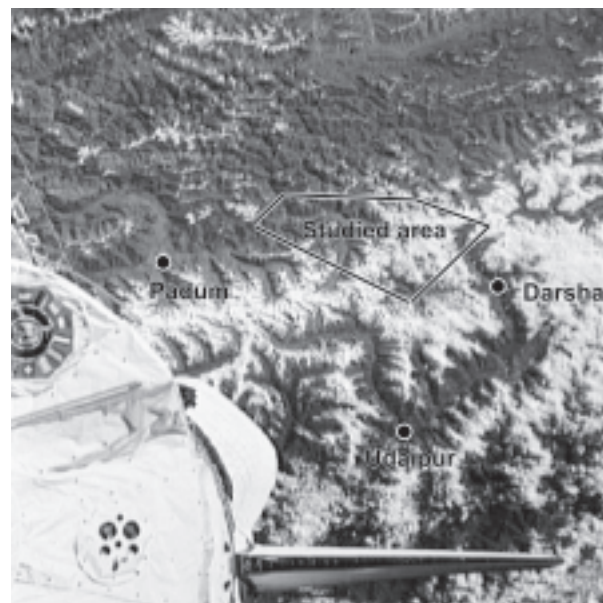


Fig. 2.3: The studied area as seen from space. This picture shows the contrast between the HHCS, covered with snow, and the TH. The snow limit follows the Zaskar Shear Zone, along the Doda, Lingti and Kurgiakh valleys.

2.4 Geological frame of this study

These crystalline rocks form as it were a wide arch or roof, with its apex greatly eroded and worn away, now mostly buried under masses of snow and ice. [...] Whilst the Southern range of the Central Himalayas is formed chiefly of crystalline rocks, mostly gneissic with metamorphic schists, it is shown that the Northern range is almost entirely composed of a vast sequence of sedimentary strata, ranging from the lower Palaeozoic to Tertiary and recent age [...] Between the Crystalline rocks and the next following, clearly sedimentary rocks, a clearly defined boundary scarcely exists. In nearly all sections I have hitherto examined, the schists seem to pass gradually into the overlying slates, phyllites and quartzites of the overlying Haimantas (Phe Fm.).

Griesbach, 1891

This study is focused on the Central Himalayan Domain in the southwestern part of Zaskar and encompasses the upper part of the High Himalayan Crystalline Sequence as well as the Proterozoic to Triassic sedimentary formations of the Tethys Himalaya.

Already on the basis of satellite imagery (Fig. 2.3), a clear topographic distinction can be made between these two contrasting domains. The HHCS forms the snow-capped towering peaks of the Great Himalayan Range, stretching along the southwestern side of the main Doda-Lingti-Kurgiakh valley. On the northeastern side of this valley, the varicoloured sedimentary formations of the Tethys Himalaya build up the smoothly shaped relief of the Zaskar Range.

The High Himalayan Crystalline Sequence of Zaskar is composed of metapelites and metapsammites, ortho- and paragneisses as well as minor calcsilicates and metabasites, cross-cut by Tertiary leucogranitic intrusions.

The structurally deepest zone of the HHCS in the studied area is formed of migmatitic orthogneisses and paragneisses, metamorphosed at upper amphibolite to granulite facies conditions. The overlying rather hornfelsic gneisses are injected by a dense network of leucogranitic dikes which ascend vertically over a distance of several hundred metres. These leucogranitic dikes are rooted into the migmatitic zone and thus seem to originate from the partial melting of these rocks. Towards the top of the HHCS, these dikes sometimes coalesce to form a ~1 kilometre thick sheet of massive leucogranitic plutons containing only scarce bits of country rocks. Although leucogranitic dikes are present all over the HHCS of Zaskar, the studied area distinguishes itself by their abundance. A striking example of these intrusions is illustrated by the snow-white cliffs of the Gumburanjun mountain (Fig. 2.4), situated in the middle of the studied area. This awe-inspiring mountain, shaped like the oversized prow of a gigantic ship, is indeed essentially carved out of leucogranitic rocks. The high-grade metamorphic rocks that make up the core of the HHCS form an elongated domal structure in Zaskar. The studied area is situated at the southeastern end of this domal structure which then disappears in the Sarchu region under the Tethys Himalaya. Therefore, the last leucogranitic intrusions crop out in this area and do not show up in the adjacent Lahul area.

The leucogranitic belt is surmounted by a major tectonic structure, the Zaskar Shear Zone. This structure corresponds to an approximately one kilometre thick mylonitic zone dipping 20° to the northeast. The Zaskar Shear Zone represents a 150-kilometres-long segment of the Central Himalayan Detachment System that runs intermittently between the HHCS and the TH along the entire length of the Himalaya. In Zaskar, this shear zone follows quite systematically the main



Fig. 2.4.: The Gumburanjun mountain at the headwater of the Kurgiakh river. Its more than 1000 m high cliffs are almost entirely carved out of leucogranites. View from the north towards the south.

Doda-Lingti-Kurgiakh valley for most of its length and marks the gradual passage between the high-grade metamorphic rocks of the HHCS and the weakly metamorphosed sediments of the Tethys Himalaya. Within this narrow zone of ductile deformation, a gradual transition between these two tectonometamorphic units is marked by a very rapid decrease of the metamorphic gradient from amphibolite facies at the base of the ZSZ to lower greenschist at its top. This is attested by the presence of a complete, although very condensed, Barrovian succession of kyanite, staurolite, garnet, biotite and chlorite mineral zones within the metapelitic schists of the Zaskar Shear Zone. The sedimentary formations of the Tethys Himalaya then form the hanging wall of the Zaskar Shear Zone. This gradual, though rapid, metamorphic transition indicates, as already observed by Griesbach (1891) for the Spiti and Sutlej regions, that the sediments from the lowermost Tethys Himalaya represent the protolith of the High Himalayan Crystalline Sequence metasediments and that a clearly defined boundary scarcely exists between these two zones. In Zaskar however, the aspect of this gradual transition between the HHCS and the TH depends on the nature of the rocks occurring within the Zaskar Shear Zone. In those regions where

these rocks are schistose, the transition is nearly perfect. Yet, in other regions as near Mune, where the rocks at the top of the HHCS are gneissic, a slickenside separates the HHCS from the TH. Structural analyses reveal that the Zaskar Shear Zone corresponds to a top to the northeast extensional shear zone which reactivates, in an opposite direction, older structures associated to the southwestward thrusting of the Nyimaling-Tsarap nappe.

Nearly all the sedimentary formations of the Tethys Himalaya are present in the southeastern part of the studied area. These formations, ranging from upper Proterozoic to Triassic are however often much less developed than in the adjacent Spiti or Lahul basins. Moreover, most of the Paleozoic formations continue to thin up towards the northeast of the studied area, until most of them totally disappear in the region of Tanze and are never to be seen again along the Zaskar range. The Tethys Himalaya in Zaskar represents the frontal part of a large-scale southwest-verging imbricate structure nappe. Several younger high-angle extensional normal faults cut through the sedimentary formations. These faults sometimes account for large relative vertical displacements as in the Sarchu region (Spring, 1993).

2.5 Purposes of the present work

This work fits in with the geological studies that were undertaken since 1979 by the University of Lausanne in the northwestern Himalaya. A complete section (Steck et al., 1993a and b) from the Indus-Yarlung Suture Zone in Ladakh to the Main Central Thrust in Himachal Pradesh was the result of several geological traverses and PhD works by this team (Stutz, 1988; Spring 1993 and Vannay, 1993). More to the west, the Ladakh, Suru, Zaskar and Kishtwar regions were the subject of several PhD works undertaken since 1978 by researchers from the University of Zurich (Honegger, 1982; Herren, 1987; Kündig, 1988, Stäubli, 1988, Guntli, 1993). There is, however, a lateral gap between the areas covered by these two research groups. This study fills this gap for the Zaskar region and in particular between the area covered by the PhD Work of Spring (1993) in the Sarchu region and the region studied by Herren (1987) along the Doda River in Zaskar.

Given the outstanding quality of the outcrops in Zaskar, this area represents one of the key localities to study the influence of extension tectonics along the Zaskar Shear Zone on the tectonic, magmatic and metamorphic evolution of the Greater Himalayan Domain.

A large part of this study was devoted to fieldwork. During the six months that lasted our three geological expeditions, we could establish a geological map of the studied region, using essentially Spot satellite images as topographic background. The mapped zone covers an area of about one thousand square kilometres at an altitude between 3500 and 6000 meters.

Structural observations were essentially focused on the transition zone between the HHCS and the TH in order to study the tectonic evolution of the Zaskar Shear Zone during the Himalayan orogen.

Petrographic observations were also an important aspect of fieldwork. A large amount of information on the metamorphic and magmatic events associated with the tectonic evolution of this area could be gathered from macroscopic observations.

The stratigraphic analyses of the sedimentary formations of the Tethys Himalaya is also part of the present work, although we did not spend much time on this aspect of the Himalayan geology since quite a lot of excellent work has already been done on this subject by previous researchers.

The second part of this study was dedicated to microscopic observations and laboratory work. A total of 252 thin sections were examined. The study of metamorphic mineral assemblages and microtextural porphyroblast-matrix relations under the microscope contributed greatly to the interpretation of the tectonic and metamorphic history of Zaskar. This optical study was completed by several analytical methods to obtain quantitative data. These methods include U/Pb and Ar/Ar geochronology, microprobe analyses, cationic and net transfer thermobarometry, isotopic thermometry and illite crystallinity.

The main purpose of the present work is to provide quantitative constraints on the age, displacement and slip rates along the Zaskar Shear Zone, on the bases of geochronological and geothermobarometrical data. Although we believe to have answered these questions in a rather satisfying manner, several other questions emerged in the course of this study:

- What role did the Zaskar Shear Zone play in the metamorphic and structural evolution of this part of the Greater Himalayan Domain?
- Why are the sedimentary rocks of the HHCS metamorphosed while their equivalents in the Tethys Himalaya are only weakly altered?

- Why is the Barrovian metamorphic zonation in the transition zone so condensed, and was this metamorphic event overprinted by a later metamorphism?
- How are the brittle normal faults in the Tethys Himalaya (e.g. the Sarchu fault) related to the Zaskar Shear Zone?
- Is the Zaskar Shear Zone correlated in time with other tectonic structures in the Himalaya?
- How are the leucogranites related to the Zaskar Shear Zone, and was the metamorphic gradient within the migmatitic zone sufficient to produce these granitic melts?
- How does a synorogenic extensional structure as the Zaskar Shear Zone form within a globally compressive system, such as the Himalaya?
- Are there Pre-Himalayan structures preserved in the Central Himalayan Domain, what are they and to what event can they be attributed?
- Why do most of the Paleozoic formations thin out and disappear towards the northwestern part of Zaskar?
- How does the geology of southeastern Zaskar correlate with adjacent regions?

We will deal with these questions throughout this work, but this monograph is not written such as to treat each of them individually. We rather tried to structure this monograph such as to tell a coherent, and if possible, linear “story”. In this introductory chapter we have given a general overview of the geodynamic settings leading to the formation of the Himalaya, as well as a description of the geologic framework of the NW Himalaya. In the following chapter, we describe the sedimentary formations that were deposited on the northern margin of the Indian continent, for they make up most of the studied area. In chapter 4, we will outline the structural geology of the north-western Himalaya and more specifically, we will see what deformation phases are observed in southeast Zaskar. Chapter 5 describes the metamorphic history of the studied area, which is a direct consequence of its structural evolution. In chapter 6 we will see how magmatic rocks formed from the sedimentary protolith, as a result of combined high-grade metamorphism and rapid tectonic uplift. In Chapter 7, we will use the data obtained from the metamorphic and magmatic rocks to constrain the age and amount of shear along the Zaskar Shear Zone. In Chapter 8, our data and observations are confronted to several models proposed to explain synorogenic extension. Finally, in chapter 9, we will make a short recapitulation of the main points covered by this work.

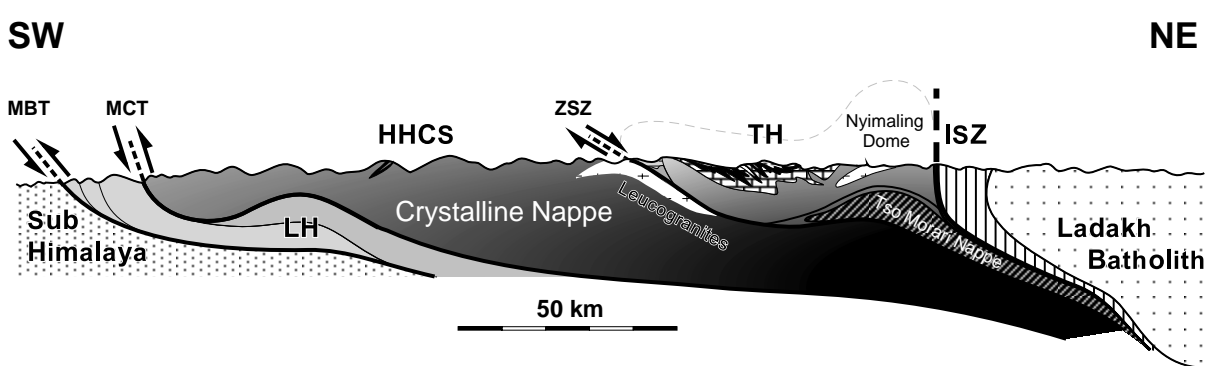
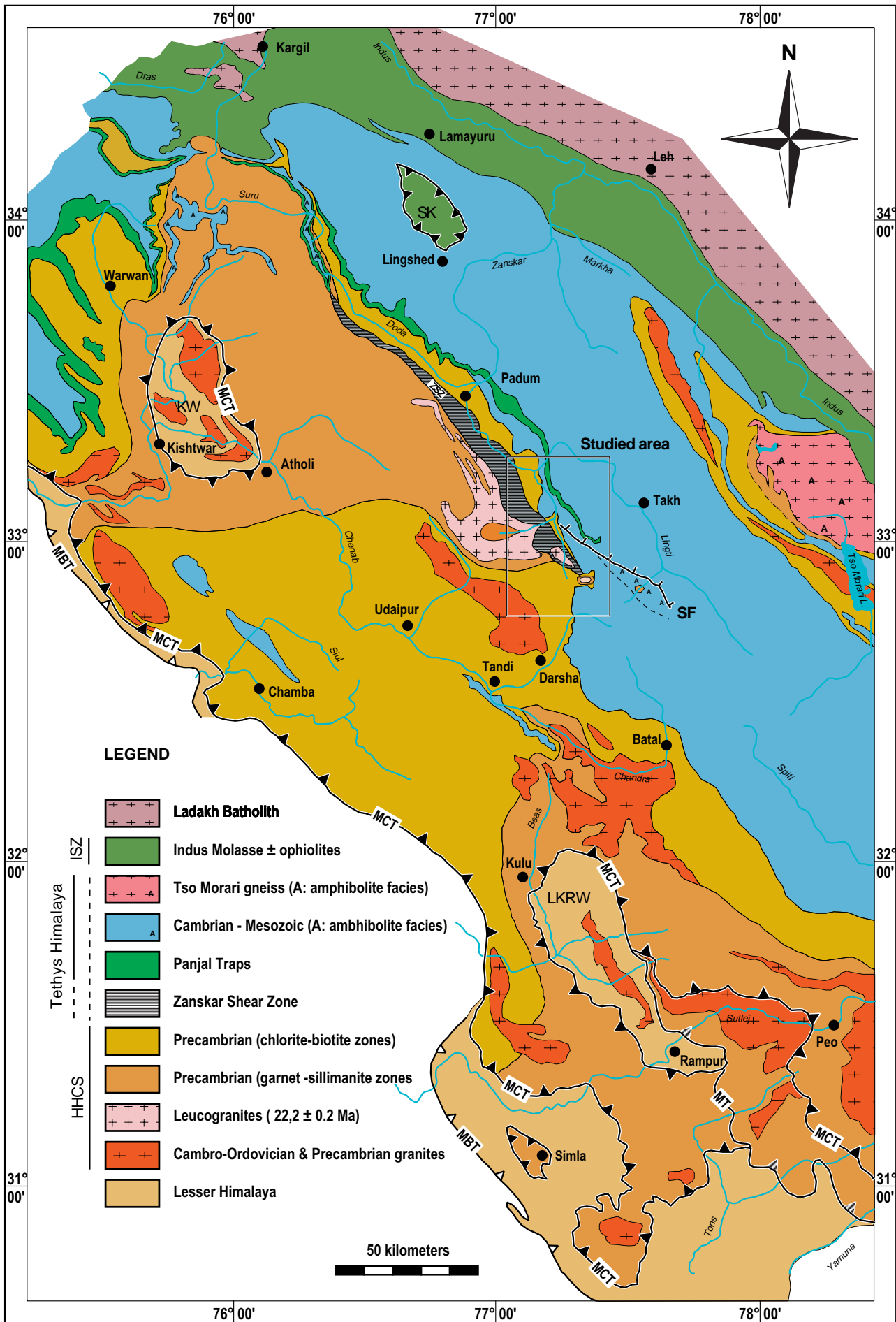


Fig. 2.5: Simplified cross-section of the north-western Himalaya showing the main tectonic units and structural elements. Shades of grey schematically represent the metamorphic gradient. LH, Lesser Himalaya; HHCS, High Himalayan Crystalline Sequence; TH, Tethys Himalaya; ISZ, Indus Suture Zone; MBT, Main Boundary Thrust; MCT, Main Central Thrust; ZSZ, Zaskar Shear Zone; SF, Sarchu Fault.



3. STRATIGRAPHY

La terre est comme une personne qui ne montre que ce qu'elle veut bien montrer. Les richesses sont au sous-sol. On ne les connaît que par les affleurements. Affleurer à la surface de la terre est une politesse que des millions d'années en roches volcaniques ou sédimentaires veulent bien nous faire. Je n'ai jamais regretté mes années de prospection à l'aveugle lisant en braille le banc de calcaire pétris de coquillages.

"Entre deux mondes", Fernand Auberjonois

3.1 Introduction

Along with the neighbouring areas of Upper Lahul and Spiti, Zaskar represents an exceptional region for the study of the sedimentary series deposited on the northern margin of the Indian plate. Many geologists were therefore attracted by this region and several Zaskari localities have given their name to stratigraphic units. We present here a compilation of these researches, mainly as a support for our geological map.

3.2 The Phe Formation (Nanda & Singh, 1977)

The name of Phe Fm. was first introduced by Nanda and Singh (1977) as an equivalent of the **Haimantas** (Griesbach 1891, Hayden 1904, Fuchs and Linner, 1995; Fuchs et al. 1995) to describe the basal formation of the sedimentary series of Zaskar directly overlying the metamorphic rocks of the High Himalayan Crystalline (their Suru Formation). As outlined in chapter 2, these authors failed to recognize that the sedimentary rocks of the Phe Fm are the same as the metasedimentary rocks that constitute their Suru Formation (HHCS). It seems important to recall the current opinion, that the sedimentary rocks of the Phe Formation belong structurally as well to the HHCS as to the TH.

The Phe Fm. is essentially formed by a monotonous alternation of grey-green siltstones, fine grained sandstones and occasional slates. These rocks show wave and current ripples, mudcracks, load casts, slump features (sometimes interpreted as flyshs), cross-bedded sand bars and minor bioturbation. Given the scarcity of fossils (cryptarchs, algae, trilobites and brachiopods) within this formation, its age is only approximately constrained between Upper Precambrian and Lower Cambrian.

The Phe Formation is commonly divided into two members. At its base, the Tsarap Member (Vannay, 1993) is richer in pelitic horizons than the overlying Doda Member (Nanda and Singh, 1977; Gaetani et al. 1986). These two members are separated by a metric to decametric layer of black graphitic sandstones and occasional conglomeratic horizons. On the left side of the Jankar river, this graphitic horizon is lying directly on the Kade orthogneiss. The transition between the Phe Formation and the overlying Karsha Formation is gradational and defined by the apparition of the first dolomitic horizons.

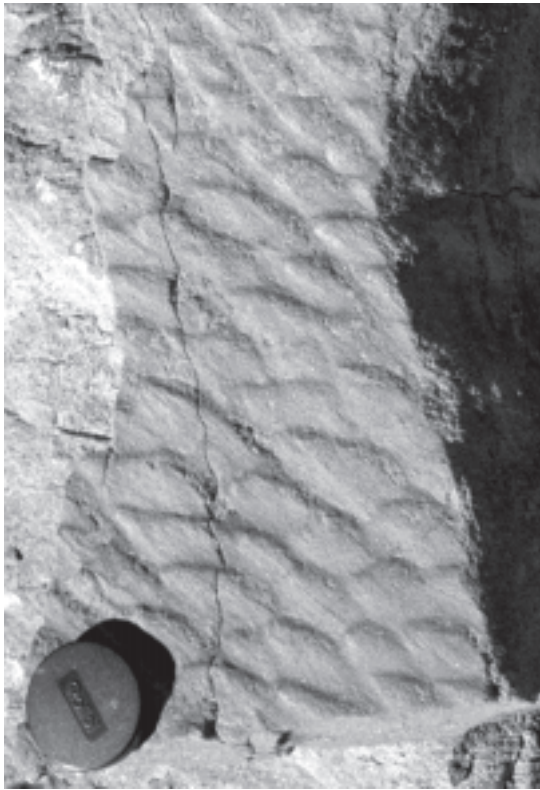


Fig 3.1: Grouped assemblage of narrow parabolic flute marks in the Phe Formation. (turn the page at right angle for a better view)

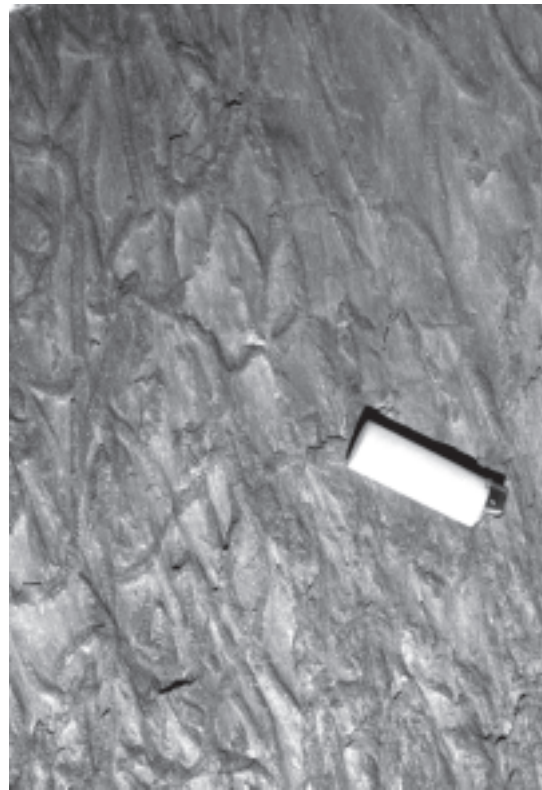


Fig 3.2: Ichnofossils, *Cruziana* isp.: these tracks are due to organisms (trilobites) moving on the sea floor while digging the soft sediments for food. (Phe Fm.)



Fig 3.3: Assymmetric sinuous ripple marks. These ripples are due to the action of underwater currents on the sea floor (Phe Formation)

The total thickness of this formation is difficult to estimate. In Zanskar the weakly metamorphosed sediments of the Phe Fm. reach a thickness of more than 800 metres, while, in Lahul, these same sediments exceed 2000 metres in thickness. The thickness of the HHCS (also partly composed of metamorphosed sediments belonging to the Phe Fm.) is even more difficult to estimate as this domain has been tectonically thickened. Estimates for the total thickness of the Phe Fm. range between 5000 metres and 10'000 metres (Fuchs and Linner, 1995; Wyss, 1998).

The Phe Formation shows many similarities with the Proterozoic series of the Lesser Himalaya (Simla Slates) and is believed to represent a sequence formed in a shallow intracontinental sea with a significant siliciclastic input (Baud et al. 1984; Gaetani et al. 1986; Garzanti et al. 1986; Vannay, 1993; Frank et al., 1995).

3.3 The Karsha Formation (Nanda & Singh, 1977)

The Karsha Fm. follows quite systematically the right bank of the Kurgiakh-Lungnak Chu until Padum where it pinches out and disappears. The maximal thickness of this formation in Zanskar is comprised between 1000 and 1200 metres, which is approximately twice as much as in Upper-Lahul. A Lower to Middle Cambrian age is attributed to the Karsha Fm. Three members can be distinguished within the Karsha Fm:

- 1) The Mauling Member (Nanda & Singh, 1977) is about 600 to 800 metres thick, and is composed of detritic sediments similar to those of the Phe Fm. They are intercalated with decimetrical to plurimetrical dolomitic beds. The transition between the Phe Fm and the Karsha formation is gradational and the lower boundary of the Mauling Member is defined by the first appearance of dolomitic beds. These dolomites are light to medium grey with a distinctive orange-brown weathering colour. The depositional environment of the Mauling Mb. must have varied between supratidal and subtidal settings (Vannay, 1993).
- 2) The Thidsi Member (Nanda & Singh, 1977) is formed by massive dolomites, reaching up to 200m in thickness. Stromatolites are frequent within this member and indicate a subtidal environment with a low terrigenous influx.
- 3) The Teta Member (Gaetani et al. 1985) is made up of alternating, well bedded, grey marly limestones and black shales. Its thickness varies between 70 and 160m. This member records an increase in water depth, from peritidal to outer shelf environment, and therefore represents a deepening upwards sequence.

3.4 The Kurgiakh Formation (Garzanti et al. 1986)

This formation is divided in two members, both approximately 150m thick. The Surichun Member is made up essentially of black shales with rare dolomitic interbeds. Trilobites of Middle Cambrian age were found within this member in Zanskar (Gaetani et al. 1986). The overlying Kuru Member has many common features with the Mauling Mb of the Karsha Fm. As no fossils were found within this member, its Middle to Upper Cambrian age is attributed on the basis of its stratigraphical position.

The Kurgiakh Fm. records a progressive change in depositional environment, from shelf to slope. This sedimentary evolution is attributed to an active tectonic subsidence following the shallow-water carbonate deposition of the Karsha Fm (Gaetani et al. 1986; Fuchs, 1987).

3.5 The Thaple Formation (Nanda & Singh, 1977)

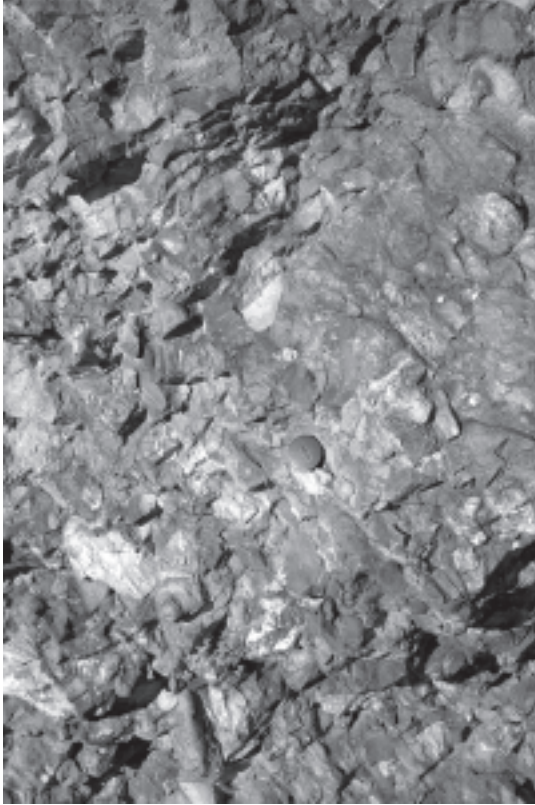


Fig 3.4: Polygenetic conglomerate of the Thaple Formation. The clasts are reworked from the Phe, Karsha and Kurgiakh Formations. Diameter of the lens cap is 4 cm.

The Thaple Fm overlies unconformably the Kurgiakh and Karsha formations (Hayden, 1904). Its thickness is highly variable, from 1200m, in the region of Kenlung Serai (Spring, 1993), to less than 100m, in the Tanze area. These lateral variations might be the result of syndepositional extension tectonics as suggested by synsedimentary faults (Spring 1993). In the studied area this formation probably ranges from Lower to Upper Ordovician as the uppermost Silurian Takche member is missing (Baud, 1984). This formation is usually subdivided into three members although up to six members have been differentiated by Spring (1993).

1) The first member is formed by red-brown sandstones alternating with polygenetic conglomerates and minor purple siltites. The clasts of the conglomerate are reworked sediments from the underlying formations, a feature indicative for a continental depositional environment (braided river, alluvial fan, channel flow).

2) The second member is composed of purple to green sandstone with siltstone and shale interbeds.

3) The third member contains gritty dolomite beds in addition to siltites and shales.

The two first members were deposited in an increasingly distal environment. The presence of dolomites, brachiopods, crinoids and bryozoans in the third member indicates a shallow water environment. (Vannay, 1993).

3.6 The Muth Formation (Stoliczka, 1866)

This massive unit is formed by mature white quartzarenites and its thickness varies between 0 and 50 metres. Very few fossils were found in this formation, and its supposed Devonian age is inferred from its stratigraphical position. Its depositional environment is litoral to supralitoral (backshore to foreshore).

3.7 The Lipak Formation (Hayden 1908)

The stratigraphy of the Lipak Formation was studied in detail by Vannay (1993) in Lahul where four members (L1-L4) were distinguished. These members can also be identified in Zaskar, although the two upper members are often missing.

- 1) Member L1 starts with several metres of orange sandstones and gritty limestones that mark a gradual transition with the underlying siliciclastic Muth Formation. These rocks are overlain by a thick (up to 120m) alternation of limestones in decimetric to metric beds and marly limestones or marls in centimetric to decimetric beds.
- 2) Member L2 does not exceed 20m in thickness and shows a change towards a partly detritical sedimentation. It is formed by gritty dolomites, limestones, black shales, gritty shales, sandstones and carbonate breccia.
- 3) Member L3 is essentially constituted of white gypsum, with rare interbeds of decimetrical dolomite beds. Some concordant dikes occur within this member. This member rarely exceeds 50 m.
- 4) Member L4 is similar to L1 but for the presence of dolomites, dolomitic limestones and sandstones.

Given the similitude between L1 and L4, Fuchs (1987) proposed that there might be a repetition of the same member by folding. This however seems very unlikely as the same succession within Lipak can be observed over too large an area to be the result of folding within this single formation.

L1, L2 and L4 represent a relatively low-energy carbonate platform in a more or less open laguna with sporadic detrital influx. L3 represents a regressive episode towards a sabkha environment.

A Lower Carboniferous age was established for the Lipak Formation since the beginning of the century (Hayden 1904).

On the basis of conodonts, Vannay (1993) proposed a Lower Tournaisian (Hastarien-Ivorien) age for this formation.

3.8 The Po Formation (Hayden, 1904)

In Spiti, where the Po Fm. is particularly well developed and reaches a thickness of 800m, Garzanti et al. (1996) have decided that it represents a group rather than a formation. Consequently, they have subdivided their Po group into four formations: the Thabo Fm., the Fenestella Shales, the Kabjima Fm. and the Chichong Fm. In Zaskar, however, this unit is much less developed (max. 200m) and shows very little variation, being formed essentially by almost pure quartzarenites. We thus have decided to keep this unit as a single formation and to stick to the name of Po Formation although Garzanti et al. (1996) suggest a correlation with their Kabjima Fm. The silty marls of the Fenestella Shales might also sporadically appear in Zaskar. When present, they form the base of the Po Fm. (Gaetani et al. 1996).

A nearshore, deltaic, high-energy depositional environment characterizes this formation. Clasts of volcanic rocks were reported to occur in this unit (Gaetani et al. 1986, 1990; Vannay, 1993; Garzanti et al. 1996).

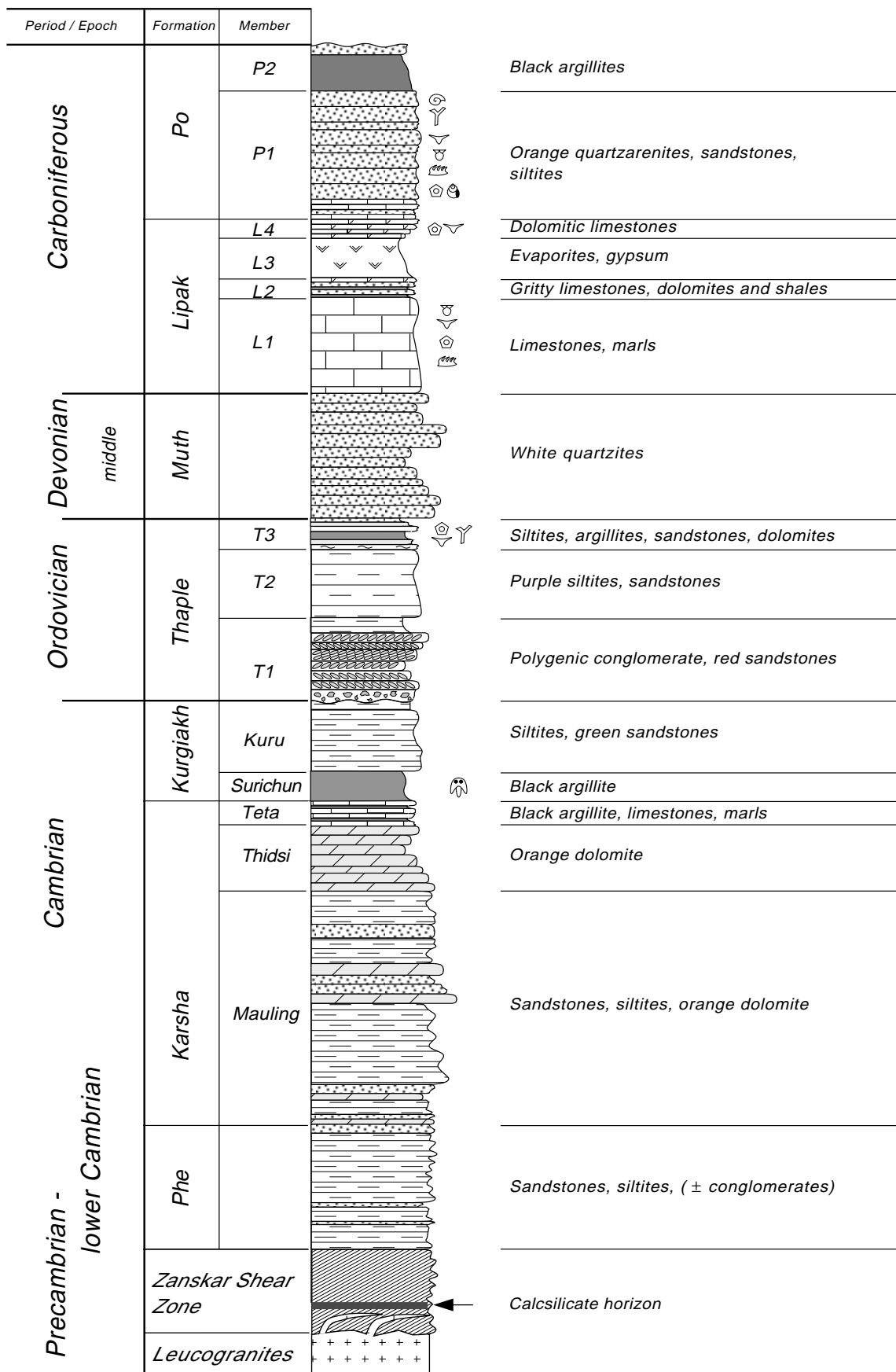


Fig 3.5: Stratigraphic column for the Precambrian to Carboniferous sedimentary formations in SE Zanskar. Because of the large variations in thickness, no scale is indicated. The thickness of individual formations and members is mentioned in text.

Lilang Group

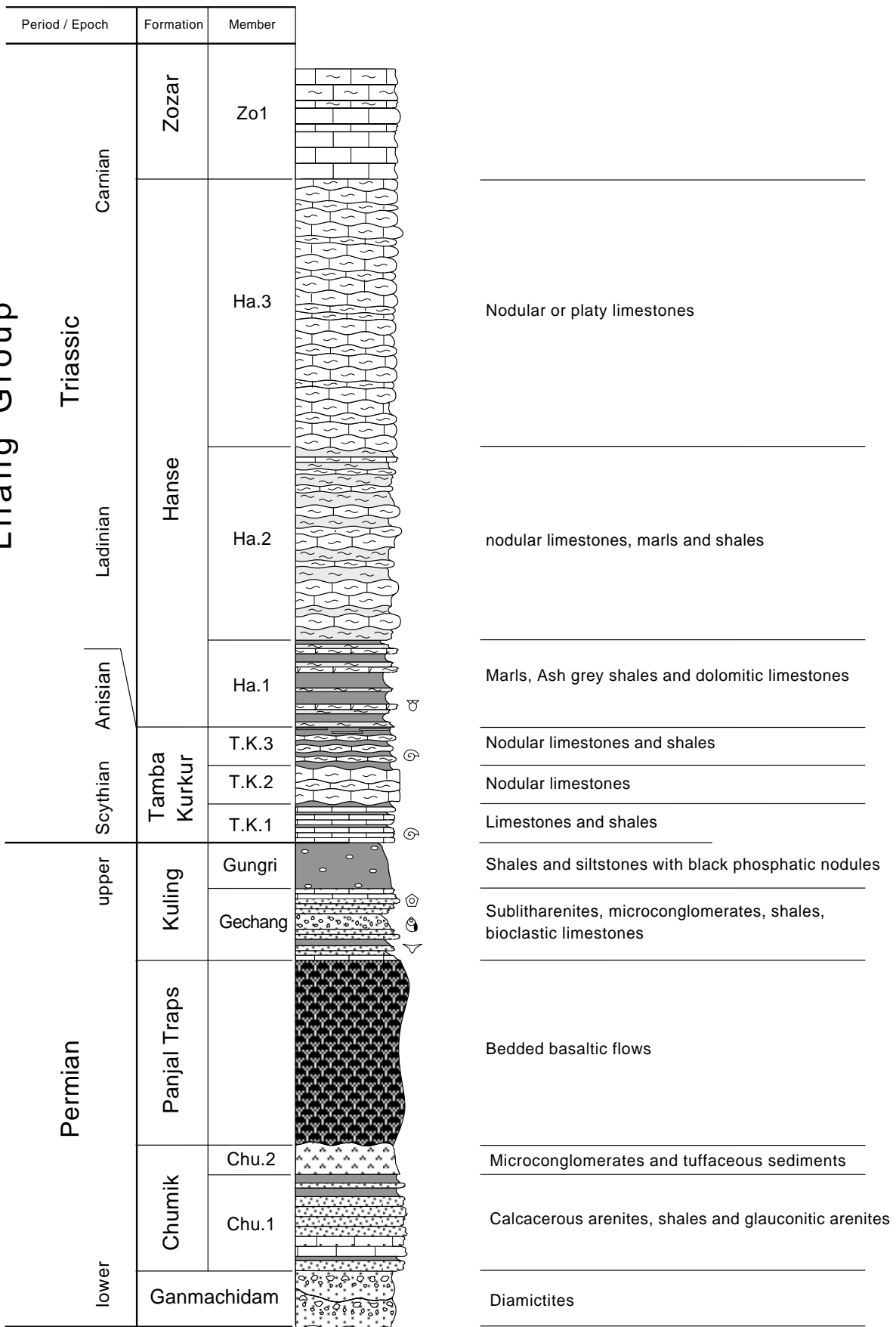


Fig 3.6: Stratigraphic column for the Permian to Triassic sedimentary formations in SE Zanskar. Because of the large variations in thickness, no scale is indicated. The thickness of individual formations and members is mentioned in text.

In Zanskar, as well as in Lahul and Spiti, the top of the Po Fm. is marked by an angular unconformity.

The age of the Po Fm. is generally accepted as Carboniferous. If the correlation between the Po Fm. in Zanskar and the Kabjima Fm. in Spiti is correct, a more specific Middle Carboniferous age could be assigned to this unit.

3.9 The Ganmachidam Formation (Srikantia et al. 1980)

The Ganmachidam Fm. was previously considered as an equivalent of the Chumik Fm. to describe supposedly similar sediments comprised between the Po Fm. and the Panjal Traps. This lack of distinction has however proven to be inaccurate (Garzanti et al. 1996a,b) and led to misinterpretation in both the age and depositional environment. The name Ganmachidam should thus only be used for the diamictite formation overlying the Po Fm.

The Ganmachidam diamictites are only sporadically present in Zanskar as they are more or less restricted to a 40 metres thick section preserved in the Tanze area. In Spiti, this formation is composed of sandstones, siltstones, dropstones and conglomerates. Clasts of plutonic granitoid rocks are quite common. The sedimentological features indicate deposition largely under glacial influence, in marine environment at high southern latitude. The age of the Ganmachidam Fm. is Lower Permian (Asselian-Early Sakmarian), but it might extend into the Upper Carboniferous (Garzanti et al. 1996a).

3.10 The Chumik Formation (Gaetani et al. 1990)

This 20 to 80 metres thick formation was originally described in the Chumik Marpo area as unconformably overlying the Po Fm. In the Tanze area, however, the Ganmachidam Fm. is sometimes sandwiched between these two formations. Two members were originally described within the Chumik Formation (Gaetani et al. 1990).

- 1) The first member consists of a calcareous, shaly and glauconitic arenite sequence. On the basis of its fauna, a Late Sakmarian age is attributed to this member. The presence of glauconitic arenites possibly indicate slow deposition during rapid eustatic rise in shoreface-to-shelfal environment and might coincide with the major worldwide transgression at the end of the Permo-Carboniferous glaciation.
- 2) The second member is made up of microconglomerates that pass upwards into greenish tuffaceous rocks. A fluvial environment is attributed to this member.

On the basis of the Late Sakmarian age of the first member, and facies similitudes in the second member, Garzanti et al. (1996) suggest that the Chumik Fm. could be correlated with the base of the Gechang Fm. in Spiti and Nepal.

3.11 The Panjal Traps (Lydekker, 1878)

The term Panjal Traps is used to designate a thick sequence of effusive basaltic rocks intercalated within the Tethyan sediments. These basaltic rocks are observed from NE Pakistan to Upper Lahul and are quite easily traceable on satellite imagery because of their dark colour.

Their maximal thickness (over 2000m) is reached in the Kashmir basin where they belong to the Panjal Volcanic Series together with the “Agglomeratic Slates”. Towards the southeast, their thickness progressively diminishes from 800m in the Doda valley to 300m in the Tanze area, 150m in Chumik Marpo until they pinch out and only sporadically appear in Upper Lahul.

Along the Doda Valley, the Panjal Traps rest directly on top of the Precarboniferous to Lower Carboniferous Phe Fm. Towards the southeast, the Panjal Traps then come to rest on progressively younger formations. From the Karsha-Padum region down to the Tanze area, they top the Lower to Middle Carboniferous Karsha Fm. In the Tanze area they transgress over the Lower Permian Chumik Fm. and then stay in this position until they disappear in Lahul.

From Zanskar to Lahul, the Panjal Traps are quite systematically overlain by the Upper Permian Kuling formation. As these effusive rocks are unfossiliferous, it is their stratigraphical position between the Chumik and Kuling formations that allows to attribute them an Upper Sakmarian to Djulfian age (Gaetani et al. 1990).

The Panjal traps are formed by a succession of bedded basaltic flows. Single beds often display a gradation from compact massive basalt at the base towards amygdale-rich basalts at the top. The upper part of these beds quite often displays ropy and braided surfaces (pahoehoe) or sometimes pillow lava. The basalts are aphyritic and display a relictual microlithic texture becoming vesicular or even spilitic at the top of the single beds.

The matrix consists of actinolite, chlorite (clinocllore), epidote, albite, hematite. The vesicles are filled with calcite, chlorite, and epidote. This mineralogy was confirmed by RX analyses (this study).

We interpret the vesicles as contemporaneous with the degassing of the lava flows in a shallow water environment. The mineral assemblage forming the mesostase might result from the transformation of basaltic glass in contact with marine aqueous solutions circulating through the lava during its outpouring.

A geochemical study of the Panjal Traps (Vannay, 1993) reveals that they correspond to tholeiitic continental flood basalts (CFB) originated from little evolved, slightly enriched P-MORB-type magmas. The geochemical signature of the Panjal Traps is quite similar to that of the tholeiitic Deccan Traps.

3.12 The Kuling Formation (Stoliczka, 1866)

This 10 to 60 metres thick formation marks the resumption of sedimentation after the episode of basaltic outflowing. Two members were distinguished within this formation:

- 1) The lower Gechang Mb. (Srikantia et al. 1980) is composed of sublitharenites, lenses of microconglomerates, black shales and arenaceous bioclastic limestones. The quite abundant fauna is indicative of a Lower Djulfian age (Garzanti et al. 1990). This member is interpreted to have

formed in shallow-water settings with minor reworked Panjal trap clasts at the very bottom and quartzose (granitoid rock derived?) detritus in the rest of the unit.

- 2) The upper Gungri Mb. (Srikantia et al. 1980) consists of black splintery shales and siltstones with randomly dispersed black phosphatic nodules suggesting a hemipelagic environment. Fossils are scarce but point to an upper Djulfian age (Garzanti et al. 1990).

3.13 The Lilang Group (Hayden, 1908)

After the mainly siliciclastic sedimentation that characterizes most of the Paleozoic, a change towards an essentially carbonate sedimentation occurs at the beginning of the Triassic.

The Lilang Group encompasses the rather uniform succession of limestones, dolomites and shales that characterizes the Triassic of the NW Himalaya. Four formations have been distinguished in Zanskar within this 1000 metre thick group: the Tamba Kurkur Fm., the Hanse Fm., the Zozar Fm. and the Quartzites Series.

3.14 The Tamba Kurkur Formation (Srikantia et al. 1980)

The mainly carbonaceous Tamba Kurkur Fm. reaches a thickness of 50-60 metres in the studied area. Three members can be distinguished within this very fossiliferous formation (Nicora et al. 1985).

- 1) The first member is composed of thin bedded, slightly nodular limestones with upwards increasing intercalation of shales. A Lower Triassic age is attributed to this member on the basis of conodonts.
- 2) The second member forms cliffs of massive thick bedded nodular limestones. The Scythian-Anisian boundary occurs within this member without any marked lithological change.
- 3) Well bedded nodular limestones with upwards increasing shaly intercalations characterize the third member. An abundant ammonoid fauna of Anisian age is present in this upper member.

According to Gaetani et al. (1986) and Vannay (1993), this formation represents a marine pelagic to hemipelagic sedimentation in upper bathial (outer shelf-talus) conditions with low sedimentation rates.

3.15 The Hanse Formation (Srikantia et al. 1980)

Three members have been defined in Zanskar within this 400 metre thick formation (Gaetani et al. 1986). A correlation of the two first members with the "Daonella Shales", the Daonella Limestones and the "Grey Beds" of Spiti was proposed by Fuchs (1987). He also suggested that the third member might correspond to the lower part of the Tropites Limestones of Spiti.

-
- 1) The first member shows a gradational contact with the underlying Tamba Kurkur Fm., marked by an increase in marls and ash-grey shales together with a thinning upwards trend. Thin-shelled bivalves of *Daonella*-type are abundant in this member.
 - 2) The second member shows thicker and more frequent limestone beds in its lower part that progressively get thinner upwards as they give way to marls and shales.
 - 3) The third member forms up to 280 metre high jagged cliffs of thick bedded nodular or platy limestones.

The age of the Hanse Fm. is mainly Ladinian. Gaetani et al. (1986) suggest that the third member, because of its great thickness, might extend into the Carnian. However, there is no paleontologic support for this hypothesis.

As for the Tamba Kurkur Fm., most of the Hanse Fm. represents a pelagic sedimentation in outer shelf conditions with, however, a significant supply of detritic clay.

3.16 The Zozar Formation (Baud et al. 1984)

This formation which reaches a thickness of about 400 metres in NW Zanskar (Ringdom) is much more reduced in the studied area where it does not exceed 160 metres. A detailed study of this unit was made by Jadoul et al. (1990), who divided it into two members. Fuchs (1987), by analogy with Spiti, includes the Zozar Fm. together with the third member of the Hanse Fm in the Tropites Limestones.

- 1) The lower member consists of bioclastic limestones (bryozoans, corals, crinoids, gasteropods, *Megalodon* sp.). These limestones sometimes become marly towards the top of the member.
- 2) The upper member is essentially dolomitic, sometimes with abundant stromatolites. Occasionally, bioclastic limestones recur at the top of this member.

The Zozar Fm. is Late Carnian in age and was deposited in a medium/high energy shallow water environment.

3.17 The Quartzites Series (Hayden 1904)

The name of Quartzites Series was first defined in Spiti by Hayden (1904) for a distinct horizon of white and brown quartzites intercalated with limestones and shales. Baud (1984) and Garzanti et al. (1986) have later used this name in Zanskar to designate the whole succession of sediments between the Zozar and Kioto Fm. Fuchs (1987) however argues that only the upper part of the unit comprised between the Zozar and Kioto Fm. strictly correspond to the Quartzites series of Spiti as defined by Hayden (1904) and that the rest of the unit should be correlated with the "Juvavites Beds", "Coral Limestones" and "Monotis shales" of Spiti. The lack of biostratigraphic evidence do not allow to ascertain whether this is correct and therefore, we prefer to stick to the name of "Quartzites Series".

The Quartzites Series in Zaskar are described in detail by Jadoul et al. (1990) who divided them into three members.

- 1) The first member starts with a biocalcarenitic interval, followed by bioturbated arkoses intercalated with limestones and micaceous pelites, and ends with coarse subarkoses and supermature quartzarenites.
- 2) The second member consists of associated micaceous siltstones, limestones and bioclastic or quartzose arenites.
- 3) The third member would be the true equivalent of the Quartzites Series of Spiti.

This formation is mainly Norian, except for the third member who might contain the Norian/Rhaetian boundary. A predominantly terrigenous input is recorded within the shallow marine, continental shelf deposits of the Quartzites Series.

3.18 Synthesis of the stratigraphic observations

The presence, since the Upper Precambrian, of an elongated and narrow intracontinental sea between the Indian continent and the Cimmerian Superterrane is documented by the sedimentary series of the Phe Formation. The sediments of this 5000 to 10'000 metres thick formation (Fuchs and Linner, 1995; Wyss, 1999; Frank et al., 1995; Steck et al., 1998) are mainly derived from the erosion of the relief fringing this trough to the north. To accommodate such a thick series of shallow water sediments either a continuous sea level rise, or more likely a major subsidence must have affected this basin.

From the Lower to Middle Cambrian, the rate of detrital input and subsidence diminished, giving way to the formation of the dolomitic horizons, stromatolitic colonies and platform carbonates of the Karsha Formation.

In the Upper Cambrian, the presence of turbidites within the Kuru Member of the Kurgiakh Formation indicates a return to a deeper sedimentation environment and of tectonic subsidence exceeding the sedimentation rate.

At the boundary between the Cambrian and the Ordovician, a major tectono-magmatic event affected a large part of Gondwana. This so-called late Pan-African event is marked by numerous ~500 Ma old granitic intrusions forming a wide belt stretching from the Alps (Bussy et al. 1996) over the Arabic peninsula, Afghanistan, Africa, India, Australia and down to Antarctica (Le Fort, 1986 and references therein). In parallel with these intrusions, some of the above mentioned areas show evidences of tectonic activity marked by an angular unconformity at the base of the Ordovician sediments.

Evidence for this late Pan-African event is also frequently observed within the Himalaya. Not only are ~500 Ma granites quite common within both the Lesser Himalaya and the High Himalayan Crystalline Sequence (see Le Fort, 1986 and Valdiya, 1995 for a review), but an angular unconformity at the base of the Ordovician Thaple Formation has long been known to exist in the Spiti region (Hayden, 1904). Moreover, the conglomeratic lithologies of the Thaple Formation testify for the uplift and erosion of parts of the underlying formations, as these conglomerates incorporate fragments of the Phe, Karsha and Kurgiakh Formations.

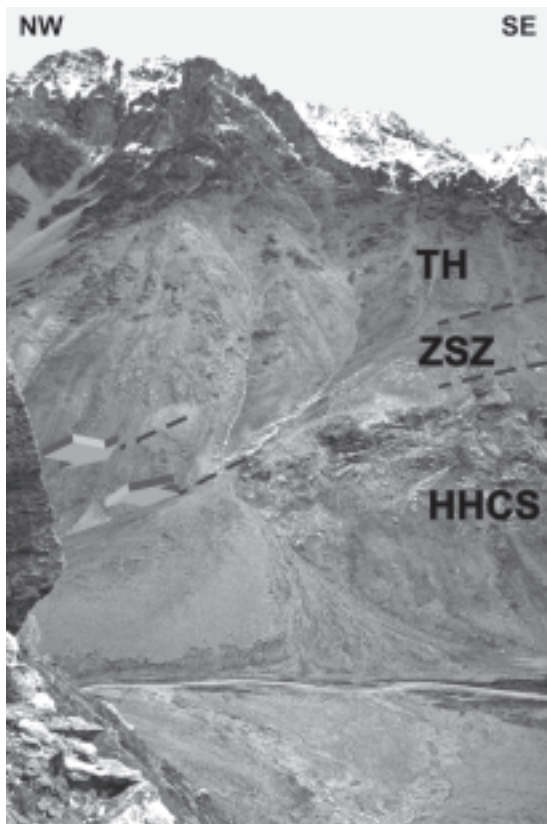


Fig 3.7: The transition between the High Himalayan Crystalline and the Tethys Himalaya in the Kurgiakh valley. Note the leucocratic dikes in the HHCS.



Fig 3.8: The angular unconformity between the Karsha Formation and the Panjal Traps NW of Tanze. Note that almost all the Paleozoic series are absent.

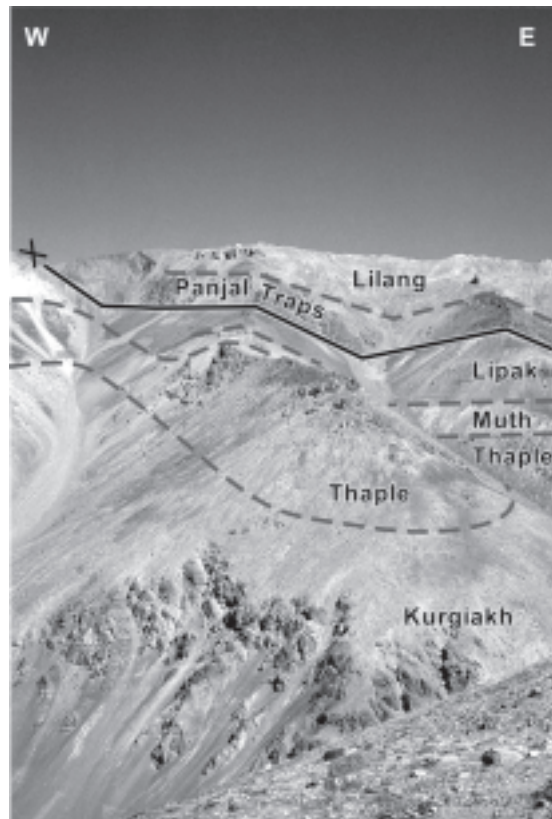


Fig 3.9: The sedimentary series on the northern side of the valley between Kurgiakh and the Surichun-La. The Panjal Traps are thrust over the Lipak Fm.



Fig 3.10: The Permian and Triassic formations above Tanze. The Permo-Triassic boundary is at the limit between the Kuling and Tamba Kurkur formations.

The nature of the late Pan-African event in the Himalaya is still poorly understood. Several authors (Srikantia et al., 1980; Baud et al., 1984; Garzanti et al., 1986; Fuchs, 1987; Valdiya, 1995) associate this event with an orogenic episode, as can be observed at the same period in Antarctica with the Ross orogeny, while others (Le Fort et al. 1986; Miller and Frank, 1992; Vannay, 1993) consider this event to be associated with an episode of vertical movements associated to extension and crustal thinning.

After the Early Ordovician continental conglomerates, the sedimentary environment in the Himalaya is essentially littoral (Middle to Upper Ordovician members of the Thaple Formation) or coastal (Devonian Muth Formation). Most of the Silurian is missing, possibly as a consequence of erosion.

Following this rather uneventful period, the rifting between the Indian continent and the Cimmerian micro-continents, followed by the opening of the Neotethys, will of course greatly affect the sedimentary record within the Tethys Himalaya. An early transtensive stage of rifting is observed since the Early Carboniferous in the Lipak Formation, where synsedimentary extension faults were described by Vannay (1993). In the Lower Permian, an episode of thermal uplift of rift shoulders is suggested in many areas by the absence, to various degrees, of the Paleozoic formations (Ordovician to Trias), whilst in adjacent graben areas the stratigraphic record is complete. A magmatic event also occurred at the boundary between the Carboniferous and the Permian, as documented by the granitic intrusion of the Yunam, in the Sarchu region. These granites yield a zircon U/Pb age of 284 ± 1 Ma (Spring et al. 1993).

The opening of the Neotethys starts in the Middle Permian with the formation of oceanic crust. This event is marked in many regions of the Himalaya by the outpouring of the Panjal Traps continental flows which, by sealing the underlying formations, sometimes reach considerable thicknesses (2000 metres as in the Kashmir basin).

Following the rifting of the Neotethys, the transgressive Upper Permian Kuling Formation testifies to the progressive subsiding of the passive Indian margin. The Triassic Lilang Group then corresponds to the formation of a carbonate platform on this flexural margin. The evolution of the northern Indian margin from the Triassic to the Eocene was described by Bassoullet et al. (1980, 1981; 1984), Baud et al. (1984), Gaetani et al. (1986, 1987), Gaetani and Garzanti (1991), Fuchs (1982a, b) and Spring (1993).

3.19 Pre-Himalayan tectonics in Zaskar

The HHCS of Zaskar is composed of metasedimentary rocks (metamorphic equivalent of the Phe Formation) intruded by orthogneisses. The protolith of these orthogneisses are essentially the Cambro-Ordovician granites associated with the late Pan-African event. This is testified by several radiometric ages. Frank et al (1975) obtained a whole-rock Rb/Sr age of 495 ± 16 Ma for the Kade orthogneiss located in the southwestern part of the studied area. Pognante et al. (1990) obtained a whole rock Rb/Sr isochron age of 549 ± 70 Ma and a zircon U/Pb age of $472 (+9, -6)$ Ma for the same intrusion. Tertiary leucogranites are also frequently present at the top of the HHCS of Zaskar. It has been shown on the bases of their isotopic composition that these leucogranites probably originated from the partial melting of both the para- and the orthogneisses of the underlying HHCS (Ferrara et al. 1991). Thus the U/Pb upper intercept age of 499 ± 235 Ma that we obtained for the monazites of the Tertiary Gumburanjun leucogranite as well as the better constrained zircon ages of 463 ± 13 Ma and 476 ± 12 Ma obtained by Noble and Searle (1995) from two leucogranitic

intrusions in NW Zaskar are interpreted as representing relictual ages of the Cambro-Ordovician granites. Recent zircon U/Pb ages obtained by Girard and Bussy (1998) for the Rupshu area also yielded ages of 479 ± 2 Ma for both the Polokonga La granite and the Tso Morari gneiss and of 482 ± 1 Ma for the Rupshu granite. All these data show that the Zaskar area was greatly affected by the intrusive episode of the late Pan-African event.

Further evidences of pre-Himalayan deformations can be observed in the Zaskar region within the Tethyan Himalaya stratigraphic record. Along most of the main NW-SE trending Doda valley, the Permian Panjal Traps rest directly upon the Precambrian to Cambrian Phe Formation and then, from Padum to Tanze, the Panjal traps top the Cambrian Karsha Formation. Both the Karsha and Phe formations form large-scale undulations of decametric to kilometric wavelength which are especially well evidenced, at a distance, by the bending of the dolomitic Thidsi Member. These undulations have axes with a general NE-SW to N-S orientation and an almost vertical axial plane. As the overlying Panjal Traps truncate these folds and as the sediments younger than the Permian are not affected by this deformation phase, these deformations must be related to a pre-Permian tectonic event.

The timing of this event can be better constrained in the Tanze area, where the Karsha Formation steeply plunges towards the southeast, whereas the Panjal Traps remain at a constant altitude. The depression that forms between these two previously superposed formations is progressively, but very quickly, filled with the complete succession of Paleozoic sediments missing to the northwest. Despite the strong Himalayan deformation affecting the sediments within this syncline, it can be observed that the Cambrian Kurgiakh Formation follows the undulation of the underlying sediments, but is unconformably overlain by the Ordovician Thaple formation. Thus, in Tanze and in Spiti, the presence of an unconformity at the base of the Ordovician points towards a tectonic event that occurred at the Cambro-Ordovician boundary.

It is also in the Tanze area that Srikantia et al. (1980) claim to have found clasts of Lower Paleozoic tourmaline bearing granites within the Kurgiakh Formation (their Thango Formation). This observation was for these authors, as also for later ones (Baud, 1984; Garzanti et al. 1986), one of the arguments for the uplift and erosion of a cratonic basement related to a late Pan-African orogenic cycle in Cambro-Ordovician time. However, we have never found any granitic clasts nor any metamorphic rock fragment within the conglomerates of the Thaple Formation. This is explained by the fact that Srikantia et al. (1980) most likely mistook Quaternary deposits for the Thaple Formation, because they associate their granitic clast with the erosion of the Gumburanjun leucogranite which they thought to be of Lower Paleozoic age, but which, in reality, is of Tertiary age!. In fact, clear evidence of a marked schistosity or regional metamorphism usually associated with an orogenic process is lacking in Zaskar.

Thus, even if we agree with the interpretation that the Cambro-Ordovician boundary is marked in the Tethys Himalaya of Zaskar by the uplift and erosion of deformed early Paleozoic sedimentary sequences, we find it very difficult to determine what caused these tectonic movements. As mentioned above, the bending of the Precambrian to Cambrian formations, the unconformity at the base of the Thaple Formation and the granitic intrusions could as well be related to extensional movements as to a pre-Himalayan orogenic event.

From the Ordovician to the Permian, we believe the Tanze area to represent the rim of a basin. This is supported by the fact that all the formations from this period thin out gradually from the southeast towards the Tanze syncline where they disappear. The Zaskar region, lying northwest of Tanze, might thus have been for most of the Paleozoic a structural height with no or very little sedimentation. Several periods of non-deposition or erosion, also within the basin, are re-

vealed by the absence of the Silurian and by unconformities at the base of most of the Ordovician to Permian formations. The more or less continuous subsidence of the basin zone until the Permian is attested by the progressive tilting of the Paleozoic formations towards the southeast. These tectonic movements are most probably related to the opening of the Neotethys and have accentuated the downwarping of the Thidsi Formation, initiated in the Cambro-Ordovician.

The subsidence or uplift movements in the Tanze area, as in the rest of Zanskar, seem to have come to an end in the “mid” Permian as is shown by the Panjal Traps which seal the underlying structures, forming what looks like a Permian peneplain. This basaltic outpouring which is related to the oceanisation of the Neo-Tethys is followed by the thermal subsidence of the whole area which is then covered by an open sea carbonate platform.

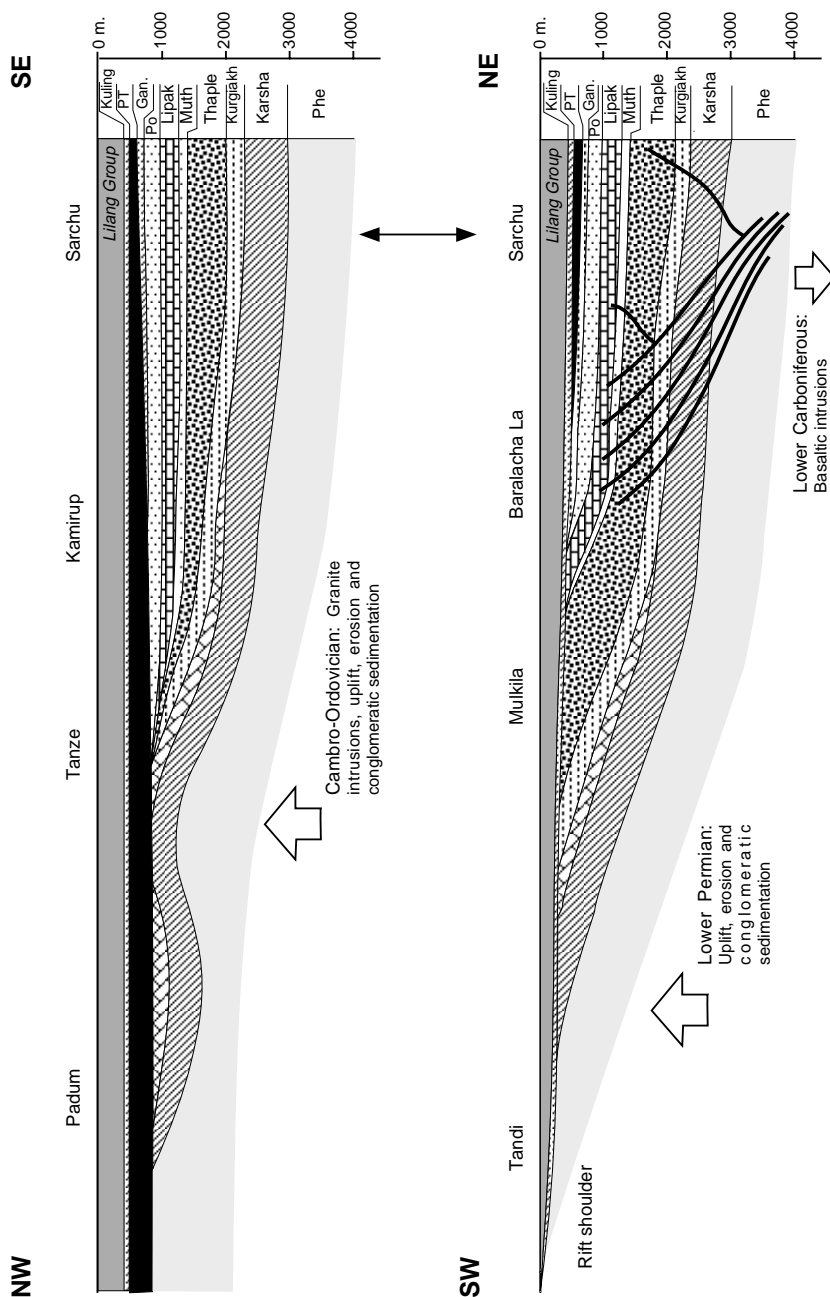


Fig 3.11: Palinspastic reconstruction of the north-west Himalaya in the middle Triassic. The lower cross-section is simplified from Vannay (1993) and shows a succession of events associated with the rifting and opening of the Neotethys. The upper cross section follows the Doda-Lingti-Kurgjakh valleys in Zanskar and intersects the cross section of Vannay in the Sarchu region. Note how all the Paleozoic formations thin out and disappear towards the northwest. Vertical exaggeration: 5X

4. TECTONICS

Nothing I had ever read or imagined prepared me for the splendour and majesty of the mountains that first day; that was the first gift Ladakh gave me, a silence before that phantasmagoria of stone, those vast wind-palaces of red and ochre and purple rock, those rock faces the wind and snow had worked over thousands of years into shapes so unexpected and fantastical the eye could hardly believe them [...] rocks tortured in as many thousand ways as the mountains they are torn from.

«A journey to Ladakh» Andrew Harvey

4.1 Introduction

We have seen in the previous chapters that the Tethys Himalaya and part of the High Himalayan Crystalline Sequence are formed by a thick pile of sedimentary rocks, deposited on the northern margin of the Indian continent and that the normal stratigraphic succession of these sediments was disturbed in places by a succession of tectonic events, that occurred mainly during the Paleozoic. The stress these events exerted on the sedimentary series are however moderate compared to the huge forces that were applied on them during the collision between India and Asia. Most of the deformations that can be observed within the Tethys Himalaya and the High Himalayan Crystalline Sequence are thus the consequence of the Himalayan orogen.

A considerable amount of work has already been done by previous researchers to decipher the rather complex Himalayan tectonic evolution of the Ladakh - Zaskar - Lahul area (Frank et al. 1973, 1977, 1987; Thöni, 1977; Bassoulet et al. 1980; Srikantia et al., 1980; Fuchs, 1982, 1987, 1989; Honegger, 1983; Keleman and Sonnenfeld, 1983; Baud et al. 1984; Gaetani et al. 1985; Colchen et al. 1986; Gilbert, 1986; Searle, 1986; Stutz and Steck, 1986; Herren, 1987; Kündig, 1988; Searle et al., 1988, 1997; McElroy et al. 1990; Pêcher, 1991; Gapais et al., 1992; Güntli, 1993; Patel et al. 1993; Routh, 1993; Steck et al., 1993, 1998; Spring, 1993; Vannay, 1993; Epard et al., 1995; Fuchs et al. 1995; Vannay and Steck, 1995; Wyss et al., in press). These studies, although sometimes contradictory, lead to a better understanding of the northwestern Himalayan tectonic history.

The tectonic evolution of the Ladakh-Zaskar-Lahul region can be subdivided in two major episodes: the first one is marked by compression tectonics related to the collision between India and Asia. This first event was responsible for crustal shortening, thickening and Barrovian metamorphic imprint on the sedimentary series of the Indian continental margin. Deformation was accommodated by thrusting, folding and the formation of both SW- and NE-directed nappes. The second major episode is marked by extensional tectonic structures related to the exhumation of the high-grade metamorphic rocks of the High Himalayan Crystalline Sequence. This second episode of syn-orogenic extension occurred while the Himalaya was still globally in compression and is expressed by ductile normal shearing, doming and brittle normal faulting.

4.1.1: Main Structural elements in the NW Himalaya

From south to north, the Himalayan belt can be divided in the following main structural elements (see also Fig. 4.1):

- The Main Frontal Thrust (MFT): It is along this still active structure that the Sub-Himalaya is thrust towards the SW over the quaternary fluvial deposits of the Indian plains.
- The Main Boundary Thrust (MBT): This structure separates the metapsammitic schists and phyllites of the Lesser Himalaya (hanging wall) from the conglomerates and sandstones of the Sub-Himalaya (footwall). The SW-directed movements associated with this structure are characterised by brittle deformation (cataclastites).
- The Main Central Thrust (MCT): This structure is one of the most important tectonic elements associated with the Himalayan orogen; it separates the high-grade metamorphic rocks of the High Himalayan Crystalline Sequence (hanging wall) from the weakly metamorphosed series of the Lesser Himalaya (footwall). Deformation along this structure was mainly ductile. The MCT can be traced along the entire frontal zone of the Himalayan belt and appears in tectonic windows as the Kishtwar Window (KW) or the Larji-Kulu-Rampur Window (LKRW) as well as in klippes as the Simla Klippe.
- The Crystalline Nappe: This SW-directed nappe is formed by the High Himalayan Crystalline Sequence and was exhumed by thrust faulting along the MCT over the Lesser Himalaya. This nappe is also sometimes referred to as «slab», «wedge» or «sheet». Internal deformation within this nappe is responsible for a large amount of crustal thickening. The Kalath Fold (Thöni, 1977; Epard et al., 1995) is a major SW vergent fold associated with the thrusting of the Crystalline Nappe on the Main Central Thrust towards the SW.
- The Shikar Beh Nappe. The existence of an early phase of NE vergent nappe stacking within the HHCS was proposed by Steck et al., 1993 and represents an exceptional feature in the Himalaya, where compression structures are classically characterised by SW-directed thrusting and folding. The Tandi syncline represents one of the most striking tectonic structures associated with this deformation phase. Vannay (1993) demonstrated that this syncline formed during a phase of NE-directed folding associated with the Shikar Beh Nappe. No thrust zone associated with this NE vergent nappe was observed along the Leh - Rohtang La transect but more to the East, along the Tso-Morari - Spiti transect. Steck et al., 1998 suggest that the Lagudarsi Thrust represents the northeastern front of the Shikar-Beh Nappe.
- The South Tibetan Detachment System (STDS), also called North Himalayan Shear Zone (NHSZ), represents a major system of north-dipping structural detachments at the boundary between the High Himalayan Crystalline Sequence and the Tethys Himalaya. This structure was first identified by Caby et al. (1983) and Burg (1984). A detailed analyses of the STDS was made by Burchfiel et al. (1992). Deformation along this structure was accommodated either by dextral strike-slip or by extensional shearing. Unlike the MCT, the STDS is not a continuous structure along the entire Himalayan belt. Various strands belonging to this structure have been identified and one of them is the Zaskar Shear Zone (ZSZ). The ZSZ is a ~150 km long extensional structure that caused a structural detachment between the HHCS and the TH. Most of the deformation along the ZSZ was accommodated by low-angle ductile normal shearing, but high-angle normal faults as the Sarchu Fault (Spring, 1993) or the Dutung-Thaktote Normal Faults (Steck et al. 1998) are

also associated with the ZSZ. Another strand of the STDS identified in the NW Himalaya is the Chandra Dextral Shear Zone (CDSZ). According to Vannay and Steck (1995), the CDSZ did not cause a structural detachment between the HHCS and the TH; deformation along this structure was essentially accommodated by ductile dextral strike-slip and is responsible for an E-W reorientation of linear structures. Although the CDSZ and the ZSZ both belong to the STDS, the relationship between these two structures is not clearly understood. It was proposed by Vannay (1993) that they form an en echelon structure.

- The Sarchu Dextral Shear Zone (SDSZ): This shear zone corresponds to a N-S couloir of ductile deformation associated with the dextral underthrusting of the High Himalayan Crystalline sequence (or Kenlung Serai Unit) below the Nyimaling Tsarap nappe (Steck et al. 1993). This structure is responsible for a N-S reorientation of linear structures and can be followed from the Nyimaling region in the north to the Main Central Thrust in the south.
- The Baralacha La Thrust System: The region of the Baralacha-La is characterised by a great number of SW vergent thrusts and folds. These low-angle decollements follow the Surichun Member of the Kurgiakh Formation and disturb only weakly the normal stratigraphic succession. Vannay and Steck (1995) conclude that the Baralacha La Thrust System is characteristic of a shallow structural level. These authors interpret these thrusts as representing an imbricate structure, that developed at the front of the SW vergent Nyimaling-Tsarap Nappe. The Parang-La Thrust at the front of the Mata Nappe represents an equivalent of the Baralacha La-Thrust along the Tso-Morari- Spiti transect (Steck et al. 1998). These two thrust systems are linked together by an en echelon structure.
- The Nyimaling-Tsarap Nappe: This name was proposed by Steck et al. (1993) for the whole thrust pile of sedimentary rocks situated between the Indus Suture Zone to the north and the Baralacha-La to the south. The internal structure of this SW vergent nappe corresponds to an imbricate structure as defined by De Margerie and Heim (1888) and updated by Steck et al. (1993, 1998). A progressive change in the style of deformation was evidenced from the northeastern part of the Nyimaling-Tsarap nappe towards the southwest as higher structural levels are exposed. Along the Indus Suture Zone in Ladakh, the root zone of the Nyimaling-Tsarap nappe is exposed as a consequence of the uplift of the Nyimaling crystalline dome. In this region, it was observed that the southwestward-directed deformations at the base of the nappe are essentially accommodated by ductile shearing. From the root zone towards the southwest, and as increasingly higher structural levels of the Nyimaling-Tsarap nappe are exposed, the deformation becomes more and more brittle. This is marked by the progressive development of a ramp-and-flat tectonic style towards the frontal part of the Nyimaling-Tsarap nappe. The upper part of the Tethys Himalaya is thus sliced into several overlapping structural units bounded by a succession of low-angle northeast dipping ramps. These brittle detachments are most likely anchored in a zone of ductile deformation towards the base of the Nyimaling-Tsarap nappe. The amount of deformation and translation becomes less important within the structural units forming the front of the nappe (Baralacha La Thrust). A recent study (Steck et al. 1998) revealed that more to the East, in the Tso-Morari area, several superposed recumbent nappes can even be evidenced within the Tethys Himalaya. According to Steck et al. (1998), the Nyimaling-Tsarap nappe represents the equivalent of the uppermost nappe (the Mata nappe) in this nappe stack.
- The HHCS Domes: the High Himalayan Crystalline Sequence is characterised by the presence of several dome structures. The Bhazun Dome, the Cishoti Dome and the Barnaj Body are such structures found north of the Kishtwar window and described by Kündig (1989); the Haptal

Dome south of Padum was described by Herren (1987). In SW Zaskar, the HHCS also forms a dome we propose to call the Gianbul Dome.

- The Nyimaling Crystalline Dome: In NE Ladakh, the Tethys Himalayan Sedimentary series are limited to the north by a dome of metamorphic rocks and Cambro-Ordovician granites similar to the High Himalayan Crystalline Sequence. The rocks from the Nyimaling Crystalline Dome recorded the ductile deformation associated with the southwestward tectonic transport of the Nyimaling-Tsarap Nappe. The dome structure corresponds to a NE vergent backfold and was acquired later on, during an episode of dextral transpression (Stutz, 1988; Stutz and Steck, 1989; Steck et al. 1993). More to the east, in the Tso-Morari region, the equivalent of the Nyimaling Crystalline Dome is structurally underlain by the Tetraogal Nappe and the Tso-Morari Nappe (Steck et al., 1998).
- The Indus Suture Zone (ISZ): This structure marks the limit between the Indian Plate and the Asian plate. It is along the Indus Suture zone that the Indian plate was subducted below Asia. Remains of oceanic crust and island arcs (Dras volcanics), mixed with flysch and molasse deposits, can be found within the ISZ as well as in the Spontang Klippe.

4.1.2: Chronology of deformation in the NW Himalaya (Fig 4.1)

The following abbreviations are used in this work for the structural analyses: D: deformation phase; S: Foliation (So = bedding; otherwise, S stands for a pervasive schistosity or a crenulation cleavage); L: Mineral or stretching lineation; F: Fold

D1: This phase corresponds to early NE-directed movements associated with the formation of the Shikar-Beh Nappe (Steck et al. 1993). The studied area is only marginally affected by this tectonic event. The Tandi Syncline and an early metamorphism of Barrovian type, restricted to the southern part of the HHCS, formed during this phase.

D2: This is the main compression phase affecting the sedimentary series of the Tethys Himalaya and corresponds to the development of the SW vergent Nyimaling Tsarap Nappe (Steck et al., 1993). Deformation associated with this phase propagated gradually from the Indus Suture Zone towards the SW as the Indian plate was progressively subducted below Asia along the Indus Suture Zone. The Baralacha La Thrust is a major frontal structure associated with this phase.

D3: This phase corresponds to the N to NNW underthrusting below the Tethys Himalaya of the series that will eventually form the High Himalayan Crystalline Sequence. The main structures associated with this phase are the Sarchu and Nyimaling Dextral Shear Zones as well as the Zaskar Shear Zone.

D4: Is a phase of extensional ductile shearing at the top of the Crystalline Nappe (HHCS) and low-angle normal faulting in the Tethys Himalaya. These deformations are associated with the southwestward-directed exhumation of the High Himalayan Crystalline Sequence from below the Tethys Himalaya. Most of the deformation related to D4 was concentrated along the Zaskar Shear Zone. Extensional movements along the ZSZ are supposedly contemporaneous with the activation of thrusting along the MCT.

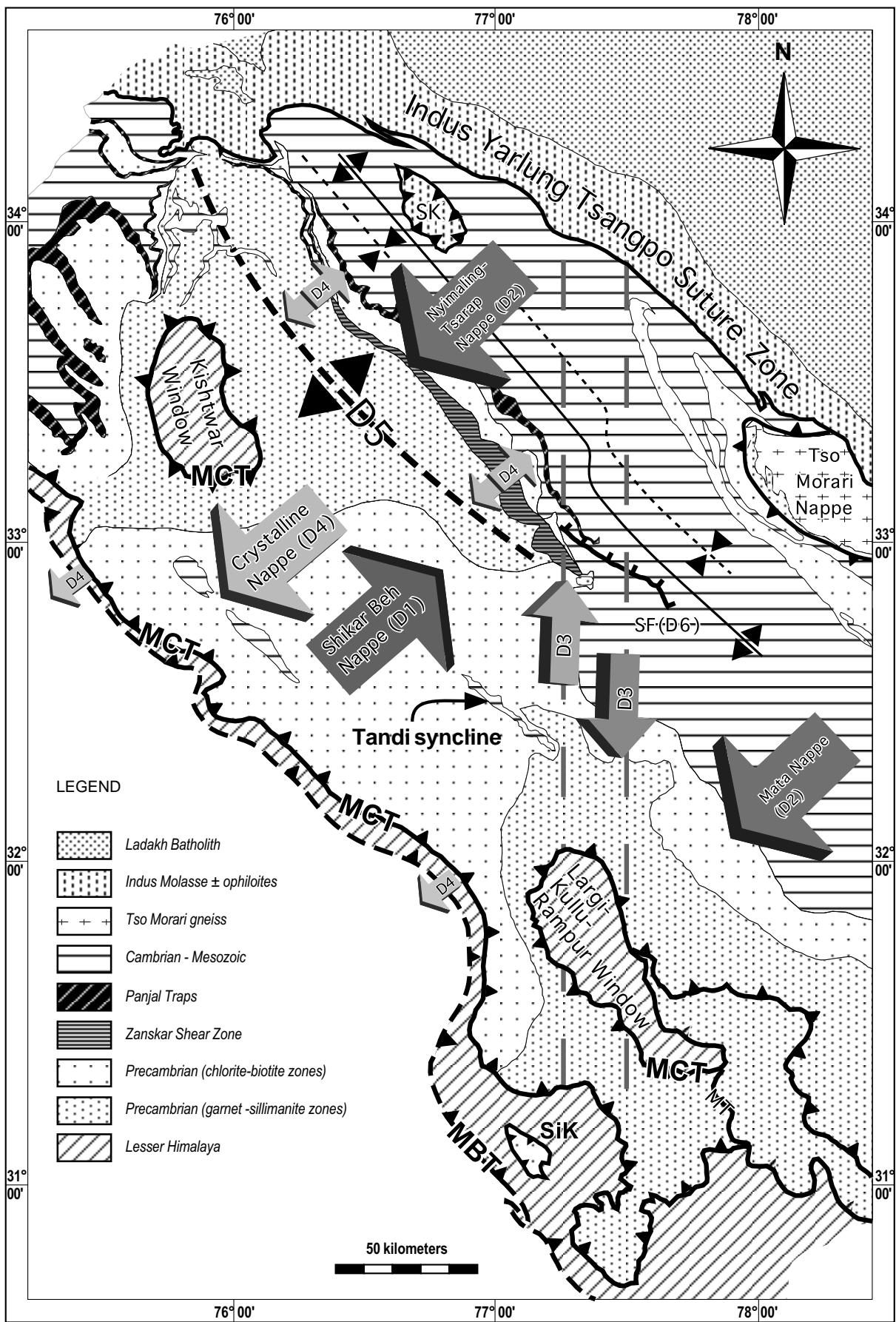


Fig 4.1: Tectonic map of the NW Himalaya, showing the main structural elements discussed in the text. MBT, Main Boundary Thrust; MCT, Main Central Thrust; SF, Sarchu Fault; SK, Spontang Klippe; SiK, Simla Klippe

D5: Corresponds to an episode of doming of the HHCS (Gianbul Dome).

D6: This last phase is marked by high-angle brittle-ductile normal faults around the HHCS domes.

4.2: Structural observations in SE Zaskar

Situated at the contact between the High Himalayan Crystalline and the Tethys Himalaya, the studied area is dominantly characterized by ductile extensional tectonics associated with D4. This deformation phase is superposed on the earlier compressive D1, D2 and D3 phases and is essentially concentrated within a 1 kilometre thick shear zone, the Zaskar Shear Zone. Two other phases, D5 and D6, are also associated with extensional tectonics and, although they appeared later than D4, their very existence is intimately associated with this main extensional phase.

4.2.1: Phase D1: the NE-directed Shikar Beh Nappe

The existence of an early NE-directed nappe in the NW Himalaya was first documented by Vannay (1993); Steck et al. (1993); Epard et al. (1995) and Vannay and Steck (1995). Their arguments are mainly based on a very detailed structural analyses of the Tandi Syncline and the distribution of the regional metamorphism. Southeast Zaskar is only marginally affected by the phase D1. Preserved structures associated with this phase are scarce and restricted to the southwestern part of the studied area. Deformation is documented by a schistosity S1 and by tight isoclinal folds F1. The foliation and folds associated with D1 overprint the sedimentary bedding S0. No thrust plane is associated with D1 in this area. A precise description of the microstructural and metamorphic evidences for this phase is given in Chapter 5.2.

4.2.2: Phase D2: The SW-directed Nyimaling - Tsarap Nappe

The Tethys Himalaya in Zaskar represents the front of the Nyimaling Tsarap nappe. In the studied area, the complete transition from ductile to brittle deformation associated with the southwestward thrusting of the Tethys Himalaya can be observed from the base to the top of the nappe. Ductile deformation is restricted to the transition zone between the HHCS and the TH and is only preserved in the upper part of this zone, where the structures related to this deformation have not been overprinted by the strong penetrative deformation related to extensional movements along the ZSZ.

The southwestward directed D2 deformation is marked in the Tethys Himalaya by three types of structures: low-angle decollements, high-angle reverse faults and folds. Open decollement folds within the calcareous sedimentary series of the Carboniferous Lipak Formation and the Triassic Lilang Group are certainly the most obvious expression of D2 (Figs 4.2 and 4.3). These superficial F2 folds with their north-south striking axes are especially spectacular within the Lilang group where they have an amplitude and wavelength ranging from ten to several hundred metres and are easily distinguishable on satellite views. These folds display long upper limbs dipping gently towards the east and short under limbs dipping steeply to the west or sometimes to the east. Their axial surfaces plunge moderately to steeply towards the east, which indicates a vergence towards the

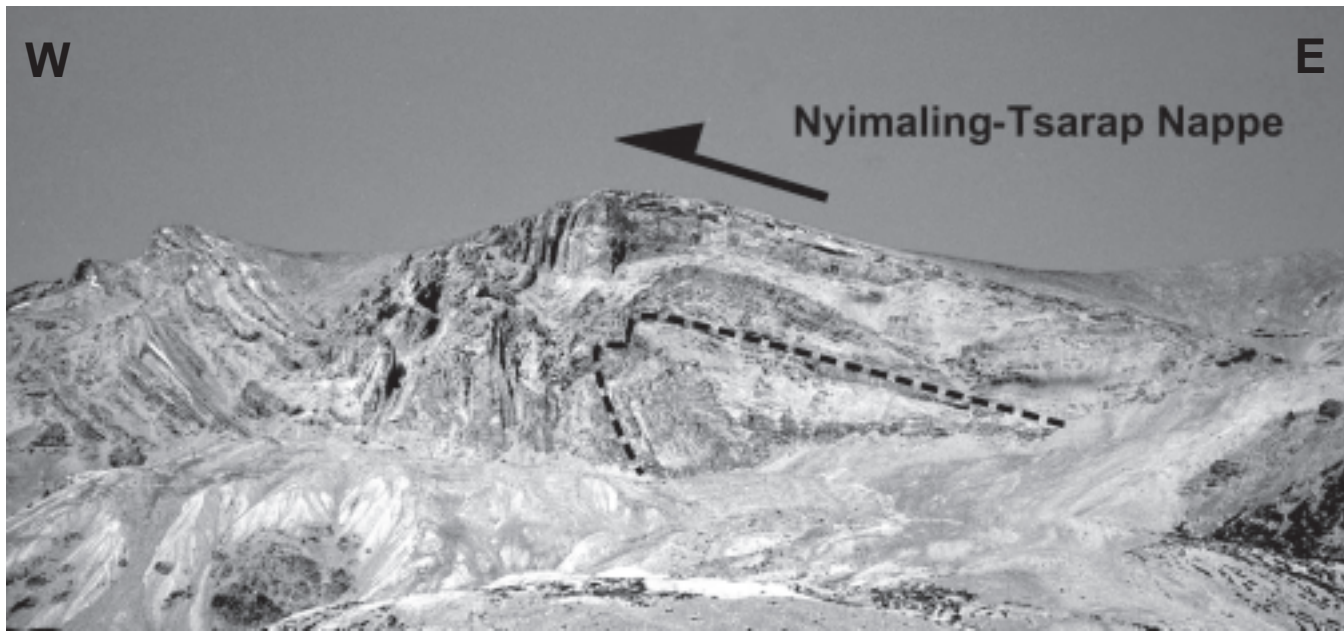


Fig 4.2: This major D2 fold is situated above de Jinshen encampment, between the Phirtse-La and the village of Taple. Such folds are frequently observed in the Triassic Lilang group, where they are associated to the south-westward thrusting of the Nyimaling-Tsarap Nappe. The present N-S orientation of the fold axes is the consequence of a dextral shear component associated to D3. The crest formed by the upper limb of the fold is 500 metres long.

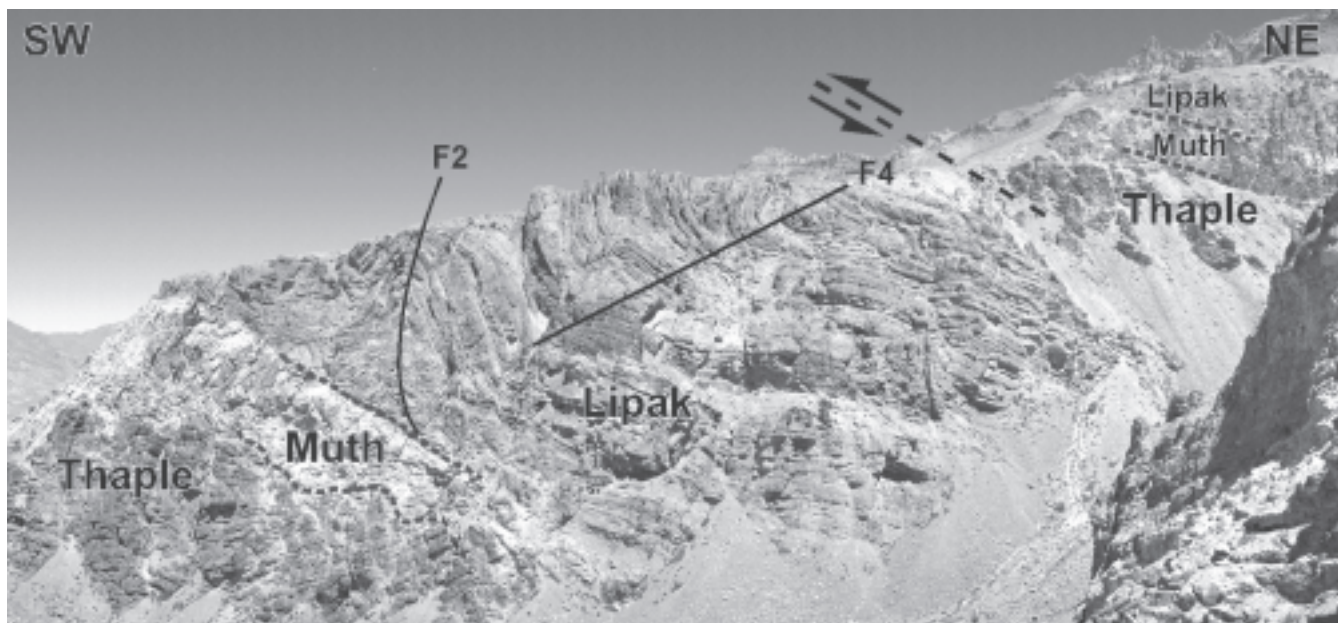


Fig 4.3: Tectonic repetition of the Ordovician Thaple, Devonian Muth and Carboniferous Lipak formations in the Tanze syncline. The D2 phase is here marked both by the formation of a thrust plane in the gypseous member of the Lipak formation and by decametric F2 folds in the Lipak limestones. These F2 folds were also reoriented during D3 and backfolded during D4. The contact between the Thaple and the Muth formations is discordant. Height of the cliff is ~20 metres

west. These folds are tectonically detached from the underlying rigid Panjal Traps along local decollement faults at the interface between these two units. Decollement faults however also occur within the different formation of the Lilang Group, giving especially to this unit a typical ramp-and flat geometry.

Decollement faults are also commonly observed within the carbonaceous Lipak Formation but are of an order of magnitude smaller than the folds in the Lilang group. The folds in Lipak are tectonically detached from the underlying rigid Devonian Muth quartzites (see Fig. 4.3) and do also have a westward vergence. The N-S orientation of the F2 fold axes in the studied area is different from the general trend of the fold axes in the rest of Zaskar, where they are systematically oriented NW-SE (Herren, 1987). We interpret this feature as a local N-S reorientation of initially NW-SE oriented fold axes during the Phase D3.

All the other formations which are not carbonaceous are only very weakly deformed by folding and rather form thrust slices, sliding over each other along local decollements. These low-angle decollements are discreet structures as they follow single stratigraphic horizons and thus do not perturb the normal stratigraphic succession. Two stratigraphic horizons were especially efficient as decollement planes. The first horizon is formed by the argillites of the Surichun member forming the top of the Cambrian Kurgikh Formation. In the Upper Lahul region, Vannay (1993) reported a major thrust plane following the Surichun Member, which is responsible in the Baralacha La area for a tectonic transport of at least 15 kilometres towards the SW. The second horizon along which layer-parallel decollement occurred preferentially is, for obvious reasons, the gypseous member of the Lipak Formation. Thus, although the normal stratigraphic succession between the Carboniferous Lipak and Permian Po Formations is nearly always preserved, this gypseous horizon certainly accommodated much of the compressive tectonics at the front of the Nyimaling Tsarap nappe. Local decollements also formed along stratigraphic boundaries between or within other sedimentary formations but are of lesser importance and spatial extent.

The third type of structures related to D2 are high-angle reverse faults which, by cutting through the sedimentary formations, disrupt the normal stratigraphic succession and cause the tectonic repetition of certain formations. Such structures are rare in the studied area and a clear tectonic repetition was only observed along one thrust plane in the Tanze syncline, where the Lipak Formation is overlain by a repetition of the Ordovician Thaple, Devonian Muth and Carboniferous Lipak Formations. More to the north, the same thrust surface superposes the Panjal Traps over the Permian Kuling Formation (Fig. 4.3).

4.2.3: Phase D3: ductile underthrusting of the HHCS below the TH

The southwestward propagation of the deformation D2 in the Nyimaling - Tsarap Nappe also affected the basal series of the Tethys Himalaya which will ultimately form the High Himalayan Crystalline Sequence. In a first stage, these, mainly proterozoic, basal series were still welded to the Tethys Himalaya, but as deformation proceeded, and as the Tethys Himalaya formed an increasingly thick stack of rocks, the lower part of the Tethys Himalaya became ductile enough to accommodate the compressive deformation through ductile shearing. From that time on, the compressive forces were essentially concentrated along a ductile shear zone at the base of the Nyimaling - Tsarap Nappe. Movements along this thrust zone contributed to the further underthrusting and metamorphisation of the basal proterozoic series, leading to the ultimate metamorphic differentiation between the Tethys Himalaya and the High Himalayan Crystalline Sequence.

In the studied area, D3 is marked by an old N-S lineation, a strong N-S elongation of the pebbles in the Ordovician Thaple conglomerates and the N-S reorientation of D2 NW-SE fold axes. These features are essentially preserved at the base of the Tethys Himalaya and to a lesser extent at the very top of the Zaskar Shear Zone where subsequent deformation associated with D4 was not strong enough to erase completely the D3 structures.

P3 folds affecting quartz ribbons and mafic horizons as well as an S3 crenulation cleavage in metapelitic rocks are preserved at the top of the ZSZ. These D3 structures show interference structures with D4. The overprint of D4 on D3 increasing gradually through the ZSZ, almost none of the S3 structures subsist at the base of the Zaskar Shear Zone.

Towards the bottom of the Zaskar Shear Zone, D3 is only preserved as inclusion trails within synmetamorphic rotated garnet porphyroblasts (fig. 4.4). These snowball garnets systematically show a top to the S-SW sense of shear throughout the ZSZ, which indicates that this structure acted as a ductile thrust zone during D3 before being reactivated as a ductile extensional shear zone during D4. This superposition of extensional shearing over an earlier thrust zone at the top of the HHCS was also recognized along other segments of the ZSZ by Patel et al. (1993).

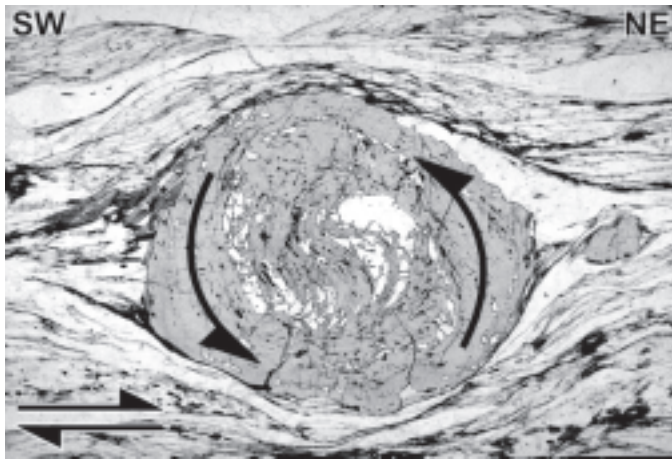


Fig 4.4: D3 syntectonic garnet porphyroblast in a metapelitic rock from the Kyanite zone (Giambul valley). Shear sense criteria deduced from the helicitic inclusion trails indicate top-to-the-SW rotation of more than 180°. Shear sense criteria in the matrix indicate an opposite top-to-the-NE movement associated to D4.

At a larger scale, D3 is marked by a zone of dextral strike-slip that can be followed from the Nyimaling region in the north down to the MCT in the south (fig. 4.1). This N-S trending structure encompasses the Nyimaling and Sarchu dextral shear zones (Steck et al. 1993) and shifts the western domains to the north with respect to the domains east of this zone of dextral strike-slip. This zone also corresponds to the westernmost end of the Nyimaling dome and the amphibolite grade rocks of the HHCS around the Kishtwar window as well as to the eastern termination of the crystalline domes of the HHCS in Zaskar.

The progressive rotation in the thrusting of the Nyimaling-Tsarap Nappe from a top-to-the-SW direction during D2 to a top-to-the-south direction during D3 is most probably related to the counterclockwise rotation of the Indian continent relative to Asia between 45 Ma and 36 Ma as documented by plate tectonic reconstitution (Patriat and Achahe, 1984; Dewey et al. 1988; Scotese et al. 1988).

4.2.4: Phase D4: ductile top to the NE extension along the ZSZ

An apparently paradoxical feature of mountain building processes is the development of major extensional structures within overall compressive systems. Although the significance of these extensional structures has been recognized only recently, such structures have been found in most orogenic belts, where they appear to play a major role in the exhumation of high-grade metamorphic rocks. In several inactive mountain belts like the **Norwegian Caledonides** (Norton, 1986; Andersen et al., 1991; Fossen, 1992; Wilks and Cuthbert, 1994, Chauvet and Séranne, 1994;), the **Variscan belt of Europe** (Malavieille, 1993), or the northwestern **American Cordillera** (Crittenden et al., 1980; Allmendinger et al., 1983; Dallmeyer et al., 1986; Metzger et al., 1991), such extensional features have been attributed mainly to late orogenic processes, developing only once shortening nearly ceased. However, in active mountain belts like the **Andes** (Dalmayrac and Molnar, 1981), the **Alps** (Steck, 1980; Ratschbacher et al., 1989; Steck and Hunziker, 1994), or the **Himalaya** (Burg, 1983; Burchfiel and Royden, 1984 & 1985; Searle, 1986; Herren, 1987 ; Copeland et al., 1990; Pêcher et al., 1991; Hubbard et al., 1992; Burchfiel et al., 1992; Hodges et al., 1992 and 1993; Brunel et al. 1994; Burg et al., 1994; Inger, 1994; Scaillet et al., 1995; Edwards et al. 1996; Sorkhabi et al., 1996; Davidson et al., 1997), clear evidence shows that major extensional structures were active contemporaneously with shortening and crustal thickening.

One of the most spectacular examples of syn-orogenic extension can be observed in the Himalaya. For nearly 2000 km along this belt, a system of north-dipping detachments separates the high-grade metamorphic sequence of the High Himalayan Crystalline Sequence from the overlying, weakly metamorphosed sediments of the Tethyan Himalaya. These extensional structures are referred to as the South Tibetan Detachment System (STDS; Burchfiel et al., 1992).

The Zaskar Shear Zone (ZSZ) is a ~ 150 km long segment of the STDS separating the HHCS from the TH in the Zaskar region of the NW Himalaya (Herren, 1987). This structure corresponds to a 1 kilometre thick zone of ductile shear, or mylonitic zone (Passhier and Trouw, 1996) following the transition domain between the Tethys Himalaya and the High Himalayan Crystalline Sequence (fig. 4.1).

The ZSZ records two major phases of deformation. As described above, relict D2+D3 microstructures, essentially expressed by rotated garnets, indicate an early top-to-the-SW sense of shear. These features indicate that the ZSZ most probably acted initially as a major syn-metamorphic thrust, along which the HHCS was underthrust below the TH (see also Patel et al., 1993).

Multi-stage extensional D4 structures are superposed on the compressional D3 fabrics. The earliest D4 phase structures correspond to pervasive C-S fabrics indicating top-to-the-NE extension. The shearing surfaces are parallel to the shear zone boundaries and define the main foliation, which bears a penetrative, down-the-dip mineral lineation. In the studied area, the ZSZ dips constantly 20° to the NE. In the lowermost part of the ZSZ, leucogranitic dikes are progressively reoriented and boudinaged through shearing, to finally become sub-parallel to the foliation (figs. 4.6 and 4.7). The main penetrative foliation is superposed by a steeper, anastomosing foliation that corresponds to a C'-type shear band cleavage (fig. 4.5). This cleavage is oblique to the shear zone boundaries and dips 40-60° to the NE. A conjugate cleavage, dipping gently toward the SW, is less well developed. These shear band cleavages record extension during a later stage of the ductile D4 deformation.

Along with the reorientation of the leucogranitic dikes and the C-S or C'-S fabrics, other shear sense indicators like mantled porphyroblasts, asymmetric P3 microfolds, back-rotated boudins



Fig 4.5: C'-type shear band cleavage transecting the main foliation (S) in an orthogneiss within the ZSZ (Reru). Notice that the cleavage does not continue in the quartz vein.



Fig 4.6: Leucogranitic dikes reoriented by ductile shearing in the Zanskar Shear Zone during D4 (Giambul valley).

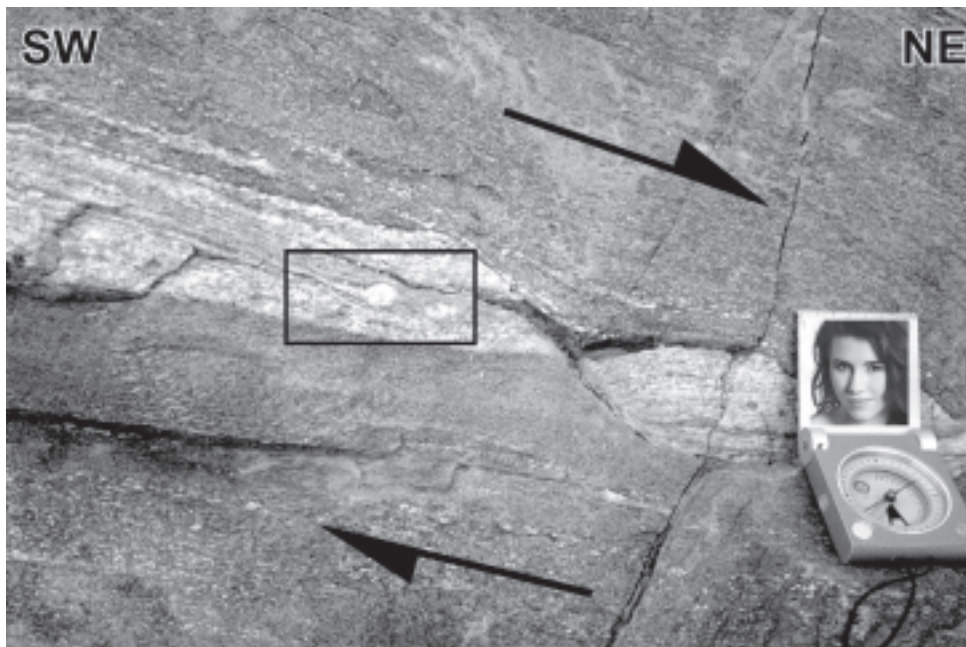


Fig 4.7: Paragneiss from the kyanite zone in the Gimabul valley. A σ -type mantled porphyroblast (in the black frame) and a back rotated boudin in an aplitic vein indicate top-to-the NE ductile extensional movements associated to D4.

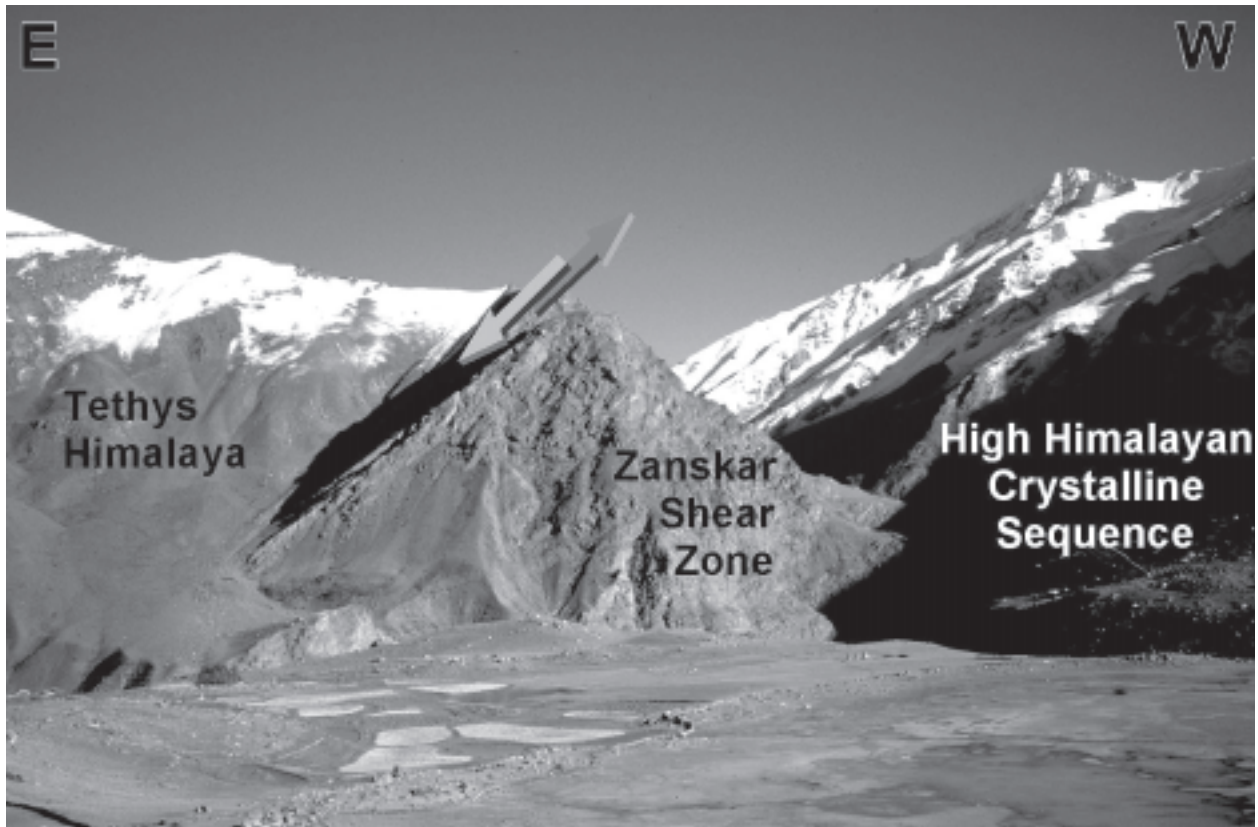


Fig 4.8: The contact between the High Himalayan Crystalline Sequence and the Tethys Himalaya, in the region of Reru, is characterized by a major slickenslide at the top of the orthogneisses that form the Zanskar Shear Zone (see Fig.4.5).



Fig 4.9: In the Gianbul valley, the Zanskar Shear Zone affected essentially metapelitic rocks, which resulted in a smooth topographic transition between the High Himalayan Crystalline Sequence and the Tethys Himalaya.

and mica fishes, systematically indicate top-to-the-NE sense of shear associated with D4. These microstructure are associated with the growth of retrograde metamorphic minerals which will be described in Chapter 5.4.

The morphology of the transition zone between the High Himalayan Crystalline sequence and the Tethys Himalaya depends on the type of rocks sheared within the Zaskar Shear Zone. In those regions where metapelitic - metapsammitic rocks were affected by ductile shearing, the transition between the HHCS and the TH is gradual and the ZSZ does not appear as a marked morphologic structure in the topography. This feature is commonly observed from the Gianbul valley to the Gumburanjun. In those regions where ductile shearing affected more competent rocks (i.e. orthogneisses), the transition between the HHCS and the TH is often brutal and the top of the ZSZ is characterised by a slickenside. Such a brutal contact is exposed in the Mune - Reru area, where it forms a marked structure that can even be recognised on satellite images.

Although most of the extensional tectonics associated with D4 were concentrated along the Zaskar Shear Zone (figs 4.8 and 4.9), the Tethys Himalaya was also affected by this phase. In this domain, D4 is marked by the reactivation of D2 thrusts as low-angle normal faults and backfolding in the carbonaceous horizons (Carboniferous Lipak and Triassic Lilang). Both low-angle folds and backfolding are, however, much less developed in Zaskar than in the adjacent Suru and Sarchu regions, most probably because in these latter regions extensional tectonics were not, or only weakly, accommodated by ductile shearing between the HHCS and the TH.

4.2.5 Phase D5: Doming

The doming episode is only apparent in the High Himalayan Crystalline Sequence, where the D5 phase is associated with an important bulging of this domain. The dome formed by the HHCS, has an approximately elliptical shape, with a NW-SE trending long axis, perpendicular to the general directions of transport of the TH nappes. The dome swells to a maximal width in the middle of its long axis and pinches at both ends, in the Suru region to the NW and in the Sarchu region to the SE. We will refer to the HHCS dome in SW Zaskar as the Gianbul Dome.

Along the Gianbul valley, we could observe that the ZSZ is warped by the doming phase. We thus disagree with the interpretation of Kündig (1988), that ductile extensional shearing along the ZSZ was the consequence of doming.

This warping or folding of the ZSZ, together with the metamorphic isograds, around a dome explains why the metamorphism decreases in the areas south of the dome as in the Chenab valley. Indeed, if the metamorphic isograds were not folded, one would expect a gradual increase in the metamorphic gradient towards the south.

Because of the folding of the ZSZ around the Gianbul Dome (fig 4.12), it is also expected that the southern side of the dome should be characterized by the presence of the ZSZ but tilted towards the south. On the southern part of the dome, the ZSZ could thus be confused with a NE vergent thrust zone because the ZSZ is here dipping to the SW and the tilted D4 shear sense criteria would still reveal a ductile top to the NE sense of shear. Preliminary data from Steck, Epard and Robyr (oral communication) reveal that, in the Miyar Valley, the southern limit of the Gianbul Dome is characterized by the presence of a ductile, low-angle, SW dipping shear zone (Miyar Thrust). The structural analysis of the Miyar Valley region reveals an early top to the NE sense of shear of the Miyar Thrust superposed by SW dipping high-angle normal faults (similar to the D6 normal faults

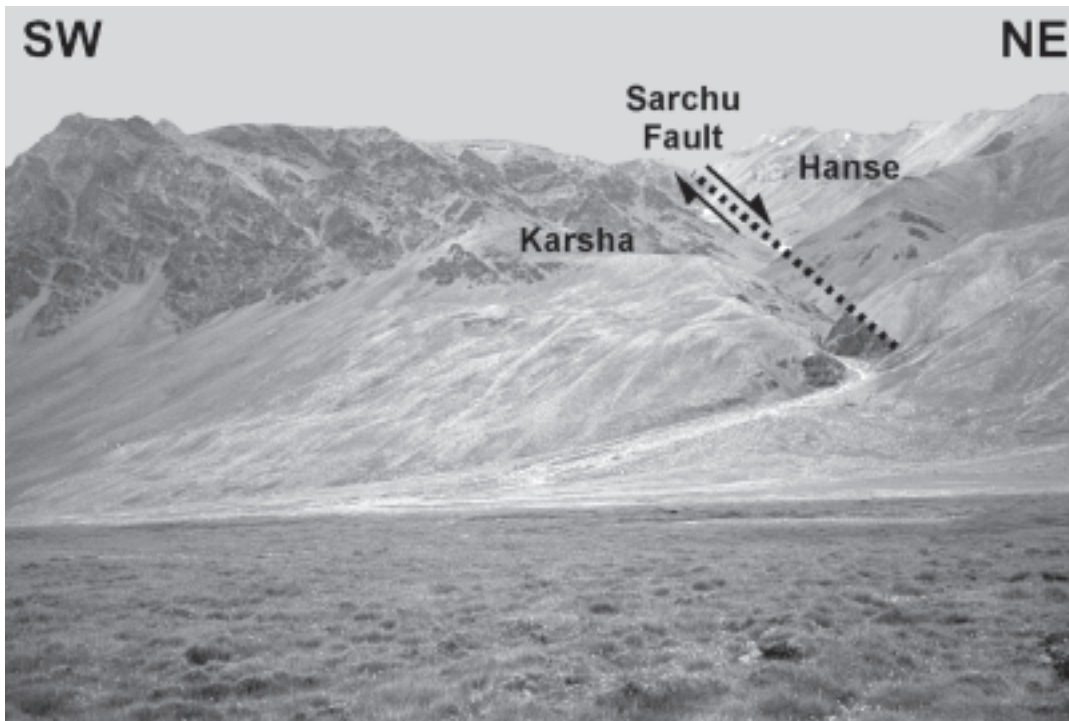


Fig 4.10: The high-angle brittle Sarchu Fault (D6) in the Kamirup valley juxtaposes the Cambrian Karsha Formation (garnet zone) with the Triassic Hanse Formation (anchizone) .

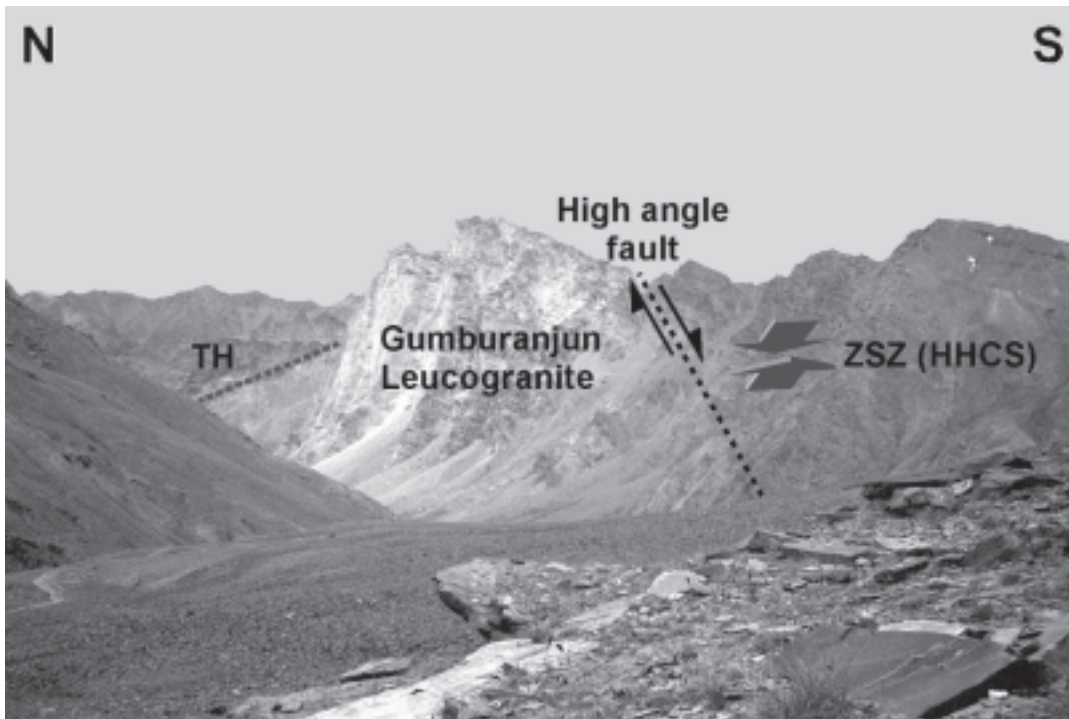


Fig 4.11: This view of the Gumburanjun mountain shows one of the major high-angle normal faults associated with D6 that borders this leucogranitic pluton. The grey arrows show the shear sense in the metapelitic rocks of the Zaskar Shear Zone.

on the northern side of the dome). Although Steck et al. (oral communication) interpret the Miyar thrust as the ductile sole of the early NE vergent Shikar-Beh Nappe, we rather consider the Miyar thrust and the ZSZ as forming a single continuous folded extensional structure (Fig. 4.12).

The consequence of the folding of the ZSZ around the Gianbul Dome, is that the shear zone has to crop out again somewhere south of the Chenab valley and the north of the MCT. Such a structure has not been described so far but the geology of this region is still little known. It is expected that the southernmost reappearance of the ZSZ should be characterised by a set of high-angle brittle normal faults, because the regions south of the Chenab are only affected by greenschist facies.

The cause of doming of the HHCS in Zanskar is unclear. It is indeed very unlikely that the doming of the HHCS is the consequence of tectonic denudation related to extensional movements along the ZSZ. Such a process is often described in zones where exhumation of high-grade rocks is associated with crustal extension as in the Basin and Range or the Cordilleran metamorphic core complex (Spencer, 1984). In these settings, the removal of a large portion of the overburden through tectonic denudation leads to isostatic rebound of the exhumed domains and to the warping of the low-angle normal shear zone. Although we observe a warping of the ZSZ around the Gianbul Dome, the doming of the HHCS occurred in a context of crustal shortening.

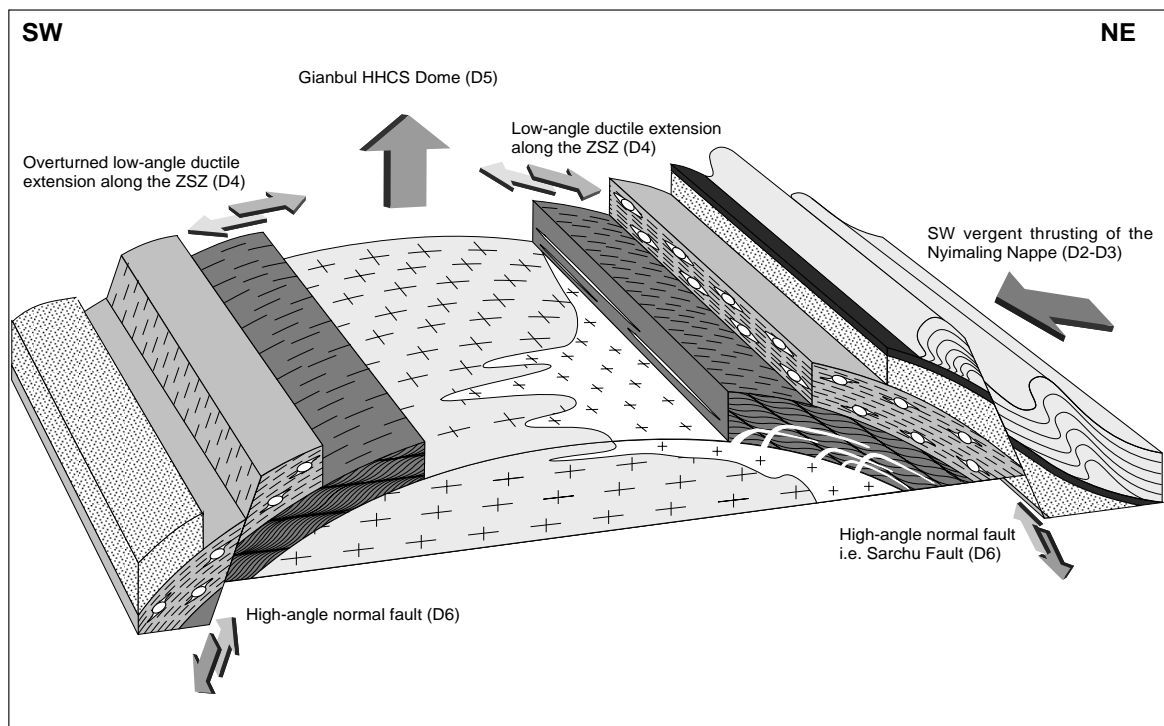


Fig 4.12: Recapitulation of the deformation phases in SW Zanskar as a block-diagram. The warping of the Zanskar Shear Zone around the Miyar-Gianbul dome during D5 rotates the shear zone, such as that this structure now dips towards the southwest on the left of the diagram. The shear sense indicators associated with D4 (ductile extension) still indicate a top to the north-east movement but which could now be interpreted as associated to a north-east vergent thrust. Note that the warping of the metamorphic isograds around the dome gives an explanation for the observed southwestward decrease in metamorphic grade towards the Chenab valley. The stippled layer represents the Paleozoic, the thin dark layer, represents the Panjal Traps and the folded layer represents the Triassic Lilang Group. The D1 phase associated to the Shikar Beh Nappe and the N-S rotation of the D2 folds are not represented.

Doming is especially pronounced in those regions where the tectonic exhumation of the HHCS is accompanied by partial melting and the formation of leucogranitic melts. By intruding the upper structural levels of the HHCS, the leucogranitic melts aggregated to form large bodies of leucogranites, which probably contributed to the bulging of the HHCS.

4.2.6 Phase D6: High-angle normal faults

The last tectonic phase D6 occurred under brittle conditions and is expressed by ultramylonites, pseudotachylites and cataclastites associated with high-angle normal faults. These young faults cross-cut the Zaskar Shear Zone and propagate through the overlying sedimentary series of the Tethys Himalaya. Normal displacement along these faults is documented in the Tethys Himalaya by the juxtaposition of younger series in the hanging wall against older series in the footwall. The most prominent of these high-angle normal faults is the Sarchu Fault (chapter 5.3.2) which juxtaposes low-grade metamorphic sedimentary series in the hanging wall against amphibolite facies metasediments in the footwall (fig 4.10).

In the Tethys Himalaya, these faults are always masked by quaternary scree. Within the ZSZ however, a clear cross-cutting relation can be established between the narrow high-angle ultramylonitic D6 faults and the low-angle mylonitic foliation associated with D4.

Along most of the ZSZ, the high-angle faults dip towards the NE at an angle between 50° and 70°. Less pronounced conjugated faults dipping towards the SW are also frequently observed. Towards the southeastern end of the HHCS, high-angle normal faults are also observed around the Gumburanjun and Kamirup leucogranitic bodies (fig 4.11). High-angle faults have also been reported in the Miyar valley, along the southern edge of the Gianbul dome, but so far only in the high-grade rocks (Steck, oral comm.).

4.3 Discussion:

The close juxtaposition of two domains, the High Himalayan Crystalline Sequence and the Tethys Himalaya, showing very different styles of deformation made it often difficult to correlate precisely a deformation phase observed in one domain with its equivalent in the other domain.

We have nevertheless subdivided the tectonic evolution of SE Zaskar into six phases of deformation. This subdivision was made on the basis of structural arguments but also on the basis of metamorphic arguments which will be presented in the next chapter.

Both the HHCS and the TH originally formed a single continuous succession of sedimentary rocks ranging from the Proterozoic to the Eocene. The now observable metamorphic difference between these now distinct domains is the result of the tectonic thickening of the sedimentary series during the collision between India and Eurasia, and thus, of the burial and metamorphisation of the mainly Proterozoic sediments at the base of the Nyimaling-Tsarap Nappe formed by the whole stack of Tethyan Himalaya sedimentary rocks. The tectonic uncoupling of the Proterozoic series from the younger series is the result of the formation of a ductile thrust, reactivated as an extensional shear zone, at the base of this nappe.

Structural observation basically reveal that the studied area underwent three clearly distinct tectonic episodes. The two first episodes are marked by compressive structures (folds, thrust planes, nappes) showing opposite sense of movement (D1, NE vergent and D2+D3, SW vergent). The third episode is marked by extensional structures (Shear Zone D4, doming D5, normal faults D6). While these three major episodes clearly succeeded one another through time, deformation phases belonging to a same tectonic episode might have occurred contemporaneously at different structural levels.

The Zaskar Shear Zone, which is marked by a top-to-the NE sense of shear, did not form in a system globally in extension but, paradoxically, this "extensional" structure formed while the Himalaya was still globally in compression. At large scale D4 does indeed correspond to the extrusion of the HHCS as a SW vergent nappe, thrust over the Lesser Himalaya along the Main Central Thrust. At the top of the HHCS, the Zaskar Shear Zone formed contemporaneously with the MCT, as a result of differential movements between the SW vergent ductile crystalline Nappe and the more rigid Tethyan Himalaya series. In other words, the southwestward extrusion of the HHCS as a large scale nappe during D4 was accommodated at its base by a thrust plane (the MCT) and at its top by an "extensional" shear zone (the ZSZ).

The superposition of high-angle ultramylonites over ductile deformation structures within the Zaskar shear zone is most probably the consequence of a single protracted episode of deformation. Continuous deformation along an extensional shear zone does indeed bring lower crustal rocks to the surface, resulting in a gradual transition from the ductile to the brittle domain within the ZSZ.

It should also be noted that, while ductile shearing occurred at depth, brittle normal faults must have started to form in the upper structural levels represented by the Tethys Himalaya. This evolution of a shear zone from a ductile to a brittle part of the crust was first proposed by Ramsay (1980), although in a basement-cover context. Such relation between discrete brittle faults in a high tectonic level and a ductile shear zone in a structural deeper level was also proposed by Steck et al. (1993) for the Nyimaling-Tsarap nappe during the compressive phase.

An interesting feature is the zone of dextral shearing associated with D3 that borders the western end of the HHCS in Zaskar, and which we have tentatively correlated with the Sarchu and Nyimaling Dextral Shear Zones. When looking at the geological map of the NW Himalaya, one can see that the domains lying west of a north-south running line connecting Leh and Kulu are shifted to the north over an horizontal distance of about 50 kilometres with respect of their equivalent lying east of this line. The eastern Zaskar dextral shear zone, together with the Sarchu and Nyimaling Dextral Shear Zones, might thus belong to a major zone of dextral strike-slip, stretching from the Indus Suture Zone to the Main Central Thrust. An equivalent structure, but of sinistral strike slip, could also be inferred from the geological map for the region of Warwan at the western extremity of the Zaskar HHCS. The delimitation of the Zaskar High Himalayan Crystalline Sequence by two zones of strike slip would explain why this particular region indents the Tethys Himalaya more than the adjacent areas, and could also explain, why the ZSZ is restricted to the Zaskar region.

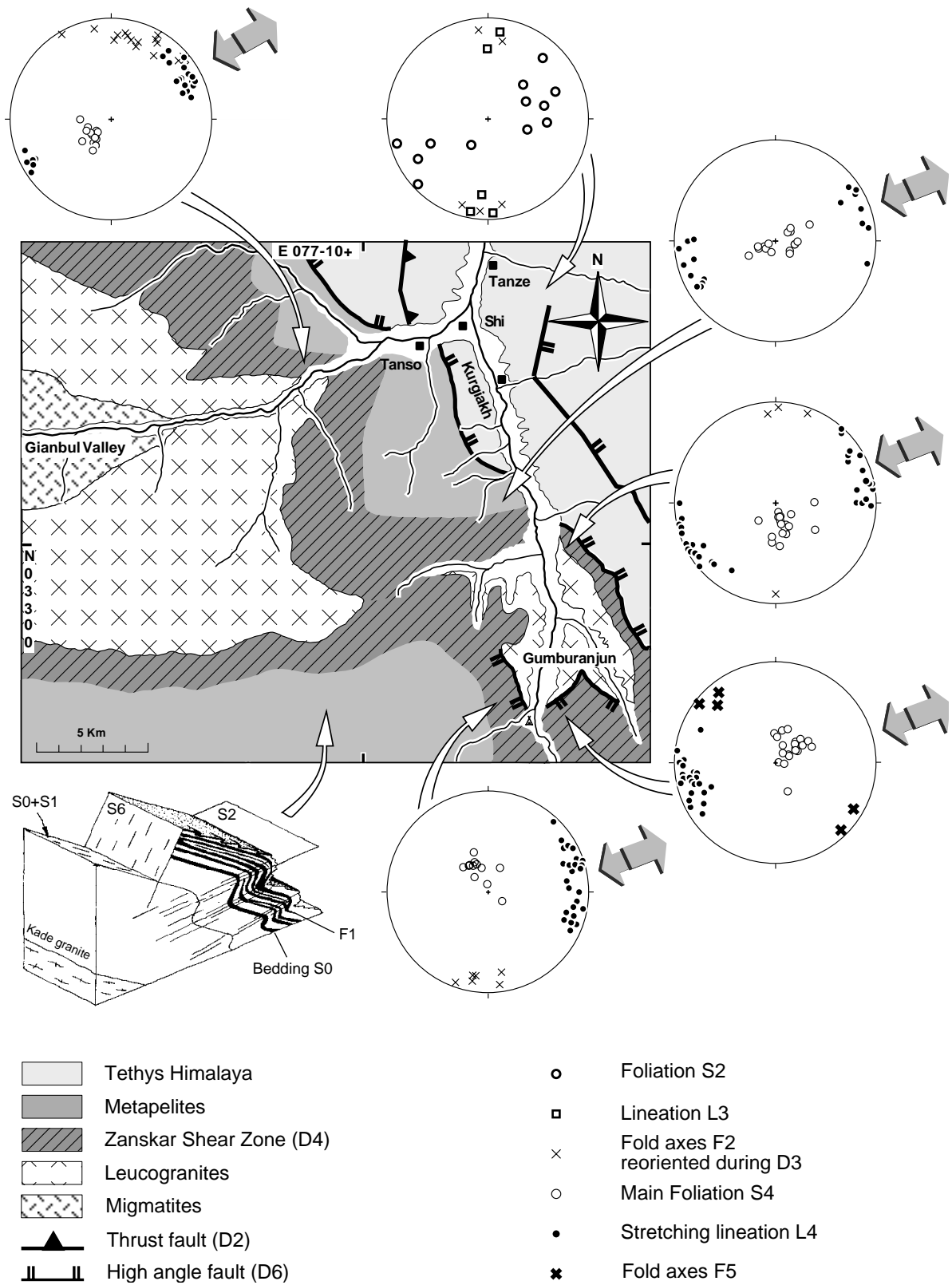


Fig 4.13: Tectonic map of SW Zaskar, showing the main structures associated to deformation phases D1 to D6. (Schmidt-Lambert projections on the lower hemisphere). Grey arrows depict the sense-of-shear during the ductile extension phase D4 (Zaskar Shear Zone S.S.).

5. METAMORPHISM

Wenn ich zehn Jahr jünger wäre, würde ich sehr versucht sein, eine Reise nach Indien zu machen, nicht um etwas Neues zu entdecken, sondern um das Entdeckte nach meiner Art anzusehen.

J.W. von Goethe, Brief an Knebel, 1787

5.1 Introduction

The studied area of Zaskar is located at the boundary between two major Himalayan domains of contrasting metamorphic grade: the High Himalayan Crystalline Sequence in the southwest and the Tethys Himalaya in the northeast. These two domains are separated by a major extensional shear zone, the Zaskar Shear Zone. This ~1 kilometre wide tectonic structure dips ~20° to the NE and runs parallel to the NW-SE trending Kurgiakh valley. It is within this narrow zone that one can observe the very rapid, though progressive, decrease in metamorphic grade between the TH and the underlying HHCS.

The footwall of the ZSZ is formed by rocks belonging to the top of the HHCS. These rocks are of high metamorphic grade and form the jagged relief of the Great Himalayan Range with its numerous glaciers and high summits often reaching over 6000 meters. In the studied area, the very top of the HHCS is characterized by the presence of a leucogranitic intrusion complex, forming a ~1 kilometre thick belt of leucogranitic plutons directly below the lower boundary of the ZSZ.

Above the leucogranitic plutons, the Zaskar Shear Zone marks the transition between the HHCS and TH. From base to top, the metapelites within the ZSZ show a reduced, but complete, succession of kyanite to biotite zone mineral assemblages, indicating a rapid upward decrease in metamorphic conditions.

The hanging wall of the Zaskar Shear Zone is formed by sedimentary series belonging to the base of the Tethys Himalaya (Karsha or Phe Formations). These sedimentary series are generally only weakly metamorphosed and form a much smoother topography.

The metamorphic evolution of the Zaskar region was already the object of several studies. Most of these studies were essentially concentrated on the high-grade metamorphic rocks of the High Himalayan Crystalline Sequence (Choudhuri, 1987; Dèzes et al. 1999; Epard et al., 1995; Fuchs, 1987; Gapais et al. 1992; Gilbert, 1986; Guntli, 1993; Herren, 1987; Jain and Manickavasagam, 1993; Kündig, 1988, 1989; Patel et al., 1993; Pognante, 1992, 1993; Pognante and Lombardo, 1989; Pognante et al., 1987, 1990; Routh, 1993; Searle and Rex, 1989; Searle et al. 1992; Spring, 1993; Steck et al., 1993; Vannay, 1993; Vannay and Steck, 1995). Fewer studies dealt with the low-grade metamorphism in the Tethys Himalaya (Fuchs and Linner, 1995; Garzanti and Brignoli, 1989; Spring, 1993; Spring et al., 1993; Steck et al., 1993, 1998).

Three successive Himalayan metamorphic events can be individualized in the studied region, The two first events are associated with crustal thickening and are of prograde regional metamorphic type. The last metamorphic event is associated with isothermal exhumation and is retrograde:

The first prograde regional metamorphism (M1) is only observed in the southwestern part of the studied area where it reaches greenschist facies conditions. This metamorphism is most probably related to the crustal thickening associated with the early NE vergent Shikar Beh nappe (D1).

The second prograde regional metamorphism (M2) is observed over the entire studied area and is characterized by a complete Barrovian metamorphic zonation ranging from anchizone in the Tethys Himalaya to sillimanite + k-feldspar zone in the lowermost part of the HHCS. This zonation which also corresponds to the gradual transition from lower greenschist to lower granulite facies, is marked by the progressive apparition of all the Barrovian index minerals. As these minerals are generally well distinguishable, even with the naked eye, a good estimation of the spatial distribution of the metamorphic mineral zone boundaries can already be established on the field. The increasing metamorphic grade is also well evidenced by the progressive transformation of the Tethyan Himalaya siltitic and arkosic sediments into the HHCS slates, schists, gneisses and migmatites. This progressive transformation of the low-grade metasediments into high-grade metamorphic rocks occurs over a surprisingly short distance which coincides with the ZSZ. The metamorphic event M2 is related to crustal thickening and underthrusting associated with the SW vergent Nyimaling-Tsarap nappe during D2 and D3.

The last metamorphic event (M3) is only clearly observed within the medium- to high-grade rocks of the High Himalayan Crystalline Sequence. M3 is marked by the apparition of low-pressure, high- to medium-temperature metamorphic minerals. These minerals grew as a consequence of retrograde re-equilibration of the high-grade M2 mineral assemblages. M3 is characterized by isothermal decompression associated with the rapid tectonic exhumation of the HHCS from below the TH during D4.

5.2 The prograde regional metamorphism M1

Two different generations of biotite occur on each side of the Shingo-La. On the southern side of this pass and above de Kade orthogneiss, the metasedimentary series of the Phe Formation are characterized by the presence of tiny (< 0,1 mm) biotite flakes. These biotite are very light coloured and their presence in hand samples can only be guessed from the slightly brownish colour of the metapsammites (fig. 5.1). The biotite flakes are closely associated with chlorite and muscovite and mark an early schistosity S1. This first schistosity corresponds to the axial plane cleavage of tight isoclinal folds P1. The sedimentary bedding S0 is still well preserved although tightly folded by the P1 folds. The main schistosity S1 is crenulated by a late deformation (D3). The biotites, muscovites and chlorite flakes are bent by this late deformation. The Kade orthogneiss below these metasedimentary rocks is also affected by a metamorphism of biotite zone grade (Vannay, 1993). Towards the top of the Shingo-la the metamorphic grade however decreases progressively and from Chumik-Nakpo up to the pass, biotite is absent and S1 is only marked by chlorite and muscovite (fig. 5.2).

On the northern side of the Shingo-La, the metamorphic grade again increases from the top of the pass towards the Lakang camping ground at the bottom of the Kurgiakh valley. On this side of the pass, the biotite zone is characterized by the presence of poikiloblastic biotite grains within the phylitic horizons of the Phe formation (fig. 5.3). These rocks have a typical grey-green lustrous

DEFORMATION				METAMORPHISM		
Crustal thickening	D1	S1 L1 F1	NE-directed thrusting of the Shikar-Beh Nappe. Structures restricted to the south of the Shingo-La.	M1	Prograde regional metamorphic event. Metamorphic gradient decreases northwards, from kyanite zone rocks in the Khoksar region to chlorite zone rocks south of the Gumburanjun	
		D2	S2 L2 F2			SW-directed thrusting of the Nyimaling-Tsarap Nappe. Formation of low-angle decollements, high-angle reverse faults and large-scale folds in the TH
			D3			S3 L3
Exhumation	D4	S4 L4 F4	Reactivation of the ZSZ as a ductile extensional shear zone. SW-directed exhumation of the HHCS from below the TH. Shearing of the M2 isograds	M3	Retrograde metamorphic event. Isothermal decompression. Growth of medium -low pressure minerals. Partial melting of the highest grade M2 rocks (migmatites)	
		D5	F5			Large-scale doming of the HHCS
		D6	S6 L6			High-angle normal faults, development of ultramylonites and pseudotachylites

Table 5.1: illustration of the relationship between the two main tectonometamorphic episodes (crustal thickening and exhumation), deformation phases (D1 to D6) and the mineral growth phases (M1 to M3). S: foliation (shistosité);, L: mineral or stretching lineation; F: folds, observed structures associated to a deformation phase.

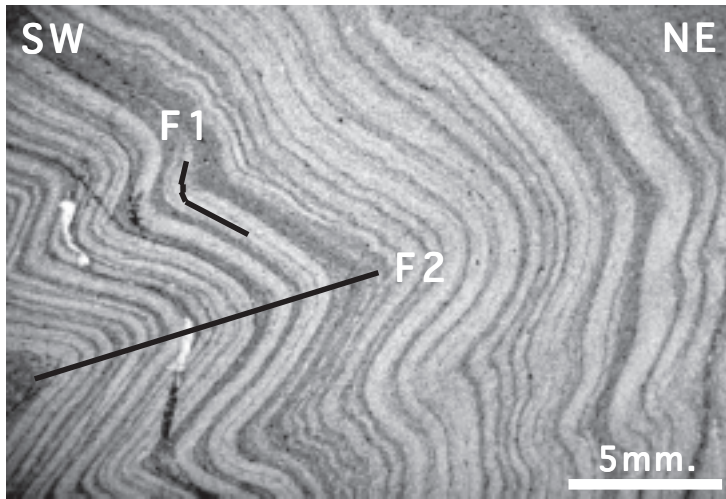


Fig 5.1: A fine-grained slate showing an alternance of clay-rich (pelites) and sand-rich (psammite) sedimentary beds. This sedimentary layering is tightly folded by F1 folds attributed to the NE vergent Shikar-Beh Nappe. Later, open, F2 folds are attributed to the SW vergent Nyimaling-Tsarap Nappe. Single biotite grains are not distinguishable at this scale but confer a brownish color to the left part of the view. Closer examination reveals that biotite formed prior to D2. Ramjak, southern side of the Shingo-La.

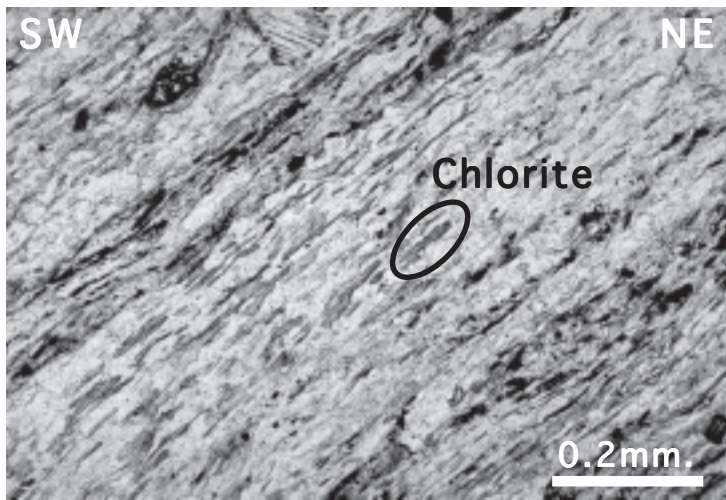


Fig 5.2: A fine-grained slate composed of an association of chlorite, muscovite, albite, k-feldspar and quartz. Biotite is lacking in this sample. Southern side of the Shingo-La, between Chumi-Nakpo and the pass.

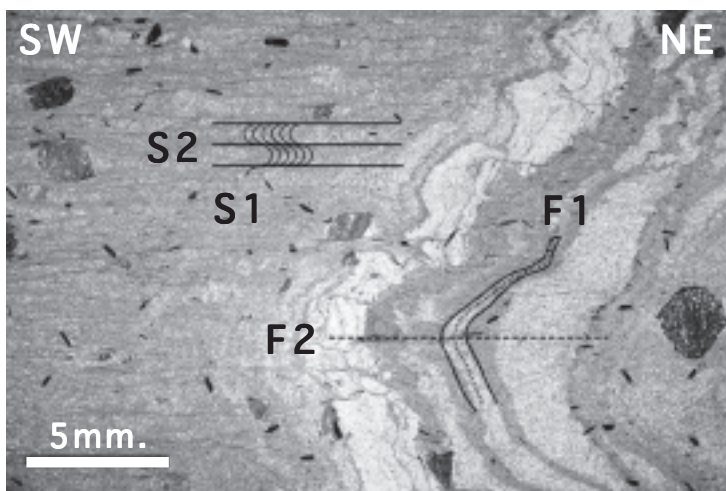


Fig 5.3: A fine-grained slate showing an alternance of clay-rich (pelites) and sand-rich (psammite) sedimentary beds. This sedimentary layering is tightly folded by F1 folds attributed to the NE vergent Shikar-Beh Nappe. Later, open, F2 folds are attributed to the SW vergent Nyimaling-Tsarap Nappe. Large biotite porphyroblasts overgrow S1 but are syntectonic with respect to D2. Matrix is composed of chlorite, muscovite, albite and quartz. Northern side of the Shingo-La.

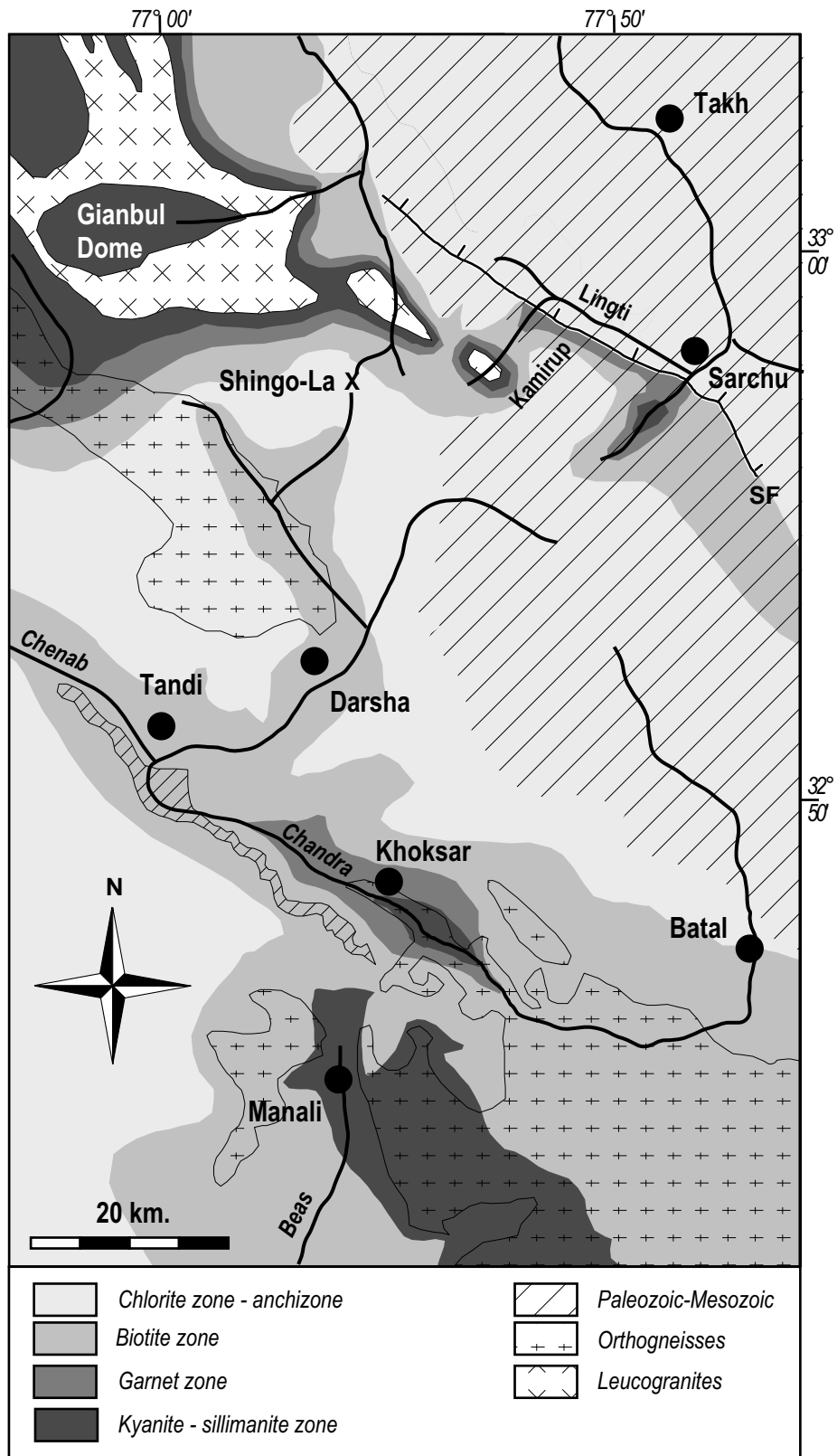


Fig. 5.4 : Metamorphic zones in the Lahul-Zaskar area. Modified after Vannay, 1993. This map shows the two distinct high-grade metamorphic domains of the Khoksar-Manali area to the south and of the Gianbul-Sarchu area to the north.

aspect and are spotted with the biotite poikiloblasts varying in size from one to five millimetres. These rocks still preserve a compositional layering which is interpreted as the sedimentary bedding S0 because of its asymmetrical internal nature (Passchier and Trouw, 1996). A first schistosity S1 defined by white micas, and to a lesser extent chlorite, is sub-parallel to S0 and is preserved within the microlithons associated with P2 folds. The cleavage domains associated with these P2 folds correspond to S2 and define the main schistosity in this area. The growth of the biotite poikiloblasts is contemporaneous with the development of S2, because an early stage of crenulation of S1, less tight than at present is preserved as inclusion trails of quartz and opaque minerals within the biotite grains. D2 and thus the growth of these biotites is contemporaneous with the crustal thickening associated with the emplacement of the Nyimaling Tsarap nappe. Such poikiloblastic biotites have also been described by Fuchs and Linner (1995) in the Kenlung Serai unit south of Sarchu.

The above-mentioned observations indicate that the biotites on the southern side of the Shingo-La belong to an earlier deformation (D1) than those on the northern side of the pass which are clearly contemporaneous to D2. The origin of D1 in this region is not clear: either it is associated with an Eohimalayan event or, more likely, to an early Himalayan event preceding the southwestward thrusting of the Nyimaling-Tsarap nappe. Such an early Himalayan event was evidenced by several authors (Steck et al., 1993; Vannay and Steck, 1995; Epard et al., 1995; Wyss et al. 1998) in the Lahul area south of Zaskar. These authors attribute D1 to the NE thrusting of a nappe stack which they call the Shikar Beh Nappe. Their arguments for this nappe are mainly based on the structural analyses of the NE vergent Tandri syncline and on the distribution of the regional metamorphism (fig. 5.4). The metamorphic grade reaches amphibolite facies in the Chandra valley (kyanite-staurolite zone near Khoksar) and gently decreases towards the north, such as to reach lower greenschist facies (chlorite zone) north of Darcha. From Darcha towards the north, the metamorphic grade increases again, to reach amphibolite facies (kyanite-staurolite zone) in the Sarchu region. As this metamorphic zonation affects sedimentary formations belonging approximately to a same structural level, they argue that the overburden required to reach amphibolite facies in the Chandra valley cannot be related to the SW thrusting of the Nyimaling-Tsarap nappe because the two high-grade metamorphic domain (Chandra to the south and Sarchu to the north) are separated by a low-grade domains (Darcha), and that the metamorphism in the southern domain can thus only be explained by the thrusting from the SW towards the NE of an earlier nappe (i.e. Shikar Beh). On the basis of these interpretations, we propose that the northwards decreasing metamorphic gradient associated with D1 observed when crossing the Shingo La from south to north is part of the general northwards decreasing trend of the southern (Chandra) metamorphic domain. The biotite zone south of the Shingo-La and our S1 are thus related to crustal thickening associated with the Shikar Beh Nappe. The biotite poikiloblasts overgrowing S1 on the northern side of the pass belong to the northern metamorphic domain and are related to the thrusting of the Nyimaling Tsarap Nappe from NE towards the SW.

5.3 The prograde regional metamorphism M2

5.3.1 Introduction

The metamorphic grade associated with the second tectonometamorphic event M2 progressively increases from the Tethys Himalaya towards the HHCS. In the studied area, the TH is characterized by slightly downwards increasing low-grade metamorphic conditions (anchizone to epizone). An exception to this rule is observed in the easternmost part of the studied area, where the metasedimentary series at the base of the Tethys Himalaya have reached lower amphibolite facies in the footwall of the Sarchu Fault. Along the Kurgiakh valley, the base of the TH forms the hanging-wall of the ZSZ and is systematically characterized by chlorite zone grade metasediments. The metamorphic grade then increases progressively, but very quickly, across the Zanskar Shear Zone from biotite grade at its top to kyanite grade at its bottom. The ZSZ thus marks the transition between the low-grade metasediments of the TH and the high-grade rocks of the HHCS. This progressive increase in metamorphic grade between the TH and the HHCS across the ZSZ is beautifully illustrated in the studied area along the Gianbul valley (fig. 5.8). This valley offers a natural cross-section through the base of the TH and the HHCS and allows to study optimally the progressive increase in metamorphic grade between these two domains. It is also along the Gianbul valley that we could reach the lowermost structural units of the HHCS, where the highest grade rocks of the studied area are exposed.

The following description of the metamorphic zonation associated with M2 starts with the low-grade metamorphism of the Tethys Himalaya with its lateral and vertical variations. We will then describe the prograde metamorphic zonation between the TH and the HHCS as observed across the ZSZ along the Kurgiakh valley and end this description with the highest grade migmatitic zone of the HHCS exposed in the Gianbul valley.

5.3.2 Metamorphism in the Paleozoic-Mesozoic (Tethyan) series

Low grade metamorphic conditions characterize most of the Tethys Himalaya sedimentary formations forming the Zanskar synclinorium. Several studies (Berthelsen, 1953; Garzanti and Brignoli, 1989; Spring, 1993; Girard, 1998; Steck et al. 1993 and 1998) however showed that the metamorphic grade increases from diagenetic conditions in the upper structural units forming the central part of the Zanskar synclinorium to reach lower amphibolite facies conditions in the lower structural units both towards the Nyimaling - Tso-Morari area to the north and in the Zanskar-Lahul-Spiti region to the south. Towards the southern rim of this synclinorium, several tectonic units have been individualized. These units are from north to south: the Kharnag, Zara and Marang-La Units (Steck et al., 1993), the Zumlung Unit (Baud et al., 1982), the Zangla Unit (Baud et al., 1982), the Chumik Unit (Spring and Crespo-Blanc, 1992) and finally the Kenlung-Serai Unit (Steck et al., 1993). Each of these units is bounded by thrust planes sometimes reactivated as normal faults and corresponds to a different structural level of the Nyimaling-Tsarap Nappe. The Kharnag Unit with its non-metamorphic grade at Lun (Steck et al., 1993) represents the highest exposed structural level, and the Padum-Kenlung-Serai Unit with its Lower greenschist to lower amphibolite facies metamorphism (Garzanti and Brignoli, 1989 and Spring, 1993) represents the lowest structural unit of this nappe. In the studied area, only the equivalents of the base of the Zangla Unit, part of the Chumik Unit and the Kenlung-Serai Unit are exposed.

The sedimentary rocks forming the Tethys Himalaya in the investigated area are generally only weakly metamorphosed. Macroscopic and microscopic investigations of both the Paleozoic or Mesozoic formations in most of the studied area rarely reveal the presence of metamorphic minerals. The only rocks which systematically yield reliable microscopic information on the metamorphic grade of the Tethys Himalaya are the effusive basaltic Panjal Traps and the mafic dikes intruding the underlying Paleozoic formations. The location of the mafic samples is shown on fig. 5.5. The magmatic texture of these rocks is generally well preserved and some relict primary augite crystals are still present in some samples. Actinote-tremolite and chlorite are however the most common mafic minerals now occurring in these rocks. The shape of the magmatic plagioclases is still recognizable although they have all been replaced by low-grade neofomed minerals. The vesicles in the Panjal traps are filled with an association of carbonates, euhedral epidote and acicular actinote-tremolite crystals. The metamorphic mineral assemblage observed in all the mafic rocks between the Phirtse-La and Purne is systematically:

albite + actinote-tremolite + chlorite + epidote + carbonates

X-ray powder diffraction analyses of eight mafic samples confirmed this assemblage and did not reveal the presence of any supplementary mineral phase. Such a mineral assemblage is typical of the lower greenschist facies or epizone metamorphic conditions.

Only one sample collected east of Chumik-Marpo in the Chumik Unit seems to indicate lower metamorphic grade as it does only contain albite + chlorite + epidote + carbonates ± quartz ± hematite. This confirms the anchizone grade of the Chumik Unit in this area as proposed by Spring (1993).

Two other mafic samples collected in the Kenlung Serai Unit at the footwall of the Sarchu Fault, one southwest of Chumik Marpo and the other at the entrance of the Kamirup valley, are characterized by the presence of metamorphic hornblende. The presence of this mineral is indicative of lower amphibolite grade. This observation is in agreement with the interpretation of Steck et al.(1993) and Spring (1993) that the metamorphic grade south of the Sarchu Fault reaches lower amphibolite facies between Chumik Marpo and Sarchu.

In order to try to detect a possible variation of the metamorphic gradient within the Tethys Himalaya, 17 samples were selected for X-ray powder diffraction analyses on clay minerals and determination of illite «crystallinity». These samples were taken either from the dolomitic Thidsi Member of the Karsha Formation or from the micritic horizons of the Lipak Formation and one sample comes from the Hanse Formation. The extraction and analytical method follows that of Holtzapffel (1985) and of Moore and Reynolds (1989) for carbonaceous rocks and is similar to the one used by Spring (1993) in the adjacent region of Sarchu.

Only 14 samples proved to be suitable for the determination of the illite «crystallinity» index (I.C.) which is obtained by measuring in mm. the width at half-height of the illite 10Å reflection on both air dried and glycolated slides (Kübler, 1968).

The results are presented in fig 5.5 and show that the I.C. values of all samples except one are comprised in a range between 1.5 and 2.0. Such values are again characteristic of epizone metamorphism or lower greenschist facies and do not show any significant variation of the metamorphic grade in the studied area. The only sample that shows a greater «crystallinity» value comes from the Hanse Formation and shows an I.C. of 2.7 indicative of upper anchizone metamorphism.

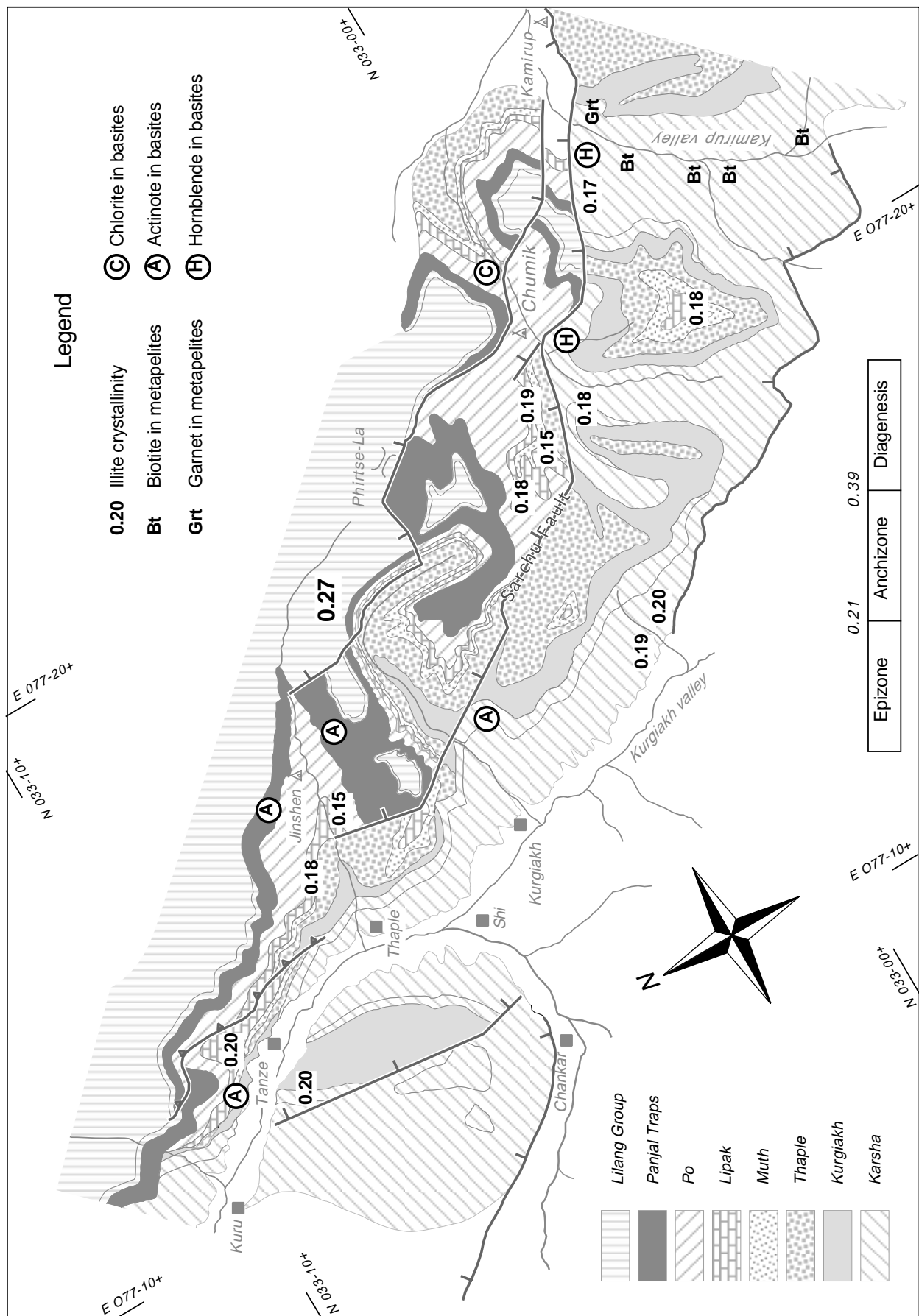


Fig. 5.5: Geological map of the Tethys Himalaya in SW Zanskar. This map shows the location of the illite samples with their crystallinity value. Also represented are the index minerals in the basic and pelitic rocks as discussed in the text.

These results are in agreement with those presented by Garzanti and Brignoli (1989) for the same area. On the Basis of X-ray powder diffraction, illite and chlorite «crystallinity» and petrographic observations, these authors also obtained lower epizone values for the Cambrian to Permian sedimentary formations (Phugtal Unit) and upper anchizone values for the Triassic Formations (Zangla Unit).

Three of the seventeen selected samples did not contain illite but revealed the presence of talc and chlorite as the dominant phyllosilicates. These three samples all come from the Kenlung Serai Unit and were taken at the base of the Cambrian Karsha Formation, at the footwall of the Sarchu Fault. A close microscopic examination of these dolomitic samples also revealed the presence of talc flakes. After Bucher and Frey (1994), talc is stable in dolomites at temperatures lower than 500° when the metamorphism is of orogenic type. This observation is again in acceptance with the interpretation of Spring (1993) that the Kenlung Serai unit, which forms the footwall of the Sarchu Fault, partly reached lower amphibolite facies.

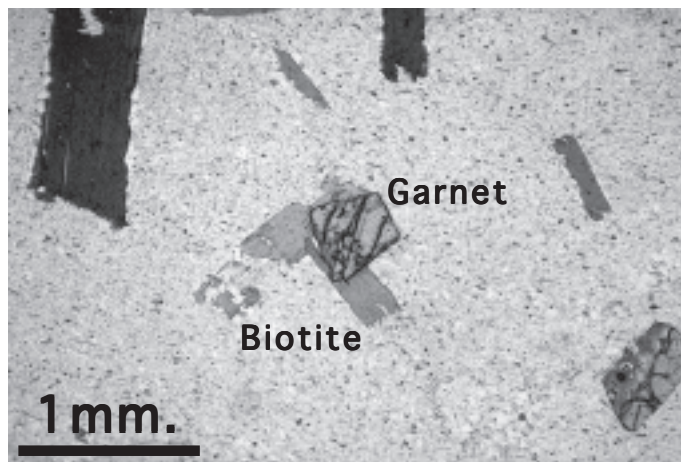


Fig. 5.6: Metapelite from the Cambrian Karsha Formation at the entrance of the Kamirup Valley. Note the randomly oriented biotite flakes

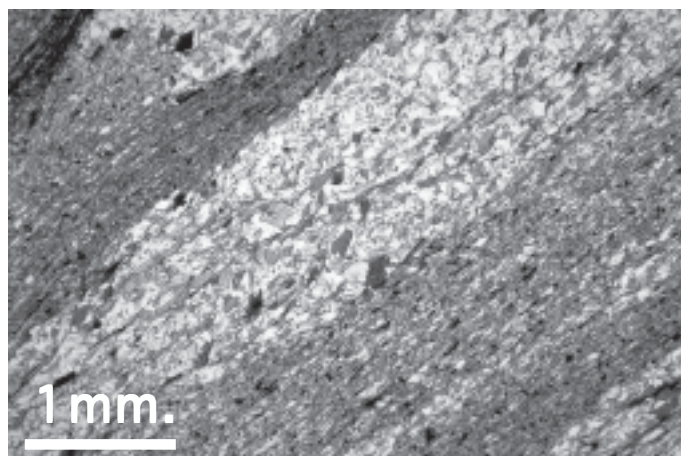


Fig. 5.7: Metapelite from the Cambrian Karsha Formation at the bottom of the Kamirup Valley. This rock is spotted with tiny biotite flakes, barely distinguishable with the naked eye.

The Kamirup valley is also the only sector of the whole investigated area where we have found biotite and garnets in the pelitic horizons of the Karsha Formation (figs. 5.6 and 5.7). Both minerals do however only occur at the bottom of the cliffs on both sides of the valley. In these samples, a fine-scale sedimentary layering is still preserved. The sedimentary layers are cut at low-angle by an oblique slaty cleavage marked by the alignment of tiny muscovite and chlorite grains. The biotite and garnet porphyroblasts are randomly oriented and grew statically over the cleavage. The fine-grained groundmass of these rocks consists of chlorite, muscovite, quartz and some tourmaline. The metamorphic gradient then diminishes upwards, for 300 meters above the floor of the valley biotite disappears and only chlorite and muscovite are present. The illites of the Lipak Formation at the top of the mountain between the Kamirup river and Chumik Marpo have an I.C. of 0.18 indicating epizone conditions. This testifies to an upward decrease of the metamorphic gradient within the Kenlung Serai unit from lower amphibolite facies at its base (Karsha Fm.) towards lower greenschist facies at its top (Lipak Fm.).

Our metamorphic study of the Tethys Himalaya also reveals a northwestward decrease of the metamorphic gradient within the Padum-Kenlung Serai Unit from the Kamirup region towards the Tanze area. The observation that the lowermost part of the Kenlung-Serai Unit reaches lower amphibolite facies between Sarchu and Chumik Marpo whereas the same stratigraphic levels exposed along the Kurgiakh river are only of lower greenschist facies is interpreted as resulting from a diminution of the overburden between these two areas. This is supported by the fact that, as described in chapter 2, the thickness of the Paleozoic formations diminishes considerably towards the northwest.

The throw of the Sarchu Fault also seems to diminish considerably towards the northwest. From Sarchu to Chumik, there is indeed a marked metamorphic contrast between the mesozonal Kenlung-Serai Unit forming the footwall of this fault and the anchizonal Chumik Unit forming its hanging wall (Spring, 1993). Such a contrast in metamorphic grade between these two units was not observed more towards the northwest, as our study shows that all the sedimentary formations below the Zangla Unit are of epizone grade along the Kurgiakh river. Moreover, the Sarchu Fault itself disappears somewhere between Thaple and Jinshen. We thus believe that the Sarchu Fault is a rotational fault and that the Kenlung-Serai and the Chumik Unit merge into a single unit, in the region of Thaple. This unit corresponds partly to the Phugtal Unit as defined by Baud et al. (1984) but only for the area NW of Thaple. The prolongation of this unit towards the Lahul as drawn by Baud et al. (1984) is indeed erroneous as was later shown by Steck et al. (1993) and Vannay (1993). In this region, there is indeed no tectonic contact between this unit and the HHCS. Furthermore, the Phugtal Unit is not an individual nappe as proposed by Baud et al. (1984). In this study, we will define the Phugtal Zone as representing the sedimentary series (Upper Precambrian to Upper Permian) comprised between the HHCS and the Zangla Unit

5.3.3 High-grade Metamorphism along the Kamirup valley

As mentioned above, the mouth of the Kamirup valley is marked by the presence of the Sarchu Fault. This high-angle normal fault brings into direct contact the Triassic rocks of the Lilang Group with the Cambrian rocks of the Karsha Formation (fig. 4.10). The rocks in the hanging wall of this fault have undergone an anchizonal metamorphism, whereas the rocks in the foot-wall of this fault are of epizone to mesozone grade. Garnet was found in a single location at the entrance of the valley in a muscovite rich metapelite of the Karsha Formation (fig. 5.6). The very limited occurrence of garnet in this area might be the result of a chemical control. Upstream and away from the Sarchu fault, the metapelitic rocks at the floor of the valley contain the mineral assemblage: biotite + chlorite + plagioclase + muscovite + quartz, typical of the Barrovian biotite zone (fig. 5.7). Seven kilometres from the mouth of the Kamirup valley, the metamorphic grade increases abruptly. Over a very short distance of less than one kilometre, one can observe the successive apparition of garnet, staurolite and finally kyanite in the metapelitic rocks. On the left side of the valley, these metamorphic zones are wrapped around a dome-shaped leucogranitic intrusion. This intrusion represents the easternmost occurrence of Tertiary leucogranites in the Zanskar-Lahul area. The zone of high-grade metamorphism is very restricted both laterally and vertically. Indeed, further upstream, the metamorphism decreases as quickly as it increased to reach again biotite zone grade. It thus appears that peak metamorphic conditions in the Kenlung Serai Unit are not found directly at the contact with the Sarchu Fault as was proposed by Spring (1993) but several kilometres to the south of the fault (fig. 5.4).

Deformation within these high-grade rocks is intense, the kyanite and staurolite prisms are systematically reoriented in a SW-NE direction. Microboudinage affects both minerals and the growth of muscovite in the necks of the boudins testifies of deformation under retrograde metamorphic conditions. The presence of late sillimanite, andalusite and cordierite crystals also testifies to a late retrograde metamorphic event. Shear sense criteria indicate nearly horizontal top to the northwest movements. Late high-angle brittle normal faults dipping 50-60° separate the high-grade rocks from the biotite zone Karsha metasediments. This small outcrop of high-grade rocks in the Kamirup valley is very similar to the restricted outcrop of kyanite grade rocks that was described by Steck et al. (1993), Spring (1993) and Fuchs and Linner (1995) several kilometres south of the Sarchu Fault along the Manali-Leh road.

We interpret these two occurrences of high-grade rocks within the Kenlung Serai Unit, both in the Kamirup valley and south of Sarchu as representing outcrops of the summit of the Gianbul dome. The combination of ductile shearing along the ZSZ and late high-angle normal faults brought the top of the HHCS dome into narrow contact with the overlying low- to medium-grade Kenlung Serai Unit. More to the west, along the Kurgiakh valley, the exhumation of the HHCS was more intense and the top of the HHCS reached higher structural level such as that the equivalent of the Kenlung-Serai unit was totally eroded. The metamorphic zonation observed along the Kurgiakh valley is the subject of the next paragraph.

5.3.4 The metamorphic transition between the TH and the HHCS across the ZSZ

All along the NW-SE trending Kurgiakh valley, the transition between the TH and the HHCS occurs within the 1 km-thick mylonitic Zanskar Shear Zone. The low-grade metasediments of the Karsha Formation at the base of the TH form the hanging wall of this structure. Within the narrow zone defined by the ZSZ, the metasediments of the Phe Formation. show, from top to bottom, a reduced but complete succession of biotite to kyanite zones, indicating a rapid downward increase in metamorphic conditions. The footwall of the ZSZ is then formed by the high-grade metamorphic rocks and leucogranitic plutons of the HHCS.

5.3.4.1 The Biotite Zone

We have already given above a description of the porphyroblastic growth of the biotites associated with the SW vergent Nyimaling Tsarap nappe (D2-D3) for the regions south and west of the Gumburanjun mountain. In the area between the northern end of the Gumburanjun and Chankar, extensional movements (D4) associated with the ZSZ are clearly evidenced by C'-type shear band cleavages (fig. 5.9). At the top of this mylonitic zone, the biotite poikiloblasts form mica fishes moulded by S4. Further down, and as ductile deformation becomes more intense, biotite forms flakes that define the main fabric associated with extensional shearing.

High angle normal brittle faults (fig. 5.10) and pseudotachylites (fig. 5.11) associated with the last episode of exhumation (D6) are frequently observed within the biotite zone. These late movements shatter the biotite blasts which are then often pseudomorphed by chlorite (retrograde pseudomorphism).

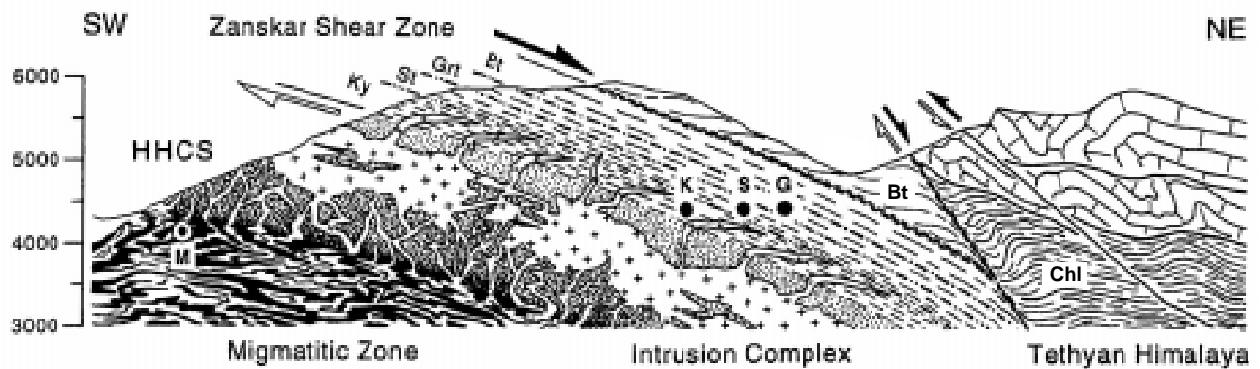
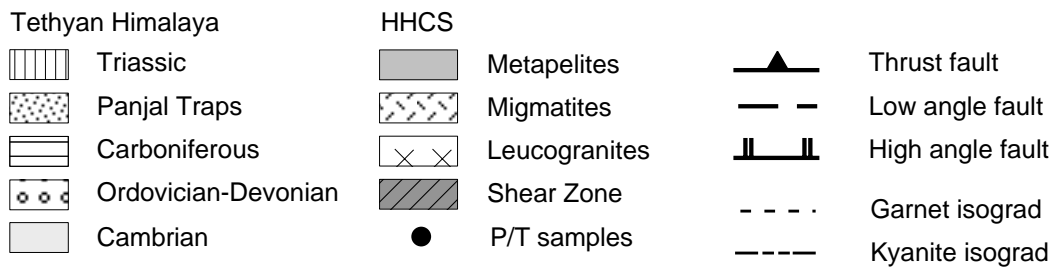
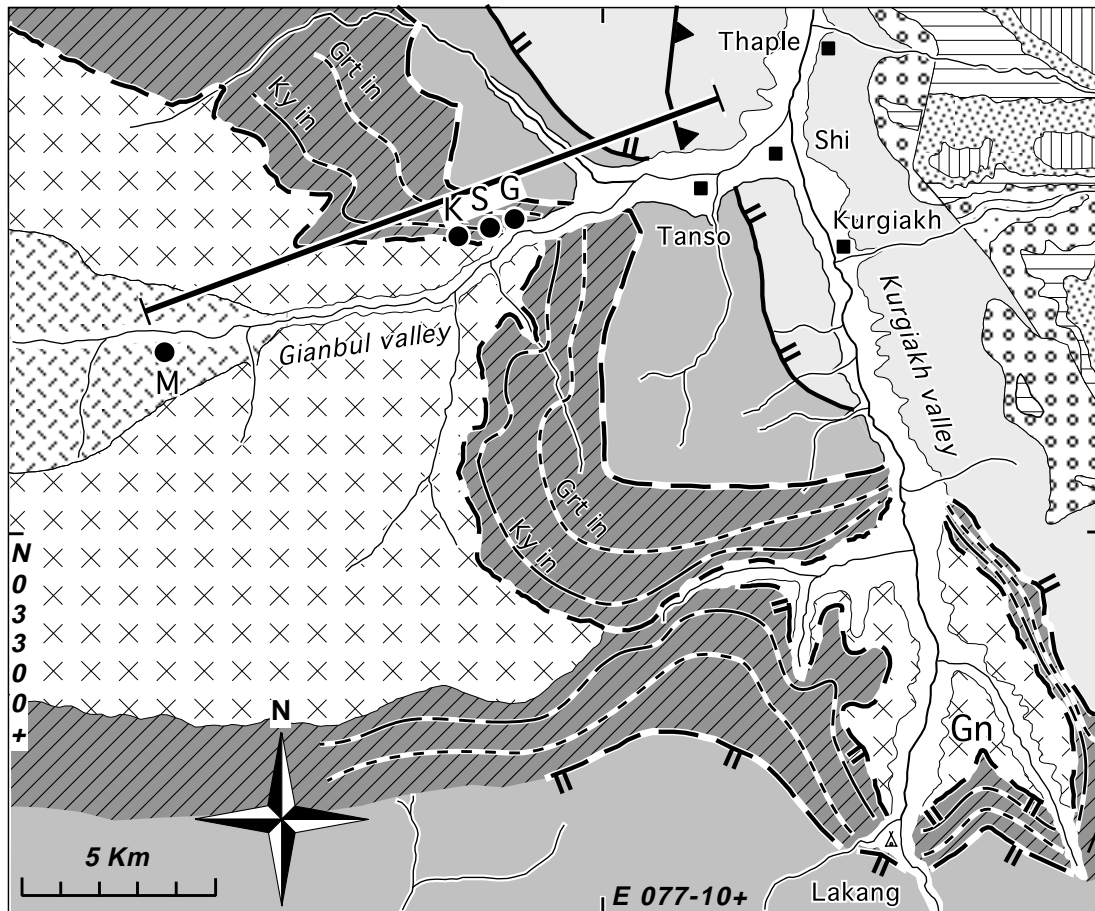


Fig. 5.8: Geological map of SW Zanskar and cross-section of the Zanskar Shear Zone along the Giambul valley. Ky (kyanite), St (staurolite), Grt (garnet) and Bt (biotite) labels refer to metamorphic mineral zones. Black dots labelled G, S, K and M indicate the position of the garnet zone to migmatite zone samples analysed for thermobarometry. Gn stands for Gumburanjun mountain. Vertical scale in meters, no vertical exaggeration.

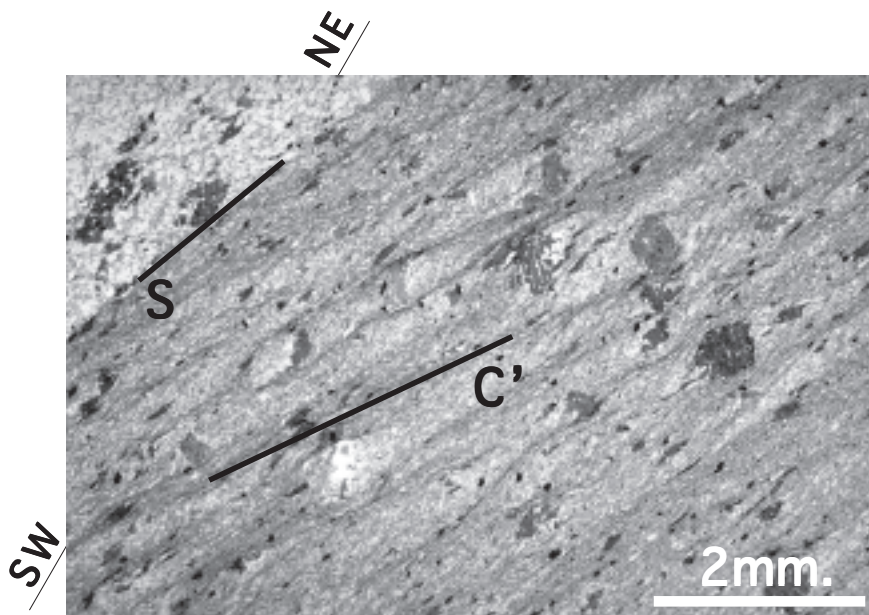


Fig. 5.9: C'-type shear band cleavage (D4) in a metapelite from the biotite zone. Top of the Zanskar Shear Zone, Giambul valley. This picture should be rotated 60° to the right.

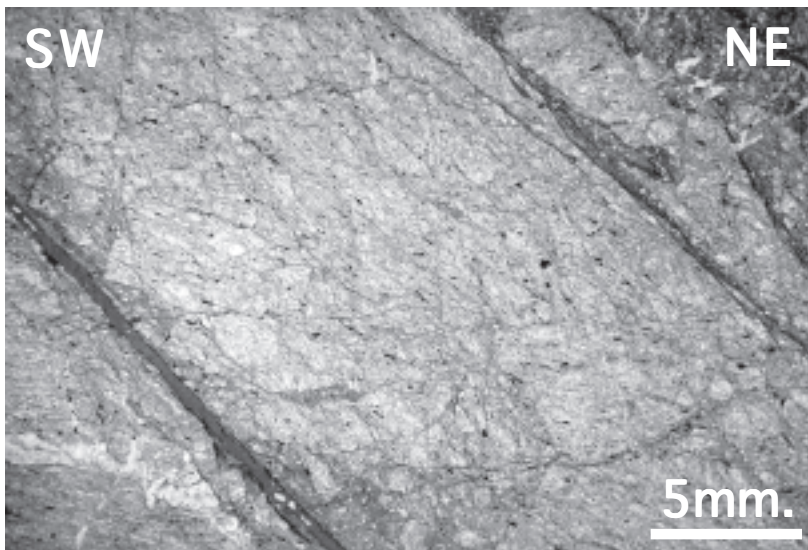


Fig. 5.10: High-angle brittle faults (D6) in a metapelite from the biotite zone. Brittle deformation transformed this rock into a cohesive cataclasite. Biotite porphyroblasts are retromorphosed into chlorite. Kurgiakh valley

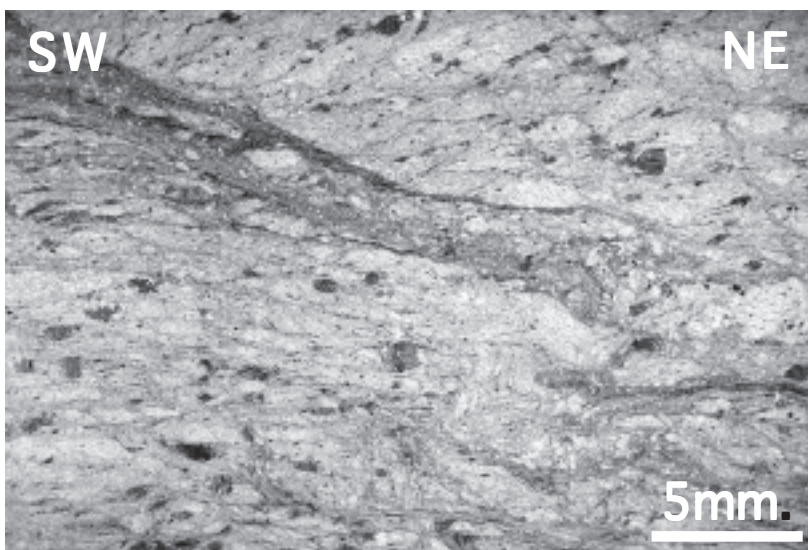


Fig. 5.11: Pseudotachylite in a metapelite from the biotite zone. The biotite porphyroblasts are shattered. fragments from a same grain display different extinction angles under plane polarised light. Kurgiakh valley.

5.3.4.2 The Garnet Zone

Garnet first appears within mafic horizons of the Phe Formation in association with amphibole, plagioclase, epidote, quartz, carbonates and titanite. These horizons have a centimetric to decimetric thickness and their contact with the surrounding rocks of the pelitic sequence is gradual. These «metabasic» strata most probably have a volcano-sedimentary origin but might also result from the metamorphic transformation of marls. The amphiboles have an elongated acicular texture and are often grouped in radiated aggregates. Their chemical composition reveals that they belong to the calcic amphibole group and plot in a field between tschermakites and ferrotschermakites. As their Al^{IV} content is greater than 1.0, they correspond to aluminotschermakites (or aluminoferrotschermakites) after the classification of Leake et al. (1997). The garnets are often found as inclusions within the amphiboles and have a composition of alm_{40-70} , grs_{10-30} , sps_{5-20} , prp_{3-10} and adr_{3-4} . The Plagioclases have a wide range of composition, their percentage of anorthite varying between 40-80%. The absence of chlorite indicates that these rocks have reached temperatures above 550°C and their mineralogical composition is typical of epidote-amphibolite facies.

Garnet then appears in the metapelitic horizons in close contact with the metabasites and finally as a commonly found mineral within the metapsammitic-metapelitic rocks of the Phe formation. The texture of these rocks also changes from phyllites in the biotite zone to micaschists in the garnet zone, showing a mylonitic texture defined by alternating quartz-rich and mica-rich layers. The typical mineral assemblage in these rocks is:

garnet + biotite + chlorite + muscovite + plagioclase + quartz ± epidote ± tourmaline

The garnets have a composition of alm_{75} , grs_5 , sps_5 , prp_{10} and adr_5 , and the anorthite percentage in the plagioclases varies between 20 and 30%. The stability of $Grt + Bt + Chl + Ms + Qtz + H_2O$ is limited by the discontinuous reactions $Clid + Bt + H_2O = Grt + Chl$ and $Grt + Chl = St + Bt + H_2O$ in the MnKFMASH system. As chloritoid is absent in the studied area, the lower limit of the stability field given above represents the minimal conditions at which garnet might appear. However, in our samples garnet most probably appears because of the continuous reaction $Chl + Ms + Qtz = Grt + Bt + H_2O$

The aspect of the biotites changes as the metamorphic conditions inside of the garnet zone increase. In the pelitic rocks close to the mafic horizons, biotite still preserves the same poikiloblastic aspect as in the biotite zone. With increasing metamorphic grade, deformation becomes more intense and the biotites, together with muscovite, are regrouped as flakes into beds that define the main foliation (S4).

The garnets are often heavily clouded, such as to sometimes appear nearly opaque in plane polarized light. Some of the garnets display an atoll texture with biotite and muscovite grains in their core. Most of the garnets do however contain inclusion trails of quartz and opaque minerals. These inclusion trails either form straight lines or helicitic structures within the garnet poikiloblasts. The garnets with straight inclusion trails are restricted to the upper structural part of the garnet zone, whereas the garnets with sigmoidal inclusion trails appear in the lower structural part of the garnet zone. Depending on their structural position, the garnets are thus either post-tectonic or syn-tectonic with respect to D3. All the garnets are then moulded by a later external mylonitic foliation (S4) and show asymmetrical strain shadows.

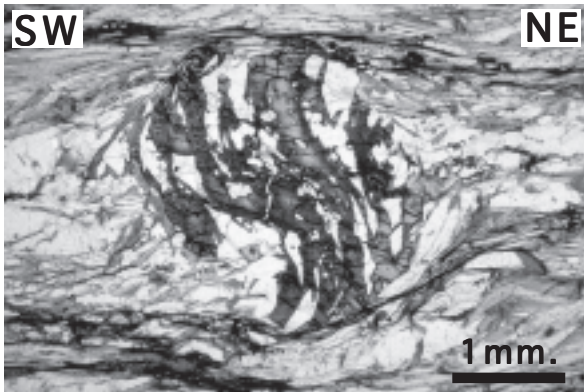


Fig. 5.12: D3 syntectonic garnet porphyroblast in a metapelitic rock from the Garnet zone (Giambul valley). Shear sense criteria deduced from the helicitic inclusion trails indicate top to the SW rotation of more than 180°.

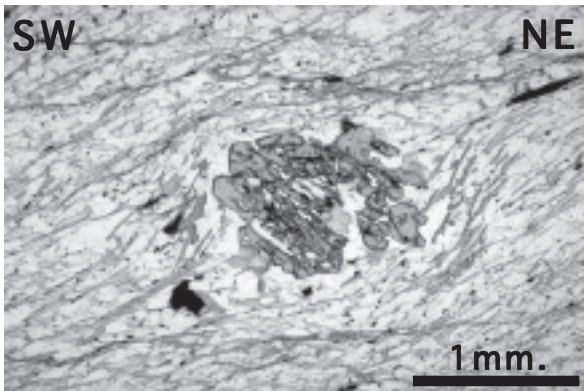


Fig. 5.13: Mantled garnet porphyroblast in a metapelitic rock from the garnet zone (Gianbul valley). Assymetrical strain shadows indicate top to the NE sense of shear (D4).

The study of the deformation structures in the mylonitic rocks from the garnet zone is very interesting as it reveals that these rocks have undergone two major phases of ductile deformation showing opposite sense of shear. The oldest phase of deformation is preserved as inclusion trails within the poikiloblastic garnet grains, and shear sense criteria for this phase are given by the syn-tectonic «spiral-Si» garnets. These spirals of inclusion show a rotation of up to 180° and systematically indicate a top to the S-SW sense of shear. This feature reveals unequivocally that the growth of these garnets is contemporaneous with ductile, top to the S-SW, shearing associated with the burial of the HHCS below the TH (D3). In the matrix, the shear sense criteria associated with this early tectonic event are totally obliterated by a later ductile deformation which shows an opposite, top to the NE, sense of shear. Shear sense criteria related to this second event are given by asymmetrical strain shadows (sigma-type tails) around the garnet porphyroblasts and the development in the matrix of a C/S fabrics followed by later C'-type shear bands. This intense late deformation is clearly caused by the top to the NE extensional movement along the Zanskar Shear Zone (D4).

5.3.4.3 The Staurolite Zone

The staurolite zone can easily be overlooked because it forms a very narrow zone and because staurolite only grows within the most pelitic horizons of the Phe formation which are rare. The rocks from this zone have a lustrous silvery aspect and are coarser grained than the rocks from the garnet zone. Staurolite when present forms honey-brown prismatic blasts which quite frequently reach centimetric size. The diagnostic mineral assemblage for this zone is:

staurolite + garnet + biotite + muscovite + chlorite + plagioclase + quartz

In the less pelitic horizons of this zone, staurolite is however absent and the mineral assemblage remains the same as for the garnet zone. The very limited thickness of the staurolite zone is partly explained by the fact that, for a Barrovian type metamorphism, the P-T conditions, where the assemblage $St \pm Grt + Bt \pm Chl + Ms + Qtz + H_2O$ is stable, are limited by the reactions $Grt + Chl = St + Bt + H_2O$ and $St + Chl = Bt + As + H_2O$ which define a very restricted domain of temperature (30°C) in the MnKFMASH system (for $X_{sps} = 0.1$, the maximum content in the analysed garnets).

As for the Garnet zone, two main phases of deformation are preserved within these rocks. The main penetrative schistosity is defined by the phyllosilicates and moulds the staurolite and garnet porphyroblasts. Some elongated staurolite grains have been reoriented NE-SW by this deformation and shear sense criteria (mantled porphyroblasts, C/S and C'-type shear bands) indicate a top to the NE sense of shear. Again, this foliation is related to ductile extensional movements along the ZSZ (D4). An earlier foliation is preserved

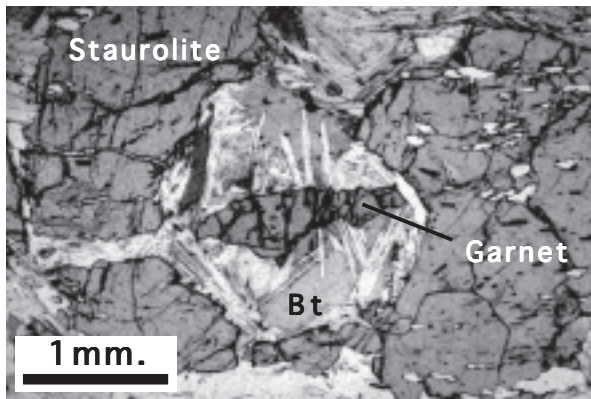


Fig. 5.14: Staurolite porphyroblast containing a relic garnet grain. Garnet is partially substituted by an assemblage of biotite and muscovite. Staurolite zone, Kurgiakh valley.

as inclusions within the staurolite blasts, but these inclusions give no information neither on the shear sense of this deformation nor on the crystallisation history of the staurolite with respect to this early tectonic event. It is however more than likely that this early event is the same D3 event as in the garnet zone. Staurolite growth is thus either syn- or post-tectonic with respect to the burial of the HHCS below the TH. Garnet is frequently found as inclusions within the staurolite poikiloblasts which indicates that the rock from the staurolite zone first underwent garnet zone metamorphic conditions.

5.3.4.4 The Kyanite Zone

Kyanite often grows as elongated tabular crystals at the contact between quartz veins and pelitic horizons of the Phe formation. Such association between kyanite and quartz veins is frequently observed also in other metamorphic terranes like the Alps and is of great help to detect the kyanite isograd. Locally kyanite forms decimetric lenses in association with staurolite, quartz and plagioclase. These lenses are wrapped by biotite-rich layers. Kyanite also occurs in pegmatitic rocks in association with quartz and plagioclase where both kyanite and plagioclase sometimes form 10 centimetre long individual crystals. Kyanite however also occurs as millimetric grains disseminated within the metapelitic horizons of the Phe Formation. The metapelitic rocks of the structurally upper part of the kyanite zone are characterized by the mineral assemblage:

kyanite ± staurolite + biotite + muscovite + plagioclase + quartz

In these rocks garnet is only preserved as inclusions inside staurolite or kyanite grains and was otherwise completely consumed by the reaction: $\text{Grt} + \text{Chl} = \text{St} + \text{Bt}$. Chlorite is also absent from these rocks, most likely because it was consumed to form kyanite by the reaction $\text{Chl} + \text{St} = \text{Bt} + \text{Ky}$. This reaction stopped once all the chlorite was consumed, which explains the presence of staurolite in association with kyanite. Staurolite is sometimes found as inclusions within kyanite grains testifying of prograde metamorphic conditions. Both Kyanite and staurolite form poikiloblasts overgrowing S3 and moulded by S4.

Lower in the kyanite zone and as metamorphic conditions increase, the metasedimentary rocks of the Phe Fm start to acquire a gneissic texture and are characterized by the following mineral assemblage:

kyanite + garnet + biotite + muscovite + plagioclase + quartz

Staurolite is only preserved as relic inclusions within garnet poikiloblasts (up to 1 cm), which indicates that staurolite was consumed and that a second generation of garnet was formed by the reaction: $St = Grt + Bt + Ky + H_2O$ (staurolite-out isograd). The garnets also contain quartz and opaque inclusion trails which often form beautiful helicitic spirals showing a rotation angle of more than 300° . As for the earlier mentioned syntectonic garnet porphyroblasts of the garnet zone, the

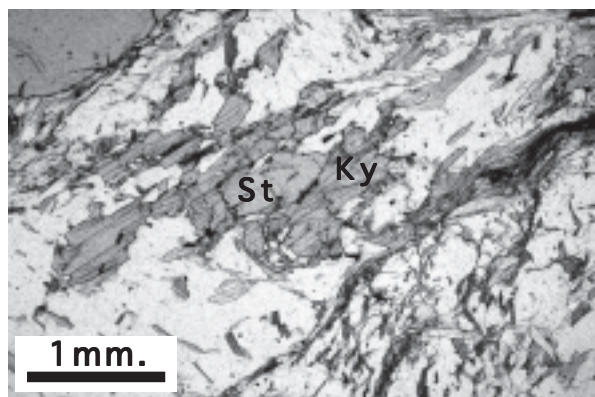


Fig. 5.15: Kyanite (Ky) porphyroblast containing a relic staurolite (St) grain. These grains are set in a matrix of quartz, plagioclase, muscovite and biotite. Upper kyanite zone, Kurgikh valley.

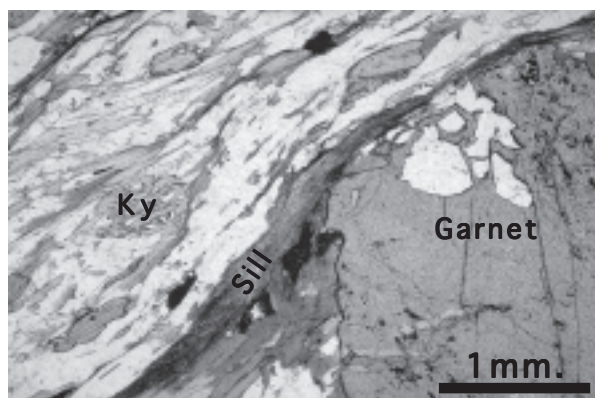


Fig. 5.16: Porphyroblasts of kyanite and garnet are set in a matrix of quartz, plagioclase, K-feldspar, biotite and muscovite. A trail of fibrolitic sillimanite is wrapped around the garnet. Although not visible on this picture, the garnet porphyroblasts frequently contain inclusions of staurolite. Lower kyanite zone, Gianbul valley.

sigmoidal inclusion trails in the present garnets do also indicate that they grew during a ductile top to the SW shearing episode associated with the underthrusting of the HHCS below the TH (D3). The garnet and kyanite poikiloblasts are moulded by the external foliation. Shear sense criteria in the matrix (winged porphyroblasts, C/S and C'-type shear bands) systematically show top to the NE movements associated with ductile extensional shearing along the ZSZ (D4).

The lowermost part of the kyanite zone is characterized by incipient migmatisation in the paragneisses. In these rocks the mineral assemblage is: **kyanite + K-Feldspar + garnet + biotite + muscovite + plagioclase + quartz.**

The apparition of K-feldspar and incipient melting of these rocks could still be related to prograde metamorphism with the reaction $Ms + Pl + Qtz = Kf + \text{kyanite} + \text{melt}$, but as these rocks also show late metamorphic growth of sillimanite associated with extensional shearing (D4), it is more likely that incipient migmatisation and the growth of K-feldspar (and sillimanite) are the consequence of a later retrograde decompression metamorphism and are due to the reaction $Ms + Pl + Qtz = Kf + Sill + H_2O$. Retrograde metamorphism will be discussed later in more details.

Directly below these migmatitic gneisses is the contact with the roof of large leucogranitic intrusion, and the lowermost kyanite zone paragneisses themselves are intruded by several generations of leucogranitic dikes escaping from the top of these magmatic bodies.

A metric to decametric layer of calc-silicate rocks quite systematically occurs close to the top of the leucogranitic intrusions. These calc-silicate are banded and are formed by garnet or vesuvianite rich layers alternating with quartz rich layers. The garnets and the vesuvianite form large crystals, often of pluricentimetric size, overgrowing millimetric diopside and forsterite grains. Titanite, carbonates and sheelite are also present in these rocks. These impure marbles are boudinaged by extensional shearing along the Zanskar Shear Zone.

5.3.4.5 The Intrusion Zone

Below the kyanite zone, the metamorphic succession is interrupted by a 1-2 kilometre thick intrusion zone, where large amounts of leucogranitic melts have been injected into the metasedimentary rocks of the HHCS. The uppermost part of this intrusion complex is marked by the presence of individual dikes which criss-cross the migmatitic paragneisses of the Phe Formation. Most of these dikes are reoriented and boudinaged by ductile shearing and represent one of the most spectacular argument for extensional, top to the NE, movements associated with the Zanskar Shear Zone.

At a structurally deeper level these dikes become more and more abundant, such as to finally form a compact leucogranitic sheet in the footwall of the ZSZ, where individual dikes cannot be differentiated any more. This sheet has an approximate thickness of one kilometre, and the massive leucogranitic cliffs of the Gumburanjun mountain are part of this zone. Scarce bits of metapelitic country rocks are preserved within these leucogranitic «plutons». These country rock fragments have an angular shape and are composed of biotite + quartz + plagioclase (oligoclase - andesine). The absence of muscovite, garnet, K-feldspar or aluminosilicates might be the consequence of a leaching process, where fluid circulation associated with the intrusion of leucogranitic magmas depleted the host-rock of certain elements.

A foliation is preserved within these blocks which shows a constant orientation as well between different blocks as with the country rock. These rocks have thus preserved their original orientation and were not tilted inside of the leucogranitic intrusion. The overall texture of the intrusion zone is agmatitic with angular rafts of country rocks cemented by leucogranites. The leucogranites will be discussed in more detail in chapter 6.

The lower part of the intrusion complex is formed by migmatitic gneisses intruded by a dense network of vertically ascending leucogranitic dikes which represent the feeder-dikes of the leucogranitic plutons. These feeder-dikes are rooted into the migmatitic zone which is the structurally lowermost metamorphic zone in this area.

5.3.4.6 The Migmatitic Zone

The Migmatitic zone has recorded the highest grade metamorphic conditions in the studied area. This zone is characterized by pervasive anatexis of the HHCS rocks and represents the most

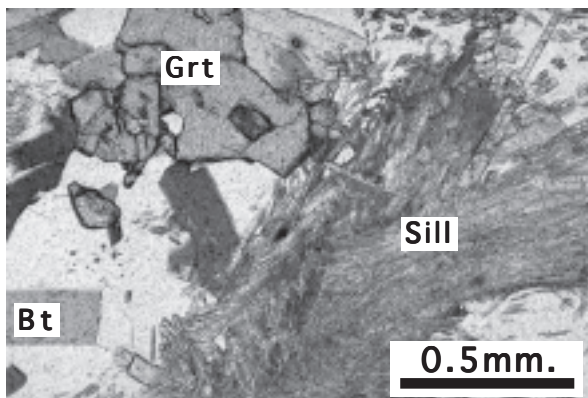


Fig. 5.17: Sillimanite k-feldspar biotite gneiss. Corroded remnants of garnet (Grt) porphyroblasts, partially replaced by biotite (bt) and sillimanite (sill). Migmatitic zone, Gianbul.

likely source for the leucogranites. The term migmatite is here used in its broad sense, a more accurate name for these rocks would be «diatexite» as they have undergone extensive partial melting and the leucosomes are volumetrically dominant over the restitic elements. Migmatization is here so intense that it is not possible to establish whether the protolith of these migmatites are the metasediments of the Phe formation or the Cambro-Ordovician granites. The leucosomes are essentially composed of K-Feldspar and quartz with minor biotite, muscovite, plagioclase, garnet and sillimanite. The

melanosomes are predominantly formed by biotite, quartz and sillimanite with minor plagioclase, garnet, tourmaline, apatite and monazite. Some muscovite grew late in replacement of sillimanite and biotite during retrograde metamorphism.

The mineral assemblages of the metapelitic (or quartzo-feldspathic) sequence give little information on the peak metamorphic condition that were reached in the migmatitic zone as they have re-equilibrated at low P/lowT during retrograde metamorphism. The virtual absence of muscovite, and the large quantities of leucogranitic melt that escaped from the migmatitic zone to form the overlying intrusion complex clearly indicate, however, that the metamorphic grade was sufficient to allow for fluid-absent melting.

Decimetric boudins of metabasic rocks sometimes occur within the quartzo-feldspathic migmatites. The core of these boudins preserves indications on the peak metamorphic condition of the migmatitic zone. These rocks show a typical granulitic texture and are formed by the assemblage

garnet + clinopyroxene + amphibole + plagioclase + quartz + titanite.

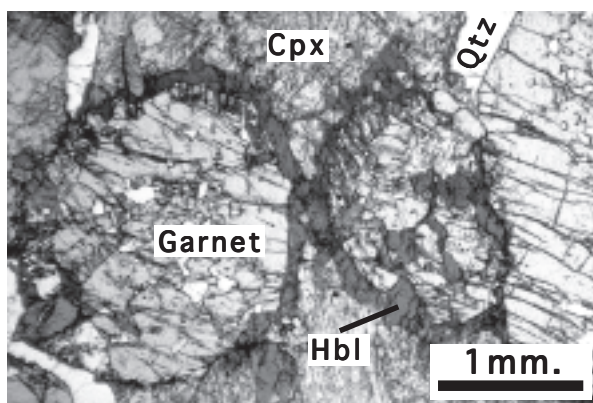


Fig. 5.18: High-pressure granulite facies metabasite composed of garnet, clinopyroxene (Cpx), plagioclase and quartz (Qtz). Retrograde hornblende (Hbl) grows preferentially at the contact between between garnets and clinopyroxenes. Migmatitic zone, Gianbul valley.

The clinopyroxenes belong to the augite group, are Calcium-rich and have the composition of salites. The amphiboles are hornblendes (s.l.) and more exactly ferropargasites. The garnets are essentially composed of almandine and grossular and the plagioclases are almost pure anorthites. This assemblage is formed through continuous reactions resulting in the modal increase of garnet and clinopyroxene at the expense of hornblende and plagioclase. This is testified by inclusions of the latter minerals in the former ones. A single relict biotite grain was also preserved in a garnet porphyroblast.

The granulitic metabasites also show evidences of retrograde metamorphism, first with the development of hornblende-rich rinds at the contact between the metabasic lenses and the surrounding quartzo-feldspathic migmatites and secondly, with the symplectic growth of hornblende and quartz at the contact between garnets and clinopyroxenes.

The mineral assemblage and the texture of the metabasic rocks typically forms along the kyanite geotherm at temperatures above 700°C (Bucher and Frey, 1994) and can be found both in upper amphibolite or high-pressure granulite facies metabasites. A clear indication that granulite facies conditions were reached would be given by the presence of orthopyroxene which appears in metabasic rocks above ~ 800°C (Spear 1993). Orthopyroxene does however not form in high-pressure granulites, even above 800°C.

As muscovite is virtually absent from the metapelitic migmatites, but biotite is still present and shows no sign of destabilisation, the metamorphic grade must have been sufficient to allow for the breakdown of muscovite but not of biotite. The break-down of muscovite occurs through the reaction:



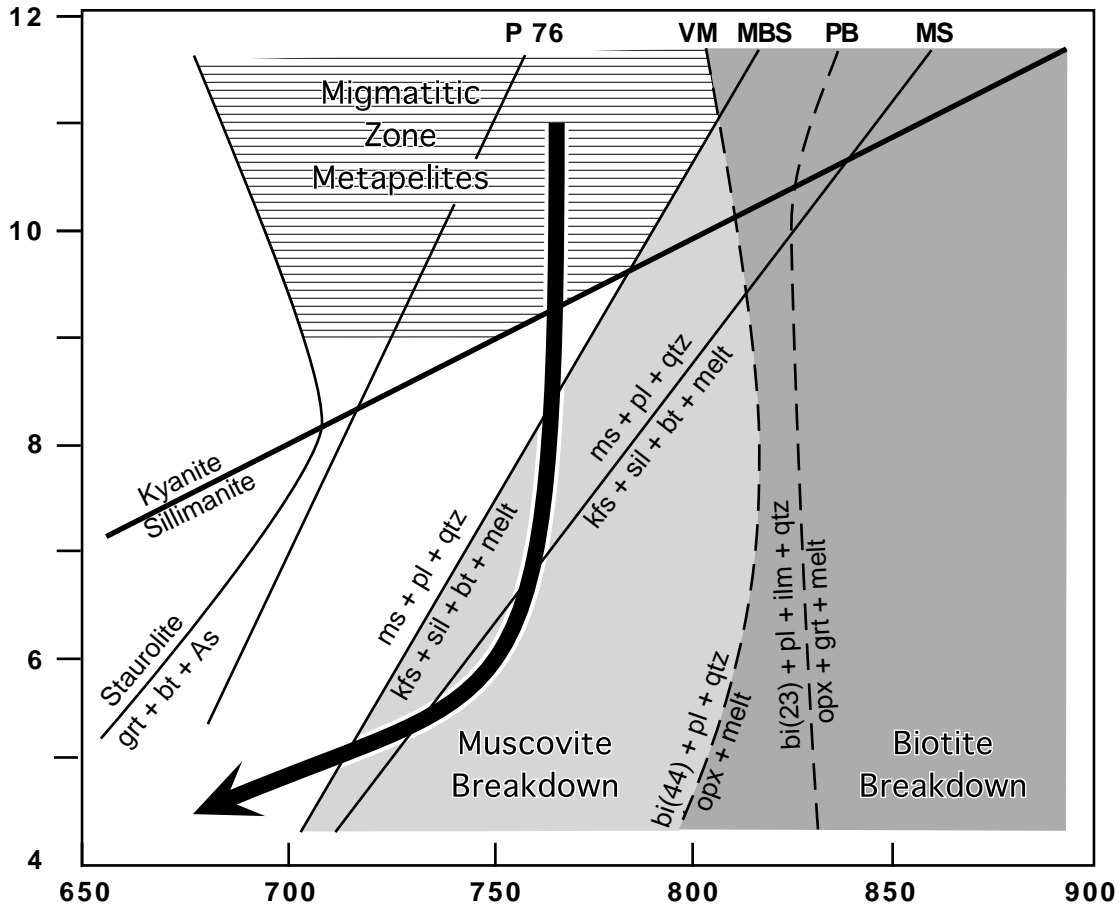


Fig. 5.19: Petrogenetic grid showing the vapor-absent melting reactions for pelites. The two muscovite dehydration-melting solidi were obtained by Patiño-Douce and Harris (1998) through experimental melting of a muscovite + biotite bearing micashist from Zanskar (MBS) and a muscovite bearing micashist from Nepal (MS). The dashed lines are solidi for dehydration melting of biotite (with mg-number in parentheses) in bulk composition lacking muscovite and an aluminosilicate phase, curve VM was obtained by Vilzeuf and Montiel, 1994 and PB by Patiño-Douce and Beard, 1996. The line labelled P 76 is the dehydration-melting solidus for end-member muscovite + albite + quartz, determined by Petö (1976). The staurolite break-down reaction curve is from Spear, 1993. The probable stability field of the migmatitic zone at peak barrovian P-T conditions is shown with a striped hatch-pattern. This field was estimated considering that metapelites from this zone must have crossed the staurolite-out reaction curve, that they were at higher pressure than the overlying kyanite zone (910 kbar from thermobarometric results) and that they have never crossed the biotite dehydration-melting curve. The thick black arrow represents the adiabatic decompression path that we propose for the metapelites of the migmatitic zone.

This figure shows that partial melting through vapour-absent dehydration of the rocks from the migmatitic zone did not occur at peak P-T conditions during the prograde M2 barrovian event but that ensuing isothermal decompression of these high-grade rocks during M3 led them to intersect the muscovite dehydration-melting curve, thus triggering anatexis and the production of leucogranitic melts.

As this reaction has a relatively low dP/dT slope, the temperatures at which the break-down of muscovite occurs are highly dependant on the pressure. Three such reaction curves are shown in figure 5.19. The first curve is a theoretical curve, obtained for the end-members muscovite + albite + quartz and predicts temperatures between 700° and 770°C for pressures between 7 and 12 Kbars (Petö, 1976). These temperatures are lower than those shown by the two other curves obtained by Patiño Douce and Harris (1998) through experimental melting of two metapelitic samples from the HHCS (one of them from Zanskar) at different P/T conditions. The natural starting material differs from the model end-member assemblage by the presence of Calcium in the plagioclase and Fe, Mg, Ti and F in the muscovite. The effect of these elements is to extend the thermal stability field of the assemblage Ms + Pl + Qtz of 50° to 80 °C relative to that of the equivalent end-member assemblage. We consider these values obtained through melt experiments on natural samples to be more reliable than the theoretical values obtained through thermobarometric modelling on end-member composition.

We have also represented in figure 5.19 the dehydration-melting curves for biotite as calculated by Vilzeuf and Montiel (1994) and Patino Douce & Beard (1996) for different Mg numbers. The minimal temperature for the break-down of biotite is 800°C and is very little dependent on pressure variations. As these reaction curves are steeper than those for the breakdown of muscovite, these two reaction curves intersect at high-pressure. The minimal pressure for this cross-over to occur is 9 kbar, above which biotite reacts before muscovite to produce melts (above 800°). As the destabilisation of biotites was not observed in our samples, the migmatitic zone should not have exceeded this temperature.

In short, both the metabasic and the metapelitic assemblages constrain the peak temperatures reached by the migmatitic zone to values slightly below 800°C. The peak pressure of the migmatitic zone can be estimated to have reached values above 9 kbar, first because of the $Grt \pm Cpx + Hbl + Pl + Qtz$ assemblage of the metabasites and secondly, because the structurally overlying kyanite zone already experienced such pressures (Staurolite-out reaction along the Ky-geotherm occurs ~ 9 Kbar).

At temperatures below 800°C and pressures above 9 kbar, it is quite unlikely that the migmatitic zone produced leucogranitic melts through dehydration melting of muscovite. On the other hand, vapour-present melting is not possible because this would result in melts of trondhjemitic composition and the observed intrusions have a leucogranitic composition.

Thus, to explain the widespread anatexis, the incongruent melting of muscovite and the production of leucogranitic melts that occurred in the migmatitic zone, we infer that these rocks must have undergone isothermal decompression such as to cross the dehydration curve of muscovite. Isothermal decompression paths (such as the one shown in fig. 5.19) intersect the relatively flat dehydration melting solidus of muscovite schists, triggering anatexis, which continues until relatively shallow depths. In contrast, the steep solidi for dehydration melting of biotite are almost parallel to isothermal decompression paths. This means that, if biotite schists remain unmolten when buried deeply in an orogen, they are also unlikely to melt during ensuing decompression.

We will see later that other independent arguments sustain the interpretation of peak metamorphic conditions followed by retrograde isothermal decompression.

5.3.4.7 Discussion

The metamorphic grade within the Tethys Himalaya increases slowly and progressively from the upper structural unit (Zangla) towards the lower structural units (Chumik and Kenlung Serai units). The metamorphic grade reaches lower greenschist facies at the base of the TH along the Kurgiakh valley and lower amphibolite facies in the Chumik Marpo - Kamirup area. The transition between the TH and the HHCS is then characterized by a very rapid, although still progressive, increase in metamorphic grade from biotite zone to kyanite zone over a vertical distance of little more than one kilometre. This transition zone coincides with a major tectonic structure, the ZSZ. The footwall of the ZSZ is formed by leucogranitic intrusions and migmatitic rocks belonging to the HHCS.

The successive prograde assemblages from the ZSZ are typical of a medium-pressure Barrovian metamorphic field gradient. The successive apparition, with increasing metamorphic conditions, of biotite, garnet, staurolite and kyanite as well as the systematic absence of Chloritoid within our rocks indicates that they correspond to low-Al metapelites. Their estimated composition is shown by a star in AFM diagrams in figure 5.20. These AFM diagrams show the most important changes that metapelitic rocks experience with increasing metamorphism along the Kyanite geotherm. Our interpretation of the pressure and temperature stability conditions of the metapelite mineral assemblages characteristic of each metamorphic zone is based on a petrogenetic grid adapted to the observed compositions (fig. 5.20). Most of the reactions limiting these stability fields have a steep dP/dT slope, implying a strong temperature control on the characteristic mineral equilibria. Little information can however be obtained from this petrogenetic grid on the pressure variation between each zone.

A Barrovian field gradient is generally the consequence of orogenic (regional) metamorphism and corresponds to a prograde metamorphic path along a kyanite-type geotherm as shown in figure 5.20. This figure however shows that such a prograde metamorphism along the kyanite geotherm implies an important pressure increase from biotite zone to kyanite zone and therefore, that a Barrovian metamorphic zonation should develop over a vertical distance of 10-20 kilometres. In the studied area, the Barrovian zones are, however, condensed in a 1-km. thick zone. We will here discuss two possible ways to produce such a condensed Barrovian zonation.

The first possible explanation is that the rocks at the base of the Tethys Himalaya reached greenschist facies conditions (biotite zone) along a particularly steep geotherm (HP / LT) such as to reach pressures of about 7-8 kbars. These rocks would subsequently have been heated by a deep-seated intrusion (i.e. leucogranites) producing a Barrow-type zonation over a short vertical distance through contact metamorphism.

The second hypothesis to explain the observed condensed Barrovian metamorphic zonation is that the rocks were initially metamorphosed along the kyanite geotherm (as would be expected in a collision orogen) and that these metamorphic zones were subsequently telescoped by extensional ductile simple shear deformation along the ZSZ during the exhumation of the HHCS.

The first hypothesis, although theoretically possible (Spear, 1993), does not seem to be appropriate in our case for the following reasons:

- In the studied area the footwall of the ZSZ is systematically in contact with large leucogranitic plutons which could be invoked as the necessary heat source. These leucogranitic bodies are however missing in northwestern Zanskar where the same telescoping of the metamorphic zones within the ZSZ was described by Herren (1987), which leaves us, for this region, without a heat source.

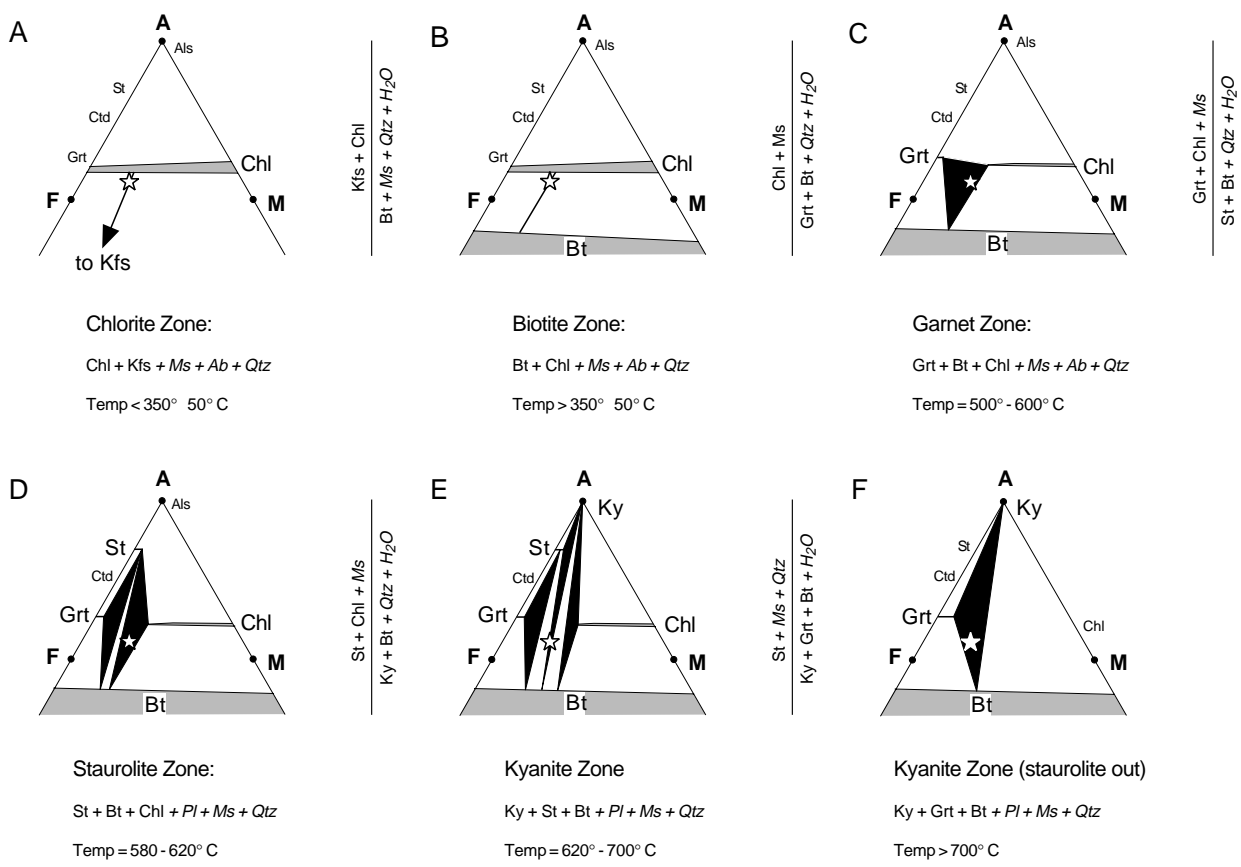
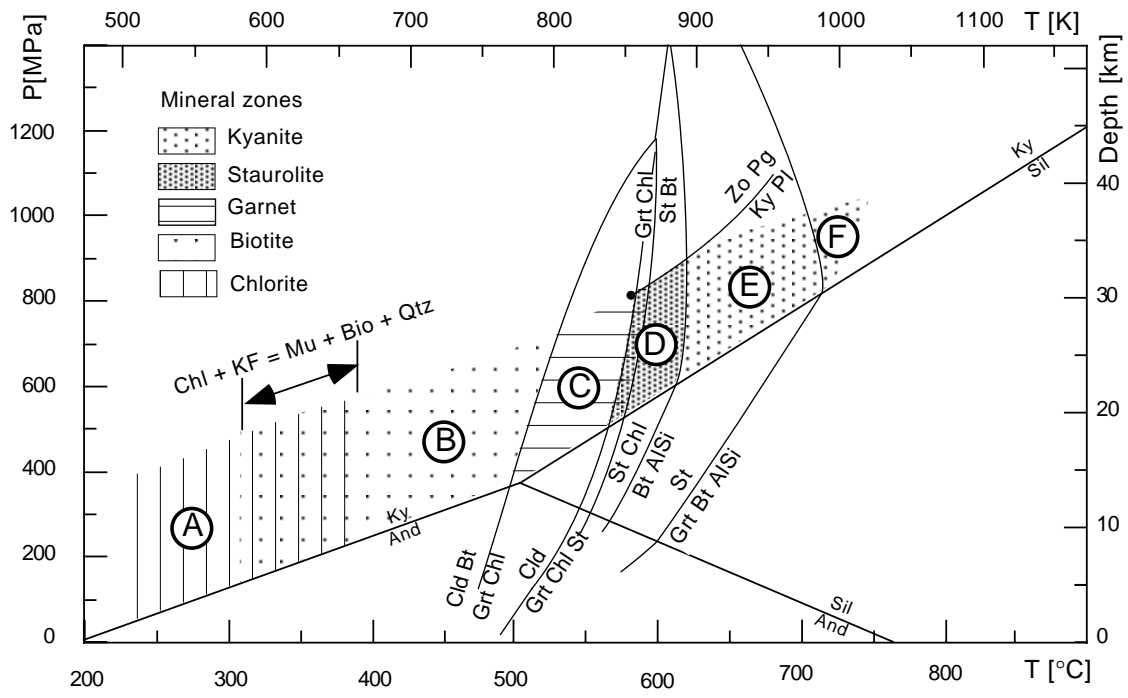


Fig. 5.20: Composite Petrogenetic grid for metapelitic rocks showing the stability fields of the successive prograde mineral assemblages observed within the transition zone between the Tethys Himalaya and the High Himalayan Crystalline. Circled letters A to G refer to mineral assemblages in Thompson (1957) diagrams depicted below. The reaction curves delimiting the garnet stability field are for $X_{\text{sp}} = 0.1$ which corresponds to the maximum value of the analysed garnets. Discontinuous reaction curves after Spear 1993.

- In the adjacent regions of Lahul and Western Suru, deformations associated with the ZSZ are weak or non-existent and the Barrovian zones in these areas are much thicker (6,3 km between the garnet and the sillimanite isograd in the region of Suru).
- Structural observations indicate that the prograde metamorphic minerals grew before the intrusion of the leucogranites.

Moreover, this hypothesis leaves us with no explanation for the cause of migmatization below the leucogranites, and thus the presence of the leucogranites themselves would be rather challenging to explain.

The second hypothesis seems much more likely because the telescoping of the Barrovian zones always coincides with ductile extensional shearing associated with the ZSZ. Moreover, the thermobarometric data presented below indicate a marked pressure difference between garnet zone and kyanite zone.

5.3.5 Thermobarometry

On the basis of the petrographic observations and the petrogenetic grid (fig. 20), we could establish pretty precisely the temperature stability conditions of the characteristic mineral assemblages of each zone. To quantify these temperatures more accurately and to obtain information on the pressure conditions of each zone, we resorted to thermobarometric analyses.

13 samples were selected for thermobarometry, on the basis of mineral and textural characteristics suggesting that peak metamorphic equilibria have been preserved. 6 of these samples are metabasites and 7 are metapelites.

Of the 6 metabasic samples, two (G1, G2) come from the garnet zone and two from the staurolite zone (S2, S3). These samples contain the stable assemblage: $\text{Hbl} + \text{Grt} + \text{Pl} + \text{Qtz} \pm \text{Ep}$. The two last samples are from the migmatitic zone (M1, M2) and are characterized by the assemblage: $\text{Cpx} + \text{Hbl} + \text{Grt} + \text{Pl} + \text{Qtz} (+ \text{Ttn})$.

Of the 7 metapelitic samples one comes from the garnet zone (G3), with the assemblage $\text{Grt} + \text{Bt} + \text{Ms} + \text{Pl} + \text{Qtz} + \text{Chl}$, one from the staurolite zone (S1), with the assemblage $\text{St} + \text{Grt} + \text{Bt} + \text{Ms} + \text{Pl} + \text{Qtz} + \text{Chl}$, three from the kyanite zone (K1, K2, K3) with the assemblage $\text{Ky} + \text{St} + \text{Grt} + \text{Bt} + \text{Ms} + \text{Pl} + \text{Qtz}$ and two from the migmatitic zone (M3, M4) with the assemblage $\text{Sill} + \text{Grt} + \text{Bt} + \text{Kfs} + \text{Pl} + \text{Qtz} \pm \text{Ms}$.

5.3.5.1 Analytical procedure

Chemical analyses were made at the University of Lausanne using a Cameca SX 50 electron microprobe operated with an acceleration voltage of 15 kv and a beam current of 30 nA for garnet, 15 nA for biotite, muscovite and hornblende, and 10 nA for plagioclase. An average of 10 analyses were made on rims of relevant minerals. Special care was taken to analyse the outermost rim of relevant adjacent phases such as to reduce the disequilibrium effects. Average rim compositions are presented in Tables A1 to A5. Analytical procedure and uncertainty propagation follow the approach of Hodges & McKenna (1987). The thermobarometry calculations were performed with a program written by K.V. Hodges, using the solution models and calibrations summarized in Table. 5.2.

A different procedure was used for samples M1 and M2 which contain the assemblage garnet + plagioclase + hornblende + clinopyroxene + quartz + titanite. The thermobarometry calculations for these two samples were performed with the thermodynamic data base and computer program TWQ 2.02 (Berman, 1991; Berman et al., 1995; and references therein).

5.3.5.2 Results:

The calculated pressures, temperatures and depth of equilibration for each sample are summarized in Table 5.1. When complete assemblages were present in the metapelites for solution of the GASP and GMAP barometers, both solutions are shown. The GAPH barometer yields two solutions.

The results of rim thermobarometry are represented in P-T diagrams (figs. 5.21 and 5.22) and are grouped by metamorphic zone. The calculated values are shown with their error ellipses. The ellipses represent 95% confidence precision of the thermobarometric calculation based on the propagation of analytical uncertainties, using the Monte-Carlo approach. The coherence between P-T results obtained with different sets of thermobarometers, either for the same metapelitic samples or for metapelitic and metabasic samples from the same zone indicates well equilibrated assemblages. All samples fit, within uncertainties, the stability conditions deduced from the petrogenetic grid for the garnet to kyanite zone assemblages. This indicates that the P-T results represent equilibration conditions close to the peak of metamorphism.

The pressure and temperature profiles through the Zanskar Shear Zone and the migmatitic zone are plotted in two schematic logs in figure 5.23 as a function of distance from the top of the ZSZ. This figure shows the rapid downward increase of both temperature and pressure.

In agreement with the field metamorphic zonation and the minerals assemblages, the P-T results confirm that a coherent and continuous Barrovian-type field gradient is preserved within the ZSZ. This gradient is characterized from the garnet zone to the kyanite zone by a temperature and pressure range of $T \sim 550^\circ$ to 700°C and $P \sim 590$ to 910 MPa.

With a «normal» lithostatic gradient of 27 MPa / km., the difference in equilibration depth between the kyanite and the garnet zone can be constrained to 12 ± 3 km. These thermobarometric data confirm that the metamorphic zones equilibrated along the kyanite geotherm at significantly different depths and that the observed telescoping of these metamorphic zones within the ZSZ is the result of extensional tectonics along this structure.

The two metabasic samples from the migmatitic zone (M1, M2) preserved peak metamorphic temperature and pressures also indicating equilibration along the kyanite geotherm. The calculated temperatures (820° and 870°C) are a little higher than the temperatures predicted by our textural and petrographic observations for the migmatitic zone. Although temperatures above 800°C could be compatible with the mineral assemblages of the metabasic rocks (orthopyroxene does not form at HP, even at T well above 800°C), such high temperature are however incompatible with the metapelitic assemblages, because the break-down of biotite, which has to start above 800°C , was not observed in the migmatitic zone. The P/T conditions obtained through thermobarometric calculations are probably overestimated because the chemical composition of the minerals is somewhat out of range for the applied calibration. Pognante (1992) obtained pressures between 9.5 and 12 kbar and temperatures between 750° and 770°C for similar Grt - Cpx - Hbl - Pl - Qtz bearing metabasites from the same area (Temasa Valley).

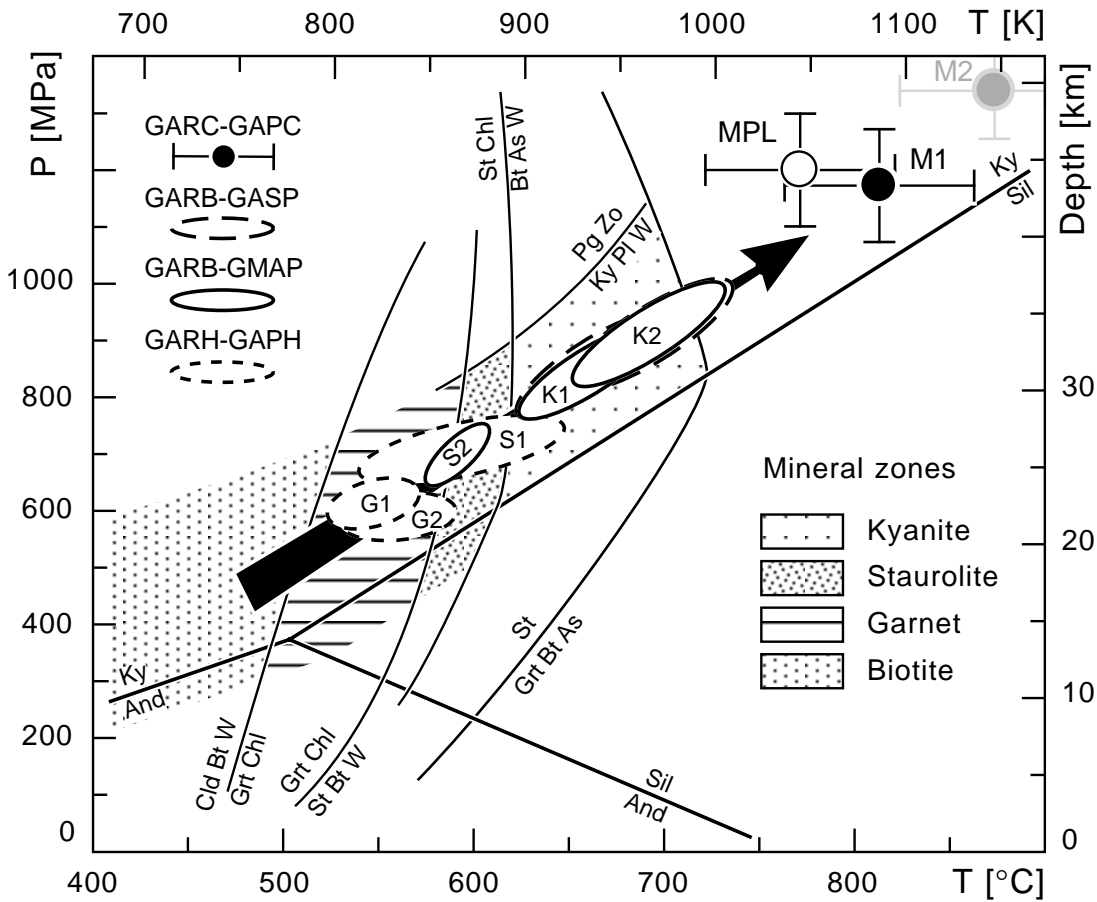


Fig. 5.21

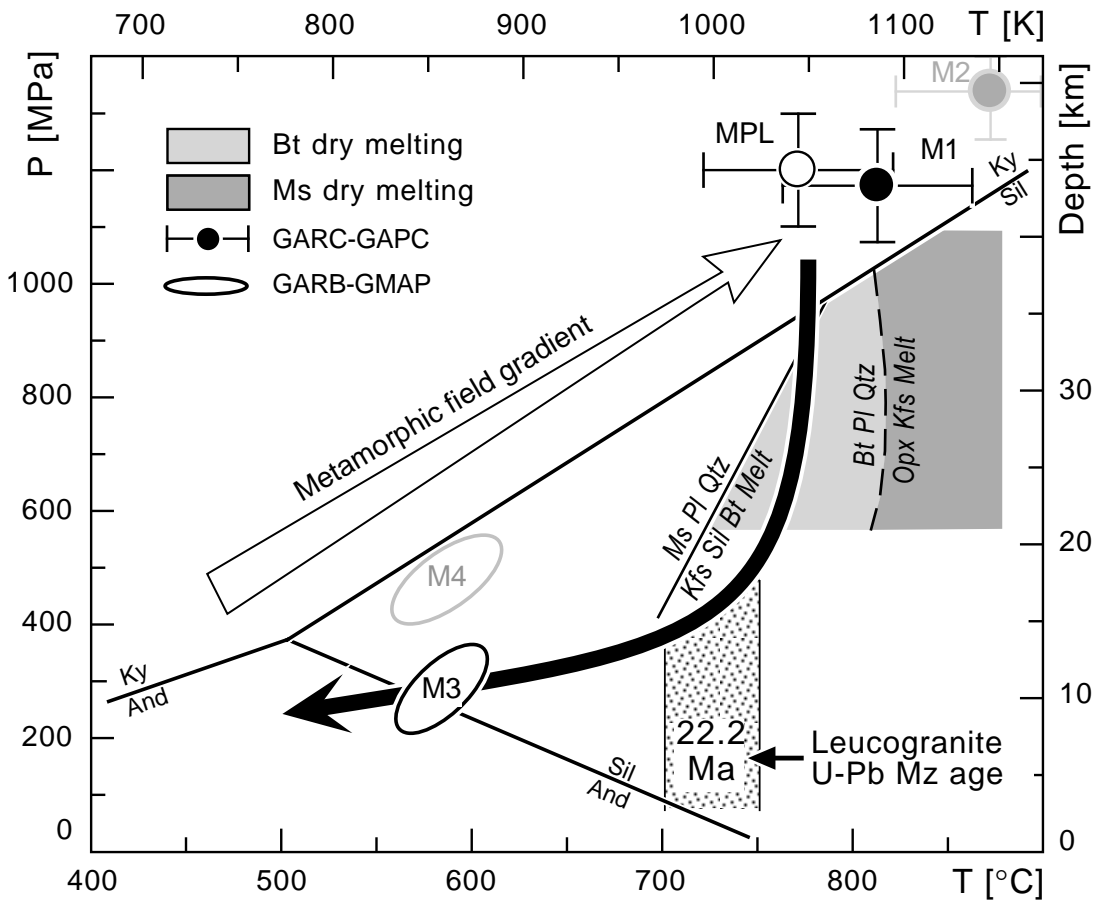


Fig. 5.22

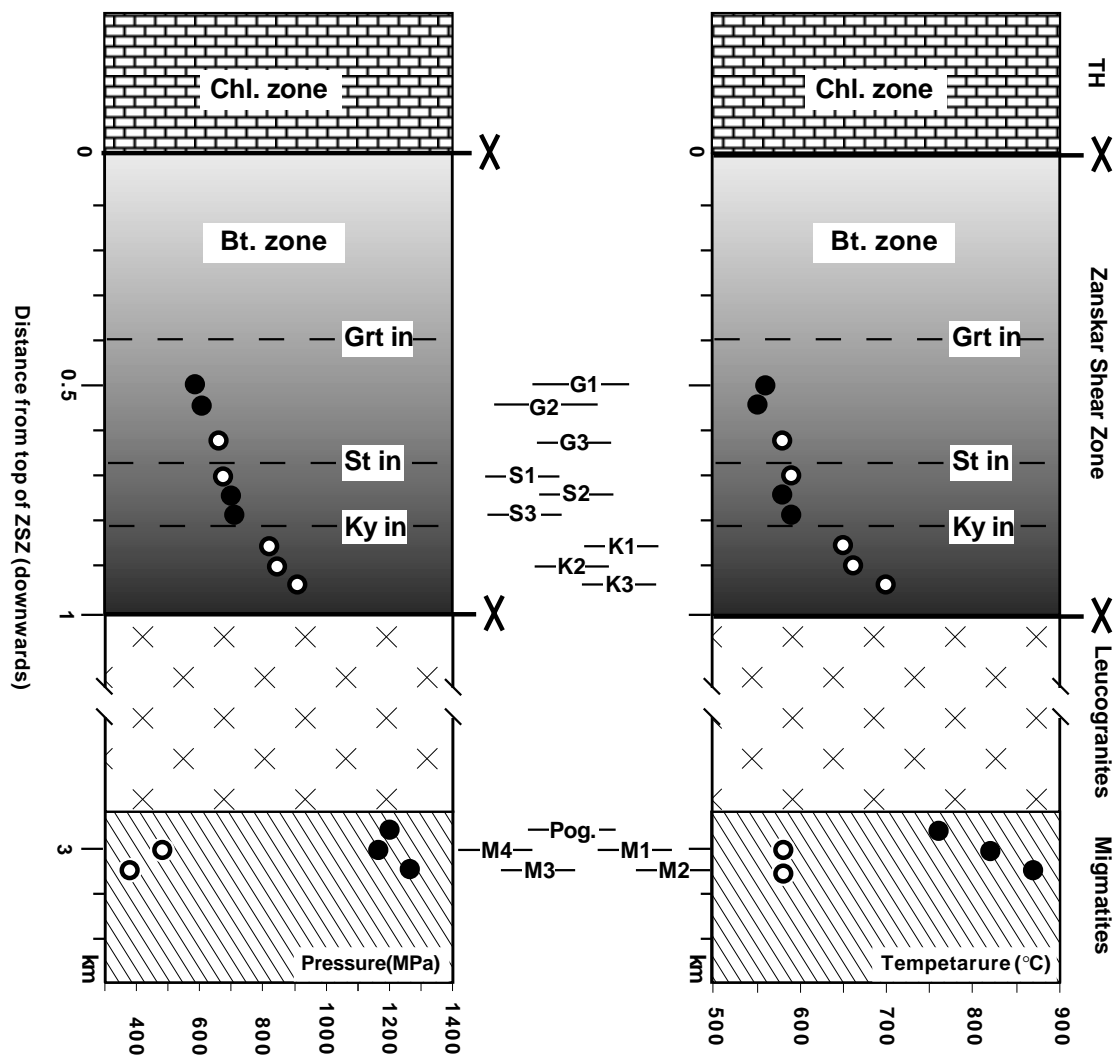


Fig. 5.23

Fig. 5.21 (facing page): Peak metamorphic conditions in the ZSZ and Migmatite Zone. The P-T stability fields for the mineral assemblages characteristic of the observed Barrovian metamorphic zones are presented in a composite petrogenetic grid. Black arrow represents the metamorphic field gradient. All reaction curves after Spear (1993). Reactions curves limiting the garnet zone field are plotted for $X_{\text{Sp}} = 0.1$ (maximum X_{Sp} content in analysed garnets). P-T determinations for the ZSZ metapelites are represented by ellipses corresponding to 2s precision. Their labels "G", "S", and "K" refer to samples from the garnet, staurolite, and kyanite zones, respectively. P-T results for the Migmatite Zone are characterized by the label "M" and nominal conservative uncertainties of ± 50 °C and ± 100 MPa are assumed for these estimates. Sample MPL after Pognante and Lombardo (1989). See Figs. 2 and 3 for sampling locations. Abbreviations: And = andalusite; As = aluminosilicate; Bt = biotite; Chl = chlorite; Cld = chloritoid; Grt = garnet; Kfs = K-feldspar; Ky = kyanite; Ms = muscovite; Opx = orthopyroxene; Pg = paragonite; Pl = plagioclase; Qtz = quartz; Sil = sillimanite; St = staurolite; W = water; Zo = zoisite.

Fig. 5.22 (facing page): Retrograde metamorphic evolution in the Migmatite Zone. Note that the arrow labelled "metamorphic field gradient" does NOT represent the prograde path followed by the samples from the migmatitic zone. The retrograde path for the Migmatite Zone is constrained by the P-T results for one metapelitic sample (sample M2), as well as by the arguments discussed in the text. For clarity, only GARB-GMAP results for metapelites are presented. Reactions after Patino Douce and Harris (1998). The 22.2 ± 0.2 Ma age corresponds to the cooling age of the Intrusion Complex leucogranite through the monazite closure temperature for U-Pb (725 ± 25 °C, Parrish, 1990), as discussed in chapter 6.

Fig. 5.23: Temperature and pressure profiles from the Zanskar Shear Zone to the migmatitic zone. Values for samples G1,2,3 (garnet zone); S1,2,3 (staurolite zone); K1,2,3 (kyanite zone); M1,2,3 and Pog. (migmatitic zone) are given in table 2. Open circles represent values for pelitic samples; solid circles represent values for mafic samples

The thermobarometric results confirm that during prograde metamorphism, the migmatitic zone reached P-T conditions close to but not necessarily sufficient to allow for the vapour-absent melting of muscovite.

The two pelitic samples from the migmatitic zone (M3, M4) yield temperatures and pressures much lower than expected ($T = 580^{\circ}\text{C}$ and $P = 3 - 4,5 \text{ kbar}$). These inconsistencies are most likely the result of late-stage re-equilibration of the phases used for thermobarometry at conditions different from maximum pressures and temperatures and thus reflect final equilibration during retrograde evolution. As mentioned earlier, in the paragraph dealing with the migmatitic zone, vapour-absent melting must have occurred through isothermal decompression of muscovite-rich rocks. The low P/T values obtained for M3 and M4 are an additional indication that isothermal decompression must have occurred at the top of the HHCS as the retrograde path joining M1 and M3 is indeed very steep (fig. 5.22).

We will see in the next paragraph, that isothermal decompression of the HHCS is also marked in the ZSZ by the growth of new mineral assemblages.

5.4 The retrograde metamorphism M3

The third tectonometamorphic event that affected the studied area is related to the exhumation of the HHCS along the Zanskar Shear Zone. During this event, the HHCS has undergone a decompression metamorphism which is marked by the growth of new metamorphic assemblages. Structural analyses reveals that the growth of these minerals is either syn-tectonic or post-tectonic with respect to extensional movements along the ZSZ. Most of these retrograde minerals were observed in the pelitic rocks of the kyanite zone and in the migmatitic zone. The order of appearance of these minerals in the kyanite zone is: sillimanite \rightarrow cordierite \rightarrow K-Feldspar \rightarrow andalusite \rightarrow margarite.

5.4.1 Sillimanite

Retrograde metamorphism starts with the apparition of sillimanite. In the kyanite zone this mineral occurs as fibrolite. This mineral is contained within the main foliation associated with extensional shearing and is oriented parallel to the main NE-SW direction of shear. Together with the apparition of fibrolite one can observe the breakdown of kyanite which reacts with quartz to produce muscovite. Kyanite grains, entirely rimmed by muscovite, are frequently observed within coarse grained samples associated with quartz veins. Fibrolite was never observed to grow directly from kyanite, or to replace it, but always to grow at the expense of micas.

In the migmatitic zone the breakdown of kyanite must have been complete as no relicts of this mineral were found. The sillimanite is here coarser grained than in the kyanite zone and forms tiny prismatic crystals. These sillimanite grains are often overgrown by quartz grains. Muscovite also grows in the rocks as a late retrograde phase.

5.4.2 Cordierite

Cordierite grains were only found in the kyanite zone. This mineral usually appears at the contact between metapelites and quartz veins where it sometimes forms decimetric nodules. Individual grains of centimetric size were observed. These are light green coloured due to their partial alteration into pinnite. Typical pleochroic halos can be observed in cordierite porphyroblasts around small monazite or zircon grains.

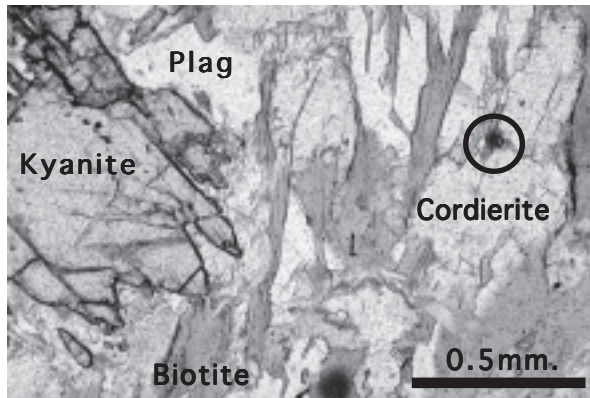


Fig. 5.24: Cordierite bearing metapelite. The cordierite grain have a slightly higher relief than the plagioclases and a pleochroic halo can be distinguished around a zircon grain within the black circle. Kurgikh valley.

into pinnite. Typical pleochroic halos can be observed in cordierite porphyroblasts around small monazite or zircon grains. Cordierite was also found to grow at the expense of kyanite grains within metapelitic schists. These cordierite-bearing metapelites are rich in light coloured biotite which testifies to a Mg-rich composition. Staurolite is systematically absent in samples where cordierite is present, which also indicates that the presence of cordierite (or staurolite) is controlled by the chemical composition of the metapelites. From an extensive review of the literature, Newton (1983) considers that cordierite is usually not stable at pressures greater than 6 kbar in most common metapelites.

5.4.3 K-feldspar

In kyanite grade metapelites, K-feldspar forms porphyroblasts sometimes overgrowing kyanite and sillimanite. The growth of K-Feldspar is syn-tectonic with respect to ductile normal shearing along the ZSZ. Fibrolite is found as inclusions within feldspar grains.

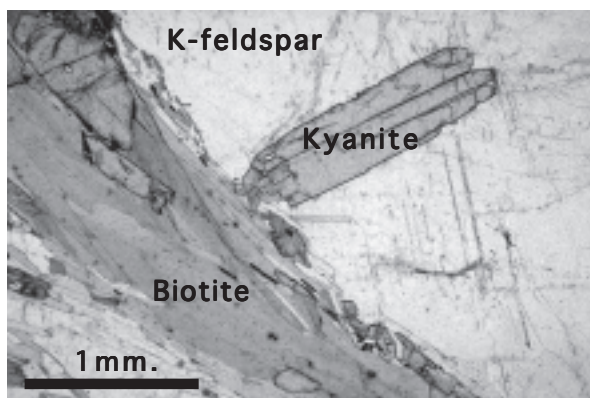


Fig. 5.25: K-feldspar porphyroblast overgrowing a kyanite grain. Lower kyanite zone, Kurgikh valley.

Large K-Feldspar crystals were also observed in pegmatitic dikes probably associated with a late pneumatolitic stage of the leucogranitic intrusions. These dikes cross-cut the kyanite zone at the base of the ZSZ without being affected by ductile extensional tectonics. In these rocks, the size of individual K-Feldspar crystals can reach up to 10 centimetres. These K-Feldspar sometimes overgrow decimetric kyanite crystals. The significance of these kyanite-bearing pegmatites is not clear.

5.4.4 Andalusite

No previous description of the occurrence of andalusite in Zanskar could be found in the literature. This mineral seems to occur rather rarely at the top of the HHCS as it has previously only been described in the Everest region (Lombardo et al., 1993; Pognante and Benna, 1993). In the studied area, andalusite forms pink euhedral crystals of centimetric size at the contact between quartz veins and metapelitic rocks. The occasional presence of relict kyanite grains within the

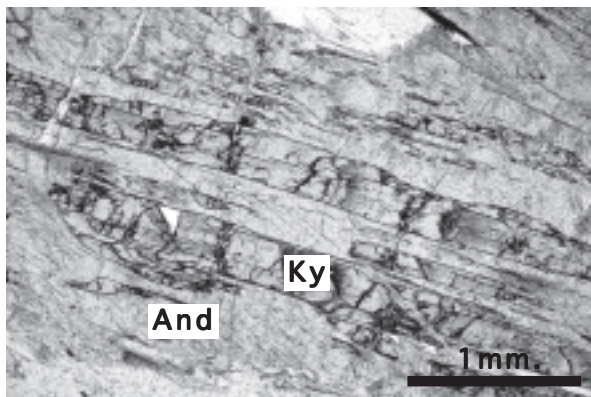


Fig. 5.26: Polymorphic transition of andalusite (And) after kyanite (ky). The field of view is dominated by a large andalusite grain with a medium relief. Some stripes of kyanite with a strong relief subsist as relicts within the andalusite. Upper kyanite zone, Kurgiakh valley.

andalusite porphyroblasts testifies to the polymorphic transition of andalusite after kyanite. In these coarse grained samples andalusite is associated with muscovite, chlorite, plagioclase, quartz and K-feldspar. In some cases, euhedral staurolite grains are preserved as inclusions within andalusite porphyroblasts. The epitaxial growth of andalusite over kyanite is also sometimes observed within the metapelitic schists. In kyanite-bearing pegmatites andalusite grows at the contact between K-feldspar and quartz in late replacement of kyanite. Andalusite is not affected by extensional tectonics and did thus crystallize once ductile normal shearing along the ZSZ had ceased.

5.4.5 Margarite

Margarite was found as a late retrograde metamorphic mineral growing at the expense of andalusite. This mineral was only found in the coarse-grained lenses of metamorphic minerals forming at the contact with quartz veins.

5.4.6 Other minerals

Retrograde metamorphic minerals are also present within calcsilicates and metabasic rocks of the kyanite and migmatitic zones.

In the calcsilicate rocks of the kyanite zone, the retrograde transformation of diopside into tremolite or chlorite is frequently observed.

In the metabasic granulites of the sillimanite zone, retrograde hornblende grows at the contact between garnets and clinopyroxenes. The growth of hornblende according to the hydration reaction: $\text{Grt} + \text{Cpx} + \text{Qtz} + \text{Pl (Na-rich)} \rightarrow \text{Hbl} + \text{Pl (Ca-rich)}$, is indicative of a pressure drop at constant temperature.

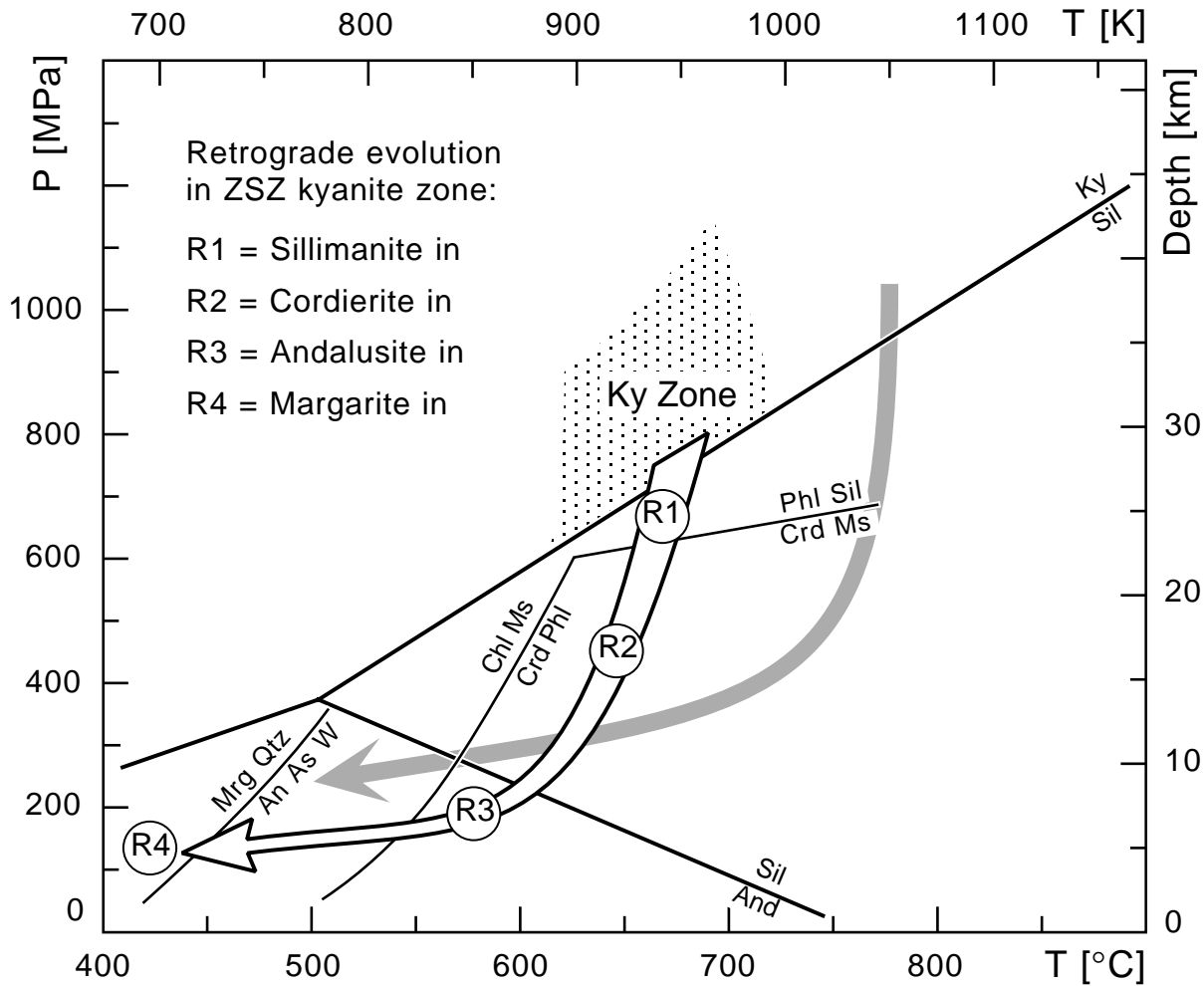


Fig. 5.27: Retrograde metamorphic evolution in the lower ZSZ. The retrograde path for the lower ZSZ (kyanite zone) is deduced from observed metamorphic mineral relations, as discussed in text. Grey arrow represents the retrograde path for the migmatitic zone as presented in fig. 5.22. Reactions after Spear (1993). An = anorthite; As = aluminosilicates; Chl = chlorite; Crd = cordierite; Ky = kyanite; Ms = muscovite; Phl = phlogopite; Mrg = margarite; Sil = sillimanite; W = water.

5.4.7 Discussion

The metapelites from the kyanite zone preserve petrographic information about their retrograde metamorphic history. The first stage of the retrograde evolution for the kyanite zone metapelites corresponds to the appearance of late fibrolitic sillimanite in some samples (fig. 5.27, point R1). The growth of sillimanite on the shearing surfaces of extensional C/S fabrics indicates extension-induced decompression. Subsequent partial replacement of kyanite by cordierite in some Mg-rich (staurolite-free) rocks confirms a decreasing pressure path (fig. 5.27, point R2). Small-scale quartz and K-feldspar segregation suggest incipient partial melting, but the presence of stable muscovite in the samples indicates that the P-T conditions reached in the kyanite zone did not induce pervasive melting. The later stages of the retrograde evolution are characterized by the appearance of andalusite as the stable aluminosilicate, which is itself subsequently replaced by margarite (fig. 5.27, points R3 and R4). These mineral changes suggest a retrograde P-T path starting with more or less isothermal decompression, and continuing with a more pronounced cooling. This retrograde P-T path, based on petrographic observations for the kyanite zone is very similar to the P-T path that can be deduced from the thermobarometric data of the underlying migmatitic zone (fig.5.22). In this zone, the metabasic granulites have retained peak metamorphic conditions associated with M2 (T ~ 800°C and P ~ 1200 MPa) but the metapelitic samples have reequilibrated at low-P / medium-T (T ~ 600°C and P ~ 350 MPa) during M3 which indicates a significant pressure drop associated with this last thermal event.

The reaction textures and mineral assemblages of the kyanite zone and sillimanite zone, together with thermobarometric data, indicate that the HHCS must have undergone isothermal decompression. Isothermal decompression of the migmatitic zone played a major role in the production of leucogranitic melts inasmuch as it maintained these high-grade rocks above the muscovite dry melting curve on a large part of the retrograde path.

The occurrence of retrograde minerals in the kyanite zone is intimately associated with the presence of leucogranitic intrusions. In the area of Mune and Reru, 30 kilometres to the NW of the studied area, leucogranitic dikes intrude the ZSZ but no large leucogranitic bodies are present in close contact with the ZSZ. The kyanite zone in this area is characterized by the presence of prograde kyanite in the metapelitic schists as well as in association with quartz veins, but none of the above-mentioned retrograde minerals could be observed within this zone. Only sillimanite occurs in this area but at a lower structural level. This sillimanite is found in migmatites showing a weaker stage of partial melting than along the Kurgiakh valley, for kyanite is still preserved as relict grains within these rocks and muscovite was never totally consumed.

There is thus a close relation between the leucogranites and the growth of late retrograde minerals. The continuous production and intrusion of leucogranites must have contributed to maintain the kyanite zone at high temperature during exhumation and thus favoured isothermal decompression and the growth of retrograde minerals in this zone. The growth of retrograde minerals was certainly also favoured by the input into the kyanite zone of enriched fluids and volatiles derived from the last stages of crystallization of the magma. A late fluid rich phase of crystallization of the leucogranites is indeed testified by the presence of late, undeformed, pegmatitic dikes.

It should, however, be emphasized that the order of crystallization of the retrograde minerals goes from high-temperature minerals (sillimanite) towards lower temperature minerals (andalusite) and that they have thus not crystallized along a prograde metamorphic path as would be expected with contact metamorphism (Buchan type). The intrusion of leucogranites within the metapelitic rocks however had a catalytic effect on the growth of retrograde minerals.

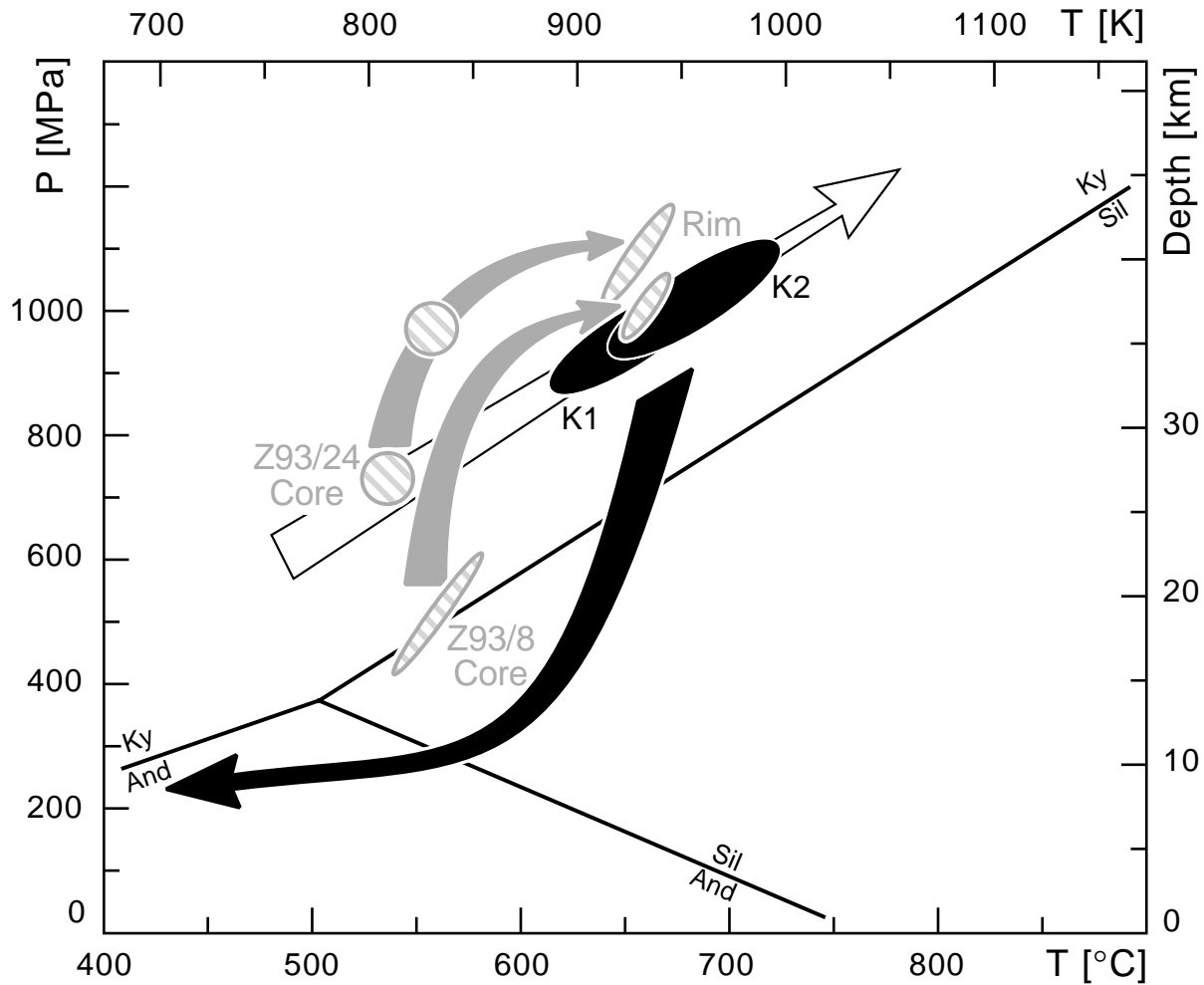


Fig. 5.28: P/T diagram showing the P-T path followed by the rocks from the kyanite zone. The grey arrows show the P-T evolution of these rocks during the growth of garnets associated to the burial of the High Himalayan Crystalline Sequence below the Tethys Himalaya (prograde metamorphic episode M2). Samples Z93/8 and Z93/24 are from the Kyanite zone in NE Zaskar. P-T condition for these two samples (grey ellipses) are from Vance and Mahar, 1998. These authors calculated the core P-T values using pseudosections and the rim values using conventional thermobarometry. Black ellipses labelled K1 and K2 are the rim values for our samples from the kyanite zone in SW Zaskar (Fig. 5.21). Black arrow represents the retrograde path followed by the samples from the kyanite zone during M3, as deduced from mineral assemblages (Fig. 5.27). White arrow represents the metamorphic field gradient within the Zaskar Shear Zone. This figure is a good illustration of the fact that the P-T path followed by a rock sample is never parallel to the metamorphic field gradient as defined by the locus of "peak metamorphic assemblages". This implies that it is not possible to infer the reaction history of a high grade rock by examination of the mineral assemblage of a rock of similar bulk composition in the low grade portion of a terrane (i.e. Spear 1993).

5.5 Conclusion

The combination of detailed petrographic observation and geothermobarometric analyses allows us to put narrow constraints on the metamorphic evolution of the studied area.

The transition between the Tethys Himalaya and the High Himalayan Crystalline Sequence is characterized by a progressive though very rapid increase in metamorphic grade which coincides with the Zaskar Shear Zone. This metamorphic zonation is the result of two subsequent tectonometamorphic events. The first event corresponds to an episode of crustal thickening associated with the southwestward thrusting of the Nyimaling-Tsarap Nappe and the burial of the HHCS below the TH, resulting in a regional metamorphism of Barrovian type. Petrographic observation and thermobarometric data indicate that the various Barrovian metamorphic zones equilibrated at significantly different peak pressures and temperatures along the kyanite geotherm.

The upper structural levels are represented by the weakly metamorphosed sedimentary series of the TH. The maximal pressures and temperatures at which these upper structural levels equilibrated (excepting the special case of the Kenlung Serai unit) can be estimated at 3 - 4 kbar and 300 - 400° C on the basis of «illite crystallinity» and mineral assemblages. Such pressures and temperatures are indicative of an overburden of 10 to 15 kilometres.

The lowermost structural level is represented by the migmatitic zone which recorded peak metamorphic pressures and temperatures of 10 - 12 kbar and 750°- 800°C corresponding to an overburden of 35 to 45 kilometres.

In-between these two extremes, all the metamorphic zone have recorded intermediate peak metamorphic P/T conditions.

The subsequent closing together of the Metamorphic zones is the result of extensional movements along the ZSZ associated with the exhumation of the HHCS. Both petrographic observation and thermobarometric estimates indicate that the exhumation of the HHCS must have been a rapid process, such as to allow for nearly isothermal decompression. The migmatitic zone is marked by a rapid pressure drop from 10-12 kbar to 3-4 Kbar. The kyanite zone records the growth of several retrograde mineral phases also indicative of isothermal decompression.

A complete P-T path (fig. 5.28) can be established for the kyanite zone of Zaskar in associating our data which constrain the retrograde metamorphic history (M3) of this zone with the data obtained by Vance and Mahar, 1998 for the prograde part of the path (M2). Peak pressure and temperature conditions that were calculated for the kyanite zone of SE Zaskar are nearly identical to those obtained by Vance and Mahar, 1998 for the same zone in NW Zaskar. This P-T path shows, in good acceptance with theoretical modelling (Spear, 1993), that crustal thickening (M2) is marked by a steep (nearly isothermal) prograde path, followed by an episode of nearly isobaric thermal relaxation. Thermal relaxation is however limited in Zaskar because crustal thickening is very quickly followed by rapid tectonic exhumation (M3), marked by an isothermal decompression path. A rapid exhumation and cooling of the HHCS might explain why, contrarily to the MCT zone (Epard et al. 1995; Vannay and Grasemann, 1998), peak metamorphic condition were very well preserved in Zaskar.

One of the major side effects of the tectonic exhumation of the HHCS was to trigger vapour-absent melting by crossing the muscovite-breakdown reaction, thus producing melts of leucogranitic composition.

TABLE 5.2: GEOTHERMOBAROMETRY RESULTS

Sample	Zone	Equilibria* (°C)	Temperature (MPa)	Pressure (km)	h† (km)	Δh#
G1	Grt	GARH-GAPH	560 ± 30	590 ± 40	22±1	0
G2	Grt	GARH-GAPH	550 ± 20	610 ± 50		
G3	Grt	GARB-GMAP	580 ± 40	660 ± 80		
S1	St	GARB-GMAP	590 ± 20	680 ± 50	26±1	4±1
S2	St	GARH-GAPH	580 ± 20	700 ± 60		
S3	St	GARH-GAPH	590 ± 50	710 ± 60		
K1	Ky	GARB-GMAP	650 ± 40	830 ± 100	31±3	9±3
K2	Ky	GARB-GMAP	660 ± 40	860 ± 90	32±2	10±2
		GARB-GASP	660 ± 40	850 ± 80		
K3	Ky	GARB-GMAP	700 ± 40	910 ± 100	34±3	12±3
		GARB-GASP	700 ± 40	910 ± 100		
Pog.	Mig	GARC-GAPC	770 ± 40	1200 ± 50		
M1	Mig	GARC-GAPC	820 ± 50	1170 ± 100	43±4	21±4
M2	Mig	GARC-GAPC	870 ± 50	1270 ± 100	47±4	25±4
M3	Mig	GARB-GMAP	580 ± 20	290 ± 80		
M4	Mig	GARB-GMAP	580 ± 30	440 ± 80		

Note: Uncertainties correspond to 2s precision, except sample M1 and M2 for which nominal uncertainties are assumed.

Methodology is given in text and mineral compositions are given in Appendix.

*Thermometers: see Table 2

† Depth of equilibration assuming a lithostatic pressure gradient of 27 MPa/km.

Difference in equilibration depths relative to garnet zone

TABLE 5.3: GEOTHERMOBAROMETRES AND CALIBRATIONS

Acronym	Reaction	Calibration
GARB	Grt (alm) + Bt (phl) = Grt (prp) + Bt (ann)	Ferry and Spear (1978)*
GASP	Grt (grs) + AlSi + Qtz = Pl (an)	Koziol and Newton (1988)†
GMAP	Grt (alm) + Grt (grs) + Ms = Pl (an) + Bt (ann)	Ghent and Stout (1981)†
GARH	Grt (prp) + Fe-Hbl = Grt (alm) + Mg-Hbl	Graham and Powell (1984)*
GAPH	Fe-actinote + Pl (an) = Hbl (Fe-Tsch.) + Grt (grs + alm) + Qtz	Kohn and Spear (1990)‡

Solution models for garnet, biotite, muscovite and plagioclase after Berman (1990), Patino Douce et al. (1993), Chatterjee & Flux (1986) and Elkins & Groove (1990), respectively. *Hodges & McKenna (1987) and McKenna & Hodges (1988) statistical treatment of the original experimental data. †Applegate & Hodges (1994) treatment. ‡Recalibrated by M. House for Elkins and Groove (1990) plagioclase solution model.

Table A1. Garnet rim compositions (12 O basis).

Sample	G1	G2	G3	S1	S2	S3	K1
SiO ₂	37.35±0.14	37.32±0.16	36.90±0.11	36.76±0.19	37.37±0.19	37.07±0.07	36.44±0.10
TiO ₂	0.03±0.01	0.03±0.02	0.04±0.02	0.02±0.01	0.05±0.03	0.09±0.03	0.04±0.02
Al ₂ O ₃	21.21±0.08	21.08±0.05	20.98±0.06	21.05±0.06	21.08±0.12	20.96±0.05	20.61±0.07
FeO	20.70±0.54	31.90±0.22	34.03±0.25	35.62±0.60	24.63±1.00	27.86±0.36	38.24±0.16
MnO	8.52±0.57	2.89±0.08	4.41±0.43	2.68±0.28	6.87±0.49	5.35±0.45	2.83±0.16
MgO	0.82±0.07	2.55±0.08	2.19±0.14	2.83±0.04	1.24±0.13	1.26±0.02	1.27±0.03
CaO	11.85±0.28	4.87±0.17	2.22±0.11	1.53±0.23	9.41±0.62	8.05±0.30	1.60±0.11
Cr ₂ O ₃	0.01±0.01	0.02±0.01	0.01±0.01	0.01±0.01	0.02±0.01	0.04±0.02	0.03±0.01
Total	100.50	100.66	100.78	100.50	100.69	100.68	101.06
Si	2.97	2.98	2.98	2.97	2.98	2.97	2.97
Ti	0.00	0.00	0.00	0.00	0.00	0.01	0.00
Al	1.99	1.99	1.99	2.00	1.98	1.98	1.98
Fe	1.38	2.13	2.30	2.40	1.64	1.87	2.60
Mn	0.57	0.20	0.30	0.18	0.46	0.36	0.20
Mg	0.10	0.30	0.26	0.34	0.15	0.15	0.16
Ca	1.01	0.42	0.19	0.13	0.80	0.69	0.14
Cr	0.00	0.00	0.00	0.00	0.00	0.00	0.00
Sum	8.03	8.02	8.02	8.03	8.03	8.03	8.04
n [*]	9	14	8	8	10	9	6

Sample	K2	K3	M1	M2	M3	M4
SiO ₂	36.87±0.28	37.10±0.15	38.09±0.24	38.12±0.21	36.58±0.16	36.29±0.12
TiO ₂	0.09±0.31	0.03±0.01	0.08±0.03	0.08±0.03	0.03±0.01	0.04±0.02
Al ₂ O ₃	21.11±0.14	21.17±0.10	21.18±0.06	21.21±0.12	20.95±0.12	20.73±0.10
FeO	33.25±0.36	33.19±0.39	22.35±0.16	21.91±0.19	30.07±0.25	31.54±0.26
MnO	3.30±0.62	3.30±0.60	0.43±0.17	0.60±0.25	11.06±0.23	9.44±0.23
MgO	3.31±0.16	3.63±0.15	1.82±0.11	1.99±0.07	1.58±0.04	1.11±0.04
CaO	2.58±0.33	2.14±0.20	16.43±0.20	16.17±0.34	0.55±0.07	1.05±0.15
Cr ₂ O ₃	0.01±0.01	0.01±0.01	0.01±0.01	0.02±0.01	0.01±0.01	0.02±0.01
Total	100.53	100.56	100.39	100.10	100.83	100.22
Si	2.96	2.97	2.99	2.99	2.97	2.97
Ti	0.01	0.00	0.01	0.01	0.00	0.00
Al	2.00	2.00	1.96	1.96	2.00	2.00
Fe	2.23	2.22	1.47	1.44	2.04	2.16
Mn	0.22	0.22	0.03	0.04	0.76	0.66
Mg	0.40	0.43	0.21	0.23	0.19	0.14
Ca	0.22	0.18	1.38	1.36	0.05	0.09
Cr	0.00	0.00	0.00	0.00	0.00	0.00
Sum	8.04	8.03	8.05	8.03	8.01	8.02
n [*]	23	10	17	20	16	18

* Average rim compositions based on n analyses. Uncertainties correspond to one standard deviation.

Table A2. Biotite rim compositions (11 O basis).

Sample	G3	S1	K1	K2	K3	M3	M4
SiO ₂	35.36±0.20	34.97±0.72	34.02±0.28	35.94±0.21	35.68±0.13	34.59±0.11	34.57±0.25
TiO ₂	1.67±0.12	1.60±0.27	1.91±0.69	1.82±0.20	1.80±0.34	2.61±0.21	2.72±0.23
Al ₂ O ₃	19.37±0.13	19.73±0.36	20.12±0.36	20.07±0.21	19.97±0.23	19.77±0.17	20.17±0.26
FeO	20.53±0.35	20.07±0.30	26.20±0.38	18.53±0.23	18.70±0.13	22.11±0.24	23.74±0.20
MnO	0.17±0.02	0.10±0.04	0.12±0.04	0.17±0.04	0.20±0.04	0.40±0.05	0.36±0.06
MgO	8.65±0.26	9.94±0.16	4.76±0.11	9.81±0.10	9.91±0.09	6.75±0.07	5.14±0.10
CaO	0.00±0.00	0.00±0.00	0.00±0.00	0.00±0.00	0.00±0.00	0.00±0.00	0.00±0.00
Na ₂ O	0.16±0.05	0.10±0.04	0.18±0.03	0.28±0.03	0.26±0.09	0.22±0.02	0.16±0.03
K ₂ O	9.11±0.12	8.46±0.35	8.98±0.11	8.93±0.09	9.39±0.25	9.30±0.07	9.30±0.27
F	0.26±0.02	0.24±0.03	0.22±0.02	0.30±0.03	0.24±0.04	0.39±0.02	0.60±0.03
Total	95.29	95.19	96.50	95.82	96.15	96.14	96.75
Si	2.70	2.66	2.65	2.70	2.68	2.66	2.66
Ti	0.10	0.09	0.11	0.10	0.10	0.15	0.16
Al	1.75	1.77	1.84	1.78	1.77	1.79	1.83
Fe	1.32	1.28	1.70	1.16	1.18	1.42	1.53
Mn	0.01	0.01	0.01	0.01	0.01	0.03	0.02
Mg	0.99	1.13	0.55	1.10	1.11	0.77	0.59
Ca	0.00	0.00	0.00	0.00	0.00	0.00	0.00
Na	0.02	0.01	0.03	0.04	0.04	0.03	0.02
K	0.89	0.82	0.89	0.86	0.90	0.91	0.03
Sum	7.78	7.78	7.78	7.75	7.80	7.76	7.73
n	10	8	11	31	14	14	14

Table A3. Muscovite rim compositions (11 O basis).

Sample	G3	S1	K1	K2	K3	M3	M4
SiO ₂	45.27±0.09	45.42±0.28	45.63±0.26	45.56±0.24	45.91±0.10	45.21±0.06	45.12±0.40
TiO ₂	0.431±0.04	0.41±0.14	0.46±0.03	0.65±0.13	0.80±0.06	0.77±0.09	0.89±0.12
Al ₂ O ₃	35.90±0.53	36.45±0.21	35.73±0.38	35.63±0.31	35.17±0.16	35.97±0.26	35.83±0.24
FeO	1.17±0.29	0.75±0.08	1.44±0.16	1.03±0.10	1.09±0.06	1.20±0.05	1.29±0.08
MnO	0.02±0.02	0.02±0.03	0.02±0.03	0.02±0.03	0.02±0.02	0.03±0.02	0.02±0.02
MgO	0.59±0.1	0.47±0.03	0.49±0.10	0.67±0.07	0.82±0.04	0.47±0.05	0.44±0.04
CaO	0.01±0.01	0.02±0.02	0.02±0.02	0.02±0.01	0.00±0.01	0.01±0.01	0.01±0.01
Na ₂ O	1.34±0.03	2.27±0.10	0.94±0.01	1.13±0.03	1.11±0.03	0.76±0.03	0.70±0.04
K ₂ O	9.24±0.09	8.00±0.07	10.02±0.08	9.73±0.07	9.73±0.04	10.31±0.06	10.43±0.08
F	0.08±0.05	0.04±0.03	0.12±0.03	0.08±0.04	0.07±0.05	0.14±0.08	0.23±0.03
Total	94.05	93.84	94.86	94.51	94.72	94.87	94.95
Si	3.04	3.04	3.05	3.05	3.07	3.03	3.03
Ti	0.02	0.02	0.02	0.03	0.04	0.04	0.05
Al	2.84	2.87	2.81	2.81	2.77	2.84	2.83
Fe	0.07	0.04	0.08	0.06	0.06	0.07	0.07
Mn	0.00	0.00	0.00	0.00	0.00	0.00	0.00
Mg	0.06	0.05	0.05	0.07	0.08	0.05	0.04
Ca	0.00	0.00	0.00	0.00	0.00	0.00	0.00
Na	0.17	0.29	0.12	0.15	0.14	0.10	0.09
K	0.79	0.68	0.86	0.83	0.83	0.88	0.89
Sum	7.00	7.00	7.00	7.00	6.99	7.01	7.01
n	7	5	8	17	7	5	10

Table A4. Plagioclase rim compositions (8 O basis).

Sample	G1	G2	G3	S1	S2	S3	K1
SiO ₂	48.12±0.97	57.72±0.71	61.50±0.41	63.46±0.22	53.70±0.83	58.31±0.45	64.74±0.20
Al ₂ O ₃	32.56±0.45	26.39±0.51	23.86±0.23	22.65±0.11	29.02±0.44	26.21±0.25	21.99±0.22
FeO	0.10±0.04	0.15±0.08	0.14±0.23	0.08±0.06	0.19±0.22	0.19±0.07	0.11±0.04
MgO	0.01±0.01	0.01±0.01	0.00±0.00	0.01±0.01	0.01±0.01	0.00±0.00	0.01±0.01
CaO	15.72±0.63	8.21±0.59	5.16±0.18	3.74±0.07	11.25±0.48	8.06±0.31	2.84±0.2
Na ₂ O	2.38±0.50	7.19±0.34	8.96±0.16	9.73±0.08	5.28±0.35	7.20±0.14	10.08±0.11
K ₂ O	0.05±0.03	0.05±0.01	0.09±0.03	0.08±0.02	0.04±0.02	0.07±0.02	0.22±0.15
Total	98.95	99.72	99.72	99.75	99.48	100.05	100.00
Si	2.22	2.59	2.74	2.81	2.44	2.61	2.86
Al	1.77	1.40	1.25	1.18	1.55	1.38	1.14
Fe	0.00	0.01	0.01	0.00	0.01	0.01	0.00
Mg	0.00	0.00	0.00	0.00	0.00	0.00	0.00
Ca	0.78	0.40	0.25	0.18	0.55	0.39	0.13
Na	0.21	0.63	0.77	0.84	0.47	0.62	0.86
K	0.00	0.00	0.00	0.00	0.00	0.00	0.013
Sum	5.00	5.02	4.99	5.02	5.02	5.00	5.01
n	5	10	7	8	9	6	6

Sample	K2	K3	M1	M2	M3	M4
SiO ₂	60.42±0.25	62.18±0.28	44.89±0.48	44.87±0.26	63.21±0.21	63.25±0.26
Al ₂ O ₃	24.46±0.17	23.47±0.19	34.71±0.24	34.62±0.17	22.95±0.14	22.91±0.20
FeO	0.07±0.05	0.10±0.05	0.07±0.04	0.1±0.04	0.05±0.06	0.04±0.06
MgO	0.01±0.01	0.00±0.00	0.00±0.00	0.00±0.00	0.01±0.02	0.01±0.01
CaO	5.92±0.20	4.80±0.11	18.25±0.31	18.25±0.28	3.88±0.14	3.86±0.20
Na ₂ O	8.45±0.08	9.00±0.14	1.06±0.18	1.10±0.01	9.46±0.10	9.46±0.10
K ₂ O	0.11±0.03	0.12±0.02	0.02±0.01	0.02±0.01	0.30±0.05	0.33±0.06
Total	99.44	99.67	99.01	98.95	99.82	99.85
Si	2.70	2.77	2.09	2.09	2.80	2.80
Al	1.29	1.23	1.91	1.90	1.20	1.20
Fe	0.00	0.00	0.00	0.00	0.00	0.00
Mg	0.00	0.00	0.00	0.00	0.00	0.00
Ca	0.28	0.23	0.91	0.91	0.18	0.18
Na	0.73	0.78	0.10	0.01	0.81	0.81
K	0.01	0.01	0.00	0.00	0.02	0.02
Sum	5.02	5.01	5.01	5.00	5.01	5.02
n	14	10	10	7	9	12

Table A5. Hornblende rim compositions (23 O basis).

Sample	G1	G2	S2	S3
SiO ₂	43.60±0.34	41.81±0.24	41.37±0.25	40.47±0.43
TiO ₂	0.25±0.03	0.39±0.03	0.35±0.07	0.27±0.09
Al ₂ O ₃	12.53±0.74	17.76±0.26	16.90±0.48	17.75±0.37
FeO	18.43±0.35	16.89±0.42	17.94±0.47	18.98±0.45
MnO	0.55±0.08	0.23±0.06	0.44±0.07	0.43±0.06
MgO	8.56±0.46	7.65±0.28	6.75±0.22	6.00±0.25
CaO	11.81±0.23	11.17±0.23	11.49±0.14	11.57±0.05
Na ₂ O	0.93±0.08	1.04±0.06	1.42±0.08	1.14±0.10
K ₂ O	0.46±0.08	0.34±0.03	0.38±0.07	0.41±0.04
Cr ₂ O ₃	0.01±0.01	0.02±0.02	0.05±0.06	0.03±0.02
F	0.46±0.04	0.20±0.04	0.67±0.09	0.16±0.06
Total	97.59	97.49	97.75	97.20
Si	6.59	6.22	6.24	6.09
Al	2.23	3.11	3.00	3.15
Ti	0.03	0.04	0.04	0.03
Cr	0.00	0.00	0.01	0.00
Mg	1.93	1.70	1.52	1.35
Fe	2.33	2.10	2.26	2.39
Mn	0.07	0.03	0.06	0.06
Ca	1.91	1.78	1.86	1.86
Na	0.27	0.30	0.41	0.33
K	0.09	0.06	0.07	0.08
Sum	15.45	15.35	15.46	15.34
n	5.00	12.00	12.00	6.00

Table A6. Clinopyroxene rim composition (6 O basis)

Sample	M1	M2
SiO ₂	52.01±0.28	51.44±0.38
TiO ₂	0.04±0.03	0.06±0.03
Al ₂ O ₃	0.48±0.32	1.12±0.49
FeO	12.50±0.63	13.17±0.89
MnO	0.22±0.05	0.21±0.04
MgO	10.21±0.31	9.79±0.47
CaO	23.86±0.43	23.00±0.50
Na ₂ O	0.12±0.08	0.19±0.07
K ₂ O	0.01±0.01	0.01±0.01
Cr ₂ O ₃	0.02±0.01	0.01±0.01
F	0.00±0.00	0.00±0.00
Total	99.49	99.00
Si	1.99	1.98
Al	0.02	0.05
Ti	0.00	0.00
Cr	0.00	0.00
Mg	0.58	0.56
Fe	0.40	0.43
Mn	0.01	0.01
Ca	0.98	0.95
Na	0.01	0.02
K	0.00	0.00
Sum	3.99	4.00
n	10	10

6. LEUCOGRANITES

The master was fond of the desert, however, and once we entered the barren landscape of rocks and cacti, he kept pointing out curious geological formations and delivering little lectures on the incalculable age of the earth. To be perfectly honest, it left me pretty cold.»

Mr Vertigo», Paul Auster

6.1 Introduction

We have decided to devote a special chapter of this work to the leucogranites, for they represent one of the rare magmatic products of the Himalayan orogen and are of paramount importance in the tectonometamorphic evolution of the High Himalayan Crystalline Sequence.

With their snow-white colour, set with tiny garnets and tourmaline prisms, their equigranular texture and lack of pronounced alteration, the Himalayan leucogranites can be qualified as being aesthetically very attractive.

One of the first descriptions of these granites is given, for the Garhwal region, by Griesbach (1891) who observed their systematic association with a «long line of dislocation» (STDS ?) at the contact between the «crystalline rocks» (HHCS) and the «Haimantas» (Phe Fm. of the TH). He also went so far as to suggest that these leucogranites might well be of Tertiary age (which is absolutely correct). Despite the fact that his age estimation is made on the basis of a somewhat shaky argumentation, it is rather impressive that he guessed them to be younger than the lowest Palaeozoic, as he himself observes that they do intrude younger formations.

Leucogranitic intrusions outcrop sporadically over a distance of more than 2000 kilometres along the strike of the Himalayan orogen (fig. 6.1), retaining remarkable uniformity in both geochemistry and in structural settings. Single intrusions do not exceed a few kilometres in thickness, and leucogranites most often form intricate sill and dike complexes. About 20 plutons of variable size do however occur along the Himalayan range, where they often form the pedestal of the highest summits in the world (Griesbach, 1891, Gansser, 1964, Le Fort, 1973). Among these plutons are the Manaslu, the Makalu, the Everest, the Langtang, the Gangotri, the Rongbuk, the Mustang, the Shisha-Pangma, the Gopu-La, the Gabug, the Monlakarchung-Pasalum, the Chung-la, the Lhozag and the Gumburanjun. These plutons are surrounded by an aureole of leucogranitic aplites or pegmatites criss-crossing the country rocks. Xenoliths of country rocks are frequently observed in the margins of the plutons, their amount diminishing progressively towards the core of the intrusions.

These High Himalaya intrusives are peraluminous, muscovite \pm tourmaline / biotite-bearing granites of minimum melt composition (Le Fort et al., 1987). They are generally emplaced in the kyanite to sillimanite grade rocks at the top of the HHCS and are associated with segments of the

South Tibetan Detachment System. Some of these intrusions however cross the STDS and intrude the weakly metamorphosed sediments of the Tethys Himalaya (Griesbach, 1891; Le Fort, 1973, Guillot et al., 1994 and 1995). Most of these leucogranites yield a monazite U/Pb age around 25-20 Ma (Schärer, 1984; Harrison et al., 1995), with no obvious variation along strike of the Himalaya (Harris and Massey, 1994). Very young leucogranites with an age < 5 Ma have however been described in the two Himalayan syntaxis (Burg et al., 1998).

The leucogranites generally have an equigranular texture and range between aplites and pegmatites. They are essentially formed of quartz + plagioclase (An₂₁ to An₂) + K-feldspar + muscovite with variable amounts of biotite, garnet and tourmaline. Accessory phases are apatite, monazite, zircon, beryl, cordierite and aluminosilicates. Despite their mineralogical uniformity, the leucogranites are commonly divided in two categories: the two-mica leucogranites and the tourmaline leucogranites. In the former category enter the granites where both muscovite and biotite are present and tourmaline is subordinate. The latter category regroups the granites where tourmaline and muscovite are widespread but biotite is virtually absent.

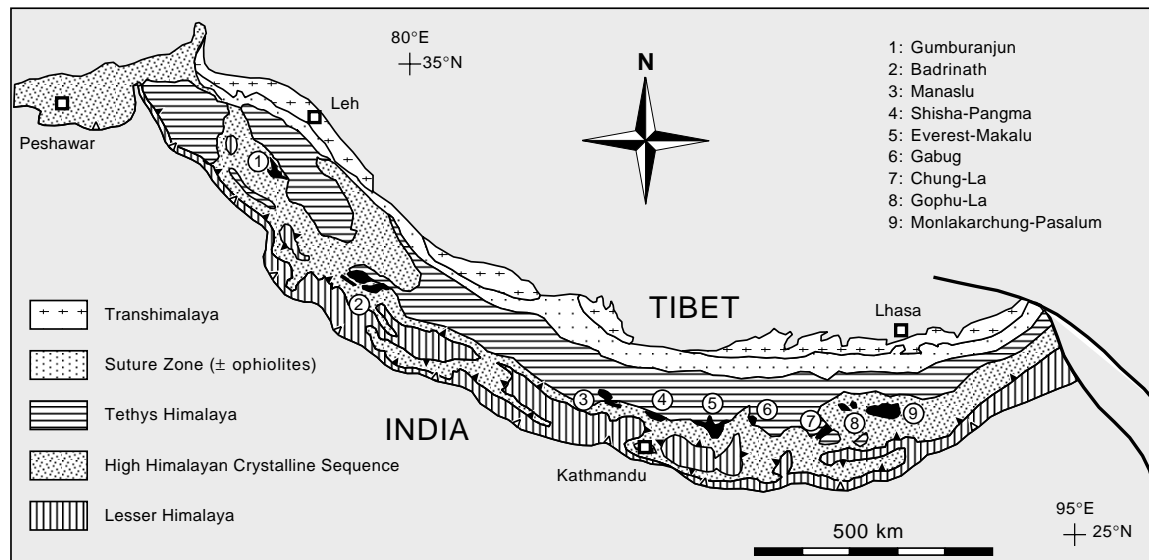


Fig. 6.1: Geologic - Tectonic map of the Himalaya, showing the location of the main Himalayan leucogranitic intrusions. Modified after Le Fort 1988.

6.2 Geological setting

Leucogranites are widespread within the upper structural levels of the HHCS in the whole Zaskar area. The abundance of these intrusions increases from north-west Zaskar towards the south-eastern parts of this area. In the upper Doda, Suru, Kishtwar and Warwan regions, the occurrence of leucogranites is limited to disseminated dikes and sills (Honegger, 1983; Herren, 1987; Kündig, 1988). The claim of Searle and Fryer (1986) that 30-50% of the granites in this region are of leucogranitic type was thus quite overoptimistic. From the region of the Haptal Tokpo valley, south of Padum, and towards the south-east, the leucogranites start to appear as frequent concordant intrusions with a size that varies between 5 mm and 600 meters (Herren, 1987). The largest amounts of leucogranites in the whole Zaskar area are undoubtedly occurring in the south-westernmost part of the HHCS, which is to say in the region covered by the present work.

In this area, the leucogranite do indeed represent a large part of the HHCS (fig. 6.9) and they occur as a more or less continuous belt of plutons of variable size from the Gianbul valley to the

Kamirup . It is in the latter valley that the leucogranites can be seen to show on the surface for the last time, for they have not been mentioned to occur more to the south-east. It is however very likely that they are still present at an unexposed level and that they might be quite close to the surface under the high-grade metamorphic outcrop south of Sarchu.

South-east Zaskar, and especially the Gianbul valley, represents probably one of the most interesting regions of the Himalaya for the study of the leucogranites as it is possible to follow these intrusions all the way from their probable source region up to their summit along this single valley.

The leucogranites in the Gianbul valley form an intrusion complex that can be divided into four zones from base to top (fig. 5.8).

The first zone is the probable production zone of the leucogranitic melts and is represented by the high-grade migmatites (fig. 6.2) that we have described in chapter 5. The restites in the migmatitic zone still contain significant quantities of both plagioclase and alkali feldspar which suggest that the production of melt occurred through vapour-absent melting of muscovite (Harris et al., 1993).

The second zone corresponds to the feeder dikes which are rooted into the migmatitic zone and ascend more or less vertically through the gneisses of the HHCS over a distance of about one kilometre (fig 6.3). As this zone is exposed in cliffs which are of very difficult access, we could not get a close view of the relation between the dikes and the surrounding country-rock gneisses.

The third zone is formed by an approximately one kilometre thick belt of massive leucogranitic plutons fed by the underlying dikes. The lower contact of these plutons is very irregular. One of these massive plutons is beautifully exposed in the northern ridge of the Gumburanjun mountain (fig. 6.4). Even if this outcrop of leucogranites is relatively small compared to those of the Gianbul valley, we will use this name for the whole set of leucogranitic bodies of south-east Zaskar as they are most likely all connected to each other and because this name was already used in the literature (Gaetani et al. 1985, Ferrara et al. 1991; Dèzes et al. 1999). Metric to decametric blocks of country rocks are preserved as xenoliths both at the base and at the top of the plutons (fig. 6.5). These rocks have a fine grained equigranular texture and are composed of a large amount of quartz (60-70%), with biotite (20-30%), albite (10-15%) and minor K-feldspar (3-5%) and tourmaline (2-3%). The amount of the rafts decreases gradually towards the centre of the plutons. These blocks have an angular shape and show a well marked foliation which is continuous from block to block and parallel with the main foliation of the country rocks (fig. 6.4). It thus appears that these xenoliths have preserved their original orientation and were not tilted within the plutons as would be expected if they were surrounded by large volumes of leucogranite in a liquid state. This is a strange feature which we tentatively attribute to the fact that the leucogranitic intrusions do not form plutons in the usual sense of the term but that they are the result of a very high concentration of dikes and sills which intruded as continuous pulses and aggregated as massive bodies of leucogranites where the individual veins are indistinguishable from one another. This interpretation is supported by the fact that in the regions outside of the plutons it is often impossible to establish a chronological relation between two dikes, as they seem to be perfectly welded together at their point of junction. Another interesting feature of the xenoliths is that they seem to be affected by some kind of leaching process. One can indeed observe that these rocks, which have no particular reason to represent a different protolith than the rest of the HHCS rocks, do show a texture and a mineralogical composition that is quite different from the usual metapelites or orthogneisses, in the sense that they are almost completely depleted in muscovite and have a fine grained equigranular texture (~ hornfelsic texture). That these rocks also initially contained muscovite is testified by the fact that we could observe, in thin section, a single perfectly rounded muscovite grain preserved inside a quartz crystal. Thus, it seems more



Fig. 6.2: The migmatites. Gianbul Valley.



Fig. 6.3: The feeder dike system. The bottom of the cliffs are formed by migmatites. Gianbul Valley.



Fig. 6.4: The Gumburanjun leucogranite. This cliff is entirely formed by leucogranites. The whiter part results from a recent rock-fall.



Fig. 6.5: Detail of a metapelitic xenolith in a boulder of leucogranite from a recent rock-fall at the Gumburanjun.



Fig. 6.6: Leucogranitic boudins in the kyanite zone of the Zaskar Shear Zone, Gianbul Valley. View towards the north.



Fig. 6.7: Two generations of leucogranitic dikes. The first generation is reoriented parallel to the ZSZ and is cross-cut by the second generation of undeformed leucogranitic dikes. Gunburanjun mountain.



Fig. 6.8: This picture shows how vertically ascending dikes are reoriented once they enter the Zaskar Shear Zone.

than likely that these xenoliths reached metamorphic conditions sufficient for the breakdown of muscovite and that they also represent a source for leucogranitic melts. The overall aspect of these leucogranitic intrusion containing angular rafts of country rocks resembles that of agmatitic migmatites (Mehnert, 1968). The xenoliths should thus be considered as restites.

The fourth zone represents the structurally uppermost levels of the intrusion complex. Above the roof of the leucogranitic plutons, a gradually decreasing array of leucogranitic veins intrudes the country rock gneisses. These veins ascend vertically for a distance of about 100 meters before most of them are reoriented parallel to the Zanskar Shear Zone (fig. 6.8) and often strongly boudinaged by extensional movements associated to the shear zone (fig. 6.6) Several dikes do however penetrate the ZSZ without being affected by extensional deformation (fig. 6.7), which clearly indicates that these dikes must have intruded the shear zone after ductile movements have ceased. The upper boundary of the leucogranitic intrusion coincides with the kyanite zone and they were never seen above the 10-50 meter thick horizon of calcsilicate rocks, which is nearly always present at this structural level in the whole studied area.

Both aplitic and pegmatitic dikes are observed towards the top of the intrusion complex and especially in the uppermost zone. The pegmatites (up to 10 meters in thickness) contain quartz, K-feldspar, plagioclase, muscovite, tourmaline, garnet, and beryl. The individual size of these minerals reaches up to 10 cm (yes, even the beryl!). In one sample from the kyanite zone, a large (12 cm) K-feldspar crystal incorporated pre-existing centimetre sized kyanite blades. Aplites, in the absence of biotite and tourmaline are pristine white with red flecks of euhedral garnets. Many of the pegmatitic dikes seem to be late as they are mostly undeformed by the ZSZ.

The association of leucogranites with pegmatites does not imply hydrous ($a_{H_2O}=1$) conditions during melting. Clemens (1984) estimated that a granitic melt produced by muscovite breakdown would be close to saturation, having ~ 10 wt. % dissolved water at 5 kbar (assuming pure OH on the hydroxyl site in micas). Crystallization of such melts can liberate a large proportion of volatiles and consequently leads to the formation of migmatites without external fluids.

6.3 Petrography

Leucogranites in Zanskar make no exception to the rule and their mineralogical composition is remarkably constant. As for the other Himalayan regions, the leucogranites in the studied area can be grouped in two categories, the tourmaline facies and the biotite facies, depending essentially on the presence or absence of biotite or garnet and the amount of tourmaline and muscovite. The texture of both leucogranitic facies is equigranular.

The tourmaline facies is formed of quartz (30 - 35 %), plagioclase (35 - 40 %), K-feldspar (15 - 25 %), muscovite (~ 5 %) and tourmaline (~ 5 %).

The biotite facies is formed of quartz (30 - 35 %), plagioclase (35 - 40 %), K-feldspar (15 - 25 %), muscovite (10 - 15 %), biotite (5 - 10%) and tourmaline (~1 %).

In general both type of leucogranites are exceptionally fresh in thin sections and sericitisation of the K-feldspar or chloritisation of the biotite is very rarely observed.

Garnet was only observed as an accessory phase in the tourmaline facies. This mineral is generally anhedral and sometimes grows as an interstitial phase.

Biotite is very rarely observed as an accessory phase in the tourmaline facies, when the two granite types are in close contact.

Plagioclase is the most abundant mineral in both facies. It is slightly zoned and optical determinations show a composition range from oligoclase ($\sim \text{An}_{20}$) in the core to albite ($\sim \text{An}_2$) at the rim. This mineral sometimes forms symplectites with K-feldspar.

K-feldspar forms among the largest crystals in the leucogranites and contains all the other phases as inclusions. They are thus the last phase to crystallize.

Muscovite is always present partly as large flakes, but its abundance decreases from the biotite facies to the tourmaline facies leucogranites. This mineral is evenly distributed throughout the granite and can be found as inclusions within plagioclase, quartz or K-feldspar. In the biotite facies, both phyllosilicates are intimately intergrown without enclosing relationships.

Tourmaline shows colour zoning from lavender blue to yellow-brown. The blue colour is generally, but not necessarily, restricted to the core of the crystals. This phase is usually euhedral although it sometimes shows a skeletal habit.

Accessory phases in both leucogranitic types are apatite, monazite, ilmenite, zircons beryl and copper mineralisations. In one aplitic sample of the Reru valley, fuchsite was observed as the dominant phyllosilicate.

Pegmatites and aplites belong to the tourmaline facies because they have all the mineralogical characteristics of this category of leucogranites. As the pegmatites and aplites are often undeformed by extensional movements, they are among the last intrusives.

Consequently we interpret the tourmaline facies as intruding chronologically later than the biotite facies and representing a later stage of the magmatic evolution.

6.4 Geochemistry

Five samples of the Gumburanjun leucogranite (Table 6.1, fig. 6.10) were analysed for major and trace element composition by Jean-Claude Vannay (unpubl. data). We incorporate these data in this work to compare them with chemical analyses made by Ferrara et al. (1991) on the same intrusion and data from Herren (1987, data from Brouand and Pêcher included) on several leucogranitic sheets and dikes from NW Zanskar (region of Padum). This set of data from Zanskar is also compared with chemical analyses made by Guillot (1993) on the Manaslu leucogranite in Nepal, which represents the largest and most studied Himalayan leucogranitic intrusion.

The purpose is to show that the chemical composition of the leucogranites is not only very homogenous within the same intrusion but also between different intrusions, even if they are separated by several hundred kilometres as for Zanskar and Nepal.

6.4.1 Major elements

The five analysed samples show a very narrow compositional range for all the major elements (table 6.1). These samples have a very high A/CNK ratio (1.30 ± 0.03), indicating a high degree of peraluminosity. These analyses also show the very low content in Fe, Mg and Mn which is in good agreement with the scarcity of ferromagnesian minerals.

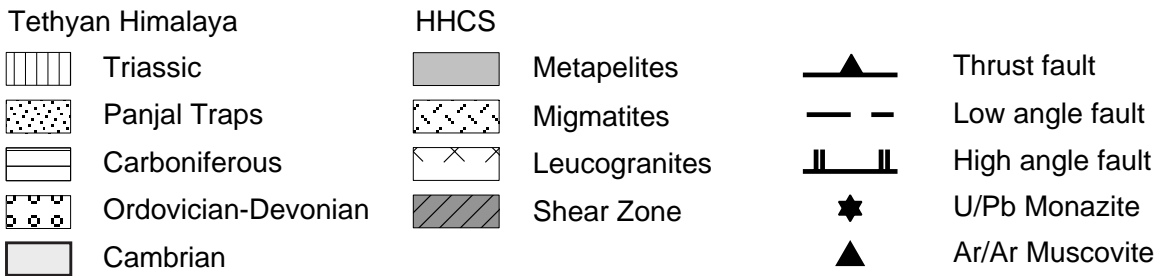
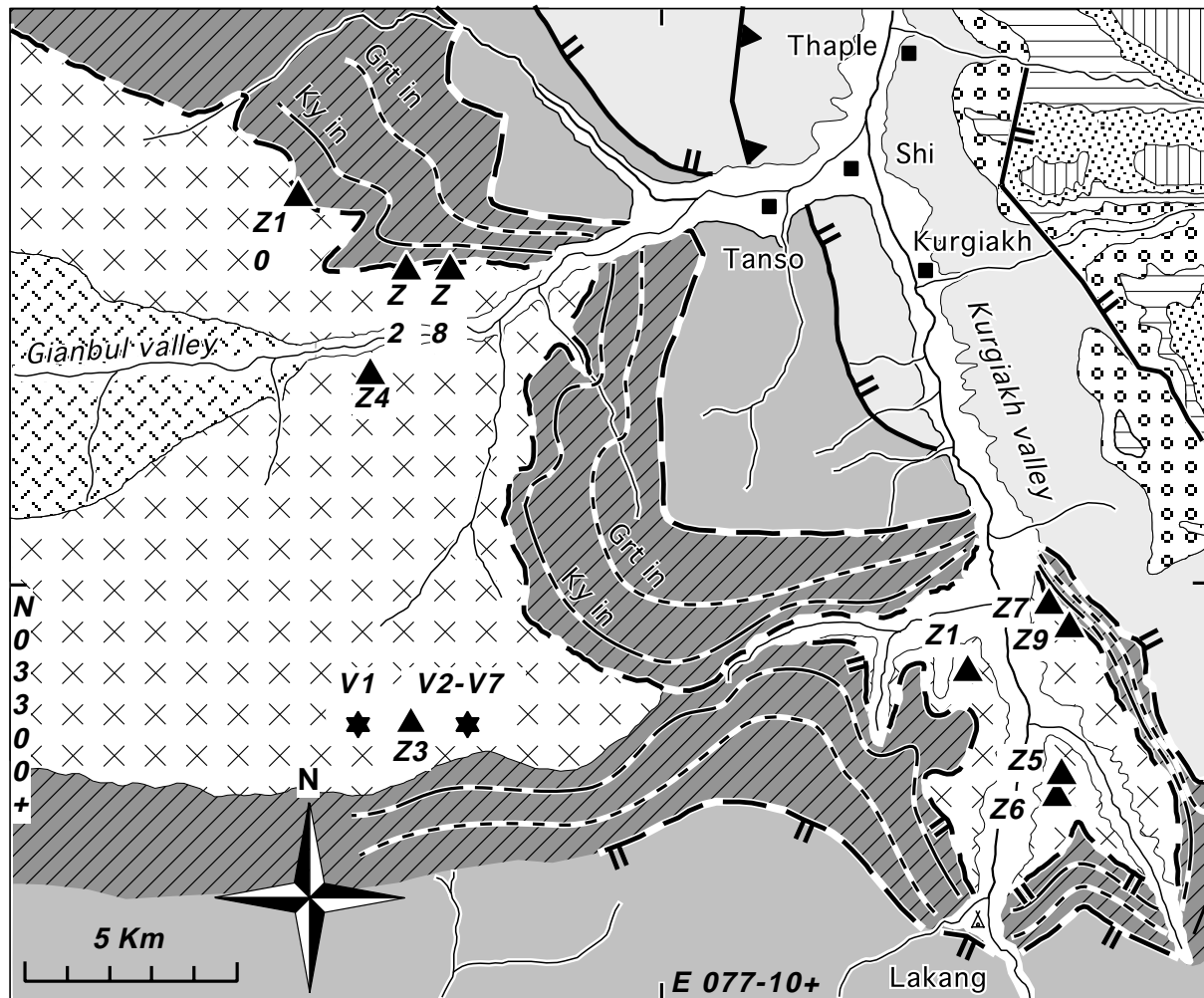


Fig. 6.9: Geological map of southeast Zanskar showing the location of the samples used for monazite U/Pb and muscovite Ar/Ar ages on the leucogranites. The 5 samples used for geochemical analyses were collected in the vicinity of point Z3, V1 and V2-V7 by Vannay (unpubl.data). The samples analysed by Ferrara et al. (1992) were collected, by these authors, close to points Z5 and Z6 . The two smaller leucogranitic outcrops of the Kamirup valley are not shown on this map.

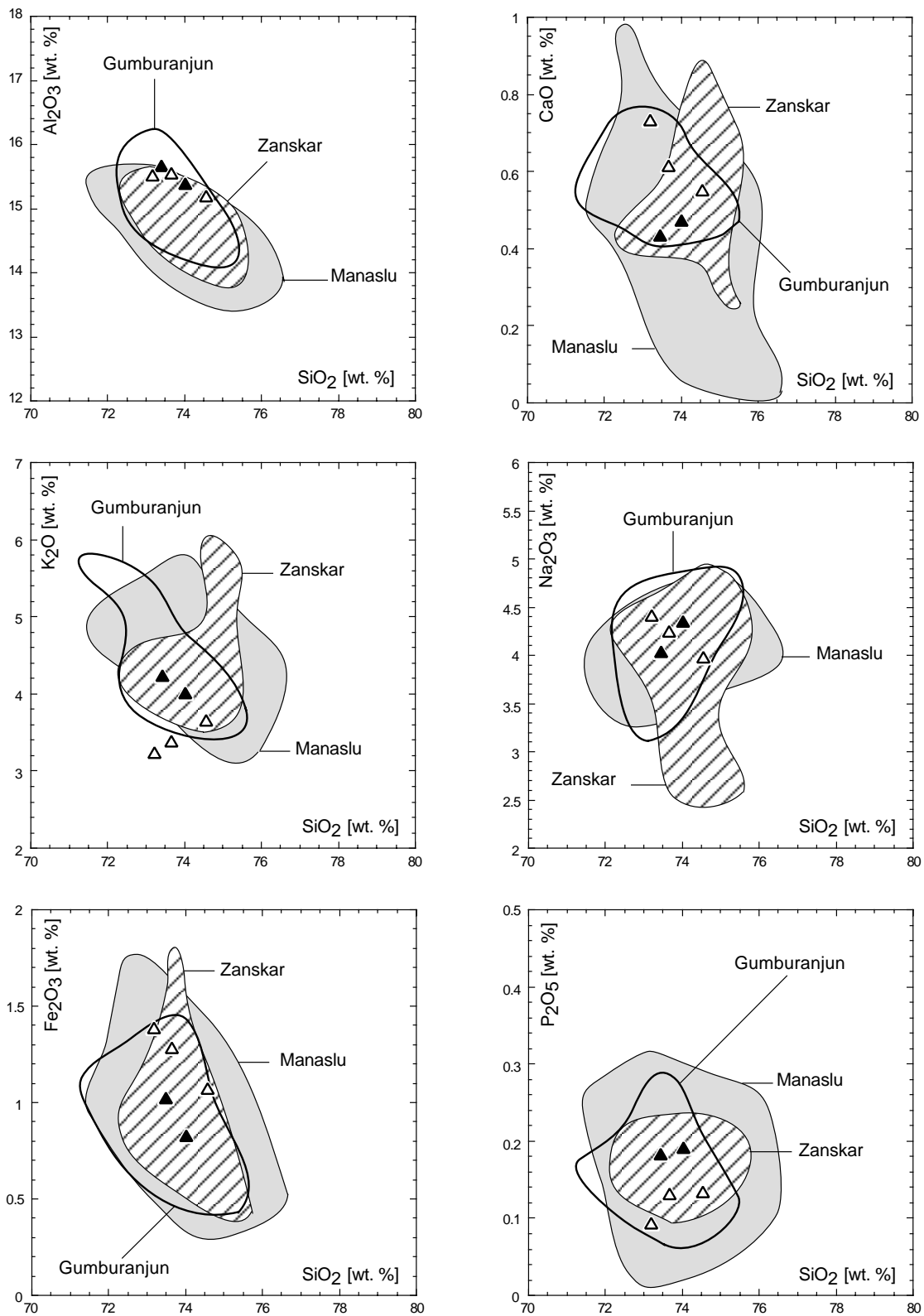


Fig. 6.10: Major-element Harker diagrams. The shaded field represents the distribution of 97 samples from the Manaslu leucogranite (Guillot, 1993). The striped field corresponds to the 19 samples of northwest Zanskar (Herren, 1993). The field with a bold line is for the 17 samples from the Gumburanjun leucogranite (Ferrara et al. 1992). The triangle represent our 5 additional analyses for the Gumburanjun. The two solid triangles are tourmaline bearing leucogranites. The three white triangles are biotite bearing leucogranites.

Major-element Harker diagrams (fig. 6.10) show that our five samples are all within the composition range of the other Zaskar leucogranites. Only two samples show a little anomaly in K_2O content. The compositional fields for the Manaslu granite encompass 97 samples, the Gumburanjun analyses totalise 17 samples, and the other samples from Zaskar amount to 19 samples. With our five samples, these Harker diagrams show the compositional range of 138 samples. The overlapping of the various compositional fields for the Zaskar samples and the Manaslu samples show that there is little variation in the major-element contents in leucogranites from two very distant intrusions. We can thus fairly assume that our leucogranites share the same characteristics with other Himalayan leucogranites. The Al_2O_3 - SiO_2 diagram however shows that our samples are amongst the most aluminium-rich Himalayan leucogranites. This is also the only diagram where a correlation between major-element concentration and silica can be observed, if all our samples are considered together.

If we consider the biotite bearing leucogranites separately, one can observe a correlation between major-element concentration and silica in all the diagrams. It can also be seen that the tourmaline bearing leucogranites seem to behave differently from the biotite bearing leucogranites. The former one are depleted in CaO and Fe_2O_3 and enriched in K_2O and P_2O_5 with respect to the latter one. Both type of granite also seem to evolve along different trends. These consideration would however greatly benefit from further analyses on both type of leucogranites as our set of data is somewhat insufficient to draw definitive conclusions.

The Gumburanjun leucogranite is peraluminous and alkali-rich, its composition in major elements is virtually identical to the other Himalayan tertiary granites.

6.4.2 Trace elements:

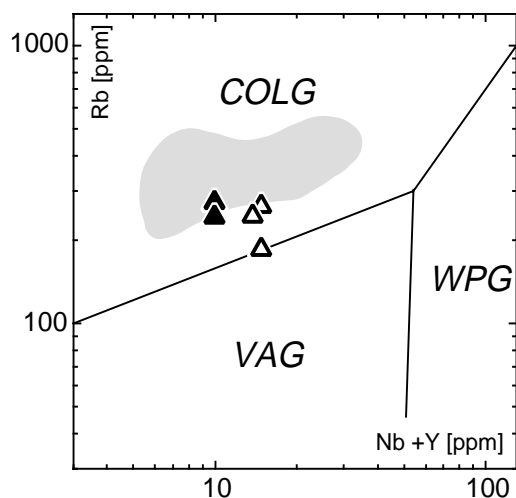


Fig. 6.11: Tectonic discrimination diagram of Pearce et al. (1984). The two solid triangles are tourmaline bearing leucogranites. COLG: syn-collisional granites; WPG: Within plate granites; VAG: volcanic arc granites. Shaded field: published High Himalayan leucogranites (Dietrich & Ganser, 1981; Scaillet et al. 1990).

Our trace element data for the Gumburanjun could only be compared with those of Herren (1993) for the larger Zaskar area, as Ferrara et al. (1992) did not analyse these elements on the Gumburanjun intrusion.

The Zaskar leucogranites quite systematically show high contents in large ion lithophile elements K, Rb, Ba, and low contents in High-field strength elements (Nb, Hf and Zr), which strongly supports a micaceous crustal source for the magmas.

The discriminant Rb versus Nb+Y diagram (fig. 6.11), not surprisingly shows that our analyses for the Gumburanjun leucogranite lie within the collisional field, as generally do the other Himalayan leucogranites (Inger and Harris, 1993).

The evolution in the content of the granites in trace elements Rb, Sr and Ba, as well as in the major elements K_2O and Na_2O , provides indication on the melting process of the source region (Inger and Harris, 1993; Guillot, 1993). Pelitic and quartzo-feldspathic rocks do produce melts essentially through fluid saturated incongruent melting of

muscovite ($Ms + Pl + Qtz + H_2O \Rightarrow Melt$), fluid absent melting of muscovite ($Ms + Pl + Qtz \Rightarrow Als + Kfs + Melt \pm Bt$) or through fluid absent melting of biotite after exhaustion of muscovite ($Bt + Pl + Als + Qtz \Rightarrow Grt + Kfs + melt$). These reactions have implications for the volume of melt produced and the mineralogy of the restites, which in turn control the trace-element chemistry of the resultant magma. Hence, depending on P-T conditions and aH₂O, one of these three reactions causes melts to be produced, modifying the orthose/albite ratio, and directly influencing the contents in Ba as well as the ratios Rb/Sr and K₂O/Na₂O in the source and the magma. In vapour-absent conditions, the amount of K-feldspar in the restites will increase, but with higher temperatures, K-feldspar will be assimilated in the melt. This will be marked by an increase in the Rb/Sr ratio and a diminution in the Ba content of the granite.

Harris and Inger (1992), Inger and Harris (1993) and Harris et al. (1995) discussed the methodology of modelling melt reactions in pelitic protoliths, and explored the geochemical consequences of muscovite and biotite melting reactions in metapelites. They showed that the three main melting reactions have a distinctive restite mineralogy that controls the trace-element distribution

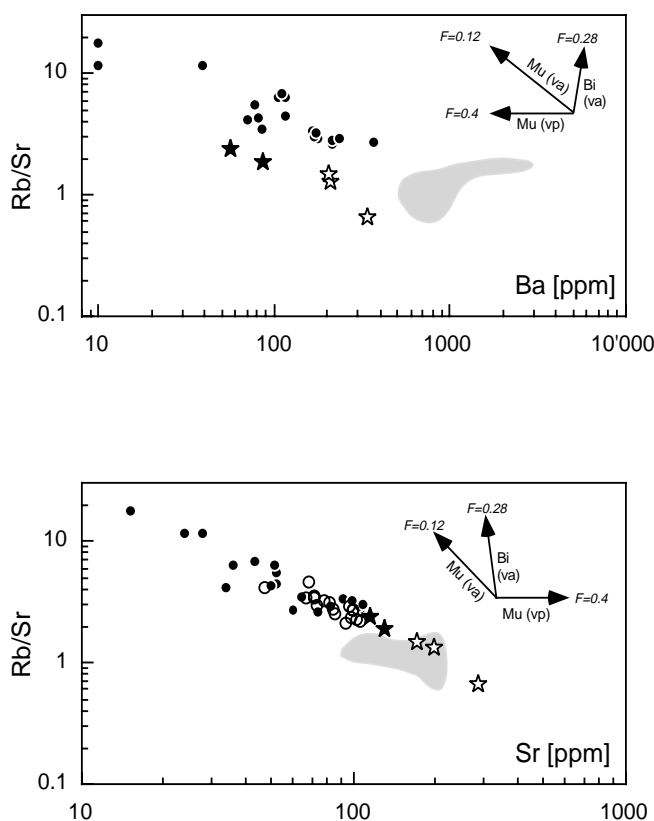


Fig. 6.12: Large ion lithophile element covariation in the Zaskar leucogranites. Stars - Our samples from the Gumburanjun; open circles - Ferrara's samples from the Gumburanjun; solid dots - Herren's samples from northwest Zaskar. Vectors represent partial melting reactions as determined by Inger and Harris (1993). The grey field corresponds to kyanite-grade micashists of the HHCS analysed by Inger and Harris (1993)

Mu (va) - vapour absent muscovite melting; Mu (vp) - vapour saturated muscovite melting; Bi (va) - vapour absent biotite melting. The observed correlation for the Zaskar samples corresponds to the fluid absent melting of muscovite. Black stars are for the tourmaline bearing leucogranites

between source and magma and that the Rb, Sr, Ba abundance in most Himalayan leucogranites are compatible with small degree ($F \sim 12\%$) partial melt of the mica schists of the source regions, under fluid-absent conditions through the muscovite dehydration reaction. These authors modelled melting vectors to illustrate the relationship of source to magma produced by the three potential melting reactions (fig. 6.12). These vectors show that a concomitant increase in Rb/Sr with a decrease in both Ba and Sr is the result of the vapour-absent breakdown of muscovite. Our analyses coupled with those of Herren (1987) and Ferrara et al. (1992), clearly show such a trend and the Zaskar leucogranites can thus be interpreted as resulting from muscovite dehydration reaction. Interestingly, our samples systematically show a lower Rb/Sr ratio than those of Herren or Ferrara et al.. Such low ratios were also found by Inger and Harris (1993) for the biotite leucogranites of the Langtang. For these authors, such low Rb/Sr ratios (< 2) indicate either that more hydrous conditions occurred during melting, or that the granite is derived from a source with a higher feldspar content. More hydrous conditions do however not signify that external fluids were incorporated into the system. The crystallization of melts derived from the breakdown of muscovite can liberate enough fluids to account for the production of subsequent magmas under hydrous

conditions. Wet magma is not synonymous with wet source!.

It should be noted that the proportion of Rb and Sr is readily modified by fractional crystallisation and therefore these elements can only be used when the granite composition is representative of a primary melt composition. The intrasuite covariations between Rb, Sr and Ba (fig. 6.12) indicate for the Zanskar leucogranite a control by alkali feldspar. Alkali feldspar may coexist with the primary melt as a peritectic phase or alternatively might be extracted from the melt by fractional crystallisation. The study of leucogranite thin section clearly indicates that quartz overgrows mica and plagioclase and is therefore the last major phase to crystallise (Harris et al. 1993). Hence, variations in Rb, Sr and Ba are determined by peritectic alkali feldspar and not by fractional crystallization.

6.5 Geochronology

Several leucogranitic samples have been selected for monazite U-Pb and muscovite Ar/Ar geochronology. The location of these samples is shown in figure 6.9. The monazite samples were collected and separated by J.C Vannay. Analyses were made by F. Bussy. The muscovite samples were collected, separated and analysed by the author.

The U-Pb analyses were made at the Royal Ontario Museum, Canada. Monazites have been isolated using conventional heavy liquid and magnetic separation techniques. Analysed crystals were selected on the basis of their high transparency, lack of inclusions and cracks, and euhedral shape. A slight air-abrasion was applied to some fractions to reduce possible surface-correlated lead-loss (Krogh, 1982). Monazite crystals were dissolved overnight on a hot plate using 6M HCL in Savillex[®] capsules. Chemistry was carried out using the standard techniques outlined in Krogh (1973), using a mixed $^{205}\text{Pb}/^{235}\text{U}$ spike, except that the capsule and column size were reduced by a factor of 10. Measurement and correction procedures follow the approach described in Bussy and Cadoppi (1996). Errors are quoted at the 95% confidence level.

The $^{40}\text{Ar}/^{39}\text{Ar}$ analyses were made at the Université de Lausanne following the analytical procedure given in Cosca et al. (1992). Samples, together with standards, were irradiated in the TRIGA reactor in Denver, USA. Gas was incrementally extracted using a low blank, double vacuum resistance furnace and analysed on a MAP 215-50 mass spectrometer. Analyses were corrected for blank, mass discrimination, isotopic decay, and interfering Ca-, K- and Cl-derived isotopes. For mass 40, blank values ranged from 4×10^{-15} moles below 1350°C to 9×10^{-15} moles at 1650°C. Blank values for masses 36-39 were below 2×10^{-17} moles for all temperatures. Isotopic production ratios for the TRIGA reactor were determined from analyses of irradiated CaF and K_2SO_4 . Correction for the neutron flux was determined using the international standards MMHB-1 and HD-BI.

The monazites from two samples of a leucogranite pluton from the Gumburanjun Intrusion Complex have been analyzed for U-Pb geochronology (Table. 6.2 and fig. 6.13). The geochemical analyses of these two samples V1(115) and V2(107) is given in table 6.1 and they have been differentiated from the three other chemical analyses in the various composition diagrams. One analysis (V1) was performed on the first sample and six (V2 to V7) on the second one. V1 to V5 yield $^{235}\text{U}/^{207}\text{Pb}$ ages ranging between 22.0 ± 0.2 and 22.5 ± 1 Ma. Except for the concordant analysis V2, these analyses plot slightly above Concordia indicating small excess ^{206}Pb , as has been inferred for some young Himalayan monazites (Schärer, 1984). XRF data indicate whole-rock Th/U ratios close to 1 for the studied leucogranite samples, which yields concordant or near concordant corrected ages using the calculation procedure of Schärer (1984). The discordant analyses V6 and

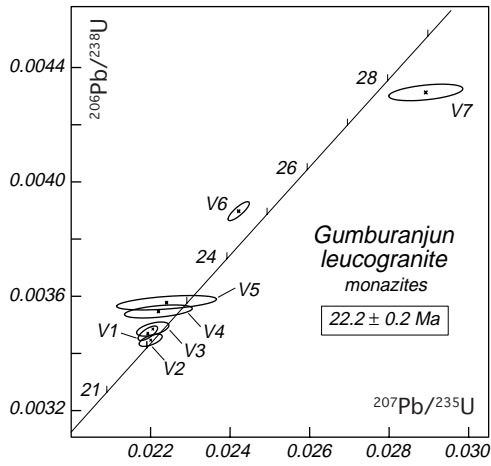


Fig. 6.13: U-Pb concordia diagram for monazites from the Gumburanjun leucogranite. The 22.2 ± 0.2 Ma age corresponds to the average of the analyses V1 to V5, and is considered as the best estimate for the leucogranite age. See text for discussion.

V7 both indicate older $^{235}\text{U}/^{207}\text{Pb}$ ages compared to the other analyses from the same sample (V2 to V5). V7 plots below Concordia and yields a $^{207}\text{Pb}/^{206}\text{Pb}$ age of ≈ 131 Ma. This feature unequivocally indicates the presence of an inherited component, as observed in some other Himalayan leucogranites (e.g. Harrison et al., 1995; Edwards and Harrison, 1997). Because the multiple-grain analysis V6 may also be affected by inheritance, we consider these two analyses as unreliable. V1 to V5 indicate an average $^{235}\text{U}/^{207}\text{Pb}$ age of 22.2 ± 0.2 Ma, which we consider as the best estimate for the age of cooling of the leucogranite through the closure temperature of monazite ($725 \pm 25^\circ\text{C}$). This result is comparable to U-Pb data from central Zaskar, 150 km to the NW of the studied area, where crustal anatexis and leucogranite intrusion in the foot wall of the ZSZ occurred between 22 and 19 Ma (Noble and Searle, 1995).

An upper intercept age of 499 ± 235 Ma. was obtained from analyses V7. Similar upper intercept ages of 463 ± 13 and 476 ± 12 Ma were obtained by Noble and Searle (1995) on monazites and zircons from leucogranites of north-west Zaskar (upper Suru valley). These ages compare well with the ages of the Cambro-Ordovician orthogneisses in the HHCS of Zaskar. Indeed, a 495 ± 16 Ma age was calculated for the Kade orthogneiss (Frank et al. 1975) and other orthogneisses in Zaskar yield Zircon ages of 472 Ma. (Pognante et al., 1990). These ~ 500 Ma orthogneisses belong to the late Pan-African event.

A total of ten muscovite $^{40}\text{Ar}/^{39}\text{Ar}$ cooling ages (Table 6.3, fig. 6.15) were obtained from both deformed dikes (Z1 and Z2) and undeformed dikes (Z7 to Z10) intruding the base of the ZSZ, as well as from the leucogranitic plutons (Z3 to Z6). The deformed dikes yield cooling ages around 22 - 21 Ma, whereas the undeformed dikes consistently indicate younger ages around 19.8 - 19.3 Ma. The plutons yield muscovite cooling ages between 20.4 - 19.5 Ma.

In figure 6.14, we have plotted the five relevant monazite U-Pb ages and the four muscovite $^{40}\text{Ar}/^{39}\text{Ar}$ ages from the Gumburanjun leucogranite, as well as biotite and muscovite Rb/Sr cooling ages from the same granite (Ferrara et al., 1991), against the estimated blocking temperatures of these minerals. The muscovite Z3 and the monazites analyses V2 to V5 come from the same sample,

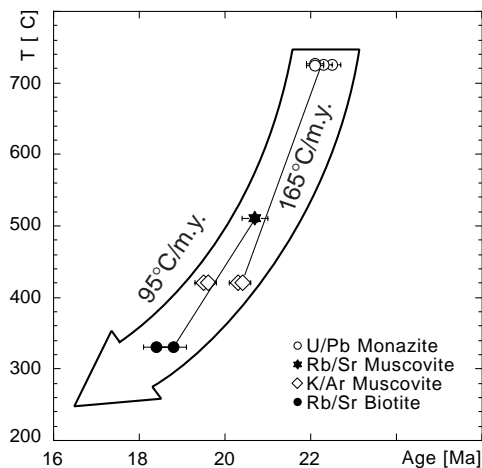


Fig. 6.14: Cooling ages versus closure temperatures from the Gumburanjun leucogranite. Rb/Sr ages are taken from Ferrara et al. (1991). Blocking temperature for U-Pb monazite = $725 \pm 25^\circ\text{C}$ (Parrish, 1990). All other temperatures as compiled by Hodges (1991): Rb / Sr muscovite = $510 \pm 50^\circ\text{C}$, K / Ar muscovite = $420 \pm 50^\circ\text{C}$, Rb / Sr biotite = $330 \pm 50^\circ\text{C}$. The solid lines represent the cooling rates of samples for which two minerals with different blocking temperatures were dated. The arrow shows the inferred overall cooling curve of the Intrusion Complex leucogranite. Symbols in isochron diagrams are larger than the uncertainties. tr: trapped argon, MSWD: mean square of weighted deviation. The $^{40}\text{Ar}/^{39}\text{Ar}$ ratio of atmosphere (Air) = 295.5.

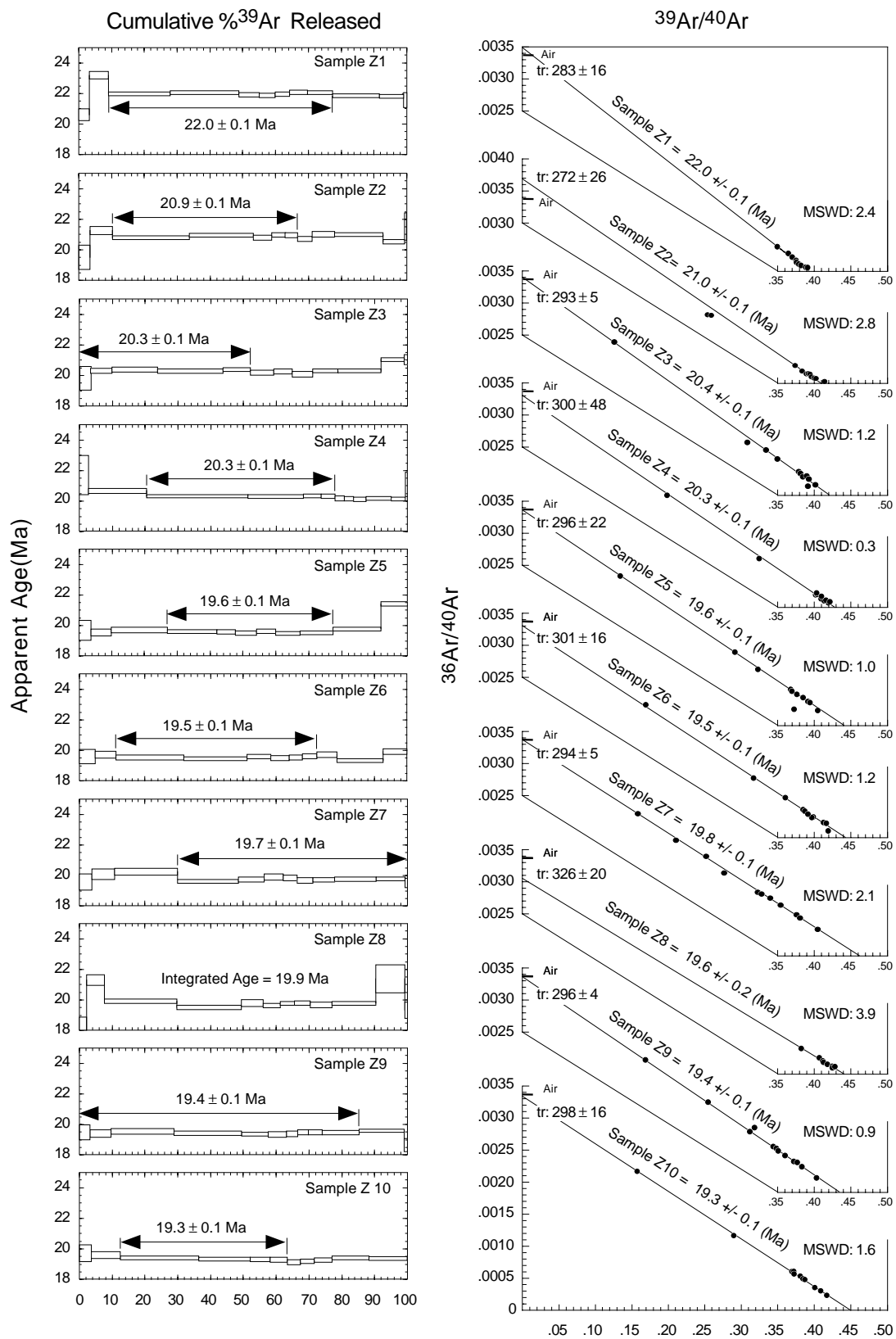


Fig. 6.15: $^{40}\text{Ar}/^{39}\text{Ar}$ age spectra and isochrons of muscovites from leucogranitic plutons and dikes. All uncertainties reported at 2s precision. Plateau ages correspond to at least three consecutive steps showing similar $^{40}\text{Ar}/^{39}\text{Ar}$ ratios within uncertainties and representing at least 50% of the ^{39}Ar released. The isochron statistics are given for the plateau steps and these results indicate trapped argon of atmospheric composition in all samples. Symbols in isochron diagrams are larger than the uncertainties. tr: trapped argon, MSWD: mean square of weighted deviation. The $^{40}\text{Ar}/^{39}\text{Ar}$ ratio of atmosphere (Air) = 295.5.

which allows us to calculate a cooling rate of 165 °C / m.y. between 725 °C and 420 °C. A cooling rate of 95 °C / m.y. between 510 °C and 330 °C can be calculated in the same way with one of Ferrara's samples. The arrow in figure 6.14 outlines the overall cooling trend of the Intrusion Complex leucogranitic plutons.

6.6 Origin of the leucogranites and melt migration

Radiogenic and stable isotopic composition of the leucogranites, their common occurrence within the high-grade regional metamorphic terranes, the lack of spatial and temporal association with basalt magmatism strongly suggest that the leucogranites are the product of pure crustal melt, uncontaminated by mantle material.

The source of the Himalayan Leucogranites is generally ascribed to the aluminous schists and gneisses of the HHCS, partly because of structural relation and partly because of isotopic systematics for Rb, Sr, Nd, O (France-Lanord et al., 1988; Deniel et al., 1987; Ferrara et al. 1991, Harris and Massey, 1994). The monazite and zircon upper intercept ages around 500 Ma of the Zanskar leucogranite clearly indicate that they must be partly derived from the melting of the Cambro-Ordovician Granites. As these old granites are relatively poor in muscovite, the leucogranite must also have had a more pelitic source. On the basis of Sr and Nd isotope ratios, Ferrara et al. (1992) found two different isotopic signatures for the Gumburanjun Leucogranite. They attribute these differences to variations in the composition of the source rocks, one yielding a characteristic signature of a metapelite protolith and the other of an igneous (granitic) protolith.

The origin of Himalayan leucogranite was believed to be related to water-saturated melting. Fluid advection from the footwall of the Main Central Thrust (Lesser Himalaya) into the relatively hot hanging wall (HHCS) was invoked as the driving mechanism for the production of water-saturated melt in the upper structural levels of the HHCS (Le Fort et al. 1987). There is however little evidence to support the notion of pervasive aqueous fluids during metamorphism of the mid-lower crust and recent trace element studies argue against fluid present melting in the formation of crustal melts (Harris et al. 1993). Also in Zanskar, metamorphic conditions and textural evidences observed in the migmatitic zone rather indicate that melts were derived from the incongruent melting of muscovite.

Lately, Himalayan leucogranitic magmas are thus increasingly thought to be initially water-undersaturated, indicating either that a fluid phase with $a_{H_2O} \ll 1$ was present during melting or that the melting reactions were fluid-absent. In the absence of free water, melting depends on the availability in the source region of hydrous minerals like muscovite or biotite which may release their water during anatexis. The amounts of water released by the breakdown of these minerals is usually not sufficient to saturate the magma and is dissolved in the melt without formation of a vapour phase (Vilzeuf and Holloway, 1988). This process is referred to as «fluid-absent melting» (Clemens, 1984), «dehydration melting (Thompson, 1982)» or «vapor-absent melting (Grant, 1985)». Aluminous schists and gneisses are generally considered to be the likely source for peraluminous granites.

The breakdown of muscovite occurs through the reaction: $22 \text{ Muscovite} + 7 \text{ plagioclase} + 8 \text{ quartz} = 5 \text{ K-feldspar} + 5 \text{ Al}_2\text{SiO}_5 + 2 \text{ biotite} + 25 \text{ melt}$ (Patino Douce, 1998), which is also known as the second sillimanite isograd (Spear, 1993). This reaction can however only produce 10-15 vol. % melt between 750° and 850°C and at 10 kbar (Vilzeuf and Holloway, 1988). Up to 50 vol. % melt can however be produced at higher temperatures (850°-900°C) with the breakdown of biotite through

the reaction: biotite + Al_2SiO_5 + plagioclase + quartz = Garnet + K-feldspar + melt. (Vilzeuf and Holloway, 1988). The amount of partial melting required before melts begin to segregate and forms plutons is called critical melt percentage. The value of this critical melt percentage is generally believed to be of the order of 25% (Spear, 1993).

A possible objection to fluid-absent melting of muscovite as the source for the leucogranites might thus be that the low melt fraction obtained through this reaction ($F < 0.15$) would preclude a critical melt percentage being obtained ($F > 0.25$) and hence prevent the melt from leaving its source. The concept of critical melt percentage does, however, assume that the melt will migrate through diapirism. We have described above that abundant feeder dikes are rooted into the migmatitic zone, which indicates that the ascent of the melts occurred through fracture propagation and was driven either by buoyancy or injection pressure, and thus diapiric arguments are irrelevant for the present case. Moreover, we have seen that the xenoliths within the leucogranitic plutons have also undergone incongruent melting and thus that the injection zone must also have contributed to the global amount of melt. Under such circumstances it is difficult to place a minimum constraint on the melt fraction that can be extracted from the source.

Patino Douce and Harris (1998) have conducted a melting experiment on two types of metapelitic rocks from the HHCS. Their results indicate that dehydration melting begins at 750°C - 800°C and produces melts that are virtually identical to the Himalayan leucogranites. Adding extra water to the starting material lowers the melting point $< 750^\circ\text{C}$, which is pretty logical, but the resulting melt has a trondhjemitic composition, which is different from most Himalayan leucogranites. For these authors, the Himalayan leucogranites were generated by fluid-absent melting at temperatures around 750°C and 6-8 kbars during adiabatic decompression and are solely the result of the breakdown of muscovite, which is in contradiction with Spear's (1993) critical melt percentage.

The dP / dT slope of the biotite dehydration curve is steep and is expected to intersect the flatter muscovite dehydration curve at high pressure. The actual pressure of the crossover is however uncertain as the exact temperature of the breakdown of biotite is highly dependant on the mg-number of biotite and the Ti and F contents of both biotite and muscovite as well as on the plagioclase composition of the source rocks. Estimation range from 9 kbar (Patino Douce and Harris, 1998) to 14 kbar (Spear, 1993).

Finally, the recognition that melting occurs essentially in the upper structural levels of the HHCS argues against the correlation of anatexis through fluid influx from the regional thrusting on the MCT, but is consistent with an association between granite formation and exhumation along the Zaskar Shear Zone.

6.6 Discussion

The Gumburanjun leucogranite is one of the pure crustal melt granites cropping out along the top of the High Himalayan Crystalline Sequence, in close association with the Zaskar Shear Zone, a segment of the South Tibetan Detachment System. This granite has a very homogenous mineral and major-element composition. Two slightly different types of leucogranites were however observed, essentially on the basis of the presence or absence of biotite. This intrusions is very similar to the other leucogranites of Zaskar which in turn show almost no mineralogical or chemical difference with other Himalayan leucogranites. Marked differences are observed in the trace-element contents of the leucogranites. These differences mainly result from the melting of an inhomogeneous source region composed of metapelites and Cambro-Ordovician orthogneisses.

Mineralogical and textural observation coupled with analytical results concur to indicate that the migmatitic zone forms the source region of the leucogranitic melts and that melting occurred through vapour-absent breakdown of muscovite, without external fluids flushed into the system. A chronological relation can be established between the biotite leucogranites and the tourmaline leucogranites. The intrusion of the former ones seems to precede the intrusion of the latter ones, which are often coarser grained and form pegmatites. It is our strong belief that the biotite leucogranites represent early melts produced in the migmatitic zone and injected in the overlying units through fracture propagation. The crystallisation of these biotite leucogranites liberated volatiles that favoured the production of additional melts of the second type (tourmaline leucogranite). This «in-situ» production of melt is testified by the presence of country-rock xenoliths whose strong depletion in muscovite argues for a restitic nature.

Vapour-absent melting of muscovite in the migmatitic zone was triggered by isothermal decompression. Isothermal decompression resulted from the rapid exhumation of the HHCS along the Zaskar Shear Zone. The production of leucogranitic melts is thus the direct consequence of extensional movements along the ZSZ.

The leucogranites cooled below the closure temperature ($725^{\circ}\pm 25^{\circ}\text{C}$) of monazite at 22 ± 0.2 Ma. This age is a close estimate of the «real» age of these granites as they underwent rapid cooling ($> 165^{\circ}\text{C}/\text{Ma}$) and the melting temperature of the protolith was $\sim 770^{\circ}\text{C}$.

The reason why leucogranites are abundant in south-east Zaskar but diminish towards the north-west is not clear. The same metamorphic conditions and extensional tectonics do indeed prevail for more than 150 km along the ZSZ. Therefore, we suggest that the main factor influencing the formation of leucogranites lies in the composition of the protolith. To produce leucogranites through decompression melting, a muscovite rich source is needed. Hence metapelites represent a more fertile source than orthogneisses or metapsammities. We could indeed observe that the studied area was rich in metapelitic horizons, but that to the north-west, (Reru-Mune area), the HHCS shows a more psammitic nature, with increasing bodies of orthogneisses, precluding the formation of anatectic melts leaving their source.

Table 6.1: Bulk chemical composition of Gumburanjun leucogranite. Analysed by Vannay (unpubl. data).

Sample	V1(115)	V2(107) T	V106	V116	V117 T	Mean \pm std. dev.
Major elements [weight %]						
SiO ₂	74.58	74.02	73.20	73.68	73.46	73.79 \pm 0.48
TiO ₂	0.10	0.07	0.17	0.13	0.08	0.11 \pm 0.04
Al ₂ O ₃	15.16	15.36	15.50	15.52	15.64	15.44 \pm 0.16
Fe ₂ O ₃	1.07	0.82	1.38	1.28	1.02	1.11 \pm 0.20
MnO	0.04	0.05	0.03	0.03	0.06	0.04 \pm 0.01
MgO	0.14	0.06	0.28	0.21	0.10	0.16 \pm 0.08
CaO	0.55	0.47	0.73	0.61	0.43	0.56 \pm 0.11
Na ₂ O	3.97	4.33	4.39	4.22	4.03	4.19 \pm 0.16
K ₂ O	3.65	3.98	3.21	3.37	4.23	3.69 \pm 0.38
P ₂ O ₅	0.13	0.19	0.09	0.13	0.18	0.14 \pm 0.04
H ₂ O	0.59	0.48	0.64	0.65	0.48	0.57 \pm 0.07
L.O.i.	0.07	0.03	0.00	0.10	0.10	0.06 \pm 0.04
Cr ₂ O ₃	0.00	0.00	0.00	0.00	0.00	0.00
NiO	0.00	0.00	0.00	0.00	0.00	0.00
Total	100.05	99.86	99.62	99.93	99.81	
A/CNK	1.32	1.25	1.29	1.33	1.30	1.30 \pm 0.03
Trace elements [ppm]						
Ba	203	87	333	206	56	177 \pm 99
Rb	250	250	188	264	267	244 \pm 29
Sr	170	130	285	199	115	180 \pm 60
Pb	119	126	152	116	127	128 \pm 13
Th	1	<1	3	3	<1	2 \pm 1
U	<2	4	4	<2	6	4 \pm 2
Nb	<5	<5	<5	<5	5	5 \pm 0
La	8	<4	14	14	<4	9 \pm 5
Ce	23	<6	21	22	17	18 \pm 6
Nd	5	<3	9	5	<3	5 \pm 2
Y	9	5	10	10	5	8 \pm 2
Zr	45	35	65	58	35	48 \pm 12
V	<3	<3	11	8	<3	6 \pm 3
Cr	<3	<3	6	<3	<3	4 \pm 1
Ni	<2	2	<2	<2	2	2 \pm 0
Co	50	32	38	39	38	39 \pm 6
Cu	<4	67	<4	12	<4	18 \pm 25
Zn	48	113	56	63	49	66 \pm 24
Ga	17	17	19	18	17	18 \pm 1
Hf	<2	<2	<2	<2	<2	2 \pm 0
S	42	49	<10	40	43	37 \pm 14

Samples V1 (115) and V2 (107) were used for U/Pb monazite age determination (table 6.5.1). Ar/Ar muscovite age was also obtained for sample V2 (107) (sample Z3 in table 6.5.2). Samples V2 (107) and V117 (**T**) are tourmaline bearing leucogranites. The three other samples are biotite bearing leucogranites.

Table 6.2: U-Pb monazite data for the Gumburanjun leucogranite

Sample#	Weight (mg)	Concentrations			Atomic ratios					Age (Ma)
		U (ppm)	Pb* (ppm)	cPb** (pg)	$^{206}\text{Pb}^\dagger$ ^{204}Pb	$^{208}\text{Pb}^\S$ ^{206}Pb	$^{206}\text{Pb}^\S$ ^{238}U	$^{207}\text{Pb}^\S$ ^{235}U	$^{207}\text{Pb}^\S$ ^{206}Pb	
[V1] 1, a fr	0.004	20322	121	10	1151	0.893	0.00347±2	0.0219± 2	0.0458± 3	22.0±0.2
[V2] 1, a fr	0.007	6120	61	15	480	2.152	0.00345±2	0.0220± 2	0.0463± 4	22.1±0.2
[V3] 2, u fr	0.006	3731	41	9	354	2.498	0.00348±2	0.0221± 4	0.0459± 6	22.1±0.4
[V4] 1, u e i	0.001	7419	74	0	228	2.107	0.00355±2	0.0222± 6	0.0454±13	22.3±0.6
[V5] 1, u tip	0.001	4789	53	0	189	2.544	0.00358±2	0.0224±10	0.0454±20	22.5±1.0
[V6] 3, a e	0.008	7837	105	8	1164	2.885	0.00390±2	0.0242± 2	0.0451± 2	24.3±0.2
[V7] 1, u e	0.001	7180	74	0	323	1.706	0.00431±2	0.0289± 8	0.0486±12	28.9±0.8

Note: Error estimates (95 % confidence level) refer to the last significant digits of the isotopic ratios and reflect reproducibility of standards, measurement errors, and uncertainties in the common Pb correction.

[i] = fraction number, 1 = number of grains analyzed, a = abraded, u = unabraded, fr = fragment, e = euhedral, i = with inclusions.

*Radiogenic.

**Common Pb.

†Corrected for spike Pb and for fractionation.

§Corrected for fractionation, spike, U and Pb blanks, and initial common Pb.

Analyses were made by F. Bussy at the Royal Ontario Museum, Canada

Table 6.3: summary of $^{40}\text{Ar}/^{39}\text{Ar}$ results on muscovites

Sample	Plateau Age (Ma)	Isochron Age (Ma)	$^{40}\text{Ar}/^{36}\text{Ar}^*$	MSWD†
Z1§	22.0 ± 0.1	22.0 ± 0.1	283 ± 16	2.4
Z2§	20.9 ± 0.1	21.0 ± 0.1	272 ± 26	2.8
Z3#	20.3 ± 0.1	20.4 ± 0.1	293 ± 5	1.2
Z4#	20.3 ± 0.1	20.3 ± 0.1	300 ± 48	0.3
Z5#	19.6 ± 0.1	19.6 ± 0.1	296 ± 22	1.0
Z6#	19.5 ± 0.1	19.5 ± 0.1	301 ± 16	1.2
Z7**	19.7 ± 0.1	19.8 ± 0.1	294 ± 5	2.1
Z8**	N.A.††	19.6 ± 0.2	326 ± 20	3.9
Z9**	19.4 ± 0.1	19.4 ± 0.1	296 ± 4	0.9
Z10**	19.3 ± 0.1	19.3 ± 0.1	298 ± 16	1.6

Note: All uncertainties reported at 2s. Methodology given in Appendix.

* Initial $^{40}\text{Ar}/^{36}\text{Ar}$ ratio.

† Mean square of weighted deviates for isochron.

§ Deformed dikes.

Plutons.

** Undeformed dikes.

††N.A. = not applicable.

7. THE ZSZ: AGE AND AMOUNT OF SHEAR

And he told stories, tracing with a finger in the dust, of the immense and sumptuous ritual of avalanche-guarded cathedrals; of processions and devil dances; of the changing of monks and nuns into swine; of holy cities fifteen thousand feet in the air; of intrigue between monastery and monastery; of voices among the Hills, and of that mysterious mirage that dances on dry snow.

«Kim» Rudyard Kipling

7.1 Introduction

We have seen in the preceding chapters that the exhumation of the High Himalayan Crystalline Sequence was assisted by extensional movements along the Zaskar Shear Zone. The exhumation of the HHCS had two major effects on the tectonometamorphic history of this unit: (1) The thickness of the Barrovian metamorphic zones has been reduced significantly through ductile shearing along the ZSZ. (2) Vapour-absent anatectic melting occurred in the highest grade Barrovian metamorphic zone, resulting in the production of leucogranitic rocks.

The thermobarometric data and the petrographic evidences we have presented in chapter 5 will be used to quantify the amount of ductile shearing along the ZSZ.

The geochronological data presented in chapter 6 will be used to constrain the age and duration of ductile extensional tectonics at the top of the HHCS.

7.2 Displacement along the ZSZ

To estimate the amount of ductile shearing that was accommodated by the ZSZ, we resorted to a simple trigonometric model which is presented in fig. 7.2.1. This model is based on the observation that, along a horizontal profile across the ZSZ, one can see the successive apparition of increasingly metamorphosed rocks, which equilibrated at very different depths, but are now at the same structural level. The net slip (s) required to bring two such rocks, initially separated by a vertical distance (ΔH), to the same structural level within a shear zone (dipping at an angle α) can easily be calculated by:

$$s = \Delta H / \sin\alpha. \quad (1)$$

The equilibration depth of the various metamorphic zones is given either by thermobarometric results or by petrographic evidences and the present dip of the shear zone is known (20°). It is thus possible to calculate the net slip along the ZSZ.

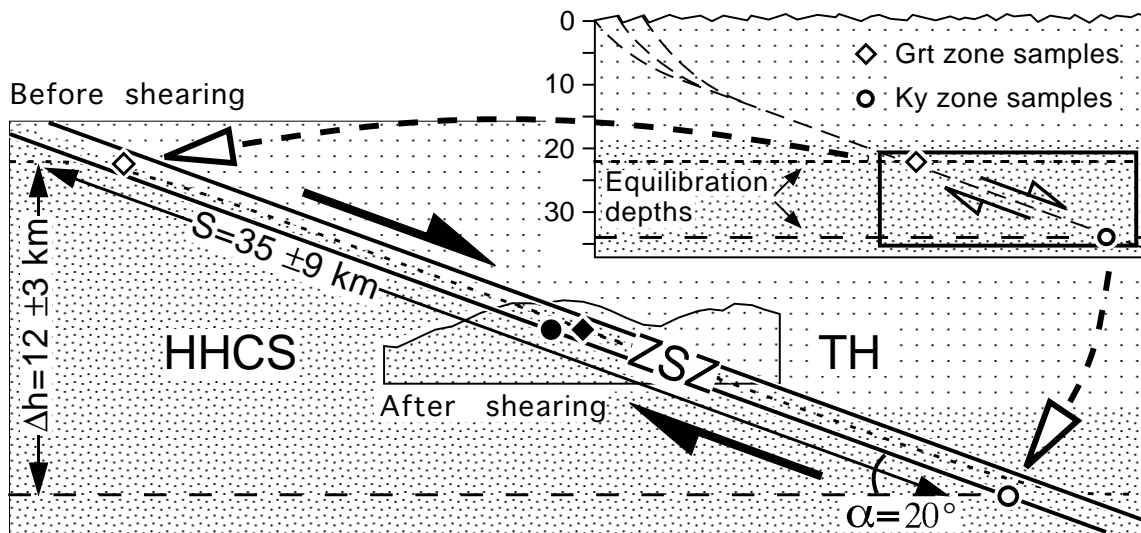


Fig. 7.1: Geometrical model for the estimation of the minimum displacement accommodated by the Zanskar Shear Zone. The small picture inlaid in the upper right corner represents the initial state after crustal thickening but before the onset of extension. The big picture is an enlargement of the black framed rectangle in the lower right corner of the inlaid picture. The cross-section in the centre of the picture corresponds to Fig. 5.8 and represents the final stage after extension. The diamond and circle represent the location of samples from the garnet and kyanite zones before extension (white) and after extension (black). α = present-day dip. No vertical exaggeration. $S = \Delta H / \sin\alpha$

Applying this equation to the Zanskar Shear Zone however requires a certain number of assumptions:

- (A) We consider the telescoping of the metamorphic zones to be essentially the result of simple shear. Pure shear is not considered in this model. Pervasive C/S fabrics within the ZSZ suggest, however, that extension occurred mainly through ductile simple shear.
- (B) The topography during peak Barrovian metamorphism is assumed to be flat, the difference in equilibration depth would indeed be overestimated if the higher grade rocks equilibrated under a significantly higher topographic relief than the lower grade samples. A southward increasing topographic gradient is however very unlikely because of the observed gradual decrease in metamorphic conditions in the TH sediments forming the hanging wall of the ZSZ.
- (C) The metamorphic field gradient observed across the ZSZ is here considered as representative of the thermal structure of the crust during metamorphism. This assumption is clearly false, because the metamorphic field gradient in any region is defined by a succession of mineral assemblages which equilibrated at peak temperature conditions but the peak temperatures were reached at different times for each metamorphic zone (fig. 7.2). The consequence is that the pressure at peak temperature is lower than immediately post-thrusting. However, as shown in figure 7.2 the difference in the depth of burial of two rocks (from two different metamorphic zones) directly after thrusting must be greater than when these same rocks have reached their respective maximal temperature. Hence, as we consider differences in equilibration depth for our calculation of the net slip, the consequence is that we under-evaluate this value.

The beauty of this trigonometric model however resides in its simplicity and in the fact that it is not influenced by the original angle formed between the metamorphic isograds and the shear zone.

The geothermobarometric data presented in chapter 5 indicate a maximal peak pressure difference of 320 ± 80 MPa between the samples from the garnet and the kyanite zone. Assuming a lithostatic pressure gradient of 27 MPa/km, this value can be converted into a vertical distance (ΔH) of 12 ± 3 km. This value represents the finite vertical displacement to bring the lowermost kyanite zone sample to the same structural level as the uppermost garnet zone sample. Using this vertical distance ΔH

$\sim 12 \pm 3$ km and the present-day dip of the ZSZ $\alpha = 20^\circ$, a net displacement $s = 35 \pm 9$ km is calculated with equation (1).

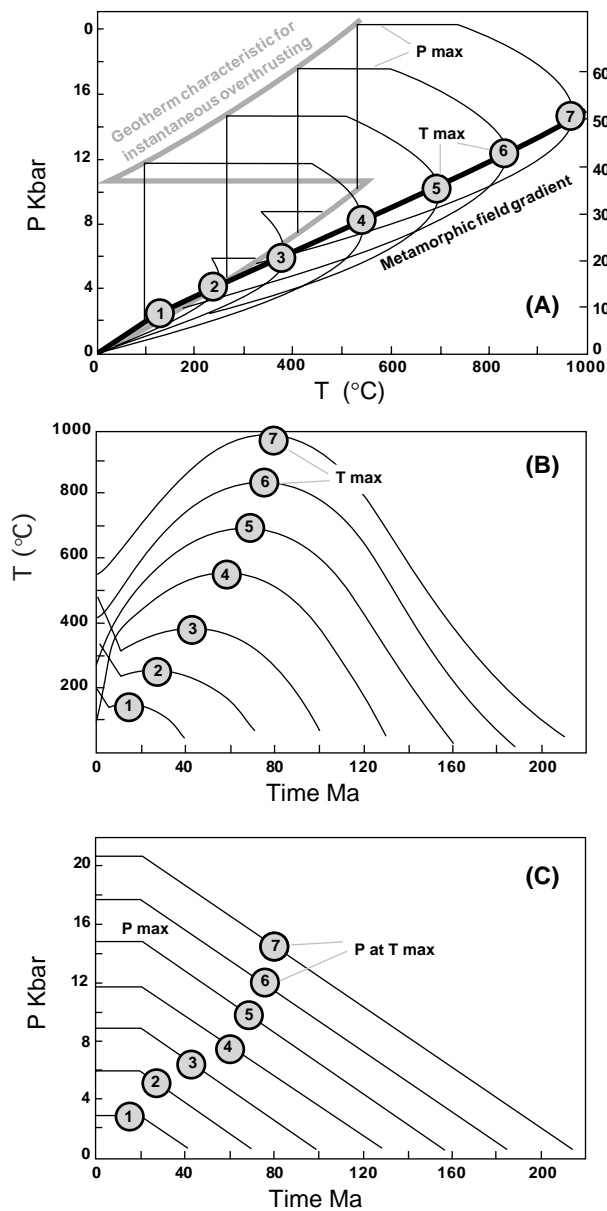


Fig. 7.2: P-T paths (A), T-time paths (B) and P-time paths (C) showing the theoretical evolution of 7 rocks after instantaneous overthrusting (Spear, 1993). Rocks 1, 2 and 3 are from the overthrusting unit and 4, 5, 6 and 7 are from the overthrust unit. The circles labelling each rock path have been placed on the peak metamorphic conditions defined by T max. (A), The line drawn through the loci of thermal maxima corresponds to the “metamorphic field gradient”. (B) Note that there is a progression in the time of T max; the deeper the rock, the later it reaches T max. (C) Note that the value of P at T max is lower than the maximum value of pressure (P max) for each rock.

Several considerations indicate that this value of 35 ± 9 km is a minimum value for the displacement along the ZSZ:

- The kyanite zone to garnet zone rocks represent only part of the sheared sequence (fig. 5.8). The deformation accommodated in the biotite zone has not been considered as no quantitative pressure constraints can be obtained for these assemblages. Additionally, more brittle extension in higher levels is also not quantified. It is however very likely that most of the deformation was concentrated in the high-grade, ductile part of the ZSZ and that the lower-grade rocks accommodated less shearing (e.g. Hacker and Mosenfelder, 1996). Petrographic evidences (staurolite out) indicate that the lowermost part of the kyanite zone equilibrated at higher pressures than those indicated by the thermobarometrical results. On the basis of these arguments, even a cautious estimation of the vertical distance between the equilibration depth of biotite zone and the lowermost kyanite zone results in a value of $\Delta H \sim 16$ km. With this value, the net slip of the ZSZ would be $s \approx 47$ km.

- The pressure estimate for peak conditions in the Migmatite Zone (fig. 5.21) indicates an equilibration depth of $\approx 43 \pm 4$ km (Table 5.1). Although this estimate is calculated with a different methodology compared to the ZSZ samples, it fits in with the metamorphic field gradient defined by these latter rocks, as well as with another estimate for comparable migmatites (fig. 5.21, sample MPL). The difference in equilibration depths between the Migmatite Zone and the ZSZ garnet zone rocks implies a vertical displacement $\Delta H \approx 21 \pm 4$ km and a net slip $s \approx 61 \pm 12$ km to bring these samples to the same horizontal level.

- Thirdly, estimates for the ZSZ net slip are highly sensitive to the dip of the structure. Because of the late large-scale doming of the HHCS in Zanskar, the original dip of the ZSZ was possibly less than its present dip of 20° . In the Qomolangma (Mt. Everest) region, where no doming is observed, the dip of the STDS varies between 15° to 5° (Burchfiel et al., 1992). Recent seismic data suggest that the dip of the STDS in the eastern Himalaya is approximately 12° , before flattening out at ≈ 20 km depth (Makovsky et al., 1996; Alsdorf et al., 1998; Hauck et al., 1998). For an original

dip of 12° and a vertical displacement $\Delta H \approx 21 \pm 4$ km, the net slip of the ZSZ could thus have been up to $s \approx 100 \pm 20$ km.

The net slip along the ZSZ in central Zanskar was estimated by Herren (1987) to be at least 25 km, on the basis of a geometrical model for the shearing of isograds. This model allows to calculate the net slip (s) along the shear zone using the equation:

$$s = (b / \sin\beta)(h / h' - \cos\beta) \quad (2)$$

where h is the thickness of a supposedly unshaped rock sequence between two known isograds outside the ZSZ (measured in the western Suru area), h' is the thickness of the same sequence sheared within the ZSZ, b is the width of the ZSZ, and β is the dip of the ZSZ relative to the dip of the isograds outside the shear zone ($\beta = 20^\circ$).

Equation (2) can be developed as:

$$s = (b \cdot h / h' \cdot \sin\beta) - (b \cdot \cos\alpha / \sin\beta) \quad (2.1)$$

$$s = (h \cdot (b/h') / \sin\beta) - (b / \tan\beta) \quad (2.2)$$

(2.2) is very similar to our own equation (1) because $h \cdot (b/h')$ is equivalent to ΔH and the term $(b / \tan\beta)$ only implies that one considers sampling perpendicular to the shear zone boundaries, instead of along a horizontal profile. The difference is anyway negligible. The major difference between the two equations is that Herren considers the angle β between the dip of the ZSZ and the dip of the isograds, where we only consider the dip of the shear zone (α)

Although this approach is broadly comparable to ours, it is based on some poorly constrained parameters. First, Herren (1987) measured a thickness $h \approx 6.3$ km between the garnet to sillimanite isograds outside the ZSZ. This value appears surprisingly small compared to the $\Delta H = 12 \pm 3$ km of initial vertical distance between the garnet zone and kyanite zone samples, as indicated by our thermobarometry results. This difference suggests that, even outside the ZSZ, the isograds may have been thinned by the late- to post-metamorphic extensional structures scattered throughout the HHCS of Zanskar (Kündig, 1989). This process would lead to an underestimation of the original thickness of the sequence bound by known isograds, and therefore of the displacement along the ZSZ, using Herren's approach. In contrast, our estimate of the vertical displacement based on P-T results for peak conditions would not be affected. Secondly, Herren (1987) calculated the total thickness of the sequence before shearing as $h (b / h')$. Because b and h' are both comparably small (0.35 and 0.25 km respectively in Herren, 1987), even small uncertainties in these two values have a major influence on the estimation of the total original thickness of the sequence now sheared within the ZSZ, and thus on the total movement. Thirdly, Herren's calculation of the net slip is dependant on the angle between the shear zone and the isograds which is difficult to estimate precisely.

Using the thermobarometric and the petrographic information to estimate the original thickness of the sheared metamorphic sequence proves to be much more accurate, as it allows to avoid most of the weakly constrained parameters used in Herren's purely geometrical model. Moreover our final calculation of the net slip along the ZSZ is independent of the original angle the isograds formed with the extensional structure.

7.3 Timing of extensional shearing along the ZSZ

Several arguments indicate close spatial and chronological relations between extension along the ZSZ, anatexis in the Migmatite Zone, and leucogranite intrusions. The coherent metamorphic field gradient defined by the P-T results (fig. 5.21) shows that the metamorphic evolution in the HHCS is the consequence of an underthrusting event which preceded the activation of the ZSZ. These results also indicate that peak metamorphic conditions in the migmatitic zone during underthrusting were close to but not necessarily sufficient for partial melting of these rocks through dehydration melting of muscovite.

The metamorphic peak conditions in the Migmatite Zone, as well as in the lower ZSZ, were followed by nearly isothermal decompression implying an exhumation faster than the thermal relaxation of the perturbed isotherms (fig. 5.22). Such a retrograde P-T path is characteristic of tectonic denudation processes (e.g. Ruppel et al., 1988) and is the consequence of the very rapid exhumation of the HHCS. Production of leucogranitic melts thus started once the decompression path of the rocks from the migmatitic zone crossed the muscovite dehydration-melting solidi.

Geochronological results indicate that the leucogranites from the Intrusion Complex cooled below $T \approx 725 \pm 25^\circ\text{C}$ at 22.2 ± 0.2 Ma (fig. 6.14). On the basis of the P-T results (fig. 5.22), we conclude that the production of leucogranitic melts was preceded by a nearly isobaric decompression which we interpret as the consequence of a rapid exhumation. This interpretation implies that cooling at 22.2 ± 0.2 Ma recorded an already ongoing stage of extension. The onset of extension (and leucogranite production) was however probably not significantly older than 22.2 Ma, although it cannot be constrained more precisely.

The magmas produced in the Migmatite Zone rose through a swarm of feeder dikes which coalesced below the ZSZ to form the flattened, sill-like plutons of the Intrusion Complex. These relations suggest that intrusion took place through fracture propagation and that the ZSZ acted as a mechanical and/or thermal discontinuity which hindered this propagation and further magma ascent (e.g. Clemens & Mawer, 1992). Several generations of leucogranitic dikes nevertheless intruded the base of the ZSZ. Most of these dikes are strongly deformed, but the presence of some undeformed dikes crosscutting the base of the shear zone clearly indicates that the leucogranite intrusion outlasted the main phase of ductile deformation.

The undeformed leucogranite dikes intruding the base of the ZSZ cooled below the closure temperature for Ar diffusion in muscovite ($T \approx 420 \pm 50^\circ\text{C}$) between 19.8 ± 0.1 and 19.3 ± 0.1 Ma (Table 6.3). These data indicate that the main ductile deformation along the ZSZ ceased before 19.8 ± 0.1 Ma. It is nevertheless likely that some brittle extension in the ZSZ hanging wall outlasted the ductile shearing (e.g. Sarchu Fault).

Consequently, our geochronological data suggest that ductile shearing along the ZSZ occurred between 22.2 ± 0.2 Ma and 19.8 ± 0.1 Ma and lasted not much more than 2.4 ± 0.2 My.

7.4 Discussion

The results of the present study show that the ZSZ accommodated at least 12 ± 3 km of vertical displacement, which corresponds to a net slip of 35 ± 9 km for the present-day dip of the shear zone. We consider these values as strict minima because several arguments strongly suggest that the ZSZ might have accommodated as much as 100 Km net slip. Geochronological data demonstrate that the main ductile shearing ceased before 19.8 Ma and that the leucogranite in the ZSZ foot wall cooled through the U-Pb closure temperature for monazite at 22.2 ± 0.2 Ma, which is interpreted as a close minimum age for the onset of the main extensional movement.

Considering these data, the slip rates along the ZSZ can be estimated to vary between 1.4 cm/y and 4.2 cm/y. Similarly, the vertical exhumation rate of the HHCS can be estimated between 5mm/y and 8.8 mm/y.

Although the STDS is not a single continuous structure along the Himalayan range, a comparison of available data reveals several first order similarities. In the Annapurna - Manaslu massifs of central Nepal, ~ 800 km to the ESE of Zaskar, several segments of the STDS appear to have been active during the 24 - 21 Ma time interval : Deorali detachment ≥ 22.5 Ma, Hodges et al. (1996); Dudh Khola - Chame detachment = 24 - 21 Ma, Coleman (1996); Manaslu detachment ≥ 22 Ma, Guillot et al. (1994) and Harrison et al. (1995). In the Mt. Everest massif, ~1000 km to the ESE of Zaskar, a minimum displacement of 34 km occurred along the Qomolangma detachment (Burchfiel et al., 1992). According to Hodges et al. (1992), this detachment was active between 22 and 19 Ma, although new data suggest a younger movement at 16.6 Ma (K.V. Hodges, personal communication, 1997). Such younger movements, as well as multi-stage extension, have been determined for other strands of the STDS, such as in the Annapurna massif (Machhapuchhare detachment ≤ 18.5 Ma, Hodges et al., 1996), in Central Nepal (Shisha Pangma detachment ≤ 17.3 Ma, Searle et al., 1997), or in Bhutan (Khula Kangri detachment ≤ 12.5 Ma, Edwards and Harrison, 1997). It is also likely that the brittle normal faulting observed in the hanging wall of the ZSZ corresponds to such late movements.

Collectively, these results indicate that synorogenic extension along segments of the STDS initiated during the earliest Miocene and that this system of detachments remained active for several millions of years until Middle to Late Miocene. This protracted extensional evolution was thus broadly coeval with thrusting of the HHCS along the MCT between the earliest Miocene (≈ 23 Ma; Frank et al., 1977; Hubbard and Harrison, 1989; Harrison et al., 1995; Hodges et al., 1996) and the Late Miocene (≈ 6 Ma; Harrison et al., 1997). These data indicate that combined thrusting at the base, and extension at the top of the HHCS, assisted the exhumation of this high-grade metamorphic sequence in the core of the Himalayan orogen.

8. MODELS FOR SYN-OROGENIC EXTENSION

*La cohérence séduisante des modèles
constitue souvent un piège en canalisant
la pensée vers une vision trop simple
d'une nature infiniment complexe.*

H. Masson

*Good field observations are hard to
refute, whereas the fun begins with the
interpretations*

G.M. Brown

8.1 Introduction:

Our study reveals that the Zaskar Shear Zone accommodated tens of kilometres of displacement and that these extensional movements at the top of the HHCS were contemporaneous with the thrusting of this domain along the Main Central Thrust. The delimitation of the HHCS by these two major structures showing opposite sense of shear indicates that the HHCS formed a slice of crustal material that moved southwards relative to both India and Tibet while regional shortening and crustal thickening was still going on.

The Zaskar Shear Zone shares the same characteristics as most normal faults; a deep, hot footwall was exhumed from beneath a shallow, cold hanging wall, resulting in the close juxtaposition of high-grade metamorphic rocks and low-grade rocks. Early ductile fabrics within the shear zone are progressively overprinted by more brittle structures as the hot footwall is cooled during its ascent to shallower crustal levels.

The tectonic settings in Zaskar are however totally different from areas of regional extension such as the Basin and Range Province of the western United States (e.g. see Wernicke, 1984; Wernicke and Axen, 1988; Platt, 1993). These latter areas are marked by crustal extension and thinning, whereas in the Himalaya, extensional shearing along the South Tibetan Detachment System formed during regional shortening and crustal thickening. This indicates that the upper crustal extensional system must have been decoupled from the underlying system dominated by convergence.

The existence of syn-orogenic extension is a relatively new discovery, which was described only since the eighties and has received quite a lot of attention in the past ten years. The mechanism or even the kinematics leading to the formation of orogen-parallel extensional structures are still little understood but several models have been proposed to cast some light on this intriguing phenomenon.

The aim of this chapter is to present and discuss several of these models.

8.2 Gravity collapse

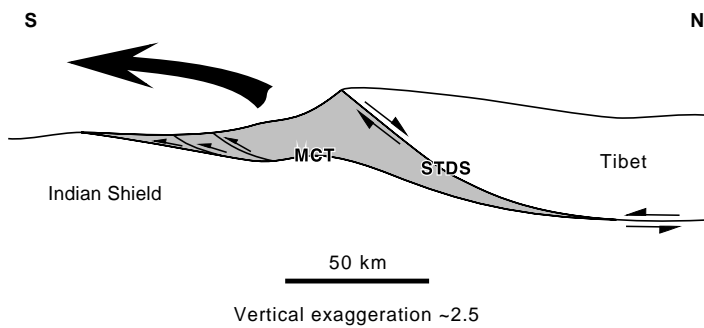


Fig. 8.1: Hypothetical cross-section showing the central Himalayan orogen as it might have looked in Miocene time. Major active fault systems include the South Tibetan Detachment System (STDS) and the Main Central Thrust (MCT). The High Himalayan Crystalline Sequence (in grey) forms a wedge that is expelled southwards by synchronous movement of the STDS and the MCT. (Hodges et al. 1993)

Himalayan topographical front. Events leading to this gravitational collapse include continental crustal thickening at the leading (southern) edge of Tibet by the underplating of the Tibetan crust with incompletely subducted material from the Indian crust. As the crustal thickness increases beneath the leading edge of Tibet, the topographic elevation increases as well and provides increased vertical stress to drive extension. Burchfiel and Royden suggest that eventually, the difference in topographic elevation between the Indian foreland and the southern end of Tibet reaches a point where the generated stress can no longer be supported by the cohesive strength of the rocks within the upper crust and gravitational collapse occurs.

Burchfiel et al. (1992) suggest that the primary trigger for the gravitation driven extensional collapse of the orogen was a major reduction in the crustal strength due to melting of the hanging wall rocks within the lower part of the upper plate. They take as a proof for this weakening of the cohesive strength of the rocks the widespread presence of leucogranites in the footwall of the detachment fault.

Hodges et al. (1996) take up the gravity collapse model of Burchfiel but propose that episodic displacement occurred on both the MCT and the STDS systems long after their initiation, which contradicts the concept of a single extensional phase of deformation (England and Molnar, 1993). For Hodges et al., the STDS must consequently have been capable of accommodating continual cycling between shortening and extension for a substantial portion (whatever that means) of the history of the orogen. In this model (fig. 8.2), extensional movements along the STDS correspond to a physical response which compensates the instability caused by over steepening during mountain building. In a continually evolving orogen, where many physical parameters are constantly changing, there is a continual alternation between extension and contraction in the wedge, as the system oscillates about the stable state. This model which is termed dynamic compensation by Hodges et al. (1996), interprets the extensional fault systems as gravitationally driven compensational structures that, along with physical erosion, helped to maintain a critical crustal profile in the orogen during continued convergence between India and Asia.

These models, which see syn-orogenic extension as a consequence of gravitational instability, are very popular among the Himalayan geologist community. Such models do however require that

Burchfiel and Royden (1985) first suggested that movements along the MCT and the STDS might have been broadly contemporaneous, and therefore presented a model where the metamorphic core of the orogen (HHCS) was represented as a northwards-tapering prism bound by these two structures and extruded southwards toward the Indian foreland (Fig. 8.1).

These authors interpret the extensional movements at the top of the HHCS as a consequence of gravitational collapse of the

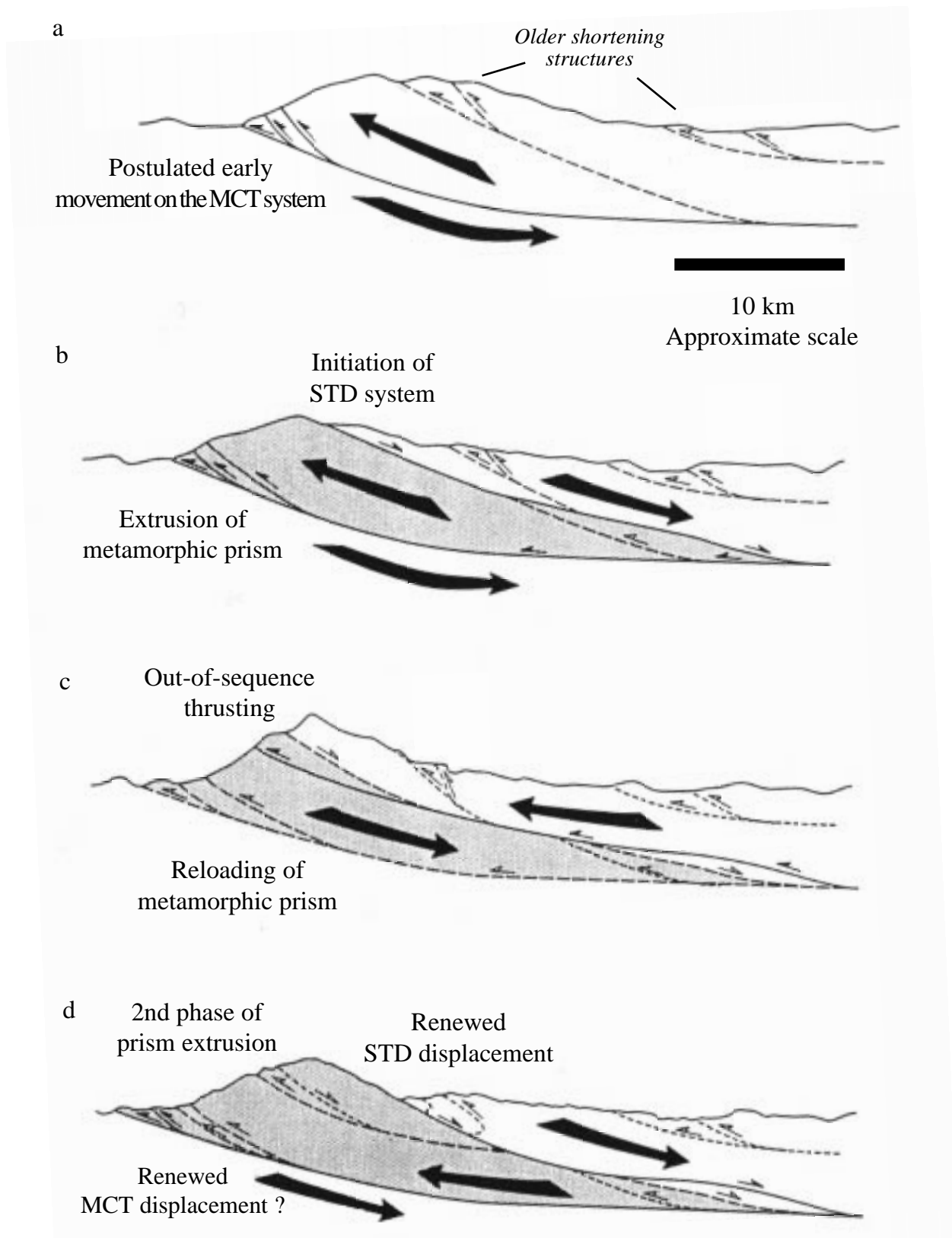


Fig. 8.2: Empirical model of Miocene dynamic compensation in the Himalaya. Copied from Hodges et al., 1996. The early history of the orogen (>22 Ma) was dominated by crustal thickening without the formation of major compensational structures. Figure a illustrates schematically the postulated architecture of the range in gross-section just prior to initiation of STD system. Solid lines indicate active faults; dashed lines are older, inactive structures. With the development of the earliest faults of the STDs, the metamorphic core of the range begins to extrude towards the Indian foreland (Fig. b). Once the system has returned to a “stable” topographic profile, it can support a second phase of shortening, this time manifested by out-of-sequence thrusting (Fig. c). The range grows vertically until, ultimately, it becomes unstable again and a second phase of compensation occurs (Fig. d).

an over-steepening state can be reached in an orogen. Reaching such a state of instability would require that the upheaval of the topographic front could not be compensated solely by erosional processes and thus had to regain equilibrium in «collapsing» along normal faults. We believe that gravity-driven extension is a process that did certainly occur in the Himalaya to produce the late D6 high-angle normal faults which compensate the gravitational instability created by the D5 doming phase. We do however think that this process could not lead to the formation of ductile low-angle extensional structures as the STDS. Our data show that crustal melting and the production of leucogranitic melts are a consequence of extension and thus cannot be the trigger necessitated to induce extensional shearing as proposed by Burchfiel et al. (1992). Moreover, multicycling between over-steepening and gravity collapse along low-angle structures as proposed by Hodges et al. (1996) could explain a certain amount of exhumation but this process is largely insufficient to explain the juxtaposition of rocks that equilibrated at depths greater than 30 kilometers with nearly unmetamorphosed sediments (Fig. 8.1 (Hodges et al. 1996)).

Finally, models based on gravity collapse do not take into account the reversal in shear sense observed along the STDS.

8.3 Ductile extrusion-channel flow model

In this model proposed by Grujic et al. (1996), the HHCS is considered as a ductile extruded wedge sandwiched between a rigid underthrusting plate (e.g. Lesser Himalaya) and a rigid buttress (Tibet-Tethyan Himalaya). The HHCS did not act as a rigid block but was deformed pervasively during its extrusion. The STDS is considered as a hinterland-dipping backstop that did not result from large-scale crustal thinning of an overthickened orogenic wedge. The normal fault geometry of the STDS is interpreted as resulting from the south-directed extrusion of the HHCS rather than by north-south extension. Extensional movements along the STDS are only relative, as the Himalaya was under compressive stress since 50 Ma. and did never undergo net crustal extension during that period (see also Searle, 1995). Ductile extrusion of the HHCS is also interpreted to be related with leucogranite intrusions.

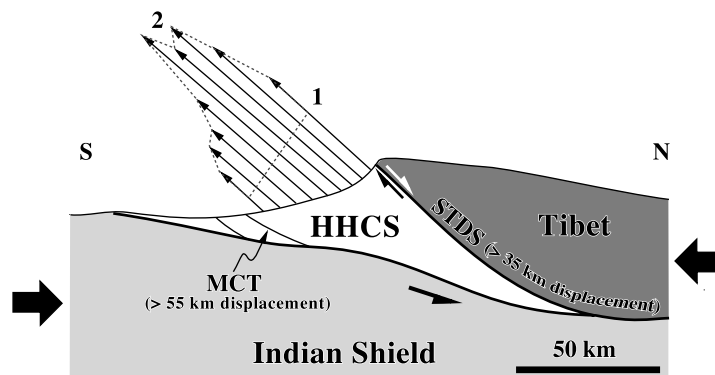


Fig. 8.3: Tectonic model for the extrusion and exhumation of the HHCS, by Grujic et al. (1996) and Davidson et al. (1997). “The arrows show schematic displacement within the HHCS relative to India and Tibet. Displacement differences, due to heterogeneous plastic flow and thrust faulting, are shown by the change in shape of an imaginary material line for two arbitrarily different times (dashed lines marked 1 and 2). However, displacements within the HHCS are not necessarily synchronous; that is,

Extensional movements along the STDS are only relative, as the Himalaya was under compressive stress since 50 Ma. and did never undergo net crustal extension during that period (see also Searle, 1995). Ductile extrusion of the HHCS is also interpreted to be related with leucogranite intrusions.

Basically, in this model the MCT zone is not restricted to the base of the HHCS but is extended to its whole thickness. The process of extrusion proposed by Grujic et al. (1996), can be approximated quantitatively by channel flow models as have been used to

describe subduction zone processes (Mancktelow, 1995). Such models characterize a thrust system (e.g. the whole HHCS) as a viscous material-filled channel lying between two rigid sheets that deform the viscous material between them through induced shear and pressure gradient within the channel. They see the resulting deformation in the HHCS as an hybrid between simple shear and pipe-flow. Pipe-flow effect is basically what happens with channelized water: highest velocities are reached in the centre of the channel and opposite vorticity occur at the boundaries. Reverse shear sense at the top of the channel is the flow-pattern inferred across the top of the HHCS, along the STDS, whereas south-directed ductile thrusting dominates at the base of the HHCS, along the MCT.

It is proposed by Grujic et al. (1996), that the extrusion of the HHCS must be the consequence of a lateral pressure gradient associated with decreasing viscosities in a channel bound by two non-parallel walls. The lateral pressure gradient develops due to the building of topography during collisional tectonics. It is also suggested that melting at the top of the HHCS lubricated and enhanced rapid tectonic exhumation.

An interesting point in this model is, that it considers the HHCS as a ductile body rather than a rigid slab and that deformation is considered as pervasive through the whole HHCS rather than concentrated at its base (MCT) and top (STDS). An other interesting point is that extensional movements along the STDS are considered as relative within an overall compressive system. It also takes into account the reversal in shear sense (top to the NE «relative extension» superposed over top to the SW simple shear) along the STDS. This model does however lack a plausible explanation for the mechanisms that lead to the extrusion of the HHCS.

8.4 Analogic physical modelling

Based on the constatation that exhumation does occur during continuing plate convergence, that the exhumation of the subducted crust is frequently associated with major normal faults (STDS) which accomodate a displacement of up to several tens of kilometres, that these faults are subparallel and dip in the same direction as major thrust faults (MCT) and that both type of faults operate simultaneously, Chemenda et al. (1995) propose an elegant experimental model which may partly explain the mechanism leading to exhumation in a compressive system.

In this model, plate collision and underthrusting is simulated in laboratory by taking different hydrocarbon compositional systems that reproduce the physical plastic properties of a lithosphere composed of a mantle layer and two crustal layers «floating» on a liquid asthenosphere (water). The collision is driven by a piston and erosion is simulated by scraping off the excess relief (corresponding to values above 6-8 km) formed by this experimental collision.

This experiment shows that at an initial stage of the collision, all layers of the continental lithosphere subduct into the mantle, but with the crust subducting slightly more slowly. At a certain point, the subduction reaches a critical stage, where the crustal sheet stops completely and fails in front of the subducted lithosphere. This sheet then begins to move back up to the surface, in an opposite direction to the rest of the crustal layer and mantle which continue to subduct. The rising crustal sheet overthrusts the subducting plate and a normal shear motion develops along the upper surface of the sheet.

The physical laws that rule this model are quite simple, subduction of the crust is driven both by the force exerted by the piston and by the drag force from the underlying mantle (gravity). These forces are counteracted by the buoyancy force which grows with increasing volume of subducted crust (Archimede's principle) until the upper crust layer fails and a slab of upper crust is detached

from the still subducting lithosphere. Push and drag forces do not affect this slab of detached crust any more, whilst buoyancy force remains the same. It is this force which causes the subsequent exhumation of this detached crust slab. Exhumation continues until the now diminishing buoyancy force is counteracted by frictional forces on the sides of the rising slab and by its own weight. As subduction of the lithosphere goes on, a new slab of upper crust is detached and undergoes the same exhumation processes as the former slab, and so on.

The authors of this model have applied these experimental results to the specific case of the Himalaya (Fig. 8.4) and have obtained comparable values in the exhumation rate, timing of events and amount of displacement.

This model is limited, however in its analogy with the reality as it considers the HHCS as a rigid slab and does not incorporate the effects of pure shear, the changes in viscosity due to increasing or diminishing temperature and the probable lubrication of the STDS through partial melting. Moreover, the STDS and the MCT are considered as parallel although they have been proven to converge.

In several ways, the Himalayan orogen can be compared to the Alps. Since the early investigation in the mid-XIX century, the geological knowledge of the Alps has been steadily refined by a large number of geologists resulting in a fairly good comprehension of the mechanism and processes that lead to the building of this mountain belt. Recent deep seismic survey of the Ecors-Crop and NFP-20 programs (Frei et al., 1990; Marchant et al., 1993; Epard and Escher, 1996; Escher and Beaumont, 1997; Steck et al., 1997) allowed to control, to some extent, the geometric extrapolation and reconstruction of the deep Alpine structures. These interpretations of what happened deep below the Alps provide a good illustration of collisional tectonics and can be extrapolated to the Himalaya, if one makes abstraction of the fact that, unlike to the Alps, Himalayan tectonics are not characterized by a basement-cover relation.

On the basis of the precursory work of Ramsay (1980), Epard and Escher (1996) propose a generic two-dimensional model to explain the possible relationship between superficial thrust sheet and deeper fold nappes and apply this model to the specific case of the Western Alps to demonstrate that the simultaneous formation of these two types of structures at different levels of the crust is possible. Contrary to the gravity collapse and ductile extrusion flow models, which isolate the upper

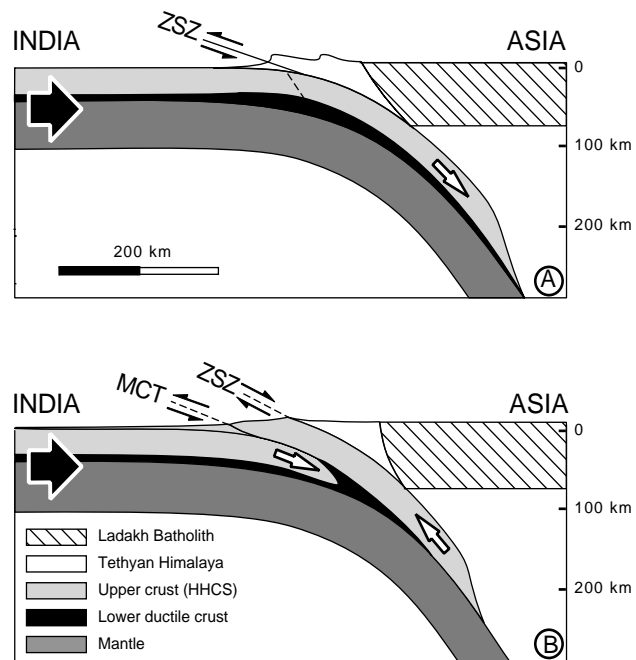


Fig. 8.4: Evolutionary model by Chemenda et al. (1995).

(A) Initial stage of the collision: Subduction of the continental crust to a depth of ca. 250 km, scraping of the sedimentary and upper crustal material from the subducting plate, formation of a huge accretionary prism (Tethys Himalaya) and a small to moderate mountain belt. This stage finishes with the formation of the MCT, ca. 20 Ma after the collision started.

(B) Uplift of the subducted crustal sheet and rapid exhumation of the crustal material. The uplift produces a normal sense motion along the upper surface of the rising sheet (along the Zanskar Shear Zone, ZSZ). On reaching the surface, the upper layers of the crustal sheet are eroded, while the deeper parts continue overthrusting the Indian plate. The rate of displacement along the MCT is roughly equal to the sum of the rates along the ZSZ and the rate of subduction of the Indian plate. The motion along the ZSZ ceases a few to several million years after its initiation, while the MCT remains active”.

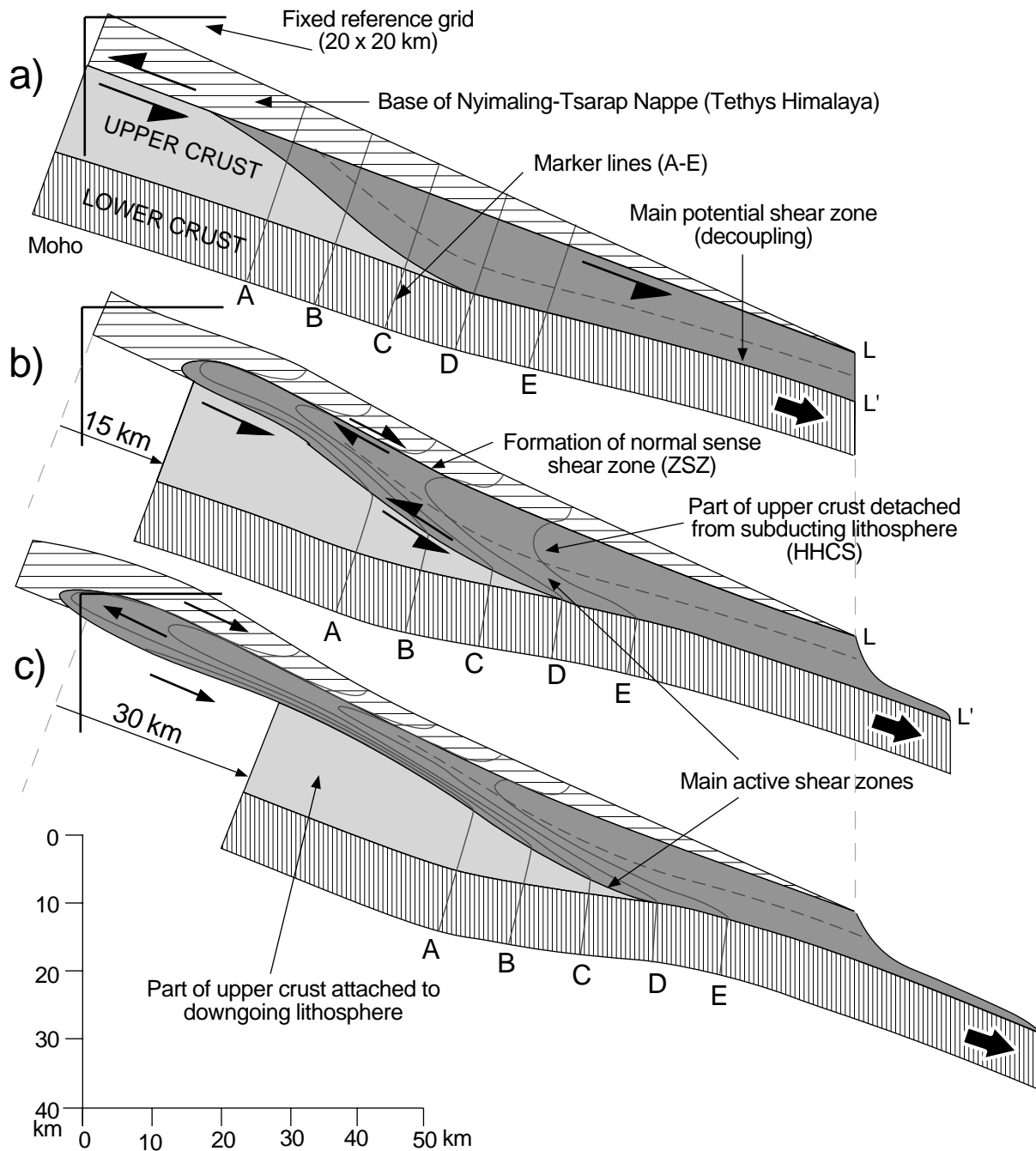


Fig. 8.5: Two-dimensional reconstruction showing the geometric consequence of combined simple shear and pure shear in a system envisaged to have generated the extrusion of nappes in the Alps, by Escher and Beaumont, 1997 and applied by the author to the Himalaya. The dark-grey area represents the southwestward extruding High Himalayan Crystalline Sequence Nappe. L-L' is taken to represent a material line in the subduction channel where the blockage has reduced the velocity at L to zero. To simplify the model, the simple shearing L-L' is mainly restricted to the decoupling zone at the base of the nappe. Given that L remains stationary and that L' is only displaced by the simple shear component, and assuming constant volume and stretching in the plane of section, the result of flattening will be the upward expulsion of the HHCS. L-L' is in this case the "pin-line" for the pure-shear component. Stage a is here similar to stage a in the model of Chemenda et al. 1995 (fig 8.4). Also in this model, Escher and Beaumont propose that buoyancy forces assist the oblique escape of the HHCS but are here not considered as the dominant factor.

crustal structures and associate extension with gravific instability or a lateral pressure gradient due to the building of a marked topographic relief, the model of Epard and Escher considers the topographic relief to be of minor geologic importance compared to the 40-60 km deep root zone (70 - 80 km in the Himalaya). As with the model of Chemenda et al (1995), lithospheric subduction is here considered to play a major role both for underthrusting and exhumation in the formation of nappes.

This model aims essentially at explaining the initial formation of ductile basement nappes, but the authors suggest, in agreement with Dietrich and Casey (1989), that the simple shear deformation in the lower structural units is often superposed by pure shear. They propose that the effect of an heterogeneous wedge-shaped pure shear would cause an upward extrusion of lower-level rocks and that this mechanism may be responsible for bringing near the surface high-pressure rocks already at an early stage of the continental subduction.

These final considerations of Epard and Escher's can be applied to the Himalaya, because the HHCS was affected by pervasive simple shear, and the effect of pure shear on the wedge-shaped HHCS is a very plausible mechanism for the lateral extrusion of this high-grade domain and could thus explain a relative extensional sense of shear along the STDS.

A model that associates the effects of both simple shear and pure shear during simultaneous underplating of the lithosphere and exhumation of the upper crust is proposed for the Alps by Escher and Beaumont (1997). These authors take up and elaborate the model of Epard and Escher (1996) to give a geometrical and mechanical explanation for the initiation and subsequent exhumation and stacking of basement nappes. Their model is based on several geological factors and previously published ideas and should also partly be relevant for the Himalaya.

An essential consideration is that originally deep basement rocks display a penetrative early foliation and stretching lineation, implying strong deformation throughout most of the volume rock. Consequently, it is unrealistic to represent large deep-seated rock bodies as having been displaced over significant distances without strong internal deformation.

The model of Escher and Beaumont for the Alps resembles that of Chemenda et al (1995) inasmuch as they also suggest that a slice of upper continental crust is detached at the front of the subducted lithosphere and that this slab moves back to the surface while the rest of the lithosphere continues to be subducted. The mechanism of ascent is, however, different as it is proposed that buoyancy forces and erosion only assist the process but are not the dominant factor. Instead it is proposed, similarly to the channel flow model, that exhumation of the detached crustal slab is the result of combined simple shear and pure shear. In other words, once a crustal slab is detached from the subducting lithosphere, further descent of this slab is hindered at a certain point and these now high-grade rocks are then flattened through pure shear between the two converging plates. The flattening of the slab implies a decrease in thickness and an increase in length. The additional length cannot be accommodated downwards and the slab is thus laterally expelled or «squeezed out» to the surface. (see also Steck et al., 1998, where geometrical proofs are given to support this model for the Tso-Morari region, south of the Indus Suture Zone)

8.5 Discussion

We have chosen to present here only models where exhumation and extensional tectonics are associated with crustal shortening and thickening and not with crustal extension as proposed by Platt (1986) or Ruppel et al.(1988).

The effect of extrusion is to place the high-grade rocks of the HHCS in contact with the overlying low-grade sedimentary series of the Tethys Himalaya along the low-angle normal Zaskar Shear Zone but in a tectonic setting without any net extension of the overall system.

On the basis of these various models and from our own observation, we infer that ductile extension along the ZSZ and conjugated thrusting along the MCT are the result of the south-westward extrusion of the HHCS. The HHCS represents a slab of upper crustal material that was first underthrust below a buttress formed by the Sedimentary series of the Tethys Himalaya (the Nyimaling-Tsarap nappe), until it reached a critical point where the downwards-pulling forces were counteracted by buoyancy. When this critical point was reached, the upper crust failed and the HHCS slab became detached from the subsiding lithosphere. Once detached, the HHCS was sandwiched between the still subsiding lithosphere and the rigid buttress formed by the TH. The compressive forces exerted by the ongoing collision lead to the deformation of the HHCS through conjugated simple shear and pure shear.



9. CONCLUSION

*Our revels now are ended. These our actors,
As I foretold you, were all spirits and
Are melted into air, into thin air:
And, like the baseless fabric of this vision,
The cloud-capped towers, the gorgeous palaces
The solemn temples, the great globe itself.
Yea, all which it inherit, shall dissolve
And like this insubstantial pageant faded,
Leave not a rack behind. We are such stuff
As dreams are made on, and our little life
Is rounded with a sleep*

«The Tempest» William Shakespeare

In this work on the structural and metamorphic evolution of SE Zaskar, we have tried to give an account of the successive events that led to the present-day close juxtaposition of two contrasted Himalayan domains, the Tethys Himalaya and the High Himalayan Crystalline Sequence. We have seen that these two domains originally formed a continuous series of sedimentary rocks deposited on the northern margin of the Indian continent and range in age from Upper Proterozoic to Upper Triassic. The contrasted metamorphic overprint of these two domains is the result of a series of strictly Himalayan events we will recapitulate.

The studied area is affected, although only marginally, by a first event of crustal thickening associated with the emplacement of the NE-vergent Shikar-Beh Nappe. This event is marked by a weak metamorphism of lower greenschist facies characterised by the growth of tiny biotite flakes on the southern side of the Shingo-La and decreases progressively towards the NE.

SE Zaskar is subsequently affected by a second event of crustal thickening associated with the emplacement of the SW vergent Nyimaling-Tsarap Nappe. Relic shear sense indicators suggest that the ductile thrust plane of this SW vergent nappe is preserved in the studied area. We propose that it is along this structure that the lowermost sedimentary series were underthrust below the Nyimaling Tsarap Nappe. It is essentially during this event that the sedimentary series acquired their metamorphic overprint.

The burial of the sedimentary series is associated with a metamorphism of Barrovian type showing a complete zonation from chlorite to kyanite zone. Our thermobarometric data confirm our petrographic interpretations that the rocks from the different metamorphic zones equilibrated at significantly different depths along the kyanite geotherm. These data also indicate that crustal thickening associated with the emplacement of the Nyimaling Tsarap Nappe was very important, for the highest grade metamorphic rocks now exhumed were buried at depths we calculated to have been over 40 kilometres.

The latest stage of emplacement of the Nyimaling-Tsarap Nappe is marked by a rotation of the underthrusting direction resulting in a reorientation of the fold axes in a N-S direction.

The subsequent stages of the tectonic-metamorphic history of SE Zaskar are related to the exhumation of the high grade metamorphic rocks. This exhumation is marked by a reversal in the shear sense of the thrust plane at the base of the Nyimaling-Tsarap Nappe. Indeed, we propose that the Zaskar Shear Zone was formed by the reactivation of this thrust plane in an opposite direction. The exhumation of the High grade rocks is responsible for the constriction of the Barrovian metamorphic isograd within the Zaskar Shear Zone and for the present-day juxtaposition of the rocks from the base of the Nyimaling-Tsarap Nappe (the HHCS) and the upper parts of this same nappe (the Tethys Himalaya).

The main issue of this work was the quantification of the amount and age of ductile extension along the Zaskar Shear Zone. On the basis of our thermobarometric results, we have shown that the highest grade rocks present in the ZSZ have equilibrated at a depth of 34 ± 3 km and that these rocks have been brought to the same elevation as rocks that equilibrated at a depth of 22 ± 1 km, implying a vertical displacement of 12 ± 3 km. The coupling of these data with a geometric model of the shear zone allowed us to estimate the net-slip along this structure to be at least 35 ± 9 km. However, a series of arguments lead us to assume that the total displacement along the ZSZ might have been up to ~ 100 km. The age and duration of ductile extensional shear was constrained by our geochronological data. The cessation of ductile extensional movements along the ZSZ was estimated at 19.8 ± 0.1 Ma through Ar/Ar muscovite cooling ages of undeformed leucogranitic dikes cross-cutting the base of this structure. A close estimate of the onset of extension was obtained through U/Pb monazite cooling age of the leucogranites, which yield an age of 22.2 ± 0.2 Ma. These data confirm the contemporaneity of extensional shearing along the ZSZ and thrusting along the MCT.

Several models are discussed to tentatively explain what processes could have led to the exhumation of the HHCS. We suggest that the HHCS represents a slice of high-grade rocks uncoupled from the subducting Indian upper-crust. This uncoupling occurred because buoyancy forces hindered further descent of this slice of crustal rocks. Consequently, the main detachment zone is transferred from the thrust plane at the base of the Nyimaling Tsarap Nappe to the Main Central Thrust. This caused the HHCS to be sandwiched between the still subducting Indian crust and a buttress formed by the Tethys Himalaya. Combined simple shear and pure shear, assisted by buoyancy forces led to the upward expulsion of the HHCS as a large-scale nappe limited at its base by the MCT and its top by the ZSZ.

The exhumation of the HHCS is marked by the apparition of a series of metamorphic minerals defining an isothermal decompression path. We suggest that the tertiary leucogranites formed in the migmatitic zone as a consequence of isothermal decompression-induced vapour-absent melting. The intrusion of these leucogranitic melt in the ZSZ might have lubricated this detachment and contributed to increase the amount of net slip along this structure.

The last stages of exhumation are marked by the formation of large domes in the HHCS and by high-angle brittle compensation faults.

This reconstitution of the sequence of events we present to explain the present geology of Zaskar is, of course, greatly influenced by contemporary models and theories on orogenic tectonics and is therefore prone to change as these ideas evolve. Nevertheless, we believe that this work contains several valuable observations on the metamorphism, the magmatism and the tectonic structures, associated with the formation of the Himalaya.

BIBLIOGRAPHY

- ALLMENDINGER P.W., SHARP J.W., VON TISH D., SERPA L., BROWN L., KAUFMAN S., OLIVIER J., SMITH R.B., (1983): Cenozoic and Mesozoic structures of the eastern Basin and Range from COCORP seismic reflection data.: *Geology*, v. 11, p. 532-536.
- ALSDORF D., BROWN L.D., NELSON K.D., MAKOVSKY Y., KLEMPERER S., ZHAO W., (1998): Crustal deformation of the Lhasa terrane, Tibet plateau from Project INDEPTH deep reflection profiles.: *Tectonics*, v. 17, no. 4, p. 501-519.
- ANDERSEN T.B., JAMTVEIT B., DEWEY J.F., SWENSON E., (1991): Subduction and eduction of continental crust: major mechanism during continent-continent collision and orogenic extensional collapse, a model based on the south Norwegian caledonides: *Terra Nova*, v. 3, p. 303-310.
- AYRES M., HARRIS N., (1997): Possible constraints on anatectic melt residence times from accessory mineral dissolution rates: an exemple from Himalayan leucogranites: *Mineralogical Magazine*, v. 61, p. 29-36.
- BARBEY P., BROUAND M., LE FORT P., PÉCHER A., (1996): Granite-migmatite denetic-link: the example of the Manaslu granite and Tibetan Slab migmatites in central Nepal: *Lithos*, v. 38, p. 63-79.
- BASSOULLET J., COLCHEN M., JUTEAU T., MARCOUX J., MASCLE G., (1980): L'edifice de nappes du Zaskar (Lakakh, Himalaya). Translated title: The structure of the Zaskar Nappes; Ladakh, Himalayas: *Acad. Sci. (Paris), C. R., Ser. D*, v. 290, no. 5, p. 389-392.
- BAUD A., ARN R., BUGNON P., CRISIMEL A., DOLIVO E., ESCHER A., HAMMER S.J.G., MARTHALER M., MASON H., STECK A., TIECHE J.C., (1982): Le contact Gondwana—Peri-Gondwana dans le Zaskar oriental (Ladakh, Himalaya). Translated title: The Gondwana-peri-Gondwana contact in eastern Zaskar, Ladakh, Himalayas: *Bulletin de la Societe Geologique de France*, v. 24, no. 2, p. 341-361.
- BAUD A., GAETANI M., GARZANTI E., FOIS E.E., NICORA A., TINTORI A., (1984): Geological observations in southeastern Zaskar and adjacent Lahul area (northwestern Himalaya): *Eclogae Geologicae Helvetiae*, v. 77, no. 1, p. 171-197.
- BAUD A., (1992): Nappe and Thrust Tectonics in Zaskar Area (NW Himalaya): Review of the so-called 'Autochtony' of the Tethys-Tibetan Zone., in A. Sinha, ed., *Himalayan Orogen and Global Tectonics: International Lithosphere Programme*: Rotterdam, A.A. Balkema, p. 45-48.
- BERMAN R.G., (1990): Mixing properties of Ca-Mg-Fe-Mn garnets: *American Mineralogist*, v. 75, no. 3-4, p. 328-344.
- BERMAN R.G., (1991): Thermobarometry using multi-equilibrium calculations; a new technique, with petrological applications.: *The Canadian Mineralogist*, v. 29, no. 4, p. 833-855.
- BERMAN R.G., ARANOVICH L.Y., PATTISON D.R.M., (1995): Reassessment of the garnet-clinopyroxene Fe-Mg exchange thermometer; II, Thermodynamic analysis.: *Contributions to Mineralogy and Petrology*, v. 119, no. 1, p. 30-42.
- BERTHELSEN A., (1953): On the geology of the Rupshu district, N.W. Himalaya.: *Medd. Dansk Geol. Foren.*, v. 12, no. 3, p. 350-414.
- BESSE J., COURTILLOT V., POZZI J.P., WESTPHAL M., ZHOU Y.X., (1984): Palaeomagnetic estimates of crustal shortening in the Himalayan thrusts and Zangbo Suture.: *Nature (London)*, v. 311, p. 621-626.
- BHARGAVA O.N., (1980): Pre-Tertiary Orogenies in the Himalaya: A Review of various evidences: *Geologische Rundschau*, v. 69, p. 811-823.
-

- BLANFORD W.T., MEDLICOTT H.B., (1879): *A manual of the geology of India*: Calcutta.
- BROOKFIELD M.E., (1993): The Himalaya passive margin from Precambrian to Cretaceous times: *Sedimentary Geology*, v. 84, p. 1-35.
- BRUNEL M., ARNAUD N., TAPPONNIER P., PAN Y., WANG Y., (1994): Kongur Shan normal fault; type example of mountain building assisted by extension (Karakoram Fault, eastern Pamir): *Geology (Boulder)*, v. 22, no. 8, p. 707-710.
- BUCHER K., FREY M., (1994): *Petrogenesis of metamorphic rocks*: Berlin, Springer-Verlag, 318 p.
- BURCHFIELD B.C., ROYDEN L.H., (1984): Large scale north-dipping, low-angle normal faults in the high Himalaya, in AGU 1984 fall meeting, San Francisco, CA, Dec. 3-7, p. 1094.
- BURCHFIELD B.C., ROYDEN L.H., (1985): North-south extension within the convergent Himalayan region: *Geology (Boulder)*, v. 13, no. 10, p. 679-682.
- BURCHFIELD B.C., CHEN Z., HODGES K.V., LIU Y., ROYDEN L.H., DENG C., XU J., (1992): The South Tibetan detachment system, Himalayan Orogen; extension contemporaneous with and parallel to shortening in a collisional mountain belt: *Special Paper Geological Society of America*, v. 269, p. 41.
- BURG J.P., (1983): Tectogenèse comparée de deux segments de chaîne de collision; le sud du Tibet (suture du Tsangpo), la chaîne hercynienne en Europe (sutures du Massif Central): Univ. Montpellier 2, 401 p.
- BURG J.P., BRUNEL M., GAPAIS D., CHEN G.M., LIU G.H., (1984): Deformation of leucogranites of the crystalline Main Central Sheet in southern Tibet (China): *Journal of Structural Geology*, v. 6, no. 5, p. 535-542.
- BURG J.P., VANDENDRIESSCHE J., BRUN J.P., (1994): Syn- to post-thickening extension: mode and consequences: *C R Acad Sci Ser II*, v. 319, no. 9 Part 2, p. 1019-1032.
- BURG J.P., DAVY P., NIEVERGELT P., OBERLI F., SEWARD D., (1998): Exhumation during crustal folding in the Namche-Barwa syntaxis.: *Terra Nova*, v. 9, no. 2, p. 53-56.
- BUSSY F., KROGH T.E., WARDLE R.J., (1995): Late Labradorian metamorphism and anorthosite-granitoid intrusion, Cape Caribou River Allochthon, Grenville Province, Labrador: evidence from U-Pb geochronology.: *Canadian Journal of Earth Sciences*, v. 32, p. 1411-1425.
- CHATTERJEE N.D., FLUX S., (1986): Thermodynamic mixing properties of muscovite-paragonite crystalline solutions at high temperatures and pressures, and their geological applications: *Journal of Petrology*, v. 27, no. 3, p. 677-693.
- CHAUVET A., SÉRANNE M., (1994): Extension-parallel folding in the Scandinavian caledonides: implication for late-orogenic processes: *Tectonophysics*, v. 238, no. Special issue: late orogenic extension, p. 31-54.
- CHEMENDA A.I., MATTAUER M., MALAVIEILLE J., BOKUN A.N., (1995): A mechanism for syn-collisional rock exhumation and associated faulting: Results from physical modelling: *Earth and Planetary Science Letters*, v. 132, p. 225-232.
- CHOUDHURI B.K., (1987): Structural, metamorphic and deformational history of a part of the Zaskar crystalline complex, NW Himalaya: *Geoscience Journal*, v. 8, no. 1-2, p. 23-31.
- CLEMENS J.D., (1984): Water contents of intermediate to silicic magmas: *Lithos*, v. 11, p. 213-287.
- CLEMENS J.D., MAWER C.K., (1992): Granitic magma transport by fracture propagation: *Tectonophysics*, v. 204, no. 3-4, p. 339-360.
- COLCHEN M., MASCLE G., VAN-HAVER T., (1986): Some aspects of collision tectonics in the Indus suture zone, Ladakh., in M. P. R.-A. Coward, C., ed., *Collision tectonics*.: Geological Society Special Publications.: London, Geological Society Special Publications., p. 173-184.

- COLEMAN M.E., (1996): Orogen-parallel and orogen-perpendicular extension in the central Nepalese Himalayas: *Geological Society of America Bulletin*, v. 108, no. 12, p. 1594-1607.
- COPELAND P., PARRISH R.R., HARRISON T.M., (1988): Identification of inherited radiogenic Pb in monazite and its implications for U-Pb systematics: *Nature*, v. 333, p. 760-763.
- COPELAND P., HARRISON T.M., LE F.P., (1990): Age and cooling history of the Manaslu Granite; implications for Himalayan tectonics: *Journal-of-Volcanology-and-Geothermal-Research.*, v. 44, 1-2, p. 33-50.
- COSCA M.A., HUNZIKER J.C., HUON S., MASSON H., (1992): Radiometric age constraints on mineral growth, metamorphism, and tectonism of the Gummfluh Klippe, Brianconnais domain of the Préalpes, Switzerland: *Contributions to Mineralogy and Petrology*, v. 112, p. 127-144.
- CRITTENDEN M.D., CONEY P.J., DAVIS G.H., (1980): *Cordilleran metamorphic core complexes*, Memoires, Geological Society of America, 490 p.
- CROOK J., OSMASTON H., (1994): *Himalayan Buddhist Villages: Environment, Resources, Society and Religious Life in Zangskar, Ladakh.*: Bristol, University of Bristol U.K., 866 p.
- DALLMEYER R.D., SNOKE.A.W., MCKEE E.H., (1986): The Mesozoic-Cenozoic tectonothermal evolution of the ruby mountains, East Humboldt Range, Nevada: A Cordilleran metamorphic core complex.: *Tectonics*, v. 5, p. 931-954.
- DALMAYRAC B., MOLNAR P., (1981): Parallel thrust and normal faulting in Peru and constraints on the state of stress: *Earth and Planetary Science Letters.*, v. 55, p. 473-481.
- DALRYMPLE G.B., ALEXANDER E.C., LANPHERE M.A., KRAKER G.P., (1981): Irradiation of samples for $^{40}\text{Ar}/^{39}\text{Ar}$ dating using the Geological Survey TRIGA reactor.: *US Geol. Surv. Prof. Pap.*, p. 1176.
- DAVIDSON C., GRUJIC D.E., HOLLISTER L.S., SCHMID S.M., (1997): Metamorphic reactions related to decompression and synkinematic intrusion of leucogranite, High Himalayan Crystalline, Bhutan.: *J. Metamorphic Geol.*, v. 15, p. 593-612.
- DENIEL C., VIDAL P., FERNANDEZ A., LE FORT P., PEUCAT J.J., (1987): Isotopic study of the Manaslu granite (Himalaya, Nepal): inference on the age and source of Himalayan leucogranites: *Contrib. Mineral. Petrol.*, v. 96, p. 78-92.
- DEWEY J.F., (1988): Extensional collapse of orogens: *Tectonics*, v. 6, p. 1123-1139.
- DEWEY J.F., CANDE S., PITMAN III W.C., (1989): Tectonic evolution of the Indian/Eurasia Collision Zone: *Eclogae geologicae Helvetiae*, v. 82, no. 3, p. 717-734.
- DEZES P.J., VANNAY J.-C., STECK A., BUSSY F. COSCA M., (1999): Synorogenic extension: Quantitative constraints on the age and displacement of the Zangskar shear Zone: *GSA bulletin*, v. 111, no. 3, p. 364-374.
- DIETRICH V., GANSSER A., (1981): The leucogranites of the Bhutan Himalaya (crustal anatexis versus mantle melting): *Schweiz. Mineral. Petrogr. Mitt.*, v. 61, no. 2-3, p. 177-202.
- DIETRICH D., CASEY M., (1989): A new tectonic model for the Helvetic nappes., in D. D. M.P. Coward, R.G. Park, ed., *Alpine tectonics*, Geological society of London Special Publications, p. 47-63.
- EDWARDS M.A., KIDD W.S.F., LI J., YUE Y., CLARK M., (1996): Multi-stage developpement of the southern Tibet detachment system near Khula Kangri. New data from Gonto La: *Tectonophysics*, 260, p. 1-19.
- EDWARDS M.A., HARRISON T.M., (1997): When did the roof collapse? Late Miocene north-south extension in the high Himalaya revealed by Th-Pb monazite dating of the Khula Kangri granite: *Geology*, v. 25, no. 6, p. 543-546.
- ELKINS L.T., GROVE T.L., (1990): Ternary feldspar experiments and thermodynamic models: *American Mineralogist*, v. 75, no. 5-6, p. 544-559.

- ENGLAND P., MOLNAR P., (1993): Cause and effect among thrust and normal faulting, anatectic melting and exhumation in the Himalaya, in P. J. T. a. M. P. Searle, ed., *Himalayan Tectonics*: London, Geol. Soc. Spec. Publ., p. 401-411.
- EPARD J.L., STECK A., VANNAY J.C., HUNZIKER J., (1995): Tertiary himalayan structures and metamorphism in the kulu valley (mandi-khoksar transect of the western himalaya) - shikar beh nappe and crystalline nappe: *Schweiz Mineral Petrogr Mitt*, v. 75, no. 1, p. 59-84.
- EPARD J.-L., ESCHER A., (1996): Transition from basement to cover: a geometric model.: *Journal of Structural Geology*, v. 18, no. 533-548, p. 533-548.
- ESCHER A., BEAUMONT C., (1997): Formation, burial and exhumation of the basement nappes at crustal scale: a geometric model based on the Western Swiss-Italian Alps.: *Journal of Structural Geology*, v. 19, no. 7, p. 955.
- FERRARA G., LOMBARDO B., TONARINI S., B T., (1991): Sr, Nd and O isotopic characterization of the Gomphu La and Gumburanjon leucogranites (High Himalaya): *Schweiz. Mineral. Petrogr. Mitt.*, v. 71, p. 35-51.
- FERRY J.M., SPEAR F.S., (1978): Experimental calibration of the partitioning of Fe and Mg between biotite and garnet: *Contributions to Mineralogy and Petrology*, v. 66, no. 2, p. 113-117.
- FOSSEN H., (1992): the role of extensional tectonics in the Caledonides of South Norway: *journal of structural geology*, v. 14, no. (8/9), p. 1033-1046.
- FRANCE-LANORD C., SHEPPARD S.M.F., LE FORT P., (1988): Hydrogen and oxygen isotope variations in the High Himalaya peraluminous Manaslu leucogranite: evidence for heterogenous sedimentary source.: *Geochim. Cosmochim. Acta*, v. 52, p. 513-526.
- FRANK W., HOINKES G., MILLER C., PURTSCHELLER F., RICHTER W., THOENI M., (1973): Relations between metamorphism and orogeny in a typical section of the Indian Himalayas; NW-Himalaya; S-Lahul, Kulu; Himachal Pradesh; first comprehensive report.: *Tschermaks Mineralogische und Petrographische Mitteilungen*, v. 20, no. 4, p. 303-332.
- FRANK W., THONI M., PURTSCHELLER F., (1977): Geology and petrography of Kulu - South Lahul area, in *Ecologie et geologie de l'Himalaya*, Paris, Dec. 7-10, p. 147-172.
- FRANK W., GANSSER A., TROMMSDORFF V., (1977): Geological observations in the Ladakh area (Himalayas); a preliminary report: *Schweiz. Mineral. Petrogr. Mitt*, v. 57, no. 1, p. 89-113.
- FRANK W., BAUD A., HONEGGER K., TROMMSDORFF V., (1987): Comparative studies on profiles across the Northwest Himalayas, *The Anatomy of Mountain Ranges*, p. 261-275. 52 Refs. IGCP Project No. 215.
- FREI W., HEITZMANN P., LEHNER P., (1990): Swiss NFP-20 program of the deep structures of the Alps., in P. H. F. Roure, R. Polino, ed., *Deep structures of the Alps*: Paris, Mémoires de la Société géologique de France, p. 29-47.
- FUCHS G., (1982a): The geology of the Pin Valley in Spiti, H.P., India: *Jb. Geol. Bundesanst.*, v. 124, no. 2, p. 325-359.
- FUCHS G., (1982b): The Geology of Western Zaskar: *Jb. Geol. Bundesanst.*, v. 125, no. 1-2, p. 1-50.
- FUCHS G., (1987): The geology of southern Zaskar (Ladakh); evidence for the autochthony of the Tethys zone of the Himalaya: *Jb. Geol. Bundesanst.*, v. 130, no. 4, p. 465-491.
- FUCHS G., (1989): Arguments for the autochthony of the Tibetan Zone discussion: *Eclogae Geologicae Helvetiae*, v. 82, no. 2, p. 685-692.
- FUCHS G., LINNEN M., (1995): Geological Traverse Across the Western Himalaya-a Contribution to the Geology of Eastern Ladakh, Lahul, and Chamba.: *Jb. Geol. Bundesanst.*, v. 138, no. 4, p. 655-685.

-
- GAETANI M., (1985): The Triassic of the Zaskar Range (NW Himalaya): *Albertiana*, v. 4, p. p. 20-24. 1.
- GAETANI M., GARZANTI E., JADOUL F., (1985): Main structural elements of Zaskar, NW Himalaya (India): *Rend. Soc. Geol. Italiana*, v. 8, p. 3-8.
- GAETANI M., CASNEDI R., FOIS E., GARZANTI E., JADOUL F., NICORA A., TINTORI A., (1986): Stratigraphy on the Thetys Himalaya in Zaskar, Ladakh: initial report: *Riv. It. Paleont. Strat.*, v. 91, no. 4, p. 443-478.
- GAETANI M., GARZANTI E., TINTORI A., (1990): Permo-Carboniferous stratigraphy in SE Zaskar and NW Lahul (NW Himalaya, India): *Eclogae Geologicae Helvetiae*, v. 83, no. 1, p. 143-161.
- GAETANI M., GARZANTI E., (1991): Multicyclic history of the northern India continental margin (northwestern Himalaya): *AAPG Bulletin*, v. 75, no. 9, p. 1427-1446.
- GANSSEER A., (1964): *Geology of the Himalayas*: london, Wiley Interscience, 289 p.
- GAPAIS D., PECHER A., GILBERT E., BALLÉVRE M., (1992): Synconvergence spreading of the Higher Himalaya crystalline in Ladakh: *Tectonics*, v. 11, no. 5, p. 1045-1056.
- GARZANTI E., CASNEDI R., JADOUL F., (1986): Sedimentary evidence of a Cambro-Ordovician orogenic event in the northwestern Himalaya: *Sedimentary Geology*, v. 48, no. 3-4, p. 237-265.
- GARZANTI E., BRIGNOLI G., (1989): Low temperature metamorphism in the Zaskar sedimentary nappes (NW Himalaya, India): *Eclogae Geologicae Helvetiae*, v. 82, no. 2, p. 669-684.
- GARZANTI E., ANGIOLINI L., SCIUNNACH D., (1996a): The Mid-Carboniferous to Lowermost Permian succession of Spiti (Po Group and Ganmachidam Formation; Tethys Himalaya, Northern India): Gondwana glaciation and rifting of Neo-Tethys.: *Geodinamica Acta*, v. 9, no. 2, p. 78-100.
- GARZANTI E., ANGIOLINI L., SCIUNNACH D., (1996b): The Permian Kuling Group (Spiti, Lahaul and Zaskar; NW Himalaya): Sedimentary Evolution during Rift/Drift Transition and Initial Opening of Neo-Tethys: *Rivista Italiana di Paleontologia e Stratigraphia*, v. 102, no. 2, p. 175-200.
- GHENT E.D., STOUT M.Z., (1981): Geobarometry and geothermometry of plagioclase-biotite-garnet-muscovite assemblages: *Contributions to Mineralogy and Petrology*, v. 76, no. 1, p. 92-97.
- GILBERT E., (1986): Evolution structurale d'une chaîne de collision: Structures et déformations dans le Nord de la plaque indienne en Himalaya du Ladakh [Doctoral thesis]: Université de Poitiers, 225 p.
- GRAHAM C.M., POWELL R., (1984): A garnet-hornblende geothermometer; calibration, testing, and application to the Pelona Schist, Southern California: *Journal of Metamorphic Geology*, v. 2, no. 1, p. 13-31.
- GRANT J.A., (1985): Phase equilibria in partial melting of pelitic rocks, in A. JR, ed., *Migmatites*, Blackie and son, p. 86-144.
- GRIESBACH C.L., (1891): Geology of the Central Himalaya: *Mem., Geological Survey of India*, v. XXIII, p. 1-232.
- GRUJIC D., CASEY M., DAVIDSON C., HOLLISTER L.S., KÜNDIG R., PAVLIS T., SCHMID S., (1996): Ductile extrusion of the High Himalayan Crystalline in Bhutan: evidence from quartz microfabrics: *Tectonophysics*, v. 260, p. 21-43.
- GUILLOT S., (1993): Le granite du Manaslu (Nepal Central) marqueur de la subduction et de l'extension intracontinentales Himalayennes: Université Joseph Fourier, 97 p.
- GUILLOT S., HODGES K.V., LEFORT P., PÉCHER A., (1994): New constraints on the age of the Manaslu leucogranite: Evidence for episodic tectonic denudation in the central Himalayas: *Geology*, v. 22, p. 559-562.
- GUNTALI P., (1993): Geologie und Tektonik des higher und Lesser Himalaya im Gebiet von Kishtwar, SE Kashmir (NW Indien). [Dissertation Nr. 10211 thesis]: ETHZ, 198 p.
-

- HACKER B.R., MOSENFELDER J.L., (1996): Metamorphism and deformation along the emplacement thrust of the Samail Ophiolite, Oman: *Earth and Planetary Science Letters*, v. 144, no. 3-4, p. 435-451.
- HARRIS N., INGER S., MASSEY J., (1993): The role of fluids in the formation of the High Himalayan leucogranites, in P. J. T. a. M. P. Searle, ed., *Himalayan Tectonics*: London, Geol. Soc. Spec. Publ., p. 391-400.
- HARRIS N., MASSEY J., (1994): Decompression and anatexis of himalayan metapelites: *Tectonics*, v. 13, no. 6, p. 1537-1546.
- HARRISON T.M., McKEEGAN K.D., LEFORT P., (1995): Detection of inherited monazite in the Manaslu leucogranite by Pb/Th ion microprobe dating: Crystallization age and tectonic implications: *Earth and Planetary Science Letters*, v. 133, p. 271-282.
- HARRISON T.M., MAHON K.I., (1995): New constraints on the age of the Manaslu leucogranite: Evidence for episodic tectonic denudation in the central Himalaya: Comment: *Geology*, v. 23, no. 5, p. 478-479.
- HARRISON T.M., RYERSON F.J., LE-FORT P., YIN A., LOVERA O.M., CATLOS E.J., (1997): A late Miocene-Pliocene origin for the central Himalayan inverted metamorphism.: *Earth and Planetary Science Letters*, v. 146, no. 1-2, p. E1-E7.
- HAUCK M.L., NELSON K.D., BROWN L.D., ZHAO W., ROSS A.R., (1998): Crustal structure of the Himalayan orogen at ~90° east longitude from Project INDEPTH deep reflection profiles.: *Tectonics*, v. 17, no. 4, p. 481-500.
- HAYDEN H.H., (1904): The Geology of Spiti, with parts of Bashahr and Rupshu: *Mem., Geological Survey of India*, v. XXXVI, no. 1, p. 1-129.
- HEIM A., GANSSER A., (1939): Central Himalaya; geological observations of the Swiss expedition 1936.: *Schweizer. Naturf. Ges., Denksch.*, v. 73, no. 1, p. 245.
- HERREN E., (1987): Zaskar shear zone; northeast-southwest extension within the Higher Himalayas (Ladakh, India): *Geology*, v. 15, no. 5, p. 409-413.
- HERREN E., (1987): Structures, deformation and metamorphism of the Zaskar area (Ladakh, NW Himalaya) [Doctoral thesis]: Swiss Federal Institute of Technology, 147 p.
- HESS J.C., LIPPOLT H.J., (1994): Compilation of K/Ar measurements on HD-B1 standard biotite; 1994 status report., in G. S. Odin, ed., *Phanerozoic Time Scale, Bull. Lias. Inform. IUGS Subcomm. Geochronol.*, p. 19-23.
- HODGES K.V., MCKENNA L.W., (1987): Realistic propagation of uncertainties in geologic thermobarometry: *American Mineralogist*, v. 72, p. 671-680.
- HODGES K.V., (1991): Pressure-temperature-time paths: *Annual Review of Earth and Planetary Sciences*, v. 19, p. 207-236.
- HODGES K.V., PARRISH R.R., HOUSH T.B., LUX D.R., BURCHFIELD B.C., ROYDEN L.H., CHEN Z., (1992): Simultaneous Miocene extension and shortening in the Himalayan Orogen: *Science*, v. 258, p. 1466-1470.
- HODGES K.V., BURCHFIELD B.C., ROYDEN L.H., CHEN Z., LIU Y., (1993): The metamorphic signature of contemporaneous extension and shortening in the central Himalayan Orogen; data from the Nyalam transect, southern Tibet: *Journal of Metamorphic Geology*, v. 11, no. 5, p. 721-737.
- HODGES K.V., HAMES W.E., OLSZEWSKI W., BURCHFIELD B.C., ROYDEN L.H., CHEN Z., (1994): Thermobarometric and ⁴⁰Ar/³⁹Ar geochronologic constraints on Eohimalayan metamorphism in the Dinggyê area, southern Tibet: *Contributions to Mineralogy and Petrography.*, v. 117, p. 151-163.
- HODGES K.V., PARRISH R.R., SEARLE M.P., (1996): Tectonic evolution of the central Annapurna Range, Nepalese Himalayas: *Tectonics*, v. 15, no. 6, p. 1264-1291.

-
- HOLTZAPFFEL T., (1985): Les minéraux argileux: préparation, analyse diffractométrique et détermination: *Société Géologique du Nord*, v. 12, p. 1-136.
- HONEGGER K., DIETRICH V., FRANK W., GANSSER A., THOENI M., TROMMSDORFF V., (1982): Magmatism and metamorphism in the Ladakh Himalayas (the Indus-Tsangpo suture zone): *Earth and Planetary Science Letters*, v. 60, no. 2, p. 253-292.
- HONEGGER K., (1983): Strukturen und Metamorphose im Zaskar Kristallin: ETH-Zürich, 117 p.
- HUBBARD M.S., HARRISON T.M., (1989): (40)Ar/(39)Ar age constraints on deformation and metamorphism in the Main Central Thrust Zone and Tibetan Slab, eastern Nepal Himalaya: *Tectonics*, v. 8, no. 4, p. 865-880.
- HUBBARD M., ROYDEN L., HODGES K., (1991): Constraints on unroofing rates in the High Himalaya, eastern Nepal: *Tectonics*, v. 10, no. 2, p. 287-298.
- INGER S., HARRIS N.B.W., (1992): Tectonothermal evolution of the High Himalayan crystalline sequence, Langtang Valley, northern Nepal: *J. metamorphic Geol.*, v. 10, p. 439-452.
- INGER S., (1994): Magmagenesis associated with extension in orogenic belts: examples from the Himalaya and Tibet: *Tectonophysics*, v. 238, no. 1-4, p. 183-197.
- JADOUL F., GARZANTI E., FOIS E., (1990): Upper Triassic-Lower Jurassic stratigraphy and paleogeographic evolution of the Zaskar Tethys Himalaya (Zangla Unit): *Riv. It. Paleont. Strat.*, v. 95, no. 4, p. 351-396.
- JAIN A.K., MANICKAVASAGAM R.M., (1993): Inverted metamorphism in the intracontinental ductile shear zone during Himalayan collision tectonics: *Geology*, v. 21, no. 5, p. 407-410.
- KELEMEN P.B., SONNENFELD M.D., (1983): Stratigraphy, Structure, Petrology and Local Tectonics, Central Ladakh, NW Himalaya: *Schweiz. mineral. petrogr. Mitt.*, v. 63, no. 2/3, p. 267-287.
- KELEMEN P.B., REUBER I., FUCHS G., SEARLE M.P., (1988): Structural evolution and sequence of thrusting in the High Himalayan, Tibetan-Tethys and Indus suture zones of Zaskar and Ladakh, western Himalaya; discussion and reply: *Journal of Structural Geology*, v. 10, no. 1, p. 129-132.
- KOHN M.J., SPEAR F.S., (1990): Two new geobarometers for garnet amphibolites, with applications to southeastern Vermont: *American Mineralogist*, v. 75, no. 1-2, p. 89-96.
- KOZIOL A.M., NEWTON R.C., (1988): Redetermination of the anorthite breakdown reaction and improvement of the plagioclase-garnet-Al (sub 2) SiO (sub 5) -quartz geobarometer: *American Mineralogist*, v. 73, no. 3-4, p. 216-223.
- KROGH T.E., (1973): A low-contamination method for hydrothermal decomposition of zircon and extraction of U and Pb for isotopic age determinations.: *Geochimica et Cosmochimica Acta*, v. 37, p. 485-494.
- KROGH T.E., (1982): Improved accuracy of U-Pb zircon ages by the creation of more concordant systems using an air abrasion technique: *Geochimica et Cosmochimica Acta*, v. 46, no. 4, p. 637-649.
- KÜBLER B., (1968): Evaluation quantitative du métamorphisme par la cristallinité de l'illite; état des progrès réalisés ces dernières années: *Bulletin de la Société Nationale des Petroles d'Aquitaine*, v. 2, no. 2, p. 385-397.
- KÜNDIG R., (1988): Kristallisation und deformation im Higher Himalaya, Zaskar (NW-Indien): ETH Zürich, 188 p.
- KÜNDIG R., (1989): Domal structure and high-grade metamorphism in the Higher Himalayan Crystalline, Zaskar Region, north-west Himalaya, India.: *Journal of Metamorphic Geology*, v. 7, p. 43-55.
- LE FORT P., (1973): Les leucogranites à tourmaline de l'Himalaya sur l'exemple du granite du Manaslu (Nepal central): *B.S.G.F.*, v. 7, no. 15, p. 555-561.
-

- LE FORT P., (1986): Metamorphism and magmatism during the Himalayan collision: *Geological Society of London William Smith conference on collision tectonics*, v. 19, p. 159-172.
- LE FORT P., DEBON F., PÊCHER A., SONET J., VIDAL P., (1986): The 500 Ma. Magmatic Event in Alpine Southern Asia, a Thermal Episode at Gondwana Scale: *Sciences de la Terre, mémoires (Nancy)*, v. 47, p. 191-209.
- LE FORT P., CUNNEY M., DENIEL C., FRANCE L.C., SHEPPARD S.M.F., UPRETI B.N., VIDAL P., (1987): Crustal generation of the Himalayan leucogranites: *Tectonophysics*, v. 134, p. 39-57.
- LEAKE B.E., AL. E., (1997): Nomenclature of amphiboles; Report of the Subcommittee on Amphiboles of the International Mineralogical Association, Commission on New Minerals and Mineral Names.: *American Mineralogist*, v. 82, no. 9-10, p. 1019-1037.
- LOMBARDO U., PETRUSATI P., BORGHI S., (1993): Geology and tectonomagmatic evolution of the eastern Himalaya along the Chomolungma-Makalu transect., in *Seventh Himalaya Karakoram Tibet workshop*, Oxford, April 6-8, p. 341.
- LYDEKKER R., (1878): Notes on the Geology of Kashmir, Kishtwar and Pangi: *Rec., Geological Survey of India*, v. XI, no. 1, p. 30-64.
- LYDEKKER R., (1883): The Geology of the Kashmir and Chamba Territories, and the British district of Khagan: *Mem., Geological Survey of India*, v. XXII, p. 1-344.
- MAKOVSKY Y., KLEMPERER L., LIYAN H., DEYUAN L., (1996): Structural elements of the southern Tethyan Himalaya crust from wide-angle seismic data: *Tectonics*, v. 15, no. 5, p. 997-1005.
- MALAVIEILLE J., GUIHOT P., COSTA S., LARDEAUX J.M., GARDIEN V., (1990): Collapse of the thickened Variscan crust in the French Massif central: Mont Pilat extensional shear zone and St-Etienne Late Carboniferous basin: *Tectonophysics*, v. 177, p. 139-149.
- MALAVIEILLE J., (1993): Late orogenic extension in mountain belts: Insight from the Basin and Range and the Late Paleozoic Variscan Belt: *Tectonics*, v. 12, no. 5, p. 1115-1130.
- MALAVIEILLE J., (in press): Normal faulting and exhumation of metamorphic rocks in mountain belts., *Evolution of geologic structures in micro- to macro-scale.*, Chapman and Hall.
- MANCKTELOW N.S., (1995): Nonlithostatic pressure during sediment subduction and the development and exhumation of high pressure metamorphic rocks.: *Journal of Geophysical Research*, v. 100, p. 571-583.
- MARCHANT R., (1993): The underground of the western Alps: *Mémoires de Géologie de Lausanne*, v. 15, p. 1-137.
- MARGERIE D.E., HEIM A., (1888): *Les dislocations de l'écorce terrestre*: Zürich.
- MCELROY R., CATER J., ROBERTS I., PECKHAM A., BOND M., (1990): The structure and stratigraphy of SE Zaskar, Ladakh Himalaya: *Journal of the Geological Society of London*, v. 147, no. 6, p. 989-997.
- MCKENNA L.W., HODGES K.V., (1988): Accuracy versus precision in locating reaction boundaries; implications for the garnet-plagioclase-aluminum silicate-quartz geobarometer: *American Mineralogist*, v. 73, no. 9-10, p. 1205-1208.
- MEHNERT K.R., (1968): Nomenclature of migmatites, *migmatites and the origin of granitic rocks*: Amsterdam, Elsevier, p. 354-357.
- MEZGER K., VAN DER PLUIJM B.A., ESSENE E.J., HALLIDAY A.N., (1991): Synorogenic collapse: a perspective from the middle crust, the Proterozoic Grenville orogen: *Science*, v. 254, p. 695-698.
- MOLNAR P., TAPPONNIER P., (1975): Cenozoic tectonics of Asia; effects of a continental collision.: *Science*, v. 189, p. 419-426.

-
- MOORE D.M., REYNOLDS R.C., (1989): *X-ray diffraction and the identification and analysis of clay minerals*: New York, Oxford Univ. Press, 332 p.
- NANDA M.M., SINGH M.P., (1976): Stratigraphy and sedimentation of the Zaskar area, Ladakh and adjoining parts of the Lahaul region of Himachal Pradesh, in S. Nautiyal, ed., *Himalayan Geology*, p. 365-388.
- NEWTON R.C., (1983): Geobarometry of high grade metamorphic rocks: *American Journal of Science*, v. 283A, p. 1-28.
- NICORA A., GAETANI M., GARZANTI E., (1985): Late Permian to Anisian in Zaskar (Ladakh, Himalaya): *Rend. Soc. Geol. It.*, v. 7, p. 27-30.
- NOBLE S.R., SEARLE M.P., (1995): Age of crustal melting and leucogranite formation from U-Pb zircon and monazite dating in the western Himalaya, Zaskar, India.: *Geology*, v. 23, no. 12, p. 1135-1138.
- NORTON M.G., (1986): Late Caledonide extension in western Norway: A response to extreme crustal thickening: *Tectonics*, v. 5, p. 195-204.
- OSMASTON H., (1994): The Geology, Geomorphology and Quaternary History of Zangskar, *Himalayan Buddhist Villages: Environment, Resources, Society and Religious Life in Zangskar, Ladakh.*: Bristol, University of Bristol U.K., p. 866.
- PARRISH R.R., (1990): U-Pb dating of monazite and its application to geochronological problems: *Can J. Earth Sci.*, v. 30, p. 1431-1450.
- PASSCHIER C.W., TROUW R.A.J., (1996): *Microtectonics*: Berlin Heidelberg, Springer, 282 p.
- PATEL R.C., SINGH S., ASOKAN A., MANICKAVASAGAM R.M., JAIN A.K., (1993): Extensional tectonics in the Himalayan orogen, Zaskar, NW India, in P. J. Treloar, and Searle, M. P., ed., *Himalayan tectonics: Geological Society of London Special Publication*: Oxford, April 6-8, p. 445-459.
- PATIÑO DOUCE A.E., JOHNSTON A.D., RICE J.M., (1993): Octahedral excess mixing properties in biotite: a working model with applications to geobarometry and geothermometry: *American Mineralogist*, v. 78, p. 113-131.
- PATIÑO DOUCE A.E., BEARD J.S., (1995): Dehydration-melting of biotite gneiss and quartz amphibolite from 3 to 15 kbar: *Journal of Petrology*, v. 36, no. 3, p. 707-738.
- PATIÑO DOUCE A.E., BEARD J.S., (1996): Effects of P, f(O₂) and Mg/Fe ratio on dehydration-melting of model metagreywakes: *Journal of Petrology*, v. 37, p. 999-1024.
- PATIÑO DOUCE A.E., HARRIS N., (1998): Experimental constraints on Himalayan Anatexis: *Journal of Petrology*, v. 39, no. 4, p. 689-710.
- PATRIAT P., ACHACHE J., (1984): India-Eurasia collision chronology has implications for crustal shortening and driving mechanism of plates.: *Nature*, v. 311, p. 615-621.
- PECHER A., (1991): The contact between the higher Himalaya crystallines and the Tibetan sedimentary series; Miocene large-scale dextral shearing: *Tectonics*, v. 10, no. 3, p. 587-598.
- PECHER A., BOUCHEZ J.L., LE FORT P., (1991): Miocene dextral shearing between Himalaya and Tibet: *Geology (Boulder)*, v. 19, no. 7, p. 683-685.
- PETÖ P., (1976): An experimental investigation of the melting reactions involving muscovite and paragonite in the silica-saturated portion of the system K₂O-Na₂O-Al₂O₃-SiO₂-H₂O to 15 kb total pressure.: *Progress in Experimental Petrology*, v. 3, p. 41-45.
- PLATT J.P., (1993): Exhumation of high pressure rocks: a review of concepts and processes: *Terra Nova*, v. 5, p. 119-133.
-

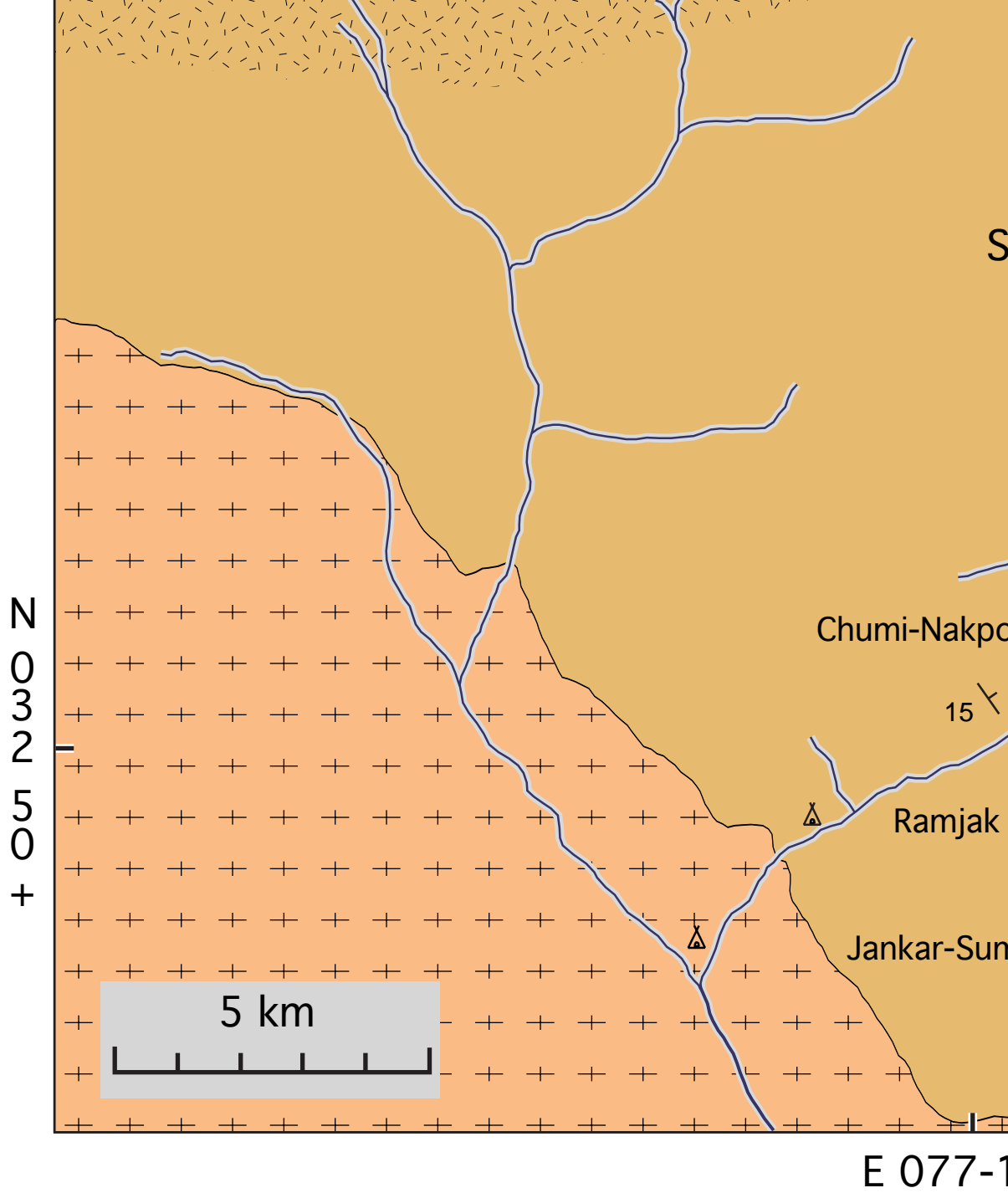
- POGNANTE U., GENOVESE G., LOMBARDO B., ROSSETTI P., (1987): Preliminary data on the High Himalayan Crystallines along the Padum-Darsha Traverse (South-Eastern Zaskar, India): *Rendiconti della Societa Italiana di Mineralogia e Petrographia*, v. 42, p. 95-102.
- POGNANTE U., LOMBARDO B., (1989): Metamorphic evolution of the High Himalayan Crystallines in SE Zaskar, India: *Journal of Metamorphic Geology*, v. 7, p. 9-17.
- POGNANTE U., CASTELLI D., BENNA P., GENOVESE G., OBERLI F., MEIER M., TONARINI S., (1990): The crystalline units of the High Himalayas in the Lahul-Zaskar region (Northwest India); metamorphic-tectonic history and geochronology of the collided and imbricated Indian Plate: *Geological Magazine*, v. 127, no. 2, p. 101-116.
- POGNANTE U., (1992): Migmatites and Leucogranites of Tertiary Age from the High Himalayan Crystallines of Zaskar (NW India): a Case History of Anatexis of Paleozoic Orthogneisses: *Mineralogy and Petrology*, v. 46, p. 291-313.
- POGNANTE U., (1993): Different P-T-t paths and leucogranite occurrences along the High Himalayan Crystallines: Implications for subduction and collision along the northern Indian margin: *Geodinamica Acta*, v. 6, no. 1, p. 5-17.
- POGNANTE U., BENNA P., (1993): Metamorphic zonation, migmatization and leucogranites along the Everest transect of eastern Nepal and Tibet; record of an exhumation history, in Seventh Himalaya Karakoram Tibet workshop, Oxford, April 6-8, p. 323-340.
- RAMSAY J.G., (1980): Shear zone geometry: a review: *Journal of structural geology*, v. 2, p. 83-99.
- RATSCHBACHER L., FRISCH W., NEUBAUER F., SCHMID S.M., NEUGEBAUER J., (1989): Extension in compressional orogenic belts: The Eastern Alps: *Geology*, v. 17, p. 404-407.
- RICOU L.M., (1994): Tethys reconstructed: plates, continental fragments and their Boundaries since 260 Ma from Central America to South-eastern Asia: *Geodinamica Acta*, v. 7, no. 4, p. 169-218.
- ROUTH J., (1993): Metamorphism and structural interpretation of the Zaskar Shear Zone, NW Himalaya, India: *Journal Geological Society of India*, v. 41, p. 187-198.
- ROWLEY D.B., (1996): Age of initiation of collision between India and Asia; a review of stratigraphic data: *Earth and Planetary Science Letters*, v. 145, no. 1-4, p. 1-13.
- RUPPEL C., ROYDEN L., HODGES K.V., (1988): Thermal modeling of extensional tectonics: Application to pressure-temperature-time histories of metamorphic rocks: *tectonics*, v. 7, no. 5, p. 947-957.
- SCAILLET B., PECHER A., ROCHETTE P., CHAMPENOIS M., (1995): The gangotri granite (garhwal himalaya): laccolithic emplacement in an extending collisional belt: *J Geophys Res-Solid Earth*, v. 100, no. B1, p. 585-607.
- SCHÄRER U., (1984): The effect of initial ²³⁰Th disequilibrium on young U-Pb ages: the Makalu case, Himalaya.: *Earth and Planetary Science Letters.*, v. 67, p. 191-204.
- SCOTese C.R., GAHAGAN L.M., LARSON R.L., (1988): Plate tectonic reconstitutions of the Cretaceous and Cenozoic basins.: *Tectonophysics*, v. 155, p. 27-48.
- SEARLE M.P., (1986): Structural evolution and sequence of thrusting in the High Himalayan, Tibetan-Tethys and Indus suture zones of Zaskar and Ladakh, Western Himalaya: *Journal of Structural Geology*, v. 8, no. 8, p. 923-936.
- SEARLE M.P., FRYER B.J., (1986): Garnet, tourmaline and muscovite-bearing leucogranites, gneisses and migmatites of the High Himalayas from Zaskar, Kulu, Lahoul and Kashmir, in collision tectonics, Geological Society Special Publication, London, p. 185-201.
- SEARLE M.P., COOPER D.J.W., REX A.J., (1988): Collision tectonics of the Ladakh-Zaskar Himalaya: *Phil. Trans. Royal Soc. London*, v. A326, p. 117-150.

-
- SEARLE M.P., REX A.J., (1989): Thermal model for the Zaskar Himalaya: *J.metamorphic Geol.*, v. 7, no. 1, p. 127-134.
- SEARLE M.P., WATERS D.J., REX D.C., WILSON R.N., (1992): Pressure, temperature and time constraints on Himalayan metamorphism from eastern Kashmir and western Zaskar: *Journal of the Geological Society of London*, v. 149, p. 753-773.
- SEARLE M., CORFIELD R.I., STEPHENSON B., MCCARRON J., (1997): Structure of the North Indian continental margin in the Ladakh-Zaskar Himalayas: implications for the timing of obduction of the Spontang ophiolite, India-Asia collision and deformation events in the Himalaya: *Geol. Mag.*, v. 134, no. 3, p. 297-316.
- SEARLE M.P., PARRISH R.R., HODGES K.V., HURFORD A., AYRES M.W., WHITEHOUSE M.J., (1997): Shisha Pangma Leucogranite, South Tibetan Himalaya: Field Relations, Geochemistry, Age, Origin, and Emplacement.: *The Journal of Geology*, v. 105, p. 295-317.
- SNELGROVE D.L., SKORUPSKY T., (1980): *The cultural heritage of Ladakh*: Warminster, Aris and Phillips.
- SORKHABI R., STUMP E., FOLAND K., JAIN A., (1996): Fission-track and $^{40}\text{Ar}/^{39}\text{Ar}$ evidences for episodic denudation of the Gangotri granites in the Garhwal Higher Himalaya: *Tectonophysics*, v. 260, p. 187-199.
- SPEAR F.S., (1993): *Metamorphic phase equilibria and pressure-temperature-time paths*, Monograph: Washington, D.C., Mineralogical Society of America, 799 p.
- SPENCER J.E., (1984): Role of tectonic denudation in warping and uplift of low-angle normal faults: *Geology*, v. 12, p. 95-98.
- SPRING L., CRESPO BLANC A., (1992): Nappe tectonics, extension, and metamorphic evolution in the Indian Tethys Himalaya (Higher Himalaya, SE Zaskar and NW Lahul): *Tectonics*, v. 11, no. 5, p. 978-989.
- SPRING L., (1993): Structure gondwaniennes et himalayennes dans la zone tibétaine du Haut Lahul-Zaskar oriental. [Doctoral thesis]: Université de Lausanne, Memoires-de-Geologie-Lausanne. 14. 148 p.
- SPRING L., BUSSY F., VANNAY J.C., HUNON S., COSCA M.A., (1993): Early Permian granitic dykes of alkaline affinity in the Indian High Himalaya of upper Lahul and SE Zaskar; geochemical characterization and geotectonic implications, in Seventh Himalaya Karakoram Tibet workshop, Oxford, April 6-8, p. 251-264.
- SPRING L., MASSON H., STUTZ E., THELIN P., MARCHANT R., STECK A., (1993): Inverse metamorphic zonation in very low-grade Tibetan zone series of SE Zaskar and its tectonic consequences (NM India, Himalaya): *Schweiz. Mineral. Petrogr. Mitt.*, v. 73, p. 85-95.
- SRIKANTIA S.V., GANESAN T.M., RAO P.N., SINHA P.K., TIRKEY B., (1980): Geology of the Zaskar area, Ladakh Himalaya, in S. Nautiyal, ed., *Himalayan Geology*, p. 1009-1033.
- STAMPFLI G.M., MOSAR J., FAVRE P., PILLEVUIT A., VANNAY J.-C., (1998): Permo-Triassic evolution of the western Tethyan realm: the Neotethys/east-Mediterranean basin connection: *Peri Thetys*, v. 3.
- STÄUBLI A., (1989): Polyphase metamorphism and the development of the Main Central Thrust.: *Journal of Metamorphic Geology*, v. 7, p. 73-93.
- STECK A., (1980): Deux directions principales de flux symmétamorphiques dans les Alpes centrales: *Bulletin de la Société Vaudoise des Sciences Naturelles.*, v. 75, no. 358, p. 141-149.
- STECK A., SPRING L., VANNAY J.-C., MASSON H., STUTZ E., BUCHER H., MARCHANT R., TIÈCHE J.C., (1993): Geological Transect Across the Northwestern Himalaya in eastern Ladakh and Lahul (A Model for the Continental Collision of India and Asia): *Eclogae Geologicae Helvetiae*, v. 86, no. 1, p. 219-263.
-

- STECK A., SPRING L., VANNAY J.C., MASSON H., BUCHER H., STUTZ E., MARCHANT R., TIECHE J.C., (1993): The tectonic evolution of the northwestern Himalaya in eastern Ladakh and Lahul, India, *in* *Himalayan Tectonics*, p. 265-276.
- STECK A., HUNZIKER J., (1994): The Tertiary structural and thermal evolution of the Central Alps-compressional and extensional structures in an orogenic belt.: *Tectonophysics*, v. 238, no. Special issue: Late Orogenic Extension., p. 229-254.
- STECK A., EPARD J.-L., VANNAY J.-C., HUNZIKER J., GIRARD M., MORARD A., ROBYR M., (1998): Geological transect across the Tso Morari and Spiti areas: The nappe structures of the Tethys Himalaya.: *Eclogae Geol. Helv.*, v. 91, p. 103-121.
- STOLICZKA F., (1866): Summary of Geological Observations during a visit to the Provinces-Rupshu, Karnag, South Ladak, Zanskar, Suroo and Dras-of Western Tibet.: *Mem., Geological Survey of India*, v. V, no. 4, p. 337-354.
- STUTZ E., STECK A., (1986): La terminaison occidentale du cristallin du Tso Morari (Haut-Himalaya; Ladakh meridional, Inde); subdivision et tectonique de nappe. Translated title: The western end of the Tso Morari crystalline complex (Upper Himalayas; southern Ladakh, India); subdivision and tectonics of the nappe: *Eclogae Geologicae Helveticae*, v. 79, no. 2, p. 253-269.
- STUTZ E., (1988): Geologie de la chaine de Nyimaling aux confins du Ladakh et du Rupshu (NW-Himalaya, Inde); evolution paleogeographique et tectonique d'un segment de la marge nord-indienne. [Doctoral thesis]: University of Lausanne, Memoires-de-Geologie-Lausanne. 3. 149 p.
- THAKUR V.C., (1980): Tectonics of the Central Crystallines of western Himalaya: *Tectonophysics*, v. 62, p. 141-154.
- THAKUR V.C., (1987): Plate tectonic interpretation of the western Himalaya: *Tectonophysics*, v. 134, p. 91-102.
- THOMPSON A.B., (1957): The graphical analysis of mineral assemblages in pelitic schists: *American Mineralogist*, v. 42, p. 842-857.
- THÖNI M., (1977): geology, structural evolution and metamorphic zoning in the Kulu Valley (Himachal Pradesh, India) with special references to reversed metamorphism: *Mitt. Ges. Geol. Bergbaustud. Osterr.*, v. 24, no. 125-187.
- VALDIYA K.S., (1995): Proterozoic sedimentation and Pan-African geodynamic development in the Himalaya: *Precambrian Research*, v. 74, p. 35-55.
- VANCE D., MAHAR E., (1998): Pressure-temperature paths from P-T pseudosections and zoned garnets: potential , limitations and exemples from the Zanskar himalaya, NW Himalaya.: *Contrib. Mineral. Petrol.*, v. 132, p. 225-245.
- VANNAY J.C., (1993): Geologie des chaines du Haut-Himalaya et du Pir Panjal au Haut-Lahul (NW Himalaya, Inde); paleogeographie et tectonique. [Doctoral thesis]: Universite de Lausanne, Memoires-de-Geologie-Lausanne. 16. 148 p.
- VANNAY J.C., SPRING L., (1993): Geochemistry of the continental basalts within the Tethyan Himalaya of Lahul-Spiti and SE Zanskar, Northwest India, *in* *Seventh Himalaya Karakoram Tibet workshop*, Oxford, April 6-8, p. 237-249.
- VANNAY J.C., STECK A., (1995): Tectonic evolution of the high Himalaya in upper Lahul (NW Himalaya, India): *Tectonics*, v. 14, no. 2, p. 253-263.
- VIELZEUF D., HOLLOWAY J.R., (1988): Experimental determination of the fluid-absent melting relations in the pelitic system: *Contribution to mineralogy and petrology*, v. 98, no. Special issue: late orogenic extension, p. 257-276.

-
- VIELZEUF D., MONTEL J.M., (1994): Partial melting of metagreywackes; Part 1, Fluid-absent experiments and phase relationships.: *Contributions to Mineralogy and Petrology*, v. 117, no. 4, p. 375-393.
- WERNICKE B., (1984): Uniform-sense normal simple shear of continental lithosphere: *Canadian Journal of Earth Sciences*, v. 22, p. 108-125.
- WERNICKE B.P., AXEN G.J., (1988): On the role of isostasy in the evolution of normal fault systems: *Geology (Boulder)*, v. 16, no. 9, p. 848-851.
- WILKS W.J., CUTHBERT S.J., (1994): The evolution of Hornelen Basin detachment system, western Norway: Implication for the style of late orogenic extension in the southern Scandinavian Caledonides: *Tectonophysics*, v. 238, no. Special issue: late orogenic extension, p. 1-30.
- WYSS M., HERMANN J., (1999): Himalayan olivine gabbros: Evidence for extension related magmatism and early granulite facies metamorphism: (*in prep.*).





Mémoires de Géologie (Lausanne)

ISSN 1015-3578

- No. 1 BAUD A. 1987. Stratigraphie et sédimentologie des calcaires de Saint-Triphon (Trias, Préalpes, Suisse et France). 202 pp., 53 text-figs., 29 pls
- No. 2 ESCHER A, MASSON H. and STECK A. 1988. Coupes géologiques des Alpes occidentales suisses. 11 pp., 1 text-figs., 1 map
- No. 3 STUTZ E. 1988. Géologie de la chaîne Nyimaling aux confins du Ladakh et du Rupshu (NW-Himalaya, Inde). Evolution paléogéographique et tectonique d'un segment de la marge nord-indienne. 149 pp., 42 text-figs., 11 pls. 1 map
- No. 4 COLOMBIA. 1989. Métamorphisme et géochimie des roches mafiques des Alpes ouest-centrales (géoprofil Viège-Domodossola-Locarno). 216 pp., 147 text-figs., 2 pls
- No. 5 STECK A., EPARD J.-L., ESCHER A., MARCHANT R., MASSON H. and SPRING L. 1989 Coupe tectonique horizontale des Alpes centrales. 8 pp., 1 map.
- No. 6 SARTORI M. 1990. L'unité du Barrhorn (Zone pennique, Valais, Suisse). 140 pp., 56 text-figs., 3 pls.
- No. 7 BUSSY F. 1990. Pétrogenèse des enclaves microgrenues associées aux granitoïdes calco-alcalins: exemple des massifs varisque du Mont-Blanc (Alpes occidentales) et miocène du Monte Capanne (Ile d'Elbe, Italie). 309 pp., 177 text-figs.
- No. 8 EPARD J.-L. 1990. La nappe de Morcles au sud-ouest du Mont-Blanc. 165 pp., 59 text-figs.
- No. 9 PILLOUD C. 1991 Structures de déformation alpines dans le synclinal de Permo-Carbonifère de Salvan-Dorénaz (massif des Aiguilles Rouges, Valais). 98 pp., 59 text-figs.
- No. 10 BAUD A., THELIN P. and STAMPFLI G. 1991. Paleozoic geodynamic domains and their alpidic evolution in the Tethys. IGCP Project No. 276. Newsletter No. 2. 155 pp.
- No. 11 CARTER E.S. 1993 Biochronology and Paleontology of uppermost Triassic (Rhaetian) radiolarians, Queen Charlotte Islands, British Columbia, Canada. 132 pp., 15 text-figs., 21 pls.
- No. 12 GOUFFON Y. 1993. Géologie de la «nappe» du Grand St-Bernard entre la Doire Baltée et la frontière suisse (Vallée d'Aoste -Italie). 147 pp., 71 text-figs., 2 pls.
- No. 13 HUNZIKER J.C., DESMONS J., and HURFORD AJ. 1992. Thirty-two years of geochronological work in the Central and Western Alps: a review on seven maps. 59 pp., 18 text-figs., 7 maps.
- No. 14 SPRING L. 1993. Structures gondwaniennes et himalayennes dans la zone tibétaine du Haut Lahul-Zanskar oriental (Himalaya indien). 148 pp., 66 text-figs., 1 map.
- No. 15 MARCHANT R. 1993. The Underground of the Western Alps. 137 pp., 104 text-figs.
- No. 16 VANNAY J.-C. 1993. Géologie des chaînes du Haut-Himalaya et du Pir Panjal au Haut-Lahul (NW-Himalaya, Inde). Paléogéographie et tectonique. 148 pp., 44 text-figs., 6 pls.
- No. 17 PILLEVUIT A. 1993. Les blocs exotiques du Sultanat d'Oman. Evolution paleogeographique d'une marge passive flexurale. 249 pp., 138 text-figs., 7 pls.
- No. 18 DI MARCO, G. 1994. Les terrains accrétés du sud du Costa Rica. Evolution tectonostratigraphique de la marge occidentale de la plaque Caraïbe. 166 pp., 89 text-figs., 6 pls.
- No. 19 JUD R. 1994. Biochronology and systematics of Early Cretaceous Radiolaria of the Western Tethys. 147 pp., 29 text-figs., 24 pls.
- No. 20 GORICAN S. 1994. Jurassic and Cretaceous radiolarian biostratigraphy and sedimentary evolution of the Budva Zone (Dinarides, Montenegro). 120 pp., 20 text-figs., 28 pls.

Order from:

Institut de Géologie et Paléontologie,

Université de Lausanne. BFSH-2. CH-1015, SWITZERLAND.

[HTTP://www-sst.unil.ch/publidep.htm](http://www-sst.unil.ch/publidep.htm)

Fax: (+41) 21-692.43.05

Bank Transfer: Banque Cantonale Vaudoise 1002 Lausanne

Account Number: **C. 323.52.56**

Institut de Géologie, rubrique: Mémoires

Price 30 CHF per volume (except volume 23 = 100 CHF). Price does not include postage

- No. 21 O'DOGHERTY L. 1994. Biochronology and paleontology of middle Cretaceous radiolarians from Umbria-Marche Apennines (Italy) and Betic Cordillera (Spain). 351 pp., 33 text-figs., 73 pls.
- No. 22 GUEX J. and BAUD A. 1994. Recent Development on Triassic Stratigraphy. 184 pp.
- No. 23 BAUMGARTNER P.O., O'DOGHERTY L., GORICAN S., URQUHART E., PILLEVUIT A. and DE WEVER P. (Eds.) 1995. Middle Jurassic to Lower Cretaceous Radiolaria of Tethys: Occurrences, Systematics, Biochronology. 1162 pp.
- No. 24 REYMOND B. 1994. Three-dimensional sequence stratigraphy offshore Louisiana, Gulf of Mexico (West Cameron 3D seismic data), 215 pp., 169 text-figs., 49 pls.
- No. 25 VENTURINI G. 1995. Geology, Geochronology and Geochemistry of the Inner Central Sesia Zone (Western Alps - Italy). 183pp., 57 text-figs., 12 pls.
- No. 26 SEPTFONTAINE M., BERGER J.P., GEYER M., HEUMANN C., PERRET-GENTIL G. et SAVARY J. 1995. Catalogue des types paléontologiques déposés au Musée Cantonal de Géologie, Lausanne. 76 pp.
- No. 27 GUEX J. 1995. Ammonites hettangiennes de la Gabbs Valley Range (Nevada, USA). 130 pp., 22 text-figs., 32 pls.
- No. 28 HÜRLIMANN A., BESSON-HÜRLIMANN A. and MASSON H. 1995. Stratigraphie et tectonique de la partie orientale de l'écaille de la Gummfluh (Domaine Briançonnais des Préalpes). 132 pp., 62 text-figs., 39 pls., 6 maps.
- No. 29 DOBMEIER C. 1996. Die variskische Entwicklung des südwestlichen Aiguilles-Rouges-Massives (Westalpen, Frankreich). 191 pp., 70 text-figs., 18 tables, 1 map.
- No. 30 BAUD A., POPOVA I., DICKENS J.M. LUCAS S. and ZAKHAROV Y. (eds.) 1997. Late Paleozoic and Early Mesozoic Circum-Pacific Events: Biostratigraphy, Tectonic and Ore Deposits of Primorye (Far East Russia). IGCP Project 272, 202 pp., 71 text-figs., 17 tables, 48 pls.
- No. 31 ARMANDO G. 1998. Intracontinental alkaline magmatism: Geology, Petrography, Mineralogy and Geochemistry of the Jebel Hayim Massif (Central High Atlas - Morocco). 106 pp.